Modelling Water and Carbon Canopy Fluxes

by

Rhys James Whitley

B.Sc in Applied Physics (Hons)

in the

Faculty of Science

Department of Environmental Sciences

A thesis submitted in fulfillment for the degree of Doctor of Philosophy

February 2011

Declaration of Authorship

I, RHYS JAMES WHITLEY, declare that this thesis titled, 'MODELLING WATER AND CARBON CANOPY FLUXES' and the work presented in it are my own. I confirm that:

- This work was done wholly or mainly while in candidature for a research degree at this University.
- Where any part of this thesis has previously been submitted for a degree or any other qualification at this University or any other institution, this has been clearly stated.
- Where I have consulted the published work of others, this is always clearly attributed.
- Where I have quoted from the work of others, the source is always given. With the exception of such quotations, this thesis is entirely my own work.
- I have acknowledged all main sources of help.
- Where the thesis is based on work done by myself jointly with others, I have made clear exactly what was done by others and what I have contributed myself.

Signed: _____

Date: _____

The thing the ecologically illiterate don't realize about an ecosystem is that it's a system. A system! A system maintains a certain fluid stability that can be destroyed by a misstep in just one niche. A system has order, a flowing from point to point. If something dams the flow, order collapses. The untrained miss the collapse until too late. That's why the highest function of ecology is the understanding of consequences.

Kynes in "Appendix I: The Ecology of Dune"

Excerpt from Dune by Frank Herbet

Acknowledgements

I must first express my gratitude and thanks to my supervisors, Prof Derek Eamus, Dr Belinda Medlyn, Dr Melanie Zeppel and Dr Cate Macinnis-Ng, who have provided me with the utmost support, encouragement, criticisms and friendship in undertaking this cyclopean project. I am also deeply grateful to my previous supervisor Dr Nicholas Armstrong, who helped to start me on the road of mathematical modelling and has provided support in his own time. I also express my thanks to my friends and fellow colleagues Dr Daniel Taylor, Dr Isa Yunusa and Dr Remko Duursma (University of Western Sydney) who have also provided invaluable support and advice in completing this work.

I would like to thank Dr Jason Berringer (Monash University), Dr Lindsay Hutley (Charles Darwin University), Dr Anthony O'Grady (University of Tasmania) and Dr Oula Ghannoum (University of Western Sydney) for supplying the data that has made this work possible.

I am grateful to Dr Mathew Williams (Edinburgh University) for supplying the source code for the Soil-Plant-Atmosphere model, and who has also made his support available in a number of ways. This thesis would not have been possible without his assistance.

I would also like to show my gratitude to Dr Gab Abramowitz (University of New South Wales) for introducing me to artificial neural networks and for supplying the necessary resources to run it.

Additionally, I would like to thank my parents, Jim and Rita Whitley, my brother Tristan Whitley and my grandmother Eva Parry for their love and support during this period. Finally, my deepest gratitude and thanks goes to the love of my life Helen Gough, whose support, encouragement and patience has made this thesis possible.

To those who I have not mentioned, I offer my regards and blessings for your support and respect during the completion of this project.

For Helen, whose patience and love was undying in completing an equally undying thesis.

Contents

List of Figures

List of Tables

Abbreviations

ANN	**A**rtificial **N**eural **N**etwork
APAR	**A**bsorbed **P**hotosynthetically **A**ctive **R**adiation
BA	**B**asal **A**rea
CUE	**C**arbon **U**se **E**fficiency
EC	**E**ddy **C**ovariance
ET	**E**vapo**t**ranspiration
GA	**G**enetic **A**lgorithm
GENOUD	**GEN**etic **O**ptimisation **U**sing **D**erivatives
GPP	**G**ross **P**rimary **P**roductivity
LAI	**L**eaf **A**rea **I**ndex
LUE	**L**ight **U**se **E**fficiency
LWP	**L**eaf **W**ater **P**otential
ME	**M**odel **E**fficiency
MJS	**M**odified **J**arvis-**S**tewart model
MNDR	**M**ultivariate-**N**onlinear-**D**ummy **R**egression
NPP	**N**et **P**rimary **P**roductivity
NSW	**N**ew **S**outh **W**ales
PAR	**P**hotosynthetically **A**ctive **R**adiation
PEP	**P**hosphoenolpyruvate
PSD	**P**article **S**ize **D**istribution
RMSE	**R**oot **M**ean **S**quare **E**rror
RuBisCO	**R**ibulose **Bis**phosphate **C**arboxylase-**O**xyganase
RuP$_2$	**R**ibulose **Bis**phosphate

SA	**S**ite-**A**average model
SOFM	**S**elf **O**rganising **F**eature **M**ap
SOLO	**S**elf **O**rganising **L**inear **O**ptimisation
SPA	**S**oil **P**lant **A**tmosphere model
SPAC	**S**oil **P**lant **A**tmosphere **C**ontinuum
SS	**S**ite-**S**pecific model
SWC	**S**oil **W**ater **C**ontent
SWP	**S**oil **W**ater **P**otential
VPD	**V**apour **P**ressure **D**eficit
WUE	**W**ater **U**se **E**fficiency
WA	**W**estern **A**ustralia

Physical Constants

Relative diffusivity of water vapour to CO_2 in air	a_c	1.56	*unitless*
Specific heat capacity of the air	c_p	1.013	MJ kg^{-1} $°C^{-1}$
Gravitational constant	g	9.807	m^2 s^{-1}
Molecular mass of air	M_a	28.96440	g mol^{-1}
Molecular mass of water	M_w	18.01528	g mol^{-1}
Atmospheric Pressure	P_a	101300.0	Pa
Universal gas constant	$\mathcal{R}$	8.1344	J K^{-1} mol^{-1}
Emissivity of the earth's surface	ϵ	0.96	*unitless*
CO_2 compensation point @ 25°C	Γ^*	36.5	μmol mol^{-1}
Psychometric constant	γ	0.066	kPa $°C^{-1}$
von Kármán constant	κ	0.41	*unitless*
Latent heat of vaporisation of water	λ	2.3845	MJ kg^{-1}
Pi	π	3.14159265	*unitless*
Density of air	ρ_a	1.204	kg m^{-3}
Density of water	ρ_w	998.2	kg m^{-3}
Stephen-Boltzmann constant	σ	5.6703×10^{-8}	W m^{-2} K^{-4}

Symbols

A_{cat}	Catchment area	m^2
A_c	RuBisCO activity-limited assimilation	μmol m^{-2} s^{-1}
A_d	Rate of CO_2 diffusion	μmol m^{-2} s^{-1}
A_g	Gross assimilation	μmol m^{-2} s^{-1}
A_j	Light-limited assimilation	μmol m^{-2} s^{-1}
A_n	Net assimilation	μmol m^{-2} s^{-1}
$C_{\%}$	Percentage of clay (PSD)	%
C_a	Ambient CO_2 concentration	μmol mol^{-1}
C_i	Intercellular CO_2 concentration	μmol mol^{-1}
C_{leaf}	Leaf capacitance	mmol m^{-2} MPa^{-1}
C_m	CO_2 concentration in the mesophyll cells	μmol mol^{-1}
C_s	CO_2 concentration in the bundle sheath cells	μmol mol^{-1}
D_v	Vapour pressure deficit	kPa
D_{vmax}	Daily maximum vapour pressure deficit	kPa
D_{peak}	Position of peak vapour pressure deficit	kPa
D_0	Lohammer constant for D_v	kPa
d_{0p}	Zero plane displacement height	m
d_{root}	Depth of roots	m
d_{soil}	Depth of soil	m
E_0	Potential evaporation	mm hr^{-1}
E_c	Canopy transpiration	mm hr^{-1}
E_{cmax}	Maximum canopy transpiration	mm hr^{-1}
E_s	Soil evaporation	mm hr^{-1}

E_t	Tree transpiration	mm hr^{-1}
E_T	Evapotranspiration	mm hr^{-1}
g_a	Aerodynamic conductance	mmol m^{-2} s^{-1}
g_b	Boundary layer conductance	mmol m^{-2} s^{-1}
g_{bs}	Bundle sheath conductance	mmol m^{-2} s^{-1}
g_c	Canopy conductance	mmol m^{-2} s^{-1}
g_{cmax}	Maximum canopy conductance	mmol m^{-2} s^{-1}
g_{plant}	Whole plant hydraulic conductance	mmol m^{-2} MPa^{-1}
g_s	Stomatal conductance to H_2O	mmol m^{-2} s^{-1}
g_{sc}	Stomatal conductance to CO_2	mmol m^{-2} s^{-1}
g_{s0}	Residual stomatal conductance	mmol m^{-2} s^{-1}
g_{smax}	Maximum stomatal conductance	mmol m^{-2} s^{-1}
g_{smin}	Minimum stomatal conductance	mmol m^{-2} s^{-1}
g_t	Total conductance to H_2O	mmol m^{-2} s^{-1}
H_s	Relative humidity	%
h	Height of canopy	m
J_e	Potential rate for electron transport	μmol m^{-2} s^{-1}
J_{max}	Maximum rate for electron transport	μmol m^{-2} s^{-1}
J_w	Flow of water to the xylem	mm t^{-1}
K	Soil hydraulic conductivity	MPA m^{-2} s^{-1}
K_c	Enzyme catalytic activity for CO_2	μmol mol^{-1}
K_o	Enzyme catalytic activity for O_2	μmol mol^{-1}
K_m	Combined enzyme catalytic activity	μmol mol^{-1}
K_p	Enzyme catalytic activity for PEP	μmol mol^{-1}
k_{D_1}	vapour pressure deficit shape parameter 1	kPa
k_{D_2}	vapour pressure deficit shape parameter 2	kPa
k_T	C_4 first order rate constant for PEP carboxylase	*unitless*
k_R	Solar radiation constant	W m^{-2}
L	Rate of CO_2 leakage from the bundle sheath to the mesophyll cells	μmol m^{-2} s^{-1}
L_{SA}	Specific leaf area	m^2 m^{-2}

M_{cj}	C_4 CO_2 flux determined by A_c and A_j	μmol m^{-2} s^{-1}
m_{root}	Root biomass	kg m^{-3}
N_f	Total leaf nitrogen content	g m^{-2}
N_{LA}	Nitrogen per leaf area	g m^{-2}
O_i	Intercellular O_2 concentration	μmol mol^{-1}
O_s	O_2 concentration in the mesophyll cells	μmol mol^{-1}
O_s	O_2 concentration in the bundle sheath cells	μmol mol^{-1}
Q_p	Quantum flux density (PAR)	μmol m^{-2} s^{-1}
$R_{a,b}$	Total above and below-ground resistance	MPa m^2 s mol^{-1}
R_d	Dark respiration	μmol m^{-2} s^{-1}
R_m	Mitochondrial respiration	μmol m^{-2} s^{-1}
R_n	Net radiation	W m^{-2}
R_s	Solar radiation	W m^{-2}
R_{plant}	Plant resistance	MPa m^2 s mol^{-1}
R_{root}	Root resistance	MPa m^2 s mol^{-1}
R_{soil}	Soil resistance	MPa m^2 s mol^{-1}
r_b	Boundary layer resistance	s m^{-1}
r_{root}	Fine root radius	m
r_s	Stomatal resistance	s m^{-1}
$S_{\%}$	Percentage of sand (PSD)	%
S_A	Sapwood area	m^2 ha^{-1}
T_a	Ambient air temperature	°C
T_{amax}	Daily maximum air temperature	°C
T_l	Leaf temperature	°C
U_z	Windspeed	m s^{-1}
V_{cmax}	Maximum rate for RuBisCO carboxylation	μmol m^{-2} s^{-1}
V_o	Rate for RuBisCO oxygenation	μmol m^{-2} s^{-1}
V_p	Rate for PEP carboxylation	μmol m^{-2} s^{-1}
V_{pr}	PEP regeneration rate	μmol m^{-2} s^{-1}
V_{pmax}	Maximum rate for PEP carboxylation	μmol m^{-2} s^{-1}
$\bar{x}_{root}$	Mean distance between roots	m

z_h	Height of humidity measurement	m
z_m	Height of wind measurement	m
z_{oh}	Roughness length governing heat transfer	m
z_{om}	Roughness length governing momentum transfer	m
α_j	Quantum yield of whole chain electron transport	mol mol^{-1}
α_{rf}	Combined constant: Quantum yield and absorbed photons used by the C_4 reaction process	mol mol^{-1}
β_e	Proportionality of error	*unitless*
β_{co}	Co-limitation between light, RuBisCO and CO_2 limited flux	*unitless*
Δ	Slope between vapour pressure and temperature	kPa $°C^{-1}$
ι_{op}	Stomatal efficiency parameter	*unitless*
λ_{cw}	Cost of water parameter	μmol mol^{-1}
Ψ_s	Soil water potential	MPa
Ψ_l	Leaf water potential	MPa
Ψ_{lpd}	Pre-dawn leaf water potential	MPa
Ψ_{lmin}	Minimum leaf water potential	MPa
θ_c	Critical point for transpiration	m^3 m^{-3}
θ_f	Field capacity of the soil	m^3 m^{-3}
θ_j	Shape coefficient for non-rectangular hyperbola	*unitless*
θ_{tr}	Transition between light-limited and RuBisCO limited CO_2 flux	*unitless*
θ_s	Soil water content	m^3 m^{-3}
θ_{sat}	Saturated water content of the soil	m^3 m^{-3}
θ_w	Wilting point for transpiration	m^3 m^{-3}

Abstract

Modelling the water and carbon fluxes from forest canopies provides useful insight into the dynamics of the exchange of water vapour for atmospheric CO_2 and the processes that govern this exchange. The work presented in this thesis aimed to answer four questions related to modelling of canopy gas-exchange. The first two questions involved the development of a simple empirical model of canopy water-use to see whether i) water fluxes from a canopy could be estimated without the need for canopy conductance and ii) could such a model be applied across multiple sites without the need for site-specific calibration? The remaining two questions involved the modification and improvement of a highly mechanistic and complex soil-plant-atmosphere (SPA) continuum model, which was done in order to iii) replicate canopy gas-exchange for a Australian tropical savanna and iv) to improve the simulated leaf gas-exchange process of a SPA model.

A simple empirical model of canopy water-use (E_c), a modified Jarvis-Stewart (MJS) model, was developed in order to circumvent the problem of requiring surface conductance as an input in order to calculate transpiration. This was accomplished by modelling an empirical relationship of the multivariate response of E_c to solar radiation (R_s), vapour pressure deficit (D_v) and soil moisture content (θ_s). The MJS model was shown to provide favourable short- and mid-term (annual) estimates of E_c that only required three more readily available abiotic inputs (R_s, D_v and θ_s) and a small set of site-calibrated model parameters. Predictions of E_c determined from the MJS model were able to replicate the observed data and compared favourably with the established Penman-Monteith (PM) equation and a statistical benchmark created using an artificial neural network (ANN).

In addition to this, the applicability of the MJS model was tested for five disparate Australian woodland sites, where model parameters were calibrated for each individual site and simultaneously for all sites. The result was that while MJS model was able to give a good representation of the measured data using site-specific parameters, using a parameter set that describes an average response of E_c to the environment performed equally well. This was despite each site being comprised of different tree species and occurring over different soil profiles. This showed that the MJS model is partially insensitive to variation in the values of the model parameters and that the number of inputs into the MJS can be

further reduced. The conclusion was that this model is broadly applicable for many sites in temperate Australia and one that can be used as a tool in the management of water resources.

While the MJS model provided a useful management tool, in order to investigate the dynamics of water and carbon gas-exchange from forest canopies, the more complex SPA model of Williams et al. (1996a) was used. While the SPA model has been applied in ecosystems globally with much success, the lack of C_4 photosynthesis has limited its application to savanna ecosystems. Modification of the SPA model was therefore undertaken in order to improve its applicability to savannas through incorporation of C_4 photosynthesis. This was an important improvement as savannas are dominated by C_4 grasses, which contribute significantly to ecosystem water and carbon fluxes. This modification allowed the SPA model to be parameterised to a savanna site in northern Australia, which was simulated over 5 years to replicate measurements of carbon and water fluxes derived from eddy-covariance. The SPA model allowed C_3 and C_4 water and carbon fluxes to be separated and this showed that the C_4 grasses contribute significantly to total savanna productivity (48%), but a much smaller amount to total water-use (23%). Additionally, it was determined the seasonal variation in leaf area index was driving the seasonality in productivity and water-use and the savanna site was determined to be energy-limited (limited by its light interception).

The modification and application of the SPA model to a savanna site highlighted important issues in the way leaf gas-exchange is represented in the model. An investigation into the leaf gas-exchange process handled by SPA showed that there was an imbalance between assimilation and transpiration, as a result of simulated stomatal conductance being increased to unreasonably high levels in order to maximise carbon gain. In order to correct this problem, the modelled gas-exchange was modified to follow the *optimality hypothesis* of Cowan and Farquhar (1977), such that carbon gain is maximised while water lost from the leaf is simultaneously minimised. This improvement was tested in a purely theoretical exercise, where leaf gas-exchange (default and improved schemes) was simulated over a drought. The result of this simulation was that the improved scheme produced a reduction in canopy water-use, while carbon gain remained high and comparable with that of the default scheme.

Chapter 1

Introduction

1.1 The Australian continent

Water is possibly the most vital resource on earth that is necessary for the existence of life. Human culture, progress and survival is heavily dependent upon it as it drives the areas of industry, urban settlement, agriculture and environmental function. However, Australia is the driest inhabited continent on earth, defined by a low mean annual rainfall ($350 - 450$ mm) and a temperature range that can be loosely termed as ranging from warm to hot. Compounding this, rainfall is highly variable resulting in prolonged droughts (that may last years), due in part to the El Niño/La Niña Southern Oscillation. Australia contains several climatic zones that encompass the extremes of desert in the interior to tropical rainforest in the far north and north-east coast of the continent. However, the majority of human urban settlement in Australia is coastal, covering the moderately temperate zones along the east and south-west coast. Most of the drier grassland interior has been used for grazing.

Only a small proportion of the total rainfall that Australia receives annually is available for human use. This fraction is approximately 10% and predominantly contributes to surface run-off (rivers) and ground-water recharge, with the other 90% returning to the atmosphere through evapotranspiration. In Australia, the fraction of water extracted from surface (lakes, rivers and reservoirs) is about 80%, while the water that is extracted

from ground-water stores is about 20% (McMahon and Finlayson, 2003; Eamus et al., 2006b). The majority of extracted water via surface and sub-surface stores is used for agriculture and equates to about $70 - 75\%$, while urban settlement and the industrial sector only use about 20%. The extraction of stored water in Australia is therefore a highly important and contentious issue; important because a large part of the Australian economy is dependent on agriculture, and contentious because the extraction of water for human use is not properly balanced in terms of the local climate and sustainability. This imbalance is largely due to irrigation, where a large volume of water is needed to produce profitable crop yields, which in most cases dictates a low commercial return of water, when thought of in terms of the volume of water spent per dollar of profit of harvested crop (Scanlon et al., 2007). This, for a continent that is characterised by low mean annual rainfall and periods of prolonged drought, shows that there is a critical need for ensuring the proper management of landscape water-use.

Water use by vegetation is defined as transpiration and is the flow of water from the soil to the leaf to the atmosphere, through the Soil-Plant-Atmosphere continuum (SPAC). The arid climate of Australia has characterised the evolution of the SPAC to be water-conservative, with native flora that is highly resilient to prolonged periods of drought. Australian native flora have had to adapt to a highly variable and low yielding rainfall, which has resulted in the development of sunken stomata, tough sclerophyllous and pendulous leaves, being drought deciduous, having increased stem water storage capacities and deep, reaching roots that are frequently able to access ground-water stores (Cook et al., 1998; Hutley et al., 2000; Eamus, 2003; O'Grady et al., 2006). Most importantly, the SPAC is the principle pathway for the flow and discharge of water from the Australian landscape, and therefore makes trees vitally important in our understanding of ecosystem water and carbon balances. The obstruction of the SPAC by the removal of vegetation results in highly negative impacts on landscape water budgets. This can include increased soil erosion, reduced primary productivity (fixing atmospheric carbon) and an increase in the development of dry-land salinity. Not only must the SPAC be considered when developing sustainable water budgets, but it also shows the important role that vegetation plays in an ecosystem's water balance.

The impact of climate change, which is forecast to increase average surface air temperatures as a result of higher atmospheric carbon dioxide (CO_2) concentrations, aggravates an already finely balance ecosystem function and the maintenance of sustainable ecosystem water balances (Whetton et al., 1993). Simulated forecasts and observational evidence suggests that water resources in Australia are highly vulnerable to the impacts of climate change. This is likely to be predominantly due to the aridity of the Australian environment, as arid ecosystems are more responsive to changes in atmospheric CO_2, temperature and precipitation (Hughes, 2003). Forcasted scenarios include a redistribution of rainfall patterns and potential changes in seasonality for parts of the continent, and an increase in evapotranspiration due to an increase in surface air temperature and a decrease in atmospheric humidity. This in turn will have an effect on the amount of water needed by the agricultural sector in Australia (Asseng et al., 2004; Anwar et al., 2007).

The problems of climate change and managing sustainable ecosystem water balances, in the present and in the future, may be investigated by the use of mechanistic and empirical mathematical equations. The use of equations allows the construction of models that capture and mimic real-world systems that can be used to simulate possible future scenarios and answer important hydrological and physiological questions. This chapter therefore outlines the underlying theory that has been used to build mathematical descriptions of ecosystem water balance and the SPAC.

1.2 The water and energy balance of a catchment

Water moves continually through a cycle of precipitation, evapotranspiration, and surface run-off, creating and maintaining the flow of rivers that eventually reach lakes or oceans; additionally part of the precipitated water penetrates into deep soil to become ground water, and is therefore thought of as stored water. The water and energy balance of a site provides the framework for studying this hydrological behaviour. It allows one to assess how changes in catchment conditions can alter the partitioning of rainfall and solar energy into different components. This may be described as a model of stored water and energy fluxes that are subject to change, by the forcing of a stochastic climate. This system is analogous to a *lumped bucket* model (Figure 1.1) that is filled and emptied of the quantity

in question (water or energy) based on current and long term climatic conditions. This is now described.

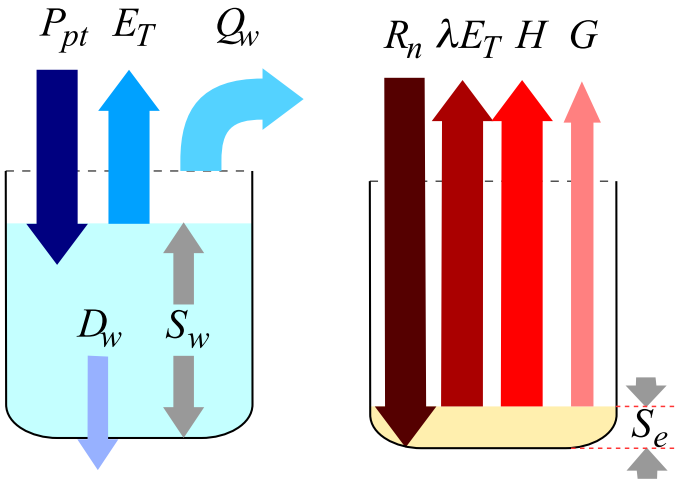

(a) Water bucket model (b) Energy bucket model

FIGURE 1.1: Illustration of site water and energy balances, using the analogy of a bucket: (a) water enters the '*bucket*' system through precipitation (P_{pt}) and leaves through evapotranspiration (E_T), ground water recharge (D_w) or surface run-off (Q_w); (b) energy enters the system as net solar energy (R_n) and leaves through latent energy (λE_T) or sensible heat (H) and soil heat flux (G). The storage in the "bucket" system is shown as (a) S_w (representing stored water) and (b) S_e (representing stored energy).

Water is accepted by the soil column and stored (S_w) during periods of precipitation (P_{pt}). Water is then lost from the soil column via evaporation (E_s), or taken up by vegetation through transpiration (E_t); the total of these two quantities is termed as evapotranspiration (E_T). Any remaining portion of S_w that is not taken up by E_T remains in the soil or is recharged to the water table (D_w). Additionally if $P_{pt} > E_T$, then water will flow out of the soil column and leave the system as surface or sub-surface run-off (Q_w). S_w is therefore subject to change over time (t), by the above processes and this may be expressed as:

$$\frac{dS_w}{dt} = P_{pt}(t) - E_T(t) - Q_w(t) - D_w(t) \tag{1.1}$$

By considering an annual water balance, and the reasonable assumption that the carry-over of S_w is negligible between years, such that $dS_w/dt = 0$, then the steady-state water balance for a catchment can be written as:

$$P_{pt} = E_T + Q_w + D_w \tag{1.2}$$

E_T is generally the second largest term in the water balance equation and is closely linked to vegetation dynamics. The proportionality between P_{pt} and E_T, depends on the type of environment. In arid regions, $P_{pt} \simeq E_T$, but in well-watered (mesic) environments $P_{pt} > E_T$.

The energy balance of a site can be described in similar terms to the water balance of the site to reflect an energy budget. Energy is supplied to the system through direct solar radiation (R_s), and is either absorbed, reflected or transmitted by the forest canopy and the soil. The absorbed energy increases the heat of an object and results in the transmission of long-wave radiation (I_w). Reflected R_s will travel back to that atmosphere unless it is intercepted by an object (i.e. the tree canopy) and therefore reflected back to the surface. Additionally I_w, once emitted, may travel through the atmosphere or to a surface. Consequently, both R_s and I_w have *up* and *down* components. The net difference between up and down components of R_s and I_w is termed as the net radiation (R_n) and is the amount of energy that is stored for use (S_e) by the catchment (Eagleson, 2002). The net energy supplied is then used (or lost) by the system through latent heat (λE_T) (where λ is the latent heat of vaporisation) and through the loss of heat from vegetation by sensible heat (H). Additionally, there is a some fraction of heat lost to the soil (G). However, the magnitude of G is small when compared with the quantities of λE_T and H (Monteith and Unsworth, 1990; Jones, 1992). The change in S_e over time is therefore given as:

$$\frac{dS_e}{dt} = R_n(t) - \lambda E_T(t) - H(t) - G(t) \tag{1.3}$$

The magnitude of S_e is generally negligible as most stored energy is lost through the emission of I_w by the leaves and soil over a 24 hour period. Leaf temperature tends to remain below that of the air when water is freely available in soil for transpiration (Eamus et al., 2006b). Therefore, it holds that $dS_e/dt = 0$, such that the steady-state energy balance of a site can be described as:

$$R_n = \lambda E_T + H + G \tag{1.4}$$

Both λE_T and H are the second and third largest terms in the energy balance equation, with the dominance of one of these terms over the other depending on the type of

ecosystem. For arid environments, $H > \lambda E_T$, and so $R_n \rightarrow H$, as limited water supplies constrain the vegetation component of E_T. For humid, sub-tropical environments the revere is true, with $H < \lambda E_T$ and $R_n \rightarrow \lambda E_T$.[1]

A relationship between the water and energy balance of a catchment in terms of its size and depth of storage can be drawn following the method outlined in Donohue et al. (2007). First, the change in soil water storage (dS_w/dt) is expressed by considering S_w is subject to change by volume (V) and the mass concentration of water ($[m_w]$); which is a first order derivative. Next, the temporal resolution is incorporated by integrating Equation 1.1 over a finite time space (τ), such that:

$$\int_0^\tau \frac{\partial S_w}{\partial V} d[m_w] + \frac{\partial S_w}{\partial [m_w]} dV \, dt = \int_0^\tau P_{pt}(t) - E_T(t) - Q_w(t) - D_w(t) \, dt \tag{1.5}$$

the integral of which is:

$$[m_w]\Delta A_{cat} z_r + A_{cat} z_r \Delta [m_w] = \tau(P_{pt} - E_T - Q_w - D_w) \tag{1.6}$$

where V can be considered in terms of catchment area (A_{cat}) and the average rooting depth of the vegetation (z_r) ($V = A_{cat} z_r$). Equation 1.6 is then described in terms of the depth of water, by dividing by A_{cat} and the density of water (ρ_w), such that the final expression for the ecosystem water balance becomes:

$$\frac{1}{\rho_w}\left([m_w]\frac{\Delta z_r}{\tau} + z_r \frac{\Delta [m_w]}{\tau}\right) = \frac{P_{pt} - E_T - Q_w - D_w}{A_{cat}\rho_w} \tag{1.7}$$

Similarly, Equation 1.3 is described replacing z_r with the depth of energy storage (z_e):

$$[m_e]\frac{\Delta z_e}{\tau} + z_e \frac{\Delta [m_e]}{\tau} = \frac{R_n - \lambda E_T - H - G}{A_{cat}} \tag{1.8}$$

The parameters A_{cat} and τ respectively determine the spatial and temporal scales of the analysis, and z_r and z_e determines the total possible soil water and energy storage respectively. The reasoning behind formulating the energy and mass balances equations

[1] Although this depends on whether the season is wet or dry.

in this way is to draw links between vegetation characteristics of the catchment and the spatial scale of the analysis, as well as to create a link between the flux and steady-state components of the relationships (Donohue et al., 2007).

1.2.1 Water- and energy-limited ecosystems

1.2.1.1 Budyko curve

In 1974, Budyko developed a framework for the mass and energy balance of demand-limited E_T, built upon the work of Schreiber (1904) and Ol'dekop (1911). Budyko performed an empirical analysis of the climate and water balance of a large number of catchments around the world, comparing how E_T and the potential evaporation[2] (R_N/λ) are limited with the respect to P_{pt} in each system. For an ecosystem where water supply is limiting, energy supplied to the catchment surpasses the water available, such that $R_n/\lambda > P_{pt}$, the maximum possible E_T is P_{pt} (assuming $Q_w = 0$) such that all water falling into the catchment is evapotranspired back out and none is stored ($S_w = 0$). For an ecosystem where energy supply is limiting, water supplied to the catchment exceeds the available energy, such that $R_n/\lambda < P_{pt}$ and the maximum possible E_T is R_n/λ (assuming $H = 0$) (Donohue et al., 2007). This allows both Q_w and S_w to increase as there is not enough available energy to evaporate all the incoming water. Based on these limits, Budyko found that different ecosystems fell along one curvilinear relationship, such that all ecosystems can be divided into energy-limited (wet) areas and water-limited (dry) areas. This, allowed Budyko to describe E_T based on these limits of available water and energy, termed as this Budyko curve, and this may be calculated as:

$$E_T = \sqrt{\frac{R_n P_T}{\lambda} \tanh\frac{1}{\Phi} \left(1 - \cosh\Phi + \sinh\Phi\right)} \tag{1.9}$$

where Φ is radiative index of dryness and is equal to $R_n/(\lambda P_{pt})$, where $\Phi > 1$ represents water limited environments, $\Phi < 1$ represents energy limited environments and $\Phi \approx 1$ represents intermediate environments (Budyko, 1974). Figure 1.2 shows the form of the Budyko curve and how E_T reaches the energy and water limits, with the line AB defining

[2]Denoted here as a measure of the available energy and R_n is divided by λ in order to express the available energy for evaporation into the depth of water evaporated.

the water limit to E_T, and the line CD defining the energy limit to E_T. An evaporative index ($\varepsilon = E_T/P_{pt}$) parameter is used to describe the partitioning of P_{pt} into E_T and Q_w. Both Q_w and H are proportional to the vertical distance from the curve to the energy and water limits respectively.

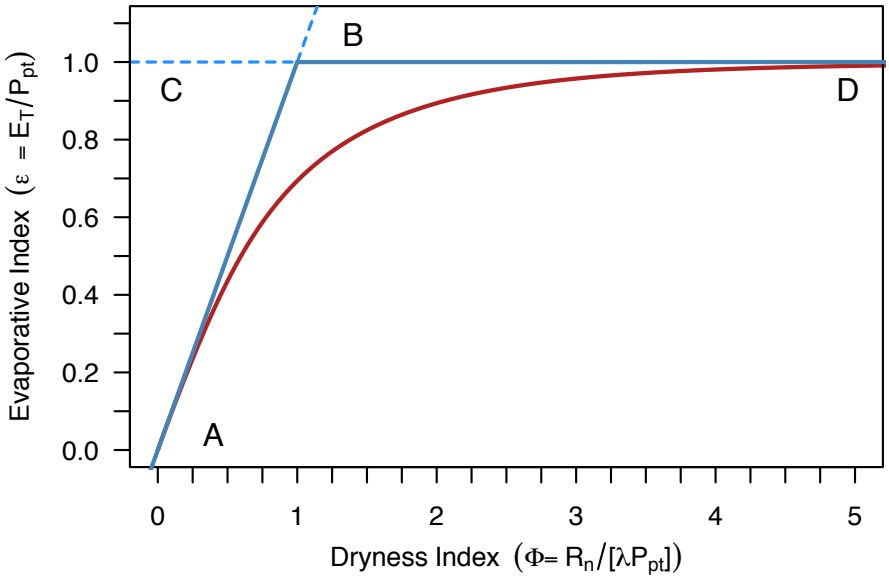

FIGURE 1.2: The Budyko framework and curve, where the curve (red line) is defined by Equation 1.9, describes the relationship between the dryness index ($\Phi = R_n/[\lambda P_{pt}]$) and the evaporative index ($\epsilon = E_T/P_{pt}$). Line AB defines the energy-limit to evapotranspiration, and line CD defines the water-limit.

The performance of the Budyko curve has been reviewed on many factors such as scale, the role of vegetation and deviations from the curve itself (Choudhury, 1999; Donohue et al., 2007). Budyko found that for large catchment areas ($A_c > 1000$ km^2), the macro-climate was the principal factor in determining E_T. However, as A_{cat} becomes much smaller, and hence the resolution becomes better, *local* conditions such as vegetation type (evergreen or deciduous species) and topography (i.e. the physical properties of the soil, slope, depth to the water table) give a larger variation in E_T due to the sensitivity of R_n at this scale (Zhang et al., 2001; Donohue et al., 2007). Budyko also considered the water and energy balance of ecosystems for large temporal scales (> 1 yr), and so the relationship described by Equation 1.9 begins to fail when the spatial and temporal resolutions are reduced. It is from Equations 1.7 and 1.8, that Choudhury (1999) and Zhang et al. (1998, 2001) have

reformulated Budyko's curve to deal with scale and vegetation more explicitly and this will be discussed in the next two sections.

1.2.1.2 Choudhury curve

Although not directly concerned with vegetation dynamics at smaller catchment scales, Choudhury (1999) explored the effects of A_{cat} on predictions of E_T. The Choudhury curve is based on the equation developed by Pike (1964) with the difference of an adjustable parameter $\overline{\alpha}$, such that E_T equals:

$$E_T = \frac{P_{pt}}{\sqrt[\overline{\alpha}]{1 + (1/\Phi)^{\overline{\alpha}}}} \tag{1.10}$$

The parameter $\overline{\alpha}$ allows for the equation to change at different spatial scales, allowing for the consequent spatial variation in R_n and P_{pt}. Choudhury found that the dependence of E_T on P_{pt} and R_n changed with the magnitude of A_{cat}, with $\overline{\alpha}$ being large at site based scales ($\overline{\alpha} = 2.6$) and decreasing to lower values at basin level scales ($\overline{\alpha} = 1.8$) (Figure 1.3). As the spatial scale increased ($A_{cat} \to \infty$), the lower the $\overline{\alpha}$, became, and this resulted in a lower E_T for a given Φ (Choudhury, 1999; Donohue et al., 2007).

1.2.1.3 Zhang curve

Zhang et al. (2001) took a more focused approach on the role of vegetation in the Budyko curve, especially concerning how the effects of vegetation on E_T become more important as the spatial scale decreases. Zhang et al. modified the Budyko framework based on previous work of Choudhury, to quantify the long-term effects of changing vegetation on E_T. This modification is given by the following equation:

$$E_T = P_{pt}\frac{1 + \omega\Phi}{1 + \omega\Phi + 1/\Phi} \tag{1.11}$$

where ω is a plant available water coefficient. The ω parameter symbolises the total water available to the plant within the root zone, which is needed for E_t, and hence, reflects the integrated role of multiple catchment processes on E_T; with notable reference to z_r

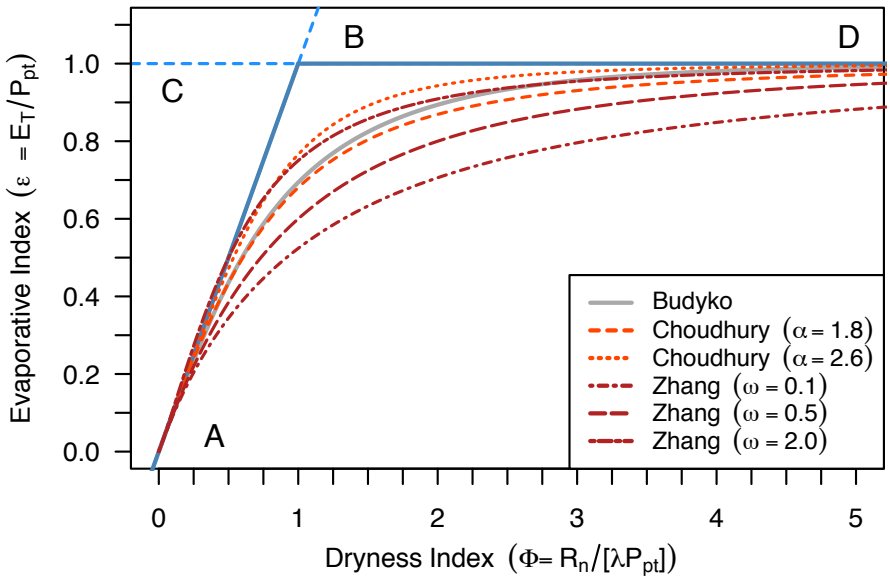

FIGURE 1.3: The Budyko curve (grey line), as compared with the Choudhury curve (orange lines) and the Zhang curve (red lines) at different spatial scales. The α values in the Choudhury curve represent the effect of the spatial scale on E_T; where $\alpha = 1.8$ is a basin, and $\alpha = 2.6$ is an entire site. The ω values in the Zhang curve represent the role of vegetation in E_T; where $\omega = 0.1$ represents bare soil, $\omega = 0.5$ represents grasses or crops, and $\omega = 2.0$ represents a forest. Line AB defines the energy-limit to evapotranspiration, and line CD defines the water-limit.

on E_T (Equation 1.7). Zhang et al. noted that for forests $\omega = 2.0$, for crops and grasses $\omega = 0.5$, and for bare soils $\omega = 0.1$. As ω increases, the larger the role of vegetation in E_T (Figure 1.3). At the limiting ends of the Budyko framework of water stress ($\Phi \to \infty$) and energy stress ($\Phi \to 0$), Zhang et al. noted the minimal effect of ω on E_T, and that ω is very sensitive to intermediate values (rather than the limits) of the dryness index (Zhang et al., 2001; Donohue et al., 2007). This additionally shows that as vegetation becomes less important, there is an increase in the magnitude in Q_w and H, as the vertical distance between the curve and the limits increases.

On a final note, Donohue et al. (2007) suggest that care must be taken when applying the Budyko curve to smaller temporal scales ($\tau < 1$ yr), as the vegetation is likely to experience a larger variation (i.e. drought, bush fires, harvesting, deforestation) and therefore show a larger variation in S_w. Vegetation dynamics can therefore present non-steady-state conditions, and if it is necessary to increase the time scale ($\Phi > 1$ yr), then the application of these models becomes less and less appropriate to areas of catchment and land

management.

1.3 Evapotranspiration

Evapotranspiration (E_T) is the combination of two separate processes, that define the energy transfer of water from the surface to the air (Figure 1.4). The first process is surface evaporation (E_s), which is defined as the water lost from some arbitrary wet surface (i.e. soil, lake or canopy during and after rain), and the second process is transpiration (E_t), which is defined as the water lost through the stomata of a leaf as a consequence of carbon uptake needed for photosynthesis (Nobel, 1999). Evapotranspiration is therefore a sum both water loss components:

$$E_T = E_s + E_t \tag{1.12}$$

and is a significant quantity in determining the water balance of a catchment (Eamus et al., 2006b).

1.3.1 Surface evaporation

Evaporation is the transfer of water from a wet surface to the atmosphere, and is the result of two distinct processes. The first process relates to the energy balance between the surface and the atmosphere, where liquid water is converted to water vapour through the energy supplied from direct R_s and air temperature (T_a). The second process describes the mass transfer of water as latent heat (or energy), and is primarily described by the movement of the water vapour from the evaporating surface to the surrounding atmosphere, as a result of the vapour pressure difference between these two points (Jones, 1992). As evaporation continues, the localised air becomes increasingly saturated, decreasing the vapour pressure gradient between surface and atmosphere, slowing the movement of water vapour across this boundary. The flow of air across this surface (wind) (U_z), replaces the local saturated air with dry air, allowing the vapour pressure gradient to remain high (Eagleson, 2002). This aerodynamic conductance (g_a) to water vapour is the primary factor responsible for the removal of water from the surface to the bulk atmosphere. These process have little biological control.

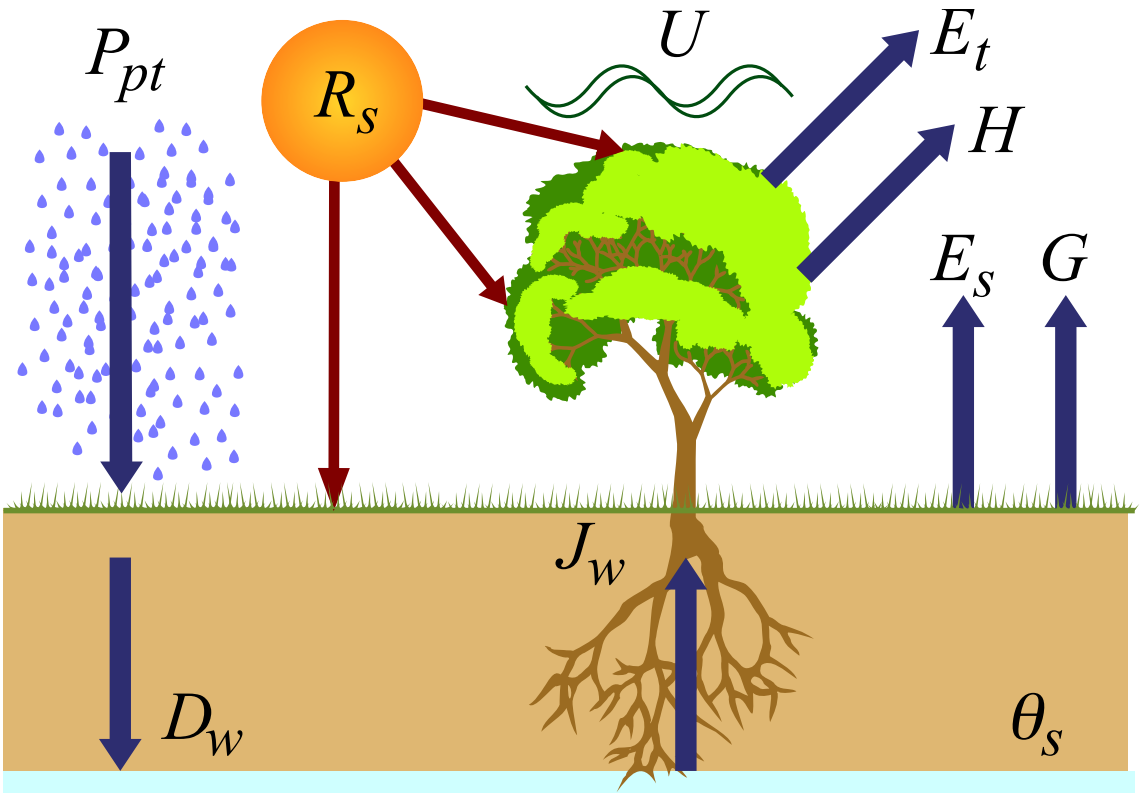

FIGURE 1.4: Water balance of an ecosystem. Rainfall (P_{pt}) which is partitioned into soil water storage (θ_s), deep drainage (D_w), and evapotranspiration (E_T). E_T is further divided into canopy transpiration (E_t) and soil evaporation (E_s). E_t is determined by incident solar radiation (R_s), turbulent transport (U), the supply of water to the canopy (J_w) and the vapour pressure deficit.

1.3.2 Transpiration

Transpiration (E_t) operates via the same mechanisms for the removal of water from a wet surface to the atmosphere discussed above. However, E_t is predominantly governed by the biological response of the plant to evaporative demand and soil water availability. This biological response is a result of the opening and closing of the stomata of the leaf; the function of which is to regulate the amount of water lost through E_t (Monteith and Unsworth, 1990; Jones, 1998). Stomatal opening of the leaves is quantified in terms of stomatal conductance (g_s), which is a measure of the conductance to vapour flow from the sub-stomatal cavity in the leaf to the layer of air at the leaf's surface. The degree of vapour flow is determined by the vapour pressure gradient and consequently transpiration is generally limited by g_s, R_s and the vapour pressure deficit (D_v) (Jarvis and McNaughton, 1986). The degree of g_s is additionally controlled by another factor, namely the volumetric

water content of the soil (θ_s). If θ_s is high, then supply of water can equal the evaporative demand and so stomata remain open. However, when θ_s is low, the evaporative demand cannot be met and so stomata will close to limit the negative impact on plant water status. Finally, the amount of water that a plant transpires is related to its leaf area; defined in terms of the leaf area index (LAI), which is the ratio of canopy leaf area to ground area. The LAI affects the interception of rainfall, radiation, and defines the canopy area available to evaporate water (Zhang et al., 1998). Therefore, the meteorological parameters that are considered to predominantly drive E_t are R_n, D_v and θ_s (Figure 1.5).

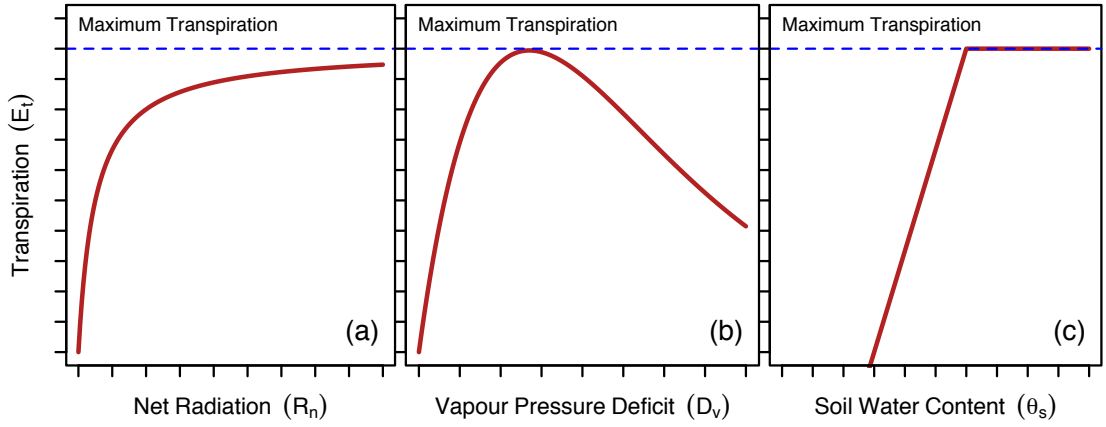

FIGURE 1.5: The predominant drivers of transpiration (E_t) from a plant are a) net radiation (R_n), b) vapour pressure deficit (D_v) and c) volumetric soil water content (θ_s).

Methods for calculating rates of E_s and E_t are now described below, and shown to be derived from the energy balance equation. Additionally methods for estimating g_s and g_c are given as well as current application of these models that have been found in the literature.

1.3.3 The Penman equation

The seminal work of Penman (1948) provided a model that describes the above process of evaporation, by arranging Equation 1.4 in terms of energy and mass transfer; assuming $\Delta S_e = 0$ and $Q_e = 0$. This gives an expression that describes the water lost from the surface (given in terms of latent energy, λE) by the sum of net energy flux ($R_n - G$) and

sensible heat (H), of the form:

$$\lambda E = R_n - G - H \tag{1.13}$$

By assuming that $\lambda E = \rho_a c_p g_v (e_s - e_a)/(\gamma[g_H/g_a])$, describing the energy driven by the pressure gradient, and $H = -\rho_a c_p g_H (T_s - T_a)$, describing the energy driven by the temperature gradient, Equation 1.13 is given as[3]:

$$\lambda E_s = \frac{\Delta(R_n - G) + \rho_a c_p D_v g_H}{\Delta + \gamma\,(g_H/g_a)} \tag{1.14}$$

where Δ is the slope of the saturation vapour pressure temperature relationship, ρ_a is the mean density of the air at constant pressure, c_p is the specific heat capacity of the air, γ is the psychrometric constant[4], g_H is the conductance of heat, and g_a is the aerodynamic conductance to water vapour, which is a function of wind speed and determined by:

$$g_a = \frac{\kappa^2 U_z}{\ln\left[\dfrac{z_m - d_{0p}}{z_{om}}\right] \ln\left[\dfrac{z_h - d_{0p}}{z_{oh}}\right]} \tag{1.15}$$

where z_m is the height of the wind speed measurement, z_h is the height of the humidity measurement, z_{oh} is the roughness length driving heat and vapour transfer, z_{om} is the roughness length driving momentum transfer, d_{0p} is the zero plane displacement height, and κ is the von Kármán constant. Equation 1.14 can be simplified by assuming that $g_H \equiv g_a$, and so becomes:

$$\lambda E_s = \frac{\Delta(R_n - G) + \rho_a c_p D_v g_a}{\Delta + \gamma} \tag{1.16}$$

This results in an equation that can be used to calculate the rate of evaporation of water from a wet surface using meteorological inputs of light, humidity, temperature and wind speed and is the universal method for calculating evaporation from a wet surface.

[3] A full derivation of the Equation 1.14 may be found in Penman (1948)

[4] $\gamma = c_p P_a/[\lambda(M_w/Ma)]$, where P_a is the atmospheric pressure at sea level, M_w is the molecular mass of water, and M_a is the molecular mass of air.

1.3.4 The Penman-Monteith equation

The model for wet surface evaporation developed by Penman (1948), was subsequently modified by Monteith (1965) to incorporate the biological mechanism of the stomata. Monteith represented the evaporating surface as a single *big leaf*, adding stomatal conductance to the mass transfer component in Equation 1.20. This was done by expressing the transfer of water vapour (g_v) to be through the stomata *and* the boundary layer ($g_v = g_a + g_s$), and again assuming that $g_a \equiv g_H$:

$$\gamma \left(\frac{g_H}{g_v} \right) = \gamma \left(\frac{g_a}{g_a + g_s} \right) = \gamma \left(1 + \frac{g_a}{g_s} \right) \tag{1.17}$$

and so Equation 1.14 is re-expressed to describe the transpiration from a vegetative surface as:

$$\lambda E_t = \frac{\Delta(R_n - G) + \rho_w c_p D_v g_a}{\Delta + \gamma(1 + g_a/g_s)} \tag{1.18}$$

This *big leaf* model is commonly referred to as the Penman-Monteith (PM) equation, and is such a versatile model that it has been successfully applied to crops (Moreno et al., 1996; Yunusa et al., 2000; Rouphael and Colla, 2004; Rana et al., 2005) and forests (Debruin and Holtslag, 1982; Gash et al., 1989; Kelliher et al., 1993; Granier et al., 2000; Leuning et al., 2008).

The PM equation additionally allows E_t to be calculated based on the ratio of g_s and g_a which is a measure of the coupling between the surface and the atmosphere (Jarvis and McNaughton, 1986). Forests are strongly coupled to the atmosphere above and are aerodynamically efficient in turbulent transport (Zhang et al., 1998). As a result, transpiration from a forest canopy is predominantly driven by D_v and g_s. Where $g_a \gg g_s$, the flow of water vapour is:

$$\lambda E_t = \frac{\rho_a c_p D_v g_s}{\gamma} \tag{1.19}$$

For short grass and crops, E_t is determined principally by R_n and g_a, and so is limited only by the atmospheric demand for water. Consequently, for a wet surface such that $g_a \ll g_s$, then the flow of water vapour is described by:

$$\lambda E_t = \frac{\Delta(R_n - G)}{\Delta + \gamma} \tag{1.20}$$

1.3.5 Methods for estimating canopy conductance

1.3.5.1 The Jarvis-Stewart model

Although the PM equation is a successful means of determining E_t, it still requires knowledge of g_s; information that is not easily attainable over the long-term, when compared with other (meteorological) inputs. Consequently, many formulations that try to quantify g_s have been developed over the past 40 years, but the most commonly used of these is an empirical method developed by Jarvis (1976). Jarvis used a set of laboratory controlled experiments, to determine the relationship between g_s and the environmental variables that limit it. Jarvis found that he could describe g_s as a function of R_s, T_a, the specific humidity deficit (H_s), atmospheric CO_2 concentration (C_a) and leaf water potential (Ψ_l), and that g_s is proportional to the joint multivariate response of these variables. Thus, Jarvis gave an empirical formulae that described this, and is given as:

$$g_s = g_{s,max} \prod_{i=1}^{M} f(X_i) \quad \forall \quad X = \{R_s, H_s, T_a, C_a, \Psi_l \dots M\} \tag{1.21}$$

where $g_{s,max}$ is the maximum stomatal conductance parameter, that is proportionally modified by the product of a set of cost functions $f(X_i)$ that describe the relationship between g_s and the environment. The array X, is the set of environmental variables described above that influence g_s; describing a five-dimensional response surface with the possibility of other dimensions, M. This allows g_s to be reduced from an idealised level (that relates to non-limiting conditions, i.e. adequate R_s, θ_s, etc), to an *actualised* level. Although the variables in X are known to affect g_s, long-term measurements of quantities such as Ψ_l are not easily acquired for use in the PM equation.

Stewart (1988) used the empirical method of Jarvis, but standardised g_s to be predominantly driven by R_s, H_s, T_a and the moisture deficit of the soil ($\delta\theta_s$), and removing the effects of C_a and Ψ_l The relationship of C_a was removed as this quantity is found to be generally static across a wide range of environmental conditions. $\delta\theta_s$ replaced Ψ_l, as this quantity was more readily available and still related the response of g_s under a water-limiting environment. Additionally, Stewart described the role of vegetation in the

transpiration process to be at the canopy level. A bulk canopy conductance (g_c) is described by the product between g_s and the LAI, so that $g_c = g_s LAI$. The resulting form of Stewart's model is therefore given as:

$$g_c = g_{c,max} f_1(R_s) f_2(H_s) f_3(T_a) f_4(\delta\theta_s) \tag{1.22}$$

where $g_{c,max}$ is a bulk canopy conductance that is modified by four cost functions ($f_{i=1...4}$) that describe the monotonic relationships between g_c and its abiotic drivers. Although not given here, the function forms of Equation 1.22 are described in detail in Chapter 2 and 3. The empirical model above is termed as the Jarvis-Stewart (JS) model, and is a very robust method for determining g_c that has been widely used in the PM equation over the past 20 years for European pine (Gash et al., 1989; Granier and Loustau, 1994), poplar (Zhang et al., 1997), beech (Granier et al., 2000) and Douglas-fir forests (Bosveld and Bouten, 2001), Amazonian pastures (Wright et al., 1995) and tropical rainforests (Dolman et al., 1991; Sommer et al., 2002; Harris et al., 2004), native Japanese plantation forests (Komatsu et al., 2006a,b), and Australian eucalyptus forests (Whitley et al., 2009). Additionally, Equation 1.22 has since been modified by other authors (Wright et al., 1995; Kelliher et al., 1995; Sommer et al., 2002) to use D_v rather than H_s, and different measures soil moisture content (θ_s).

1.3.5.2 The Tardieu-Davies model

Although the JS model provides an effective way of estimating g_c based on the ambient environmental conditions, other methods are available that relate more strongly with the plant's physiology. Past studies such as those of Hartung (1983), Wartinger et al. (1990), Tardieu and Davies (1992) and Zhang and Davies (1990, 1991), have used soil drying experiments to investigate stomatal control by chemical signalling through abscisic acid (ABA), a plant hormone that is synthesised by dehydrating roots and leaves. The authors found that variations in ABA concentration in the xylem sap ([ABA]) were strongly correlated with g_s. The generation of ABA by the roots creates a long-distance signal that communicates θ_s to the leaf. ABA travels with the transpiration stream, to eventually reach the guard cells of the stomata whereby it causes an increase in the osmotic potential

of guard cells and causes the stomata to close (Wilkinson and Davies, 2002). Tardieu and Davies (1993) built upon this work by developing a model that set out to describe g_s as a function of both [ABA] and Ψ_l, given as:

$$g_s = g_{s,min} + \alpha_k \exp\{\beta_k[\text{ABA}] \exp(\delta_k \Psi_l)\} \tag{1.23}$$

where $g_{s,min}$ is the minimum stomatal conductance, α_k, β_k and δ_k are fitted parameters, where β_k is the basal sensitivity of [ABA] to stomatal conductance at $\Psi_l = 0$, δ_k describes the increase in stomatal sensitivity to [ABA] as $\Psi_l \to -\infty$, α_k is the difference between the maximum and minimum stomatal conductance, $\alpha_k = g_{s,max} - g_{s,min}$, and [ABA] may be expressed as,

$$[\text{ABA}] = \frac{a_1 \Psi_r}{J_w + b_2} \tag{1.24}$$

where Ψ_r is the root water potential, J_w is the flow of water through the SPAC, and a_1 and b_2 are empirically derived coefficients. Equation 1.23 has since been called the Tardieu-Davies (TD) model and has been applied in hydrological frameworks with the PM model to investigate the drought behaviour of plants (Sage, 1994; Tardieu et al., 1996; Tardieu and Simonneau, 1998), and coupled with photosynthesis models (Dewar, 2002). Although the TD model has been effective in the above studies, there is still some difficulty in applying it due to the needed for data on Ψ_l and Ψ_r which are infrequently measured. It will be shown however in Section 1.4 that the TD model can be a critical component in models of canopy gas-exchange.

1.3.6 Application of the Penman-Monteith equation to remote sensing

As has already been shown, the PM equation has been applied successfully to many ecosystems. However, scaling the PM model to larger spatial and temporal scales has not been widely investigated. This is largely due to to the use of the water balance models mentioned in Section 1.2, when operating at the catchment scale, which avoids the need to define a catchment g_c and complex parameterisations. Although these models can provide estimates of E_T, they over-simplify the processes that are involved in transpiration, and offer no way of separating E_T into the E_t and E_s components. Consequently, attempts

have been made to couple the PM equation to remotely sensed data. This idea behind a remote-sensing Penman-Monteith (denoted as RS-PM) model, is to give the ability to estimate latent energy fluxes that can be partitioned into vegetation and bare surface components, using readily available data from satellite sources. These can then be used for short or long-term reference in developing catchment water balances. The following are three methods that have recently been proposed in the literature, and offer promising applications of an already robust model.

1.3.6.1 The Cleugh model

Cleugh et al. (2007) propose a method of applying the PM equation from $1-2$ km to continental spatial scales using surface meteorology measurements and remotely sensed data. They also suggest a simple model for calculating g_c at these larger scales using the same data.[5] No modifications have been made to the structure of the PM equation, thereby retaining the energy balance constraints that make it a robust model. Because most g_c models, such as those developed by Jarvis (1976), Stewart (1988) and Tardieu and Davies (1993), require re-parameterisation over different sites, their widespread applicability is lacking. However, Cleugh et al. (2007) suggest that LAI, normalised difference vegetation index (NDVI), and the fractional vegetation cover (f_c) are adequate surrogates for g_c. The reasoning behind this is that the development of a vegetated land surface requires adequate θ_s to be available, and changes in θ_s will be reflected in the changes in NDVI (and to a lesser extent of LAI), such that they operate on the same time-scale (Cleugh et al., 2007). Hence, low values of g_c are expected at low values of LAI and low θ_s, while the inverse is also true. Therefore the following model for g_c, based on the assumption that $E_s \ll E_t$, is defined as:

$$g_c = g_{c,min} + c_L \max\{LAI_{min}, f_c LAI_{max}\} \tag{1.25}$$

where c_L is the mean canopy conductance per unit leaf area index, $g_{c,min}$ is the canopy conductance controlling soil evaporation and conductance through the leaf cuticle (generally

[5] Although the authors refer to surface conductance, rather than canopy conductance, both terms are considered synonymous in this study as the authors ignore the effects of soil evaporation.

$g_{s,min} = 0$), and f_c is defined as:

$$f_c = \left(\frac{NDVI - NDVI_{min}}{NDVI_{max} - NDVI_{min}} \right)^2 \tag{1.26}$$

Cleugh et al. (2007) applied this model across two sites and found that the parameter c_L was remarkably similar, despite their different vegetation types and climate. Comparing the PM model using the site-specific and numerical averaged c_L values, showed no difference in the explained variance (74%), suggesting that Equation 1.25 may have broad applicability. Cleugh et al. (2007) additionally showed that for both sites at local spatial scales there was a good agreement between estimates from the RS-PM model and measured data. This model was subsequently applied to data from non-local sources, such as those from the Australian Bureau of Meteorology, and compared against outputs from the RS-PM model using local measurements. Again, the RS-PM was shown to hold up sufficiently well with only a slight decrease in performance, with the explained variance dropping form 74% to 73%. Finally the RS-PM approach was applied to a continental scale, with estimates of E_T comparing well with the climatological averages of evapotranspiration provided by the Australian Bureau of Meteorologys Morton model (Morton, 1983).

1.3.6.2 The Mu model

Following the methodology of Cleugh et al. (2007), Mu et al. (2007) built upon the RS-PM model, with an improved calculation of surface conductance. Cleugh et al. (2007) originally stated that $E_s \ll E_t$, such that Equation 1.25 is only applicable for sites with adequate vegetation ground cover. Additionally, Mu et al. (2007) suggest that a dependence of T_a or D_v on g_c should be included to account for the opening and closing of stomata. The first concern is especially valid when LAI is low and there is a high ratio of E_s to E_t. However, this is only a problem when the soil surface is wet as E_s rapidly declines to zero within a day or two after rain. Ecosystems that have a consistently low LAI are arid and therefore the number of rain days per year is small and so the contribution of E_s to annual E_T is likely to be small (Eagleson, 2002; Eamus et al., 2006b). In order to overcome these issues, Mu et al. (2007) partitioned the calculation of E_T into separate components of E_t and E_s,

and re-formulated the linear surface conductance model by replacing the maximum LAI and f_c term, with temperature and humidity modifiers, such that Equation 1.25 becomes:

$$g_c = L_{AI}\, c_L\, f(T_{a,min}) f(D_v) \tag{1.27}$$

where $f(T_{a,min})$ and $f(D_v)$ are cost functions (much like in the JS model) that limit potential surface conductance by $T_{a,min}$ and D_v respectively (see Mu et al. (2007) for the expansions of these functions). The f_c parameter was then used to allocate the available energy $(R_n - G)$, in Equation 1.18, to the canopy and the soil surface. Additionally, NDVI is replaced in Equation 1.26 with enhanced vegetation index (E_{NI}) for reasons of higher resolution (see Mu et al., 2007). These modifications to Cleugh et al. (2007)'s model is denoted as the Revised RS-PM model. Mu et al. (2007) have shown that the Revised RS-PM model performs better than the RS-PM model, substantially reducing the root mean square error (RMSE) by almost 60%. The revised RS-PM model has also shown a slight decrease in performance when replacing local flux data with non-localised measurements, with explained variance dropping from 76% to 70%. Finally the Revised RS-PM was applied at a global scale, and was found to agree well with MODIS observations.

1.3.6.3 The Leuning model

Leuning et al. (2008), have developed a RS-PM model that can be applied to large-scale analysis, which overcomes some of the short-falls of the two methods of calculating surface conductance given above. Leuning et al. (2008) introduce a new model for g_c that is based on the model proposed by Kelliher et al. (1995) that replaces Equtions 1.25 and 1.27. Additionally a much simpler soil evaporation model than that used by Mu et al. (2007) is incorporated in this model. Given that E_T is the sum of soil and canopy evaporating components, Leuning et al. (2008) have expanded Equation 1.18 to include a E_s component, which assumes that E_s occurs at some fraction (f_S) of the equilibrium rate at the soil surface. Equation 1.18 can therefore be re-expressed as:

$$\lambda E_T = \underbrace{\frac{\epsilon(1 - f_S) + g_a/g_i}{\epsilon + 1 + g_a/g_c}}_{\text{Canopy}} + \underbrace{f_S \frac{\epsilon\tau}{\epsilon + 1}}_{\text{Soil}} \tag{1.28}$$

where $\epsilon = \Delta/\gamma$, τ represents the partitioning of the available energy ($A_e = R_n - G$) into canopy ($\tau = A_{e,c}/A_e$) and soil components ($\tau - 1 = A_{e,s}/A_e$) respectively and is formulated as, $\tau = \exp\{-k_A L_{AI}\}$, where k_A is an extinction coefficient for available energy. The parameter g_i is the climatological conductance as defined by Monteith (1965) and is expressed as, $g_i = A_e D_v/(\rho_a c_p/\gamma)$. The expression for g_c is a modification of that developed by Kelliher et al. (1995), introducing a component that expresses the influence of D_v on g_c, and is given as:

$$g_c = \frac{g_{sx}}{k_Q} \ln\left[\frac{Q_h + Q_{50}}{Q_h \exp(-k_Q L_{AI})}\right]\left[\frac{1}{1 + D_v/D_{50}}\right] \tag{1.29}$$

where, Q_h is the visible radiation at the top of the canopy (approximately 50% of R_s), g_{sx} is the maximum g_s of leaves at the top of the canopy, k_Q is the extinction coefficient for R_s and Q_{50} and D_{50} are the Q_h and D_v at half of the maximum g_s respectively. Leuning et al. (2008) applied their model to 15 flux station sites from around the world. These sites covered a wide range of climates and ecosystems such as deciduous and evergreen forests, corn crops, wetlands, grasslands and woody savannas. For each flux site, Equation 1.28 was parameterised, and then compared with numerically averaged parameters values (excluding g_{sx} and f) over the 15 sites, which resulted in no significant reduction in performance. The model was able to explain variance between $83 - 96\%$ and RMSE range of $0.09 - 0.50$ mm d^{-1} over these 15 sites, showing the robustness of the model in estimating evaporation rates from land surfaces over large spatial and temporal scales.

1.4 Leaf gas-exchange

The previous section has covered the physics of water loss from a leaf's surface and the importance of its role in catchment water balances at various spatial scales. The other important role of vegetation water-use is now discussed in terms of its linked dependence with photosynthesis. The dependence between transpiration and photosynthesis is described by the exchange of water vapour for CO_2 between the canopy and the atmosphere, and is generally termed as *canopy gas-exchange*. Leaf gas-exchange is an important process in the SPAC that describes the net carbon gain by leaves, while restricting the amount of

water lost through transpiration (Figure 1.6). The relative amount of carbon gained per unit water lost, is a function of g_s, which is adjusted through a set of physiological control mechanisms that respond to changing environmental conditions (Nobel, 1999). Although a complete understanding of these physiological mechanisms are still not well understood, the gas-exchange process can be described in terms of a supply and demand regime, that links transpiration and photosynthesis with stomatal control as follows (Figure 1.6).

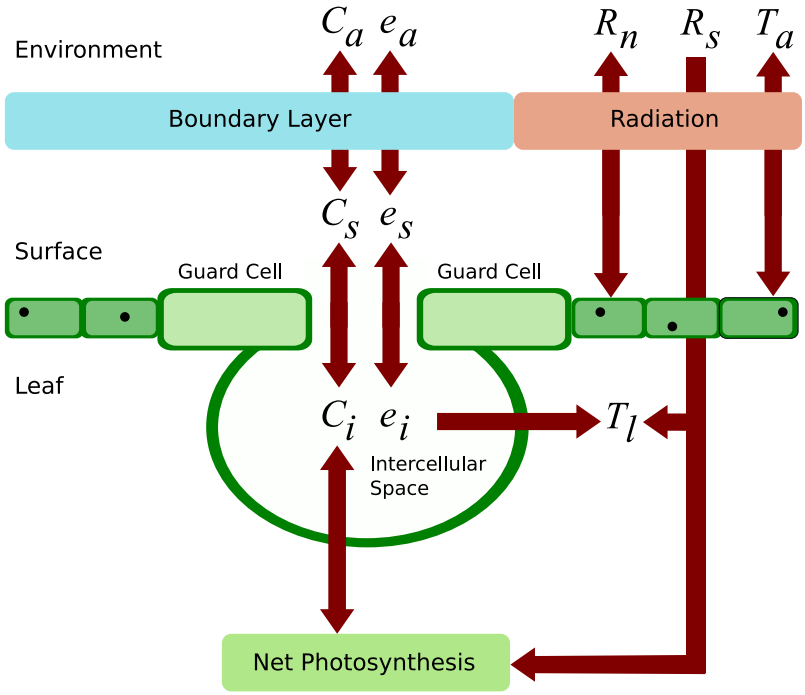

FIGURE 1.6: A schematic representation of a partial cross-section of a leaf, showing the mass and energy fluxes in leaf gas-exchange. Fluxes are shown by the red arrows, where C, e and T stands for the CO_2 concentration, H_2O vapour concentration and temperature respectively. The subscripts a, s and i, refer to properties in ambient air, at the leaf surface and in the intercellular air space of the leaf, respectively. R_n specifies the net radiation input from the sky and R_s represents solar radiation. The diagram is from Collatz et al. (1991)

As the sun rises in the morning, the supply of R_s to the leaf increases and consequently T_a increases and the stomata open. Absorbed energy increase leaf temperature (T_l) and vaporises water, with the vapour moving from the cell walls, to the sub-stomatal cavity, to the leaf surface due to the vapour pressure difference. As water leaves the stomata, Ψ_l drops, creating a potential difference between the leaf and roots, creating a movement of water from the roots to the leaves. As a consequence of open stomata, CO_2 gas is supplied from the atmosphere into the sub-stomatal cavity due to a concentration gradient created

by higher atmospheric concentration at the leaf surface than in the cavity. The CO_2 in the sub-stomatal cavity is then fixed through the process of photosynthesis. Water moves across the boundary layer to the atmosphere assuming adequate turbulent transport (high wind speed). As the day progresses T_a and T_l increase, and so the vapour pressure gradient between the leaf and the atmosphere increases. In some circumstances the supply of water to the leaf can not match the demand for water by the atmosphere. In order to prevent hydraulic failure of the SPAC, partial or complete stomatal closure may occur.

This process of leaf gas-exchange between atmospheric CO_2 and H_2O vapour from the leaf that is well coupled to the atmosphere, can be described by following an Ohm's law analogue.[6] The supply of atmospheric CO_2 needed for assimilation (A_d) by the leaf is given as:

$$A_d = g_{sc}(C_a - C_i) \tag{1.30}$$

where g_{sc} is the stomatal conductance to CO_2 and C_i is the intercellular CO_2 concentration. Similarly, the demand for H_2O by the atmosphere (E_t) is given as:

$$E_t = a_c g_{sc}[e_i(T_l) - e_a(T_a)] \simeq g_s D_v \tag{1.31}$$

where $a_c = 1.6$ and is the relative diffusivity of water vapour to CO_2 in air, such that the stomatal conductance to water is $g_s = a_c g_{sc}$, e_i and e_a are the intercellular and atmospheric water vapour pressures, which are functions of leaf temperature (T_l) and T_a respectively, and the term $e_i(T_l) - e_a(T_a)$ is equivalent to D_v. Additionally, Equation 1.31 can be replaced with Equation 1.18, which includes the effects of the leaf boundary layer, through g_a, and the available energy to the leaf, through R_n.

The net biochemical demand for CO_2 can be described by the C_3 photosynthesis model of Farquhar et al. (1980), which describes the net carbon assimilation of the plant (A_n) as being limited by either biochemical activity or light, such that:

$$A_n = \min\{A_c, A_j\} - R_d \tag{1.32}$$

[6] For the sake of simplicity the boundary layer conductance is assumed sufficiently large, such that the CO_2 concentration and vapour pressure at the leaf surface is equal to that of the atmosphere.

where A_c is the gross rate of assimilation when Ribulose Bisphosphate Carboxylase-Oxygenase (RuBisCO) activity is limiting, A_j is the gross assimilation rate limited by Ribulose Bisphosphate (RuP_2) regeneration when electron transport is limiting, and R_d is the rate of respiration. Both A_c and A_j are described by Michaelis-Menten rate equations and are given as:

$$A_c = V_{cmax} \frac{C_i - \Gamma^*}{C_i + K_m} \tag{1.33}$$

$$A_j = \frac{J}{4} \frac{C_i - \Gamma^*}{C_i + 2\Gamma^*} \tag{1.34}$$

where, V_{cmax} is the maximum rate of RuBisCO activity, Γ^* is the CO_2 compensation point, J is the rate of electron transport and K_m is the Michaelis-Menten coefficient for the carboxylation of RuBisCO. A more in-depth discussion on C_3 as well as C_4 photosynthesis is given in Chapter 4, along with the models that are used to calculate these quantities. Finally, the supply of water to the leaf from the roots of the plant (J_w) is described using the same Ohm's law analogue used to describe Equations 1.30 and 1.31, and is given as:

$$J_w = \frac{\Psi_s - \Psi_l}{R_{soil} + R_{plant}} \tag{1.35}$$

where Ψ_s and Ψ_l are the soil and leaf water potentials respectively (the difference between these is the potential difference), and R_{soil} and R_{plant} are the respective soil and plant resistances to water flow.

Equations 1.30, 1.31, 1.32 and 1.35 give a framework for the exchange of CO_2 and H_2O vapour between the plant and the atmosphere. However, these equations do not give a closed form expression for A_n, that is coupled with g_{sc}, and by extension E_t. In the previous section, the JS model was introduced as a suitable method of expressing g_s, which describes how stomatal aperture can vary under *independent* environmental factors. The problem of using the JS model is that it does not acknowledge the interaction of leaf physiology with g_s. In order for a g_s model to close the above expressions for the supply and demand of CO_2 and H_2O, it must recognise the evolution of stomata in maximising carbon gain while minimising water loss (Cowan, 1977; Cowan and Farquhar, 1977). Work by Wong et al. (1978, 1985a,b,c) has shown that there is a strong correlation between g_{sc} and A_n,

such that $g_{sc} \propto A_n$ under a range of nutrient and CO_2 concentrations, and irradiance and humidity conditions. A number of semi-empirical formulations for g_{sc} have been developed that describe both the strong correlation between g_{sc} and A_n, and their interactions with the environment. Given below are a number of the most important semi-empirical models of g_{sc} and A_n that have been widely cited in the literature.

1.4.1 The Ball-Woodrow-Berry model

Ball et al. (1987) developed a semi-empirical relationship that uses the relation of $g_{sc} \propto A_n$, to be dependent on the effects of humidity and ambient CO_2 concentration, such that g_{sc} may be described as,

$$g_{sc} = g_{s,0} + \frac{a_1 \, A_n \, H_s}{C_a} \tag{1.36}$$

where H_s is relative humidity, and $g_{s,0}$ and a_1 are fitted parameters that are equivalent to the intercept and slope of the relationship between g_s and A_n,[7] where the former is the residual stomatal conductance in the absence of light ($R_s \to 0$) and photosynthesis ($A_n \to 0$), and the latter is a coefficient that describes the relationship $\partial A_n / \partial g_s$. Equation 1.36 predicts that g_{sc} will increase with A_n and H_s assuming that C_a is constant, and predcits a decrease with increasing C_a assuming that $\partial A_n / \partial C_a$ is small (otherwise g_{sc} remains constant). Additionally, environmental effects such as R_s, T_a, etc. are incorporated through A_n which is expressed through Equation 1.32. Equation 1.36 is generally referred to as the Ball-Woodrow-Berry (BWB) model and has been used in many gas-exchange models, from the leaf and canopy scales (Leuning, 1990; Collatz et al., 1991) to landscape and global scales (McMurtrie et al., 1992a,b; Sellers et al., 1992; Baldocchi et al., 2004; Medlyn et al., 2005a).

1.4.2 The Ball-Berry-Leuning model

There are some problems with the formulation of the BWB model described above. Principally, it has no mechanistic basis due to the use of C_a and H_s parameters and also that it is only applicable under well-watered conditions. Mott (1988) has shown definitively

[7] The relationship is actually between g_s and $A_n H_s / C_a$

that stomata respond to C_i rather than C_a. However, the use of C_a may still be justified, so long as the ratio of C_i/C_a remains constant with increasing A_n and changing environmental conditions (Leuning, 1995). Mott and Parkhurst (1991) have additionally shown that stomata respond to E_t, rather than H_s, such that there is a linear dependence between g_{sc} and E_t, and therefore D_v as expressed by Equation 1.31. Leuning (1995) built upon the work of Ball et al. (1987) by modifying the BWB model to address these issues. First, C_a is replaced by the term $(C_a - \Gamma^*)$ where Γ^* is the CO_2 compensation point, which accounts for the behaviour of the stomata at low C_a. Second, H_s is replaced by the hyperbolic function $(1 - D_v/D_0)$ of Lohammer et al. (1980), which Leuning found to give the best results in explaining the variation of g_{sc} and the ratio C_i/C_a with variation in D_v. Finally, an expansion of Leuning's work by Wang and Leuning (1998) incorporated a cost function that allowed the BWB model to operate under changing soil water conditions and enhancing its applicability. The BWB has therefore been modified to express g_{sc} as:

$$g_{sc} = g_{s,0} + \frac{a_1 \, A_n f_w}{(C_a - \Gamma^*)(1 - D_v/D_0)} \tag{1.37}$$

where D_0 is an empirically determined coefficient, and f_w is a monotonic cost function describing the penalty on g_{sc} and A_n as the soil water content moves towards the wilting point (θ_w), and is expressed as:

$$f_w = \min \left\{ 1.0, \; \frac{s_1(\theta_s - \theta_w)}{s_2(\theta_c - \theta_w)} \right\} \tag{1.38}$$

where θ_c is the critical point of θ_s, and s_1 and s_2 are empirically determined coefficients. This modification of the BWB model has since been coined the Ball-Berry-Leuning (BBL) model and has since been widely used to investigate many physiological questions (Buckley et al., 2003; Katul et al., 2003; Tuzet et al., 2003; Misson et al., 2004) and applied to various landscapes (Leuning et al., 1998; van Wijk et al., 2000; Cramer et al., 2001; Novick et al., 2004; Medlyn et al., 2005b; Uddling et al., 2005; Vico and Porporato, 2008). Although the BBL has since largely replaced the use of the BWB model in canopy gas-exchange simulations, it is still applicable, especially for cases where there is little variation in D_v (Medlyn et al., 2005a).

1.4.3 The Dewar model

Dewar (2002) combined the work of Ball et al. (1987), Tardieu and Davies (1993) and Leuning (1995), to reach an expression of g_{sc} that combines the essential features of Equation 1.37 and Equation 1.23 to give a more complete description of stomatal behaviour within a mechanistic framework. Dewar's model therefore describes g_{sc} to be:

$$g_{sc} = \frac{a_1(A_n + R_d)}{C_i(1 - D_v/D_0)} \exp\{\beta_k[\mathrm{ABA}] \exp(\delta_k \Psi_l)\} \tag{1.39}$$

Notable changes are made to the BBL model, the most critical being the replacement of the term $A_n/(C_a - \Gamma^*)$ with $(A_n + R_d)/C_i$, so as to be in line with the findings of Mott (1988), where g_{sc} is regulated by C_i not C_a. Additionally, g_{sc} now responds to D_v through water loss and chemical signalling, via the expressions of $1/(1-D_v/D_0)$ and $\delta_k \Psi_l$. This model, has since been applied by Verbeeck et al. (2007) into the Analysis of Forest Ecosystems (ANAFORE) model in estimating stored water-use of Scots pine. Although largely unchanged, Verbeeck et al. reintroduced the $g_{s,0}$ parameter to the BBL component of Equation 1.39, so as to include the effects of night-time transpiration.

1.4.4 The Cowan and Farquhar optimisation hypothesis

The physiological models of stomatal conductance described above, predominantly define the environmental regulation of stomata; that is, variations in ambient climatic forcing dictate the degree of stomatal opening. The degree of opening can, however, be expressed in terms of the regulatory role rather than one of response. This means that instead of determining the degree of opening via the local environmental conditions, aperture can be determined through a consideration of a *cost-benefit* scheme, where the plant is hypothesised to operate in terms of a water-carbon economy. Although the models that have been described so far in this section operate under such a regime, they still rely on environmental forcing to determine g_s. Cowan (1977) and Cowan and Farquhar (1977) established that stomatal opening is *optimised* so that the carbon gained for photosynthesis is maximised while water lost through transpiration is minimised. Consequently, Cowan and Farquhar (1977) expressed that over some arbitrary period of time ($t_1 \rightarrow t_2$), the total

water lost for carbon gained by the plant can be expressed as:

$$\int_{t_1}^{t_2} A_n(t) - \lambda_{cw} E_t(t) \; dt = 0 \tag{1.40}$$

where λ_{cw} is a non-physical *cost of water* parameter, that dictates the optimal unit amount of carbon gained per unit water lost.[8] Although a non-physical parameter, λ_{cw} can be thought of in terms of a plant's water-use efficiency (WUE), which can be expressed as:

$$\lambda_{cw} = \frac{\partial A_n / \partial g_{sc}}{\partial E_t / \partial g_{sc}} \tag{1.41}$$

Equation 1.40 can be expressed in terms of an objective function:

$$f_{\min}(g_{sc}) = A_n(g_{sc}) - \lambda_{cw} E_t(g_{sc}) \tag{1.42}$$

where the value of λ_{cw} is optimal when $f_{\min}(g_{sc}) = 0$. This expression allows stomatal closure to be described due to the excessive water loss (increasing E_t), following the observations of Mott and Parkhurst (1991). Equation 1.42 can be expanded to include the Equations 1.30, 1.31 and 1.32, that make up the gas-exchange framework, discussed at the beginning of this section. The relative amount of carbon gained is expressed by solving Equations 1.30 and 1.32 for steady-state conditions and eliminating C_i as a *nuisance* parameter, such that:

$$A_n(g_{sc}) = \frac{4g_{sc}(C_a - 2\Gamma^*) + J_e - \sqrt{[4g_{sc}(C_a - 2\Gamma^*) + J_e]^2 - 16 g_{sc} J_e (C_a + \Gamma^*)}}{8} \tag{1.43}$$

[8] Cowan and Farquhar (1977) use the inverse of this parameter, i.e. unit of water lost per unit of carbon gained.

and the water lost can be described by using Equation 1.31. Therefore the objective function that describes the balance between carbon gained and water lost is expressed as:

$$\begin{aligned} f_{\min}(g_{sc}) = & \frac{g_{sc}(C_a - 2\Gamma^*)}{2} + \frac{J_e}{8} \\ & - \frac{\sqrt{[4g_{sc}(C_a - 2\Gamma^*) + J_e]^2 - 16g_{sc}J_e(C_a + \Gamma^*)}}{8} \\ & - \lambda_{cw} a_c g_{sc} D_v \end{aligned} \tag{1.44}$$

The λ_{cw} that maximises the above expression, can be determined by taking the partial derivative of Equation 1.44 with respect to g_s:

$$\frac{\partial f_{\min}(g_{sc})}{\partial g_{sc}} = \frac{C_a}{2} - \Gamma^* - \frac{2g_s(C_a - 2\Gamma^*)^2 - J(C_a - \Gamma^*)}{\sqrt{16g_s^2(C_a - \Gamma^*)^2 - 16Jg_s(C_a - \Gamma^*)}} - \lambda_{cw} a_c D_v \tag{1.45}$$

and by rearranging Equation 1.45 in terms of g_{sc} for $\partial f_{\min}(g_{sc})/\partial g_{sc} = 0$ gives an expression for the optimal g_{sc} at a given value of λ_{cw}:

$$g_{sc} = \frac{J(2C_a - 2\Gamma^*) - (2\lambda_{cw} a_c D_v - C_a + 2\Gamma^*)\sqrt{16g_s^2(C_a - 2\Gamma^*)^2 - 16g_s J(C_a - \Gamma^*)}}{4(C_a - 2\Gamma^*)^2} \tag{1.46}$$

The framework above developed by Cowan and Farquhar, is generally referred to as the stomatal optimisation (SO) model, although the word *optimisation* is a misnomer, as λ_{cw} defines the level at which A_n and E_t operate constantly rather than a level that is optimal. Additionally λ_{cw} has no physical basis in reality and must be empirically determined for the model to work, and is perhaps the reason as to why the SO model has not been incorporated into global climate models (GCM). However, several studies have used the SO model to investigate physiological questions on stomata (Hari et al., 1986; Mäkelä et al., 1996), and against field data (Berninger and Hari, 1993; Berninger et al., 1996; Hari et al., 1999; Thomas et al., 1999a,b; Thum et al., 2007; Schymanski et al., 2007, 2008b,a, 2009; Katul et al., 2010).

1.5 A Soil-Plant-Atmosphere continuum model

The preceding sections have given examples of model frameworks that are used in investigating ecosystem water balance and canopy gas-exchange. We now look at a model that uses the above theories to simulate the SPAC. The Soil-Plant-Atmosphere (SPA) model of Williams et al. (1996a) is a process-based model that simulates ecosystem photosynthesis and water balance at fine temporal and spatial scales. The model is written in FORTRAN and is freely available for download (http://www.geos.ed.ac.uk/homes/mwilliam/spa.html). The SPA model focuses on canopy processes, and explores links between leaf-level water loss, leaf and soil water status, and water fluxes from the soil through the plant. Additionally, it simulates surface energy and water balance, heat and water transport and root water uptake, and the interception and evaporation of intercepted rainfall (Williams et al., 2001c). The model framework partitions the forest canopy and soil-root system into 10 layers each respectively (the number of layers can be increased by the user), and operates on a 30 minute time-step (Figure 1.7).[9] The 10 canopy layers describe the vertical variation in light interception, leaf area, distribution of foliar nitrogen, and the rates of photosynthesis and transpiration. Light interception through the canopy is handled by a comprehensive radiative transfer scheme, whereby the canopy is divided into sunlit and shaded foliage (Williams et al., 2001a). The 10 layers of the soil profile describe the rooting depth, distribution of root biomass, hydraulic properties (particle size distribution, hydraulic conductivity, etc), water content and temperature (Williams et al., 2001c). The entire framework of the SPA model is too extensive to cover here, so only the gas-exchange process will be briefly covered, while the canopy light-interception and soil water balance theory may be referred to in Williams et al. (2001a) and Williams et al. (2001c) respectively; SPA's gas-exchange framework is given more extensively in Chapters 4 and 5 of this thesis.

What differentiates the SPA model from other models, is its unique method of simulating canopy gas-exchange. In their work, Williams et al. (1996a) developed a similar method to that of Cowan and Farquhar (1977), whereby gross carbon gain is maximised by maximising stomatal conductance, but independent of the water-use needed to reach this level

[9] The time-step may be changed according to the user's preference.

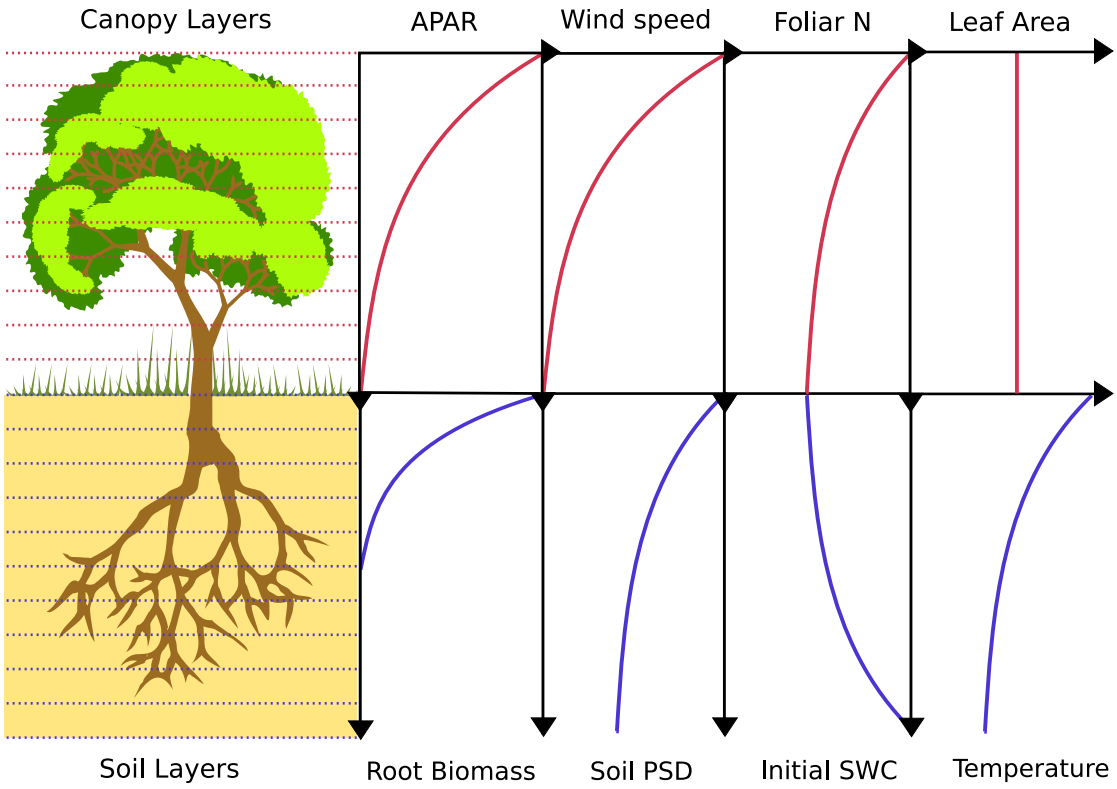

FIGURE 1.7: The soil-plant-atmosphere model partitions the forest canopy and below-ground root system into 10 layers each respectively. The canopy layers describes the vertical distributions in sunlit and shaded leaf area, distribution of foliar nitrogen (N), absorbed photosynthetically active radiation (APAR) and the rate of photosynthesis and transpiration. The soil layers describe below-ground energy and water balance, as well as root distribution and hydraulic properties, such as the initial soil water content (SWC) and the particle size distribution (PSD) of the soil (percentage of sand and clay).

of productivity. Williams et al. (1996a) explain their model in terms of the efficiency of carbon uptake, whereby the leaf will increase g_s incrementally and thereby A_n, until such a point that any further increase in g_s does not result in an appreciable increase in A_n. This conceptually ignores the increase in E_t, such that the plant operates to spend the extra water needed to gain that fraction more of carbon. This process may be formulated as:

$$\iota_{op} = \frac{\delta A_n}{\delta g_{sc}} = A_n(g_{sc,t_2}) - A_n(g_{sc,t_1}) \tag{1.47}$$

where ι_{op} is the operating or efficiency point, which defines the degree of stomatal opening of the plant under well-watered conditions. For the instance where soil water availability becomes limiting there is a hydrological limit on the leaf water status, through Ψ_l, that stops g_{sc} reaching ι_{op} in order to prevent xylem embolism. As g_{sc} increases, Ψ_l will drop

due to an increase in E_t, following the formulation of Equation 1.35. If Ψ_l falls to the critical threshold at which xylem cavitation occurs ($\Psi_{l,min}$) then the stomata will shut in order to prevent a critical failure of the hydraulic architecture. The effect of increasing g_{sc} on $d\Psi_l/dt$ is described by:

$$\frac{d\Psi}{dt} = \frac{\Psi_s - \Psi_l - E_t R_{a,b}}{C_l R_{a,b}} \tag{1.48}$$

where Ψ_s is the soil water potential, $R_{a,b}$ is the total below-ground resistance to water flow and C_l is the leaf capacitance. This formulation links the gas-exchange component of the SPA model with the hydraulic architecture and prevents excessive water loss by the simulated canopy. Additionally, this gives an extra constraint in the optimisation such that a plant will increase g_{sc} incrementally while $\Psi_l > \Psi_{l,min}$.

This stomatal optimisation theory has been incorporated into the SPA model of Williams et al. (1996a) and successfully used it to describe water and carbon relations for a number of ecosystems such as an Amazonian rainforest (Williams et al., 1998; Fisher et al., 2006, 2007), Arctic tundra (Williams et al., 2000, 2001c, 2004), temperate ponderosa pine (Law et al., 2000; Williams et al., 2001a,b), boreal (Hill et al., 2008), oak (Engel et al., 2002; Hernandez-Santana et al., 2009) and an Australian Eucalypt forest (Zeppel et al., 2008a) and tropical savanna (Chapter 4). The SPA model has also been tested by Misson et al. (2004) against the JS and BBL models and show to perform equally well, and has been incorporated into the global climate model (GCM), the Joint U. K. Land Environmental Simulator (JULES) (Alton et al., 2009).

1.6 Work to be presented in this thesis

Having covered the background theory on surface evaporation and the exchange of water vapour and CO_2 between the atmosphere and the canopy, a set of questions are raised which this thesis will attempt to address. These questions have been developed from some of the common issues of modelling water and carbon fluxes from a forest canopy. The first issue is whether a simple model (as opposed to a highly complex one) can be used to determine canopy water fluxes without the need for a large number of inputs and detailed

descriptions of a site. The second issue is, given a highly complex LSM such as the SPA model, how is it limited in its application to some ecosystems such as tropical savannas. Additionally, is the modelled description of leaf gas-exchange in the SPA model correct? Below are listed the four questions that encompass this thesis, as well as a description on how each chapter will attempt to address these questions.

Question 1:

> *"Can water fluxes from a canopy be estimated using a simple empirical model without the need for canopy conductance?"*

The current and ongoing issue with using the PM equation is that it requires a formulation of g_c in order to derive an estimate of canopy water-use (E_c). Although the JS and TD models offer a means of estimating g_c and have been highly successful in their own right, they still require specific calibration to site-derived data in order to be used. Chapter 2 will therefore describe the conceptualisation of a simple empirical model of E_c that removes the need for g_c as an input. This model, a modified Jarvis-Stewart (MJS) model, will follow a Jarvis-type structure, whereby a measure of the maximum rate of canopy water-use is proportionally modified by a set of empirical relationships; these relationship being based on the multivariate response of E_c to R_s, D_v and θ_s. The performance of this model will be compared against the PM equation and a statistical benchmark created using an artificial neural network (ANN).

Question 2:

> *"Can a simple empirical model of canopy water-use be applied across multiple sites without the need for site-specific calibration?"*

Following on from Question 1, Chapter 3 will look at the applicability of the MJS model across five disparate Australian woodland sites. This will involve a calibration of the model to each site individually and then to all sites simultaneously, with the aim being to determine a set of *site-specific* and *site-average* parameters that can be used in the model

to derive estimates of E_c at each site. The idea of this approach is to see how sensitive the model is to variation in the value of the model parameters and whether or not an set of *site-average* parameters can give reasonable predictions of site E_c. If a set of *site-average* parameters do not result in a decline in model performance, then this will remove the need to calibrate the model at each site and reduce the amount of required information to run the model.

Question 3:

> *"Can the Soil-Plant-Atmosphere model be used replicate canopy gas-exchange for a Australian tropical savanna?"*

A distinct limitation of the SPA model is that it only considers C_3 photosynthetic processes (Appendix A). Although this is not a problem for many temperate landscapes, tropical savannas (an important global biome) are dominated by C_4 grasses that make significant contributions to ecosystem biomass (Hutley et al., 2000; Chen et al., 2002, 2003; Kanniah et al., 2010a). Chapter 4, details the incorporation of C_4 photosynthesis into the SPA model necessary in extending its applicability towards tropical savannas. The reasoning behind using savannas as the test-bed for this exercise is as that they are a dominant ecosystem globally and consequently they influence regional and global carbon budgets extensively. Despite this, savannas have not been extensively modelled in the literature, and there is a major gap in savanna research; especially as most models do not include a C_4 photosynthesis model. This will involve the testing of two C_4 photosynthesis sub-models as well as the parameterisation of the SPA model to a savanna site. The consequence of this will provide a way of investigating the contribution of C_4 vegetation to total savanna ET and gross primary productivity (GPP). Additionally, the question of what drives the seasonality of ET and GPP in a savanna will be investigated.

Question 4:

> *"Can the leaf gas-exchange process in the SPA model be improved so as to maximise carbon gain while simultaneously minimising water loss from the leaf*

following the Cowan and Farquhar optimality hypothesis?"

The current framework of the leaf gas-exchange process in SPA works towards maximising A_n by increasing g_s; that is, g_s is increased until there is no appreciable increase in A_n. This representation of leaf gas-exchange, causes the SPA model to transpire copious amounts of water in order to gain an infinitesimal amount of carbon. This process ignores the *"optimality hypothesis"* of Cowan and Farquhar (1977) who state that the leaf must maintain some balance between the water lost from the leaf and the carbon gained by the leaf. Chapter 5, describes a possible solution to this problem by introducing the limitation of E_t on gas-exchange into Equation 1.47 following the *optimality hypothesis* (Cowan and Farquhar, 1977). This modification to the SPA model will be tested over a 30 day drying period, in order to observe any benefits of this modification and to highlight the effects of soil drying on leaf gas-exchange. The goal of this chapter will be to determine whether or not the SPA model responds correctly to drought.

Chapter 2

Comparing the Penman-Monteith equation and a modified Jarvis-Stewart model with an artificial neural network to estimate stand-scale transpiration

The work presented in this chapter was first conceptualised, peer reviewed and published in a special edition of Plant and Soil, volume 305 (2008), pages 35-47. This work was then further extended, peer reviewed and published in the Journal of Hydrology, volume 373 (2009), pages 256-266. I acknowledge that the work presented here is my own, and that any involvement by other persons has been duly acknowledged in the text. The publication Whitley et al. (2009) has therefore been incorporated almost verbatim as a chapter in this thesis. Specifically, I acknowledge that all the field data used in this chapter were collected by Zeppel et al. as described in Zeppel et al. (2004)

2.1 Introduction

Measuring tree water-use is an important step in determining the water balance of woody landscapes (Komatsu et al., 2006a; Wullschleger and Hanson, 2006; Rollenbeck and Dieter, 2007; Simonin et al., 2007) and determining landscape water balances is important to forestry and mining industries, to water and landscape management agencies and the land-atmosphere modelling community. Whilst estimating tree water-use can be undertaken using sapflow technologies (O'Grady et al., 1999; O'Grady, 2006), such measurements are made at the scale of individual trees, usually over relatively short time frames (days and weeks) and typically only during the growing season (Wullschleger et al., 1998; Lundbald and Lindroth, 2002). However, to obtain the required annual estimates of stand transpiration rates, up-scaling spatially and temporally is required; even when there is continual monitoring of a few trees at a site. Whilst eddy covariance (EC) measurements of stand water-use give integrated measures of vegetation water-use (Hutley et al., 2000; Eamus et al., 2001; Ewers et al., 2007), EC is expensive, technically challenging and requires large, flat homogenous landscapes. Key end-users who require annual estimates of vegetation water-use (including mine-site managers, catchment management authorities and water resource managers) require a methodology that is sufficiently robust to be useful, but not too resource (time, equipment, data) intensive and one that is applicable to uneven terrain or small plots. An application of a simplified model of vegetation water-use, as applied to management of groundwater dependent ecosystems, can be found in Howe et al. (2005).

Water flux through trees is a principal pathway for the discharge of soil water. Consequently, to determine the water budget of woody landscapes, tree canopy water fluxes must be known, either through direct measurement or through modelling (Komatsu et al., 2006a; Wullschleger and Hanson, 2006; Rollenbeck and Dieter, 2007; Simonin et al., 2007). Stomatal conductance (g_s), solar radiation (R_s), vapour pressure deficit (D_v) and soil moisture content (θ_s) are the major determinants of tree water fluxes (Jarvis and McNaughton, 1986; Wullschleger et al., 2001; Zeppel, 2006; Zeppel and Eamus, 2008; Zeppel et al., 2008b) and seasonal variations in these three abiotic variables cause seasonal variation of canopy conductance (g_c) and canopy transpiration (E_c) (Harris et al., 2004; Komatsu

et al., 2006b). Measuring seasonal variations of these abiotic variables and parameterising their impact is important for quantifying intra-annual variation in g_c and E_c.

The Penman-Monteith (PM) equation (Monteith, 1965) is commonly used to estimate evapotranspiration of crops (Yunusa et al., 2000; Lu et al., 2003) and forests (Gash et al., 1989; Kosugi et al., 2007; Zeppel and Eamus, 2008). In the past two decades the PM equation has been simplified by assuming forest canopies are highly coupled to the atmosphere (Granier et al., 1996b; Whitehead, 1998; Granier et al., 2000; Ewers et al., 2007). The base assumption is that transpiration (E_t) is controlled by stomatal resistance to water flow (r_s; the inverse of g_s) in response to meteorological forcing and assuming that atmospheric resistance (r_a) in the soil-plant-atmosphere pathway is very low ($r_s \gg r_a$). The rate of water loss from the surface of a leaf is calculated as:

$$\begin{aligned} E_t &= g_s(e_s - e_a) \\ &= g_s D_v \end{aligned} \tag{2.1}$$

where e_s and e_a are the vapour pressures at saturation and in the air, such that $D_v = e_s - e_a$. Water lost from the leaf, can then be scaled up to the water lost from the surface of the forest canopy by multiplying the right-hand side of Equation 2.1 by the leaf area index (LAI) (Whitehead, 1998), such that:

$$\begin{aligned} E_c &= LAI \cdot g_s D_v \\ &= g_c D_v \end{aligned} \tag{2.2}$$

The regulation of g_c and E_c has received extensive investigation (Jarvis, 1976; Stewart, 1988; Granier and Loustau, 1994; Harris et al., 2004; Komatsu et al., 2006b). Such studies use measured values of sap-flow or EC and an inversion of the PM equation to derive measurements of g_c. In most applications of the PM equation, a Jarvis-type model (Jarvis, 1976; Stewart, 1988) is used to quantify g_c via set of seasonal response terms, describing the functional relationships relating to R_s, D_v and θ. This approach has been applied over the past 30 years to various stands comprised of different species, such as temperate poplar, maritime pine, oak, spruce and pine forests (Gash et al., 1989; Dolman et al., 1991;

Ogink-Hendriks, 1995; Wright et al., 1995; Zhang et al., 1997; Lagergren and Lindroth, 2002; Sommer et al., 2002), Amazonian pastures and rainforests (Harris et al., 2004) and Japanese conifer forests (Komatsu et al., 2006a,b). Parameterisation of a Jarvis-type model over an annual cycle for Australian native woodlands and forests has not yet been conducted. Responses of g_s and E_t to D_v have been investigated for northern Australian savannas by Thomas and Eamus (1999); Thomas et al. (2000) and Eamus and Shanahan (2002) and soil moisture responses of E_c and g_c have been investigated (Hutley et al., 2001; Zeppel and Eamus, 2008; Zeppel et al., 2008b).

Jarvis-type models have been used extensively because of their simplicity and they allow calculation of g_c as a function of meteorological variables and soil water availability. However, one problem in applying Jarvis-type models is the requirement for a large degree of spatial and temporal replication in g_c and subsequent use of the PM equation in order to calculate E_c. Consequently, the frequent problem of having to quantify g_c poses difficulties in readily applying the PM equation. Furthermore, the PM equation is known to predict E_c poorly under limiting soil moisture conditions and it may correlate with observations best when E_c is large (David et al., 1997; Rana et al., 2005). In order to overcome this problem, the work contained herein describes a relatively simple empirical model whereby scaled estimates of E_c can be made from readily available meteorological measurements (R_s, D_v and θ_s) without the need to measure g_c. This model is conceptualised on the empirical framework of Jarvis (1976) and Stewart (1988) and in reference to this it has been coined as the modified Jarvis-Stewart (MJS) model. Additionally, this model is compared against the PM equation, with the performance of both models (MJS and PM) being tested against a statistical benchmark, which has been created using an artificial neural network (ANN). Finally, the results are compared with those found in previous studies to show the spatial variability of models parameterised over different sites and ecosystems.

2.2 Methods

2.2.1 Site description

A remnant open woodland site located approximately 70 km south of Tamworth, in north-western NSW (31.5°S, 150.7°E, elevation 390 m), was used in this study. A full description of the site is provided in Zeppel et al. (2004) and Zeppel and Eamus (2008). In summary, the average height of the trees was 15 m and is dominated by *Eucalyptus crebra* and *Callitris glaucophylla*. These two species contributed approximately 75 % of the tree basal area at the site. Total tree basal area was 23.8 ± 3.4 m^2 ha^{-1}. The eucalypts had a lower density than the *Callitris* (42 stems ha^{-1} compared to 212 stem ha^{-1}) but contributed most (approximately 75 %) to the basal area of the two species combined because its average diameter was much larger than that of the *Callitris*. The understorey was dominated by grasses, predominantly *Stipa* and *Aristada* species. Soils at the site were shallow with well-drained acid lithic bleached earthy sands (Banks, 1998) with occasional exposed sandstone.

Incoming solar radiation and wet and dry bulb temperature were measured at hourly intervals at a weather station located in a cleared pasture ($>$ 4 ha) approximately 100 m from the remnant woodland. Wind speed was measured with a cup anemometer situated about 3 m above the canopy and soil moisture was measured with Theta Probes (Delta-T Devices, UK) at 50 cm depth at two locations. LAI was measured at seven locations in the woodland, as previously described (Zeppel, 2006) using a Li-Cor 2000 Plant Canopy Analyser, four times during the year of study (2004). LAI ranged from 0.9 to 1.0 on these four occasions (data not shown).

2.2.2 Water use by individual trees

The rate of water-use by individual trees (L d^{-1}) was measured by Zeppel et al. (2004) at 15 minute intervals using sap-flow sensors (model SF100, Greenspan Technology, Pty Ltd, Warwick, Australia). For each species 10-12 trees were chosen to sample the full range of tree sizes and each tree was instrumented with 4 sensors. Sensors were stratified with

depth (at 1/3 and 2/3 of the depth) through the sapwood (Medhurst et al., 2002; Zeppel et al., 2004). sap-flows were corrected for wound effects, sapwood area, radial variability in flow and volumetric fractions of water and wood (Zeppel et al., 2004). Wound width was measured for both sensor sets in each of seven trees of both species at the end of the sampling period, following the method of O'Grady et al. (1999). A wound width of 2.5 mm for *C. glaucophylla* and 3.7 mm for *E. crebra* was used to correct velocity estimates. Basal area and diameter at breast height (DBH) of all trees were measured in 7 replicate 50 m x 50 m plots (Zeppel et al., 2004).

2.2.3 Scaling to stand transpiration

Scaling from individual trees to stand transpiration was done by multiplying the average hourly sap velocity (V_{sap}) by the sapwood area per unit ground area (A_{sap}); further details of this can be found in Zeppel et al. (2004) and Whitley et al. (2008). $A_{S\,plot}$ was calculated from measurements of sapwood depth for both tree species and from plot-level measurements of the stand. Each 24 hour period was summed to give the daily sap flux (cm^3 $plot^{-1}$ d^{-1}). The water-use (cm^3 H_2O $plot^{-1}$ d^{-1}) of each plot (with an area of 2500 m^2) was converted to the stand scale (mm^3 H_2O mm^{-2} ground area [GA] d^{-1}). The DBH of all trees in 7 replicate plots was measured and therefore there were 7 estimates of stand water-use (cm^3 sapflux cm^{-2} GA d^{-1}) for each day. The mean and standard error of all 7 plots, for each day, was then estimated, and converted from cm^3 H_2O cm^{-2} GA d^{-1} to yield stand water-use (E_c, mm hr^{-1}).

2.2.4 Models

The goals for this analysis were threefold. First, to parameterise two transpiration models in order to derive a set of seasonal response terms describing the responses of E_c and g_c to changes in their driving environmental variables. Second, to compare estimates of modelled E_c made via an empirical model (Whitley et al., 2008) with those made from the PM equation. Finally, to quantify the performance of these models statistically by comparing model outputs, against that of an artificial neural network (ANN). I now outline the two models used in this study and then describe the ANN applied to the data.

2.2.4.1 The Penman-Monteith model

The PM equation calculates the latent energy lost from the canopy as:

$$\lambda E_c = \frac{\Delta R_n + \rho_a c_p D_v g_a}{\Delta + \gamma(1 + g_a/g_c)} \tag{2.3}$$

where Δ is the slope of the relationship between the saturation vapour pressure and temperature (kPa $^{\circ}C^{-1}$), ρ_a is the air density (1.204 kg m^{-3} @ 20°C), c_p is the specific heat of air (1.013 MJ kg^{-1} $^{\circ}C^{-1}$), γ is the psychometric constant (0.066 kPa $^{\circ}C^{-1}$), λ is the latent heat of vaporisation (2.39 MJ kg^{-1}), R_n is the net radiation above the forest canopy (MJ m^{-2} hr^{-1}; converted from W m^{-2}) and is calculated from R_s using an expression from Eagleson (2002) given as:

$$R_n = R_s(1 - \alpha) - 57.65 \tag{2.4}$$

where α is the albedo of the earth's surface (≈ 0.2) and 57.65 represents a constant level of longwave radiation (W m^{-2}). Lastly, g_a is the aerodynamic conductance (m s^{-1}) and is estimated from:

$$g_a = \frac{(1 + 0.54U)}{4.72 \ln(Z/Z_0)^2} \tag{2.5}$$

where U is the wind speed above the canopy (m s^{-1}), Z is the height of the forest canopy (m) and Z_0 is the roughness length for the forest type (1.95 m for this forest type; from Zeppel et al. (2008b)). Using a Jarvis-type model, g_c is expressed empirically as:

$$g_c = g_{c\,max} f_1(R_s) f_2(D_v) f_3(\theta) \tag{2.6}$$

where the functions f_i are a set of scaling terms that reduce $g_{c\,max}$ in response to changes in R_s, D_v and θ; scaling from leaf to canopy level and vice versa is achieved through the LAI term, incorporated via the $g_{c\,max}$ parameter such that $g_{c\,max} = LAI\, g_{s\,max}$. The functions f_i take on values between 0 and 1, proportionally modifying $g_{c\,max}$ to give modelled estimates of g_c[1]. The functional forms for climatic forcing on stomatal aperture used in

[1]It is assumed that the responses to each driving variable are independent (Jarvis, 1976).

this study are taken from Harris et al. (2004), and are expressed as:

$$f_1(R_s) = \left(\frac{R_s}{1000}\right)\left(\frac{1000 + k_1}{R_s + k_1}\right) \tag{2.7}$$

$$f_2(D_v) = \exp(-k_2 D_v) \tag{2.8}$$

$$f_3(\theta) = \min\left\{1,\ \frac{\theta - \theta_w}{\theta_c - \theta_w}\right\} \tag{2.9}$$

where the parameters $g_{c\,max}$, k_1, k_2, θ_w and θ_c are free parameters determined through least-squares optimisation. Equation 2.7 describes the asymptotic response of increasing R_s, with saturation occurring at approximately 1000 W m^{-2} and k_1 (W m^{-2}) describing the curvature of the relationship. Hyperbolic saturating functions describing Rs have been applied extensively at leaf, tree and canopy scales for conductance (Kelliher et al., 1993; Granier et al., 2000) and for tree water-use (Komatsu et al., 2006b). Equation 2.8 describes the exponential decay of g_c due to increasing D_v, where k_2 (kPa) describes the rate of decay. Equation 2.9 shows the soil moisture response to be a piece-wise relationship, where θ_w and θ_c (m^3 m^{-3}) denote the points of inflection in the relationship and can loosely be termed as the wilting and critical points respectively.

In order to parameterise Equation 2.6, an inversion of the PM equation was solved in order to derive measurements for g_c (mm s^{-1}) and is given as:

$$g_c = \frac{\gamma \lambda E_c g_a}{\Delta R_n + t_c \rho_a c_p D_v g_a - \lambda E_c(\Delta + \gamma)} \tag{2.10}$$

The parameters $g_{c\,max}$, k_1, k_2, θ_w and θ_c are determined by minimising the difference between Equations 2.6 and 2.10, using a nonlinear optimisation method (explained later in this chapter). The optimised parameter values are then used in Equation 2.6 to determine modelled values of g_c which are then inserted into Equation 2.10 in order to derive modelled estimates of E_c.

2.2.4.2 The modified Jarvis-Stewart model

Following the formulation and theory given by Equation 2.2, E_c can be modelled empirically using a Jarvis-type approach that can circumvent the need for g_c as a model input. For a well-coupled forest, where water lost from the leaf is controlled by stomatal aperture in response to meteorological changes, the mass transfer of water can be equated to follow an Ohm's law analogue, such that water lost from the canopy surface can be described by the equation:

$$E_c = g_c D_v \tag{2.11}$$

Following that, g_c is primarily controlled by variations in R_s, D_v and θ, and Equation 2.6 can be inserted into Equation 2.11, such that:

$$E_c = g_{c\,max} f_1(R_s) f_2(D_v) f_3(\theta) \cdot D_v \tag{2.12}$$

and noting that:

$$E_{c\,max} = g_{c\,max} D_v \tag{2.13}$$

it follows that water lost from the surface of the forest canopy can be described empirically as:

$$E_c = E_{c\,max} f_1(R_s) \hat{f}_2(D_v) f_3(\theta) \tag{2.14}$$

where once again the functions f_i describe a set of modifiers that proportionally modify $E_{c\,max}$ in response to changes in R_s, D_v and θ. The functional responses of E_c to variations in R_s and θ are the same responses as described by Equations 2.7 and 2.9. However, the response of E_c to increasing D_v is different as it includes the response of stomata shutting down at high D_v to maintain turgor and conserving water supply. This is generally referred to as the *three-phase response* (Monteith, 1995). Therefore, a new function is defined to explain the variation of E_c with D_v and is given as:

$$\hat{f}_2(D_v) = k_2 D_v \exp(-k_3 D_v) \tag{2.15}$$

where, the parameters k_2 and k_3 describe the rate of change at low and high atmospheric demand. This is a new term and follows the shape of a Bolztmann distribution function. Examination of Equation 2.15 shows that it replicates the three-phase response of transpiration to variation in g_s as D_v is increases from low to high values. Monteith (1995) has reviewed this topic and Eamus and Shanahan (2002) and Thomas and Eamus (1999) provide experimental and model verification. However, this is not normalised as Equations 2.7, 2.8 and 2.9 are, and some care is needed optimising Equation 2.14. Hourly estimates of modelled E_c (mm hr^{-1}) were determined from functions f_i.

The formulation given in Equation 2.14 is functionally equivalent to the PM equation, yet is much simpler to fit, requires fewer measurements and specifically removes g_c as a model input, a problem concurrent in all studies that use the PM equation (Ewers and Oren, 2000; Lu et al., 2003; Pataki and Oren, 2003); but retains it structurally within the model through the parameter E_{cmax}. Additionally, Equation 2.14 Is structurally equivalent to Equation 2.3 assuming that the forest canopy is highly coupled to the atmosphere, such that $g_c \ll g_a$, and so Equation 2.3 reduces to:

$$\begin{aligned} \lambda E_c &= \frac{\rho_a c_p D_v g_c}{\gamma} \\ E_c &= \frac{\rho_a c_p}{\lambda \gamma} \cdot g_c D_v \end{aligned} \tag{2.16}$$

Expressing E_c as function of R_s, D_v and θ in this way, follows the model structure defined by Jarvis (1976) and Stewart (1988), and so this empirical equation has been coined (in the context of this study) as the modified Jarvis-Stewart (MJS) model.

2.2.4.3 Model parameterisation

Both models were parameterised from experimental (measured) data using a genetic algorithm and weighted least squares (WLS). A weighting term (σ_i) was incorporated to better quantify the distribution of error in the measurements and hence ensure the optimised free parameters were closer to maximum likelihood. The parameters $E_{c\,max}$, $g_{c\,max}$, k_1, k_2, θ_w and θ_c are the optimised free parameters that represent response constants in the JS models. A multivariate optimisation for Equations 2.6 and 2.14 was done by minimising the

weighted sum of the square of residuals (WSSR). Given that the model parameters are set at some arbitrary starting values, we express the WSSR as:

$$\chi^2_{\min} = \sum_{i=1}^{N} \left(\frac{Y_i - f(X_i, \beta)}{\sigma_i} \right)^2 \tag{2.17}$$

where

$$\sigma_i = b\, Y_i \tag{2.18}$$

and Y_i is the ith experimental value, f is the model equation, where X_i and β being the ith model variables and parameters respectively, σ_i is the ith standard deviation and N is the number of data points. It is assumed that the heteroscedasticity is explained by Equation 2.18; expressing the standard deviation to be proportional to the experimental data Y_i, multiplied by an error constant of proportionality b (Kirkup et al., 2004). In order to specify whether σ_i is normally distributed, it is assumed that the residuals are a surrogate for σ_i such that $\sigma_i = Y_i - \hat{Y}_i$. For this study, random measurement error (σ_i) has been assumed to be normally distributed and heteroscedastic based on observations of the weighted residuals. The parameters values necessary to run the PM equation can therefore be found by inserting Equations 2.6 and 2.10 into 2.17:

$$\chi^2_{g_c} = \sum_{i=1}^{N} \left(\frac{\frac{\gamma \lambda E_{c,i} g_{a,i}}{\Delta R_{n,i} + t_c \rho_a c_p D_{v,i} g_{a,i} - \lambda E_{c,i}(\Delta+\gamma)} - g_{c\,max} f_1(R_{s,i}) f_2(D_{v,i}) f_3(\theta_i)}{b \, \frac{\gamma \lambda E_{c,i} g_{a,i}}{\Delta R_{n,i} + t_c \rho_a c_p D_{v,i} g_{a,i} - \lambda E_{c,i}(\Delta+\gamma)}} \right)^2 \tag{2.19}$$

and the parameter values necessary to run the MJS model are found similarly by inserting Equation 2.14 into 2.17:

$$\chi^2_{E_c} = \sum_{i=1}^{N} \left(\frac{E_{c,i} - E_{c\,max} f_1(R_{s,i}) \hat{f}_2(D_{v,i}) f_3(\theta_i)}{b\, E_{c,i}} \right)^2 \tag{2.20}$$

The two formulations above, show the difficulties in optimisation that are commonly experienced when using a least squares criterion at large dimensionalities. As the problem moves from linear to non-linear, the parameter space very quickly becomes increasingly populated by local minima and is therefore increasingly difficult to find the global minimum pertaining to the correct parameter values. Where local minima occur over the

large parameter space, early convergence of the solution is likely to occur, hampering the optimisation. To overcome these problems, a genetic algorithm was incorporated instead of the traditional Levenberg-Marquardt or Gauss-Newton algorithms. Unlike the gradient descent methods, a genetic algorithm is able to cover the entire parameter space with a large set of possible solutions. These solutions evolve and undergo a simulated process of natural selection until the best solution and hence the global minima equating to parameter values that are maximum likelihood, is found. A more detailed explanation of genetic algorithms and their design can be found in (Goldberg, 1989). For this study we used a pre-built genetic algorithm package in the Mathematica© software called *Differential Evolution*. The cross probability (probability of mating) was set to 50%, while population size was set automatically by the algorithm and run for 100,000 iterations to give an adequate amount of generations to find the global maxima.

2.2.4.4 Artificial neural network

In order to test the MJS model and PM equation against some form of statistical benchmark, an ANN was used as a comparator (Kohonen, 1989; Hsu et al., 2002; Abramowitz, 2005). A multivariate ANN procedure called a Self-Organising Linear Output map (SOLO) developed by Hsu et al. (2002) was used for this study to create this statistical benchmark and Figure 2.1 shows a diagram of this process. SOLO learns the relationship between inputs and outputs through the use of a training data set. Input information (R_s, D_v and θ) is classified in a Self Organising Feature Map (SOFM) (Kohonen, 1989). The SOFM is built by grouping parcels of input information into groups or *nodes* and are assigned a weighting term, where each weighting term corresponds to a specific pattern of input data. This SOFM is then connected to a prediction map, which is constructed by a multiple linear regression between input information (three abiotic drivers) and output information (canopy water-use). Regression parameters are determined from each node and are selected according to the supplied input data at a specific time-step; that is, a set of R_s, D_v and θ values will correspond to a specific E_c value. Thus, SOLO produces a piece-wise linear reconstruction of any functional relationship between these two groups (inputs and outputs) of variables (Abramowitz et al., 2009). The limitation of this process is that it requires a large amount of data (which determines the number of nodes) to construct

significant relationships so as to give an effective statistical reconstruction of the desired output. Although this is the basic idea behind the SOLO ANN, the theory behind this process is given in greater detail in Hsu et al. (2002).

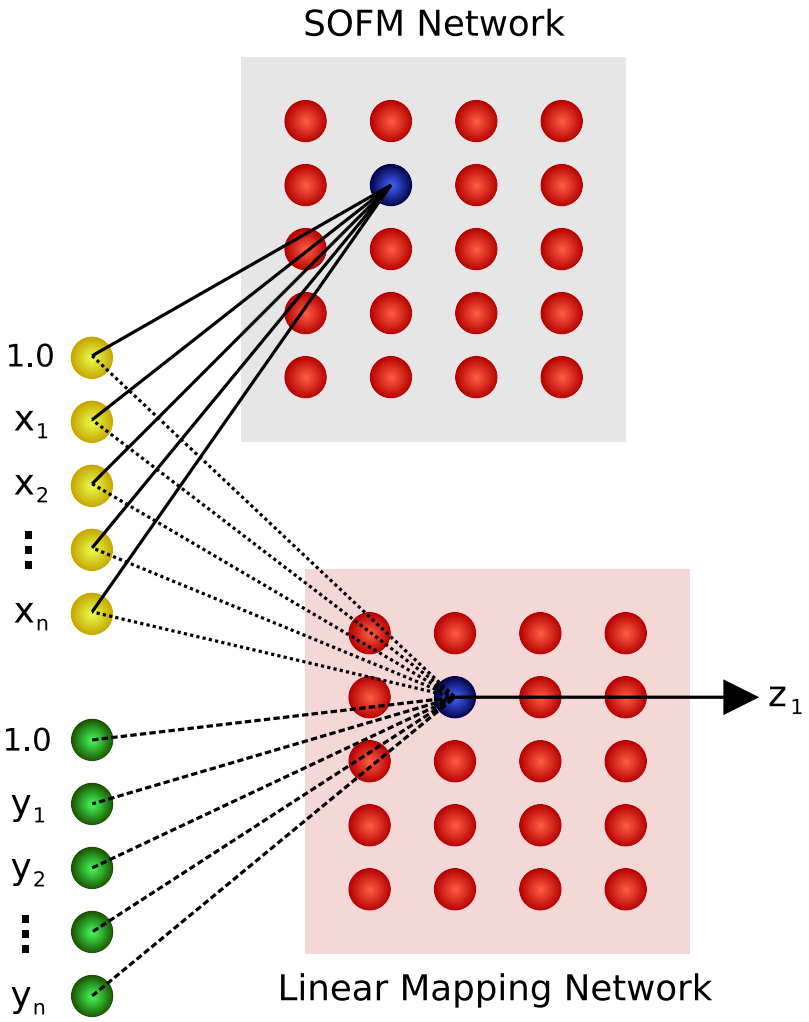

FIGURE 2.1: Diagram of the self-organising linear optimisation (SOLO) artificial neural network (ANN). The grey square denotes the self-organising feature map (SOFM) which contain nodes (red circles) of grouped input information, i.e. solar radiation, vapour pressure deficit and soil moisture content (yellow circles; $x_1, x_2 \ldots x_n$), where the data contained in each node are linearly related. Nodes in the SOFM network are compared with measurements of the desired output, i.e. canopy transpiration (green circles; $y_1, y_2 \ldots y_n$) through a multivariate linear regression in the linear mapping network. This allows functional relationships between the input and output information to be developed. Further input data can then be fed into SOLO to reconstruct the desired output (z_1).

The ANN is a pure statistically-based response to the meteorological forcing on a per time step basis (Abramowitz, 2005). The purpose of comparing a conceptual model against an

ANN output must be clearly understood. The ANN will always outperform mechanistic, conceptual models because it effectively has up an infinite number (theoretically) of optimised parameters, whereas most conventional models have at most 10 to 30. A direct comparison is therefore inappropriate. However, the ANN informs us about the information content of the data-set. That is, it indicates whether a model is performing badly because it fails to capture underlying relationships in the data, or whether it is performing badly because the dataset is too noisy. Thus, it offers a statistical evaluation of model performance.

In this study, a statistical benchmark was created using the SOLO ANN, where the three meteorological drivers (R_s, D_v and θ) containing 2616 data points (per variable) were used to construct a 5 x 5 SOFM. The size of the SOFM was kept small due to the low number of data points. The 5 x 5 SOFM was then used in SOLO along with E_c data in a training process, which was then subsequently used to simulate purely statistical predictions of E_c.

2.2.4.5 Filtering the data set

Sap flow data were filtered to avoid division by zero errors by including data only between 0900 h and 1600 h. This exclude hours when solar radiation was zero. To avoid wet-canopy conditions, days with rainfall events were also excluded. This filtered data-set was used to define the boundary conditions for Equations 2.7, 2.8, 2.9 and 2.15. To avoid circularity (using the same data to both parameterise the model and to compare with model outputs), the total 109 day data set spanning the year containing measurements from Jan-Feb, Jun-Jul and Aug-Sep, were partitioned into two separate data sets of alternate days. The first set (days 1, 3, 5 .) was used to optimise the seasonal response parameters, and the second set (days 2, 4, 6 .) was used to validate the model. No systematic patterns were evident in the data and there was no change in model outputs when allocation of each half of the data set to either optimisation or validation was reversed. However, it is noted that this does not result in two truly independent data-sets as, for example, rainfall on one day will affect E_c on the following day.

2.3 Results

2.3.1 Meteorological and sap-flow data

Maximum daily R_s ranged from 100 to almost 1400 W m^{-2} in summer and from 100 to 800 W m^{-2} in winter whilst the maximum daily D_v ranged between 0.5 to 7.0 kPa in summer and 0.1 to 1.6 kPa in winter (Figure 2.2a). The Liverpool Plains are characterised by summer dominant rainfall and a drier winter and this was evident during the study period, when there were 19 rain events during January and late February and 6 smaller events in July, August and September (Figure 2.2b). Summer maximum daily soil moisture content reached 13.9 % after two consecutive rain events during January, with subsequent decreases in E_c resulting from a gradual decline in θ to a minimum of 9 % (Figure 2.2b). During winter maximum daily θ reached a maximum of 10.8 % after a small 2 day rain event and a minimum of 9.4 % (Figure 2.2b). Mean daily E_c measured with the sap-flow sensors (scaled by sapwood area) varied up to 8-fold on consecutive days, with a range of from 0.09 mm d^{-1} during a rainy day (24th Feb) up to approximately 2.8 mm d^{-1} (28th Feb) on a rain-free day in the summer (Figure 2.2c). During winter, E_c varied between no measurable transpiration ($E_c << 0.01$ mm d^{-1}) on a rainy day (11th Jul) up to 2.08 mm d^{-1} on a rain-free day (28th Jul). Declining E_c between the 4th Feb and 22nd Feb was associated with declining θ, whilst large increases in E_c occurred after the 13th Jan and after 24th Feb following large rain events and hence soil recharge. An increase in soil moisture was evident from the 1st Aug, and was associated with an increase in stand water-use. The three largest rainfall events during the summer period increased soil moisture at 60 cm depth, whereas during winter most rainfall events had little effect on soil moisture at 60 cm depth (Figure 2.2 b).

2.3.2 Modelled stand water-use

The five parameters in Equation 2.6 and six parameters in Equation 2.14 were optimised by minimising the WSSR by using the Differential Evolution genetic algorithm in Mathematica©. Results from the genetic algorithm produced a set of maximum likelihood parameters that best describe seasonal responses. Figure 2.3 a, b, c shows the

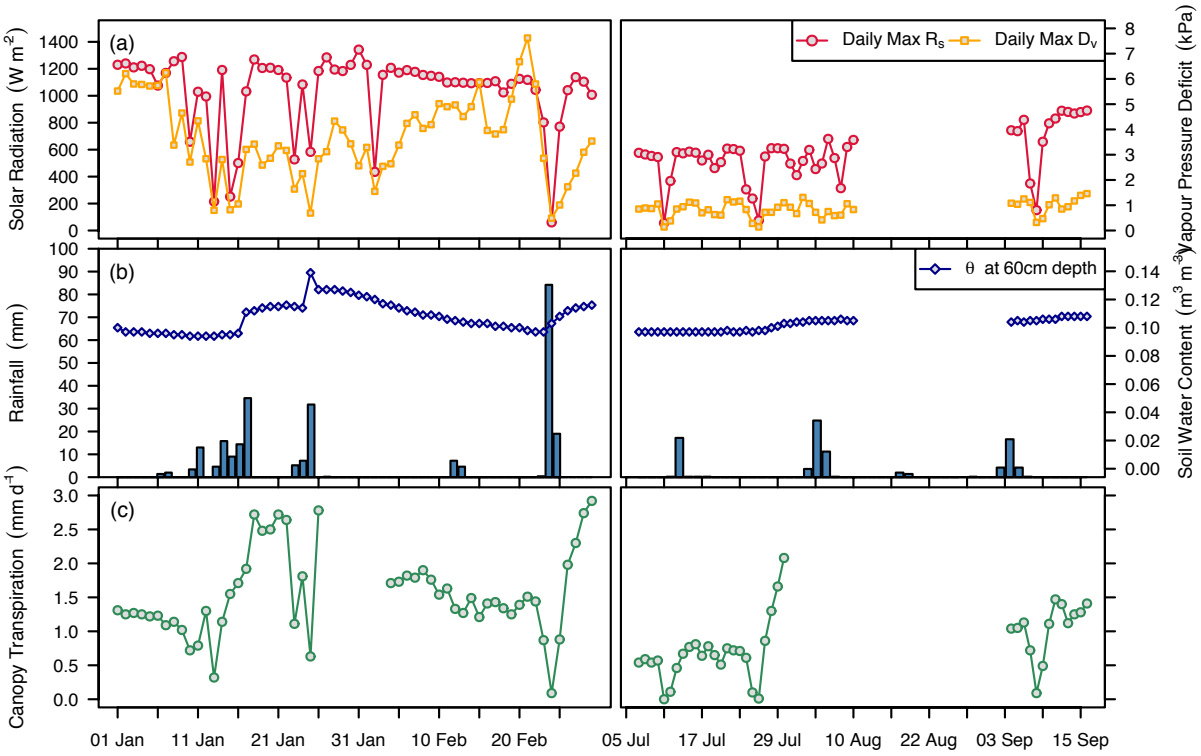

FIGURE 2.2: Day-to-day variation in canopy transpiration and its driving variables at Paringa. Data shown is the (a) daily maximum incident solar radiation (R_s), daily maximum vapour pressure deficit (D_v), (b) total soil water content to a depth of 60 cm (θ_s), daily rainfall and (c) total daily stand transpiration (E_c) for the periods of (left) January - February and (right) July - September 2004.

relationships between E_c and the driving variables R_s, D_v and θ and Figure 2.3 d, e, f shows the relationships of g_c against the same driving variables. Generally the functional forms fit well to the boundary regions described by the data, except for the response of E_c to D_v for the winter (Figure 2.3b). The residuals between measured and modelled data (Figure 2.4) reveal a minor heteroscedasticity, as evident by the slight pattern of the residuals. In order to properly account for this heterscedascticity, we used a weighting term (Equation 2.18). Using this weighting term explained the random errors (ϵ) in the measurements to be normally distributed, with the 68% confidence interval being within ± 1 standard deviation (data not shown). Table 2.1 contains the best estimates of the parameters in Equations 2.7, 2.8, 2.9 and 2.15 along with their respective standard errors. All parameter values were found to be statistically significant ($P < 0.05$).

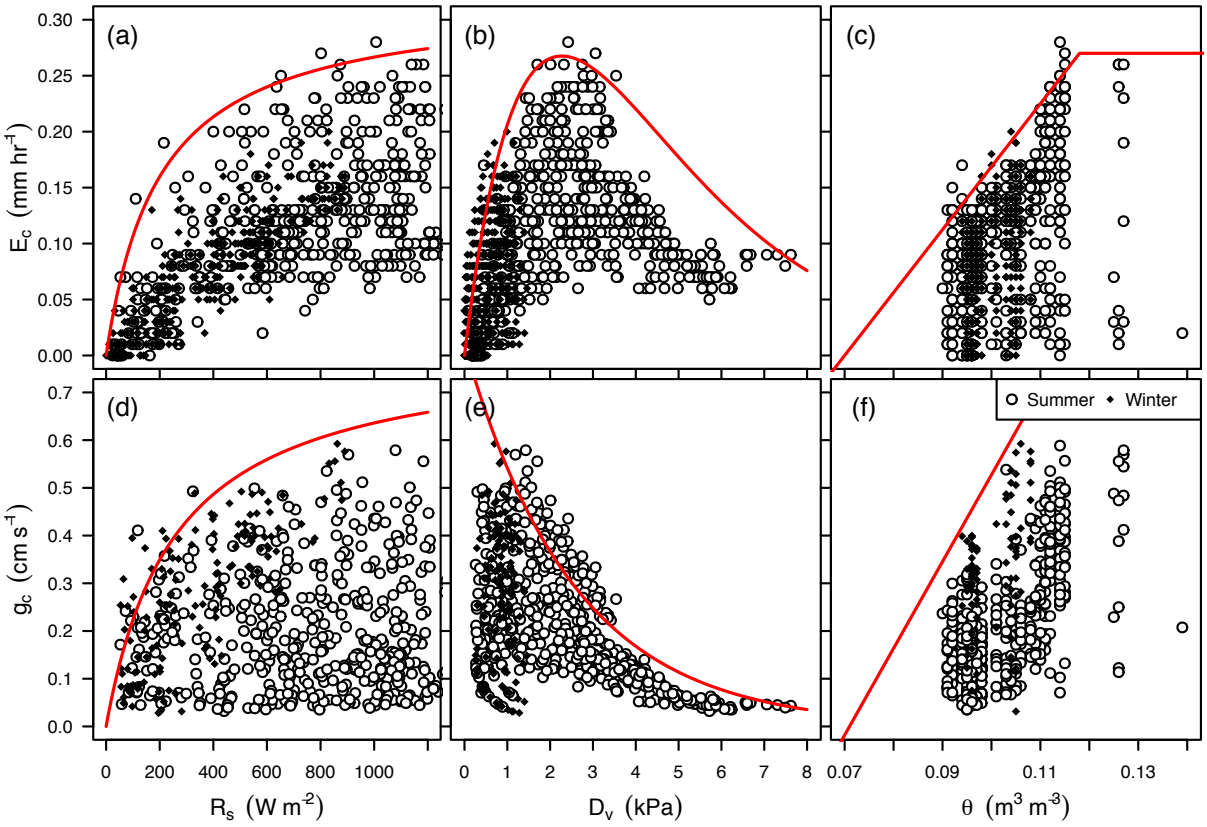

FIGURE 2.3: The functional dependencies based on the optimised parameters of canopy transpiration (E_c) on: (a) solar radiation (R_s), (b) vapour pressure deficit (D_v) and (c) soil water content at a depth of 60 cm (θ); and canopy conductance (g_c) on (d) R_s, (e) D_v and (f) θ_s. Relationships are given by white circles for summer (○) and black diamonds for winter (p). The red lines are the functional response curves ($f_{1...3}$) that describe non-limiting relationships between the quantities of E_c and g_c, and its environmental drivers.

The seasonal response parameters relating to g_c were used in Equation 2.6, which in turn was used in the PM equation (Equation 2.3) to give estimates of canopy water-use (E_c^{PM}). The seasonal response parameters relating to E_c, were used in MJS model (Equation 2.14) to derive estimates of canopy water-use (E_c^{JS}). Figure 2.5 shows a comparison of E_c estimates from both the PM equation and MJS model, against scaled measurements (E_c^{Obs}) and predictions from an ANN (E_c^{AN}) over the January-February summer period and July-September winter period. There was a slight under-prediction of E_c^{Obs} using both models, from the 17th-23rd Jan and 25th-29th Feb, which coincides with prior large rain events. Under-prediction of E_c^{Obs} was observed throughout the winter period but it was only

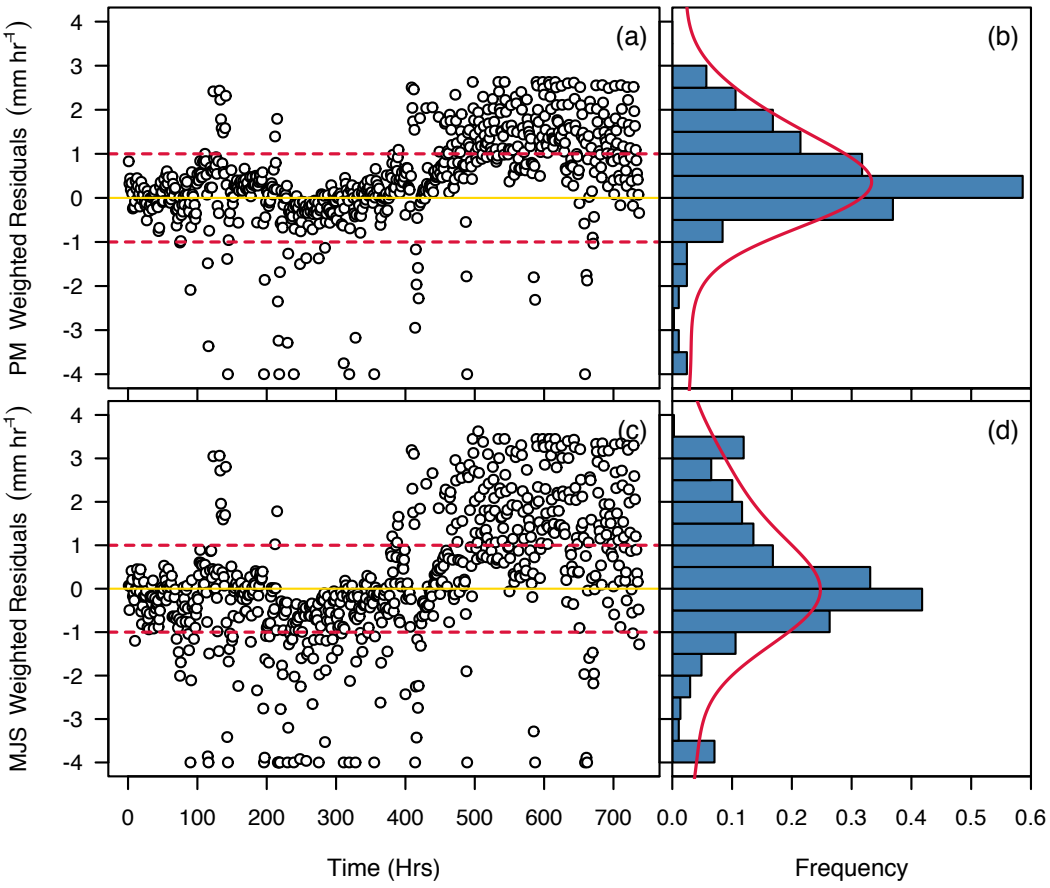

FIGURE 2.4: Weighted residuals (*measured* − *modelled*) for (a) the Penman-Monteith (PM) equation and (b) their distribution of error, and the weighted residuals for (c) the modified Jarvis-Stewart (MJS) model and (d) their distribution of error. The dashed lines show the regions for which the residuals fall between ±1 standard deviations, representative of the 68% confidence region. Both models conform to the assumption of a normally distributed error about a mean 0 and standard deviation 1.

occasionally seen in the summer. This under-prediction in both cases affects the total daily sums of E_c from both models. The ANN shows a night-time bias in its fitting, resulting in predictions of night-time E_c during both summer and winter periods which are not always measured by the sap-flow sensors, especially in winter. The ANN was unable to account for night-time E_c from the 27th-31st July. Points of failure in the fitting seem to be replicated across both models and the ANN. A comparison of both models shows that E_c^{JS} is much closer to the ANN in terms of explaining observed variations in E_c.

To allow a more detailed comparison amongst the ANN and model outputs, changes in

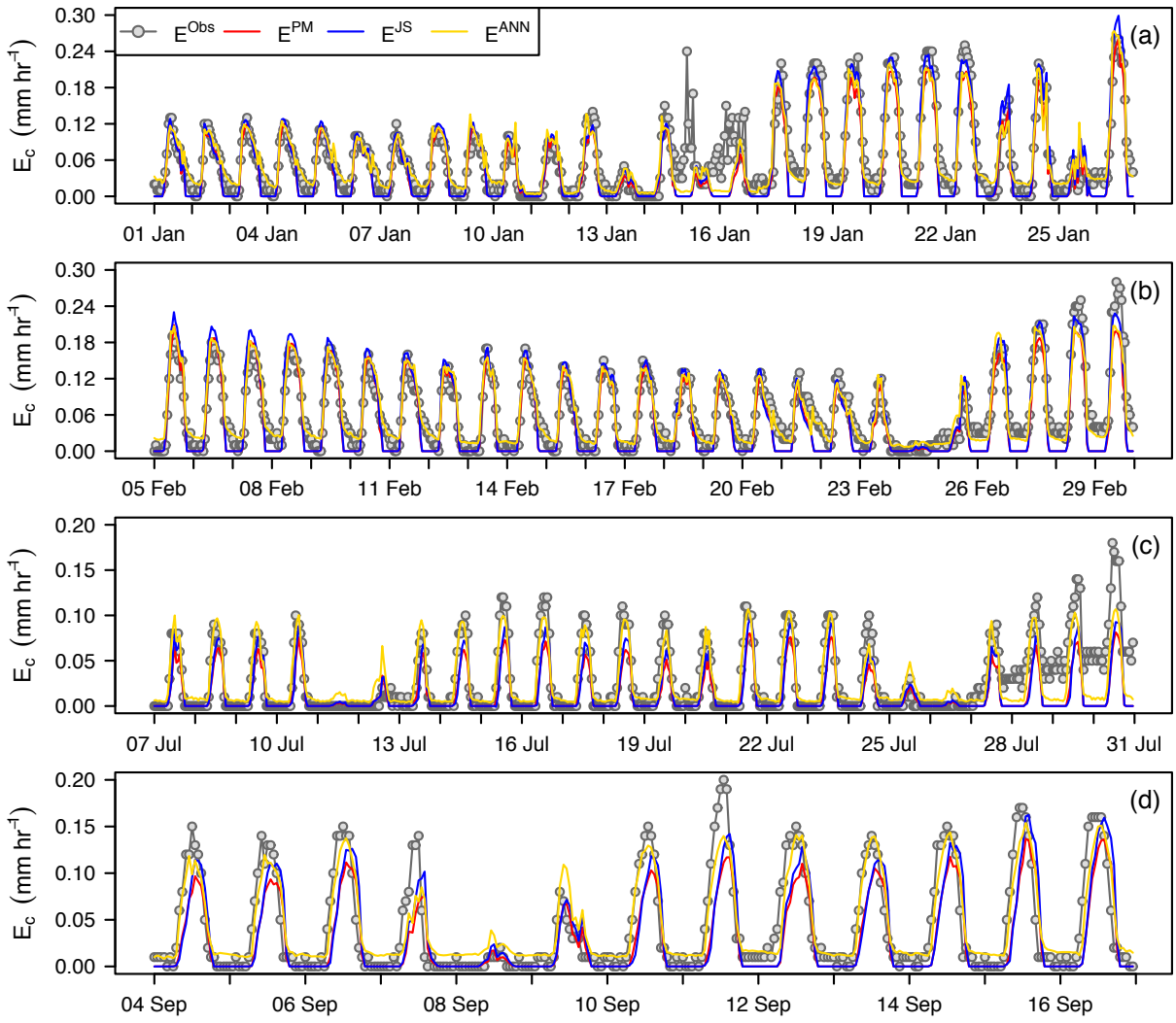

FIGURE 2.5: Canopy transpiration (E_c) measured with sapflow sensors (data points) and estimated E_c from the modified Jarvis-Stewart (MJS) (blue line), the Penman-Monteith (PM) equation (red line), and the statistical benchmark created using an artificial neural network (ANN; gold line) over the sampling periods in (a) January, (b) February, (c) July and (d) September 2004.

TABLE 2.1: Parameter estimations resulting from an optimisation of the modified Jarvis-Stewart (MJS) model and Penman-Monteith (PM) equations using a genetic algorithm. Parameters defined here are both maximum reference values for maximum canopy conductance ($g_{c\,max}$; m s^{-1}) and canopy transpiration ($E_{c\,max}$; mm hr^{-1}), environmental functional dependencies on solar radiation (R_s), (k_1; W m^{-2}), vapour pressure deficit (D_v), (k_2 and k_3; kPa), and soil water content (θ_s) at wilting (θ_w), and critical points (θ_c; mm^2 mm^{-2}), the constant of proportionality associated with error (b) and explained variance (R^2). Standard errors (S.E.) are given as a fraction of the parameter value in brackets.

	E^{PM}		E^{JS}	
Parameter	Value	S.E.	Value	S.E
$g_{c\,max}/E_{c\,max}$	0.0082	(0.02)	0.267	(0.02)
k_1	257.99	(0.19)	200.38	(0.20)
k_2	1.08	(0.02)	–	
k_3	0.39	(0.03)	0.44	(0.11)
θ_w	0.071	(0.02)	0.07	
θ_c	0.115	(0.01)	0.118	(0.01)
b	0.38		0.29	
R^2	0.86		0.87	
RMSE	0.0159		0.0042	
slope	0.92		0.91	
intercept	0.023		0.025	

hourly rates of E_c for four representative days are presented in Figure 2.6. In summer months, the MJS and PM models represent the morning trend of increasing sap-flow equally well but neither was able to represent the late afternoon/early evening trends in sap-flow very accurately. On average, in summer, the MJS model either slightly ($< 10\%$) under-estimated or slightly over-estimated mid-day rates of E_c, whilst the PM equation either closely matched or under-estimated by a larger margin (15%) mid-day rates of E_c. The ANN consistently followed the changes in E_c more closely throughout the 24 hr period.

The performance of both models was less satisfactory in winter than summer (Figure 2.6). The PM model consistently under-estimated the rate of E_c, particularly in the morning, but over-estimated E_c in the afternoon on some days. The MJS model performed better than the PM model in winter by a better representation of the maximum rates of E_c. However, it failed to adequately represent the early morning increase in E_c observed in the data. As expected the ANN closely matched the daily trends in E_c. The sap-flow

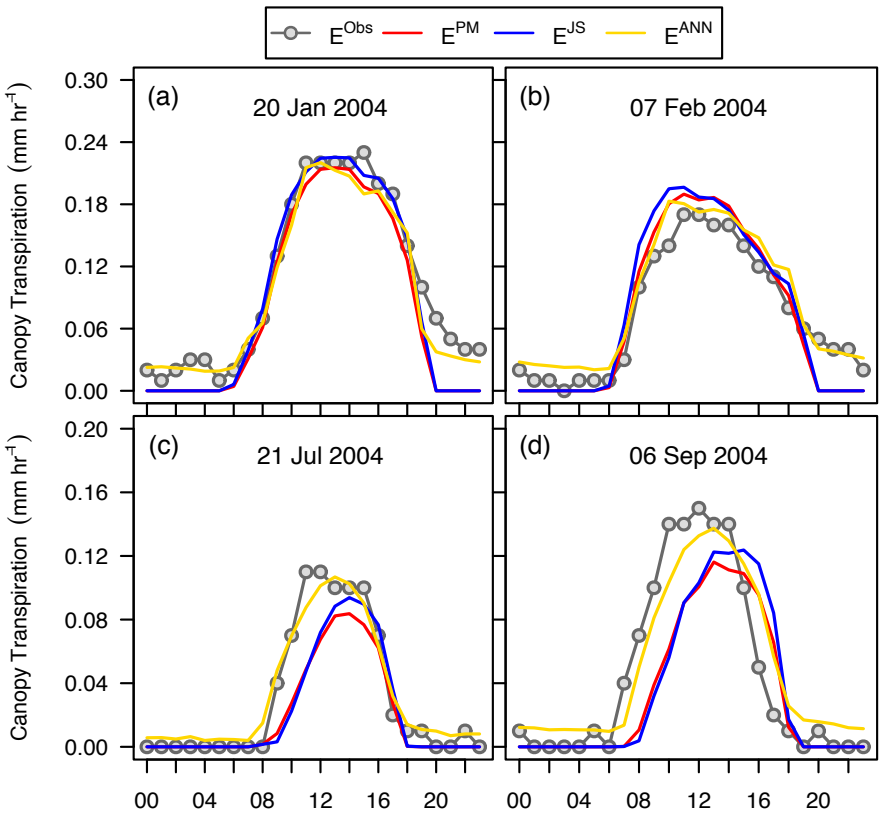

FIGURE 2.6: Diurnal variation in canopy transpiration (E_c) measured with sapflow sensors and modelled with the Penman-Monteith (PM) equation (red line), the modified Jarvis-Stewart (MJS) model (blue line) and the statistical benchmark created using an artificial neural network (ANN; gold line) for (a) 20th January, (b) 7th February, (c) 21st July and (d) 6th September 2004.

sensors measured a total of 75.4 mm of transpiration by the canopy for the 109 day study period between 0900 h and 1600 h. All three models gave a similar sum: the MJS sum for 109 days was 84 mm; for the PM model the sum was 75 mm; the ANN sum was 76.4 mm. Regression analysis revealed strong linear relationships between measured and modelled rates of stand water-use (Figure 2.7). In all cases the slope of the regression for summer data was closer to one than the slope for the winter data, which was always significantly less than one. Furthermore, in all cases the goodness-of-fit for the summer data was better than for the winter data. Thus, slopes of 0.86 and 0.79 for and respectively were observed and explained 87% of the variance and explained 86%. The ANN gave a slope of 0.85 and explained 86% of the variance.

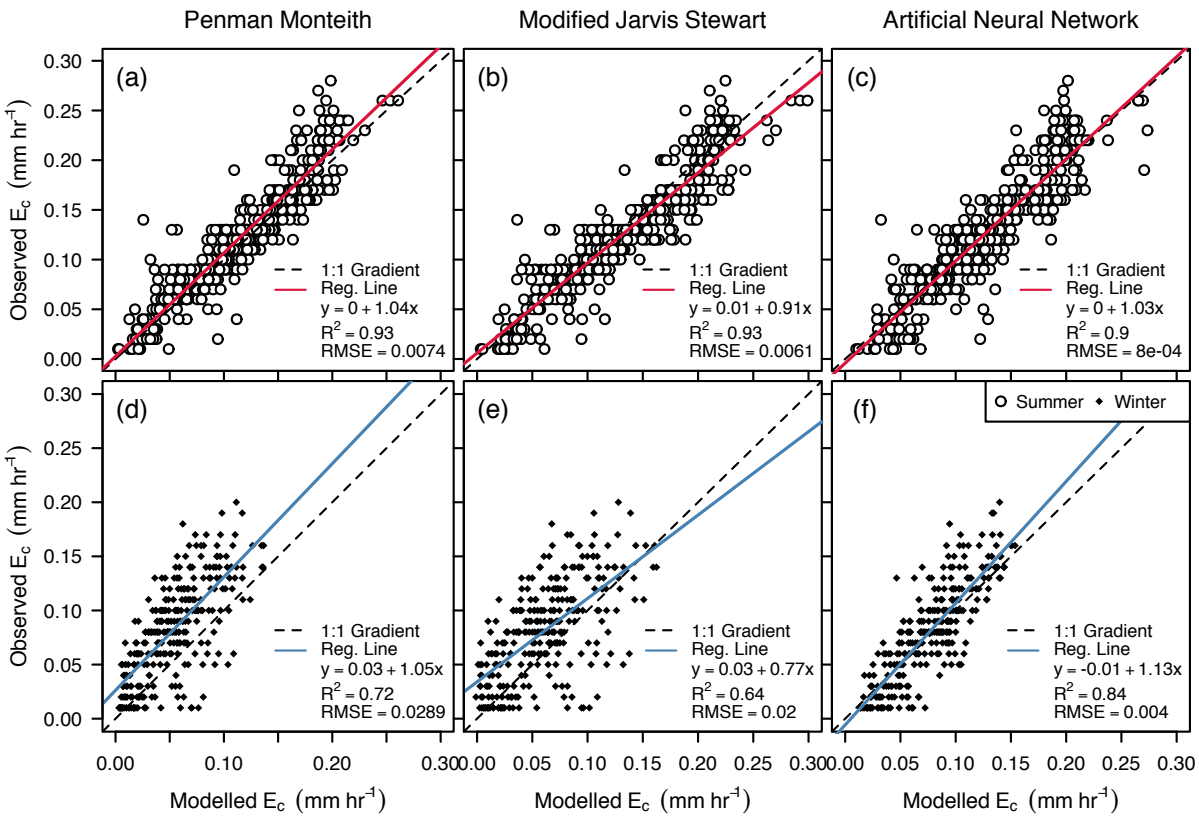

FIGURE 2.7: Summer (white circles, a-c) and winter (black diamonds, d-f) comparisons between measured and modelled stand transpiration (E_c) from (a) modified Jarvis-Stewart (MJS) model, (b) Penman-Monteith (PM) equation and (c) the statistical benchmark created using an artificial neural network (ANN). The 1:1 line is given by a black dashed line, and the regression lines are given in red (for summer) and blue (for winter)

2.4 Discussion

The responses of g_c and E_c (Figure 2.3) to each abiotic driving variable agree well with responses observed previously in a range of different forest types (Zhang et al., 1997; Sommer et al., 2002; Silberstein et al., 2003; Harris et al., 2004; Komatsu et al., 2006b) (Figure 2.7). Values for $E_{c\,max}$, $g_{c\,max}$, k_1, k_2, θ_w and θ_c (Table 2.1) also compare well with previous studies (Harris et al., 2004; Komatsu et al., 2006b). The estimated value for $E_{c\,max}$ of 0.267 mm hr^{-1} from the MJS model is comparable to the measured maximal value of 0.280 mm hr^{-1}. However, the estimated value of 0.0082 m s^{-1} for $g_{c\,max}$ is significantly over-estimated compared to the measured value (0.0058 m s^{-1}). The reason

why the modelled estimate of $g_{c\,max}$ is larger than the measured value is because the maximum value of E_c occurs in the mid-range of D_v (Figure 2.3b) but the modelled $g_{c\,max}$ predicts maximum values under conditions of low D_v and high R_s (Fig 2c, d) and such conditions do not occur in the field. Consequently there are no (large) values for observed $g_{c\,max}$ corresponding to these modelled environmental conditions. This also means that the MJS model is easier to fit than the PM model. However, this over-estimation of $g_{c\,max}$ had little impact on hourly values of E_c because of good agreement between modelled and measured hourly values of g_c. Conversely, E_c^{PM} under-predicted E_c^{Obs}, to a larger degree (especially in winter) when compared with E_c^{JS} because of the poor ability of E_c^{PM} to account for the impact of the generally lower θ_s in winter. Additionally, the value of $g_{c\,max}$ may be too low for the model, such that in order for the PM equation to better predict E_c, the required value for modelled $g_{c\,max}$ may need to be much higher.

As R_s increased, g_c and E_c increase asymptotically from zero to a maximum. At low levels of incident radiation, energy supply limits evaporation, but at high levels of radiation, other factors (especially soil moisture content and hydraulic conductance of soil and plant), limit evapotranspiration (Williams et al., 1997). The boundary curves for R_s show that both the E_c and g_c responses are almost identical and provide a good description of the asymptotic increase of E_c and g_c with increasing R_s. It was found that incorporating the soil moisture response function was critical for the model to satisfactorily describe variations in E_c and g_c, especially under limiting soil water conditions. Such a conclusion has been made previously (Wright et al., 1995; Harris et al., 2004). The observed patterns in the response of E_c and g_c to θ_s compares well with those found by Kelliher et al. (1993); Harris et al. (2004) and Komatsu et al. (2006b) and is attributed to the impact of a declining θ_s on stomatal, and hence canopy, conductance (Eamus et al., 2006a; Zeppel et al., 2008b) and the need to avoid excessively low leaf water potentials and hence xylem cavitation (Thomas and Eamus, 1999).

In contrast to the relatively simple relationship linking θ_s and E_c and g_c, the relationship between E_c, g_c and D_v was more complex. The functional responses of E_c and g_c to D_v differ because the response of E_c to D_v is determined by both the direct response of stomata to D_v, or rather, E_c (Mott and Parkhurst, 1991; Monteith, 1995; Eamus et al., 2008) and the response of diffusion *per se* to D_v. The response of g_c to increasing D_v compares well

with other studies that have found an exponential response (i.e. Granier and Loustau, 1994; Wright et al., 1995; Harris et al., 2004). The three-phase behaviour of E_c is comparable to that of stomatal behaviour observed at the leaf (Monteith, 1995; Thomas and Eamus, 1999; Eamus et al., 2002) and canopy scales (Komatsu et al., 2006b; Zeppel, 2006) and is the result of a feedback between increasing cuticular water loss as D_v increases and a declining supply of water to guard cells (Eamus et al., 2008). The initial response of E_c for low values of D_v is unlikely to be a response to the covariance of R_s in the morning, because even under a constant saturating level of light, the same three-phase behaviour was observed (Thomas and Eamus, 1999). The threshold of $2.0-3.0$ kPa for the transition to declining transpiration with increasing D_v observed in the present study is larger than that observed by Pataki and Oren (2003) and Komatsu et al. (2006b) and the decline in E_c was more severe than the decline in g_c they observed. This difference is probably because the site used in the present study is much drier, experiences a much larger range of D_v (as high as 7.0 kPa) and was recovering from a long period of drought, compared to those used by Pataki and Oren (2003) and Komatsu et al. (2006b). The response of stomata (and hence E_c) to D_v is strongly influenced by soil moisture content (Thomas and Eamus, 1999; Thomas et al., 2000) and therefore the long-term ($>$ 4 yr) drought experienced at the present site is likely to have influenced the response we observed.

Daily variations in E_c were captured well by both the MJS and PM models. Observed hourly E_c varied 12 fold over a period of one week in mid-January and the model was able to replicate this range and the time course of the response of E_c to fluctuations in R_s, D_v and θ_s. Similarly, more gradual declines in the maximum rate of E_c that were observed during drying periods (late Jan to late Feb) were captured in the models as well as the drier periods in winter. Poor model performance was generally seen during and immediately after large rainfall events, where large increases in observed rates of stand transpiration (15th -17th Jan and 27th-31st Jul) were not captured by the models. This could be because the sap-flow sensors, located at the base of the tree stem, were measuring a significant volume of canopy recharge in the absence of significant rates of transpiration (because of low values of R_s and D_v). Such recharge is driven by gradients of water potential between soil and leaf (Dawson et al., 2007), which may have been large in the present study but neither model incorporate such a mechanism for driving water flux up

the stem. Similarly the presence of nocturnal flows on several nights (for example, January 14th to January16th, February 25th to February 27th and July 28th to July 30th) were not captured by either model as both models assume stomatal closure at night. A simple calculation can estimate the potential contribution of canopy recharge to these two issues. The basal area of the two dominant tree species is 20.4 m^2 ha^{-1}. Average bole height of these two species is approximately 10 m so the total stem volume (ignoring branches and wood in the canopy) is 204 m^3 ha^{-1}. The average water content of the sapwood for the two species was 37.5 % (Zeppel et al., 2004) and it was assumed that the daily fluctuation in water content resulting from depletion and recharge of stem storage is no more than 50 % of this. Therefore a maximum of 38.25 m^3 ha^{-1} of stored water is available for nocturnal flow. Over the study period, actual rates of nocturnal flow range from 0.5 mm ha^{-1} $night^{-1}$ (25th/26th February) to 1 mm ha^{-1} $night^{-1}$ (14th/15th January), or 5 to 10 m^3 ha^{-1} $night^{-1}$. This range of nocturnal flow is less than estimated maximum volume of water that may be discharged and recharged in one night (38.25 m^3 ha^{-1}) and was therefore seen as reasonable.

Nocturnal flows were not observed on every night and were most commonly observed after significant rain had wet the soil profile. When this occurs, the gradient of water potential between soil and canopy is increased, the soil-to-root hydraulic connectivity is increased and nocturnal atmospheric humidity is generally increased. Such conditions favour canopy recharge (Dawson et al., 2007). If the hydraulic conductivity of the soil-plant transport pathway is 2.0 mmol m^{-1} s^{-1} (Zeppel, 2006) and the gradient in water potential is 1.0 MPa, then the maximum volume of recharge that can occur in a single 10 h night is 12.96 m^3 ha^{-1} $night^{-1}$, a value that agrees well with the estimated range of nocturnal flows (5-10 m^3 ha^{-1} $night^{-1}$). It would appear that canopy recharge is a very large fraction (up to 100 %) of the nocturnal flow observed and nocturnal transpiration through open stomata is therefore a small fraction of the total sap-flow measured at night with sap-flow sensors located at the base of the stem.

To compare daily performance of the models in more detail a sampling of 2 days from the summer and winter periods is considered (Figure 2.6). Differences between the MJS model and PM model in summer were marginal and both follow a trend similar to the ANN. In winter, however, the performance of the PM model dropped significantly with

an underestimation of up to 50 % during daylight hours. The MJS model reduced this underestimation to less than 20 % and compares well against the ANN. There was also a bias towards over-estimates of sap-flow in the afternoon for both models in winter, which the ANN did not exhibit.

The outputs of both models in winter lagged the observed values in the morning or morning and afternoon (Figure 2.6). The relative failure of the MJS model to fit to some days in winter appears to be because of the large number of winter data values which lie to the left (that is, outside) of the boundary line defined by Equation 2.18 (Figure 2.3). The boundary line defines the boundary well for summer data but fails to define the boundary in winter and this leads to the lag between model and measurement on some winter days. A slight but significant improvement in fit (reducing the time lag between JS and observed rates of sap-flow) of the modified JS model was produced if the model, when applied to the winter period, used parameter values derived only from winter data, rather than parameterising with the entire data set (data not shown). Failure to accurately predict E_c by the models during some of these winter days was not due to the data set being too small, as the ANN was able to accurately replicate all daily patterns (include night time fluxes) across both seasons. On a statistical basis, variations in R_s, D_v and θ are measured with sufficient frequency and resolution to account for observed changes in E_c.

The effect of temperature on E_c was also investigated. However, it was found that incorporating temperature in either the PM or MJS models had a negative impact on model performance and increased the error in the seasonal response parameters. Consequently the temperature response function was omitted. Similar problems in the use of a temperature function were found by Wright et al. (1995) and Sommer et al. (2002).

The MJS model was applicable to conditions of low and high E_c in summer at hourly time-steps with a slope of the regression of model versus observed values of 0.92. In winter, the MJS performed less well when E_c was large. In both summer and winter the PM model performed less well than the MJS at both low and high rates of E_c (Figure 2.5) and therefore at short time-frames (hourly) the MJS was generally more applicable than the PM model, which appears to be less successful under conditions of low E_c at hourly

time-steps in some studies (David et al., 1997; Rana et al., 2005) or less successful under conditions of high E_c in the present study (Figure 2.6)

The sum of water-used between 0900 h and 1600 h across the entire 109 day period was 75.4 mm. The PM model predicted a 109 day sum of 75 mm and the modified JS model predicted 84 mm whilst the ANN model predicted 111 mm. The ANN model has a very large number of parameters and is expected to fit the data extremely well because the size of the data set was sufficiently large to allow this. In summer the fit of the MJS data to experimental data was very good (Figure 2.7) and despite the poorer fit in winter on some days because of the poor definition of the winter boundary values for the response function for D_v, the 109 day sum of water-used derived from the MJS model was very close to the actual sum of water-used. It is apparent that despite limitations of both the PM and MJS models on some days under some conditions, at hourly time-steps (Figures 2.6, 2.7) the aggregate behaviour over a sufficient number of days (Figure 2.7) results in a close agreement between observed and modelled total sums of water transpired.

2.5 Conclusions

For this study, a standard (via the PM equation) and a new empirical (via the MJS model) approach was used to model the responses of stand-scale water-use to changes in R_s, D_v and θ_s. Both models were successfully parameterised using a limited number of sap-flow measurements and corresponding environmental driving variables over 55 days, incorporating data from both summer and winter periods. Model response functions for g_c and E_c were found to describe variation in water-use due to R_s, D_v and θ_s. These responses compared well with those found in previous studies on different forest types. Both models performed equally well during summer when soil water content was fairly high. During winter the MJS model performed significantly better than the PM model, especially under conditions of high transpiration. However, over the entire 109 day study period the total modelled daytime sums of water-used were all very close to the observed sum of 75.4 mm.

Chapter 3

Application of the modified Jarvis-Stewart model across five contrasting Australian ecosystems

3.1 Introduction

The water used by vegetation through the process of transpiration, is the principle pathway by which water is discharged from vegetated land surfaces in Australia. Investigating the vegetation component of evapotranspiration and quantifying it through mathematical models, allows one to observed how forest canopies, shrubs and grasses influence the water balance of an ecosystem (Eagleson, 2002). By extension, this allows the sustainable management of local catchment water-balances, which are subject to variation as a consequence of changes in land-use or climate (Zhang et al., 2001). Such information helps in the verification of other hydrological quantities when partitioning rainfall into its constituent components; where these components are evapotranspiration, water yield, canopy interception[1] and groundwater recharge. This is especially important for dry and arid ecosystems, like those that dominate Australia, as the determination of water fluxes

[1]While for some canopies canopy interception is a significant component of a site's water balance, for most open Eucalypt woodlands canopy interception is a small and is therefore no considered in this chapter.

is important in the effective management of water, vegetation and land resources (Eamus et al., 2006b).

Transpiration from a forest canopy depends upon a number of site specific parameters that relate to the physical properties of the soil, vegetation and ambient meteorological conditions. Three environmental variables, R_s, D_v and θ_s are seen as the primary driving forces behind transpiration (Jarvis and McNaughton, 1986; Wullschleger et al., 2000; Lagergren and Lindroth, 2002; Lundbald and Lindroth, 2002; Harris et al., 2004; Zeppel et al., 2008a). The sensitivity of transpiration to these drivers may vary depending on species (Pataki and Oren, 2003; O'Grady, 2006) and site (Leuning et al., 2005). Energy limited sites (those limited by available sunlight) will have a stronger relationship between water-use and available energy, while those that are water limited, show a stronger relationship with evaporative demand and the regulation of water-use by leaf stomata (Budyko, 1974; Whitehead, 1998; Oren et al., 1999). Consequently models need to be able to replicate such sensitivity to responses in order for them to be useful in estimating vegetation water use across many ecosystems.

There are numerous methods available to derive estimates of evapotranspiration, evaporation and transpiration. Some rely on describing the semi-empirical relationship between soil, vegetation and atmosphere, such as the Penman-Monteith (PM) equation (Monteith, 1965), while others use purely empirical relationships between canopy water fluxes and meteorological drivers, such as Jarivs-type models (see Chapter 2 and Whitley et al., 2008, 2009). Because of the semi-mechanistic basis of the PM equation, there is wide appeal in using it to make estimates of tree water-use. However, its implementation is often limited by the need for aerodynamic and stomatal conductances to be known; a problem that is compounded with trying to define stomatal conductance without the need for complex parameterisations. As stomatal conductance varies widely across species, sites and time of day, a stomatal conductance model, such as those developed by Jarvis (1976), Ball et al. (1987) and (Leuning, 1990) are generally used. However, these still require calibration against the site to be modelled and so requires a complex number of steps. Consequently, some authors such as Cleugh et al. (2007), Mu et al. (2007) and Leuning et al. (2008) have developed more accessible methods of calculating canopy conductance to be used with the PM equation. Empirical Jarivs-type models however, can be more useful and offer

similar results to the PM equation when canopy water fluxes, along with its drivers, are known (Chapter 2). The problem arises from the requirement for site-specific parameters to also be known, where the term *site-specific parameters* equates to parameters that are derived from independent data-sets; that is, each site (data-set) has its own set of parameters. Site-specific parameterisations however, may not be necessary if the responses of tree water-use to variable climatic conditions among tree-species and stands can be shown to be functionally equivalent. Mäkelä et al. (2008) have shown that when using an empirical Jarvis-type model, a set of *average* parameters are suitable enough to make long-term predictions of stand gross primary productivity. They suggest that there is some convergence in the relationships between productivity and its environmental drivers across the five ecosystems that were used in their study. It therefore follows that a set of parameters that describe the average response across multiple sites are capable of giving good model predictions. Functional convergence of water-use across species at a site has been reported by Meinzer (2003), Wright et al. (2006) and O'Grady et al. (2009) to name a few, and so the question is raised as to whether the response of canopy water fluxes to variable environmental conditions is similar across multiple ecosystems in Australia.

The rate of canopy water-use by different ecosystems varies across a large number of sites (i.e. Bosveld and Bouten, 2001; Wullschleger et al., 2001; Zeppel and Eamus, 2005; O'Grady, 2006; Kelley et al., 2007). The question may be asked: what is the cause of this large variation among ecosystems? Have species developed functional traits that are adapted to different climates, or is variation the result of differences in tree size and hence LAI? The literature is dominated by ecophysiological research into contrasting species-specific behaviour or strategies in physiological processes such as transpiration, photosynthesis and growth, expressing the diversity of plant function among species (Meinzer, 2003). Whilst this has provided enormous understanding into the environmental adaptations of plants, it has led to a misunderstanding that plant species are always functionally divergent (Reich et al., 2003). This divergence becomes less apparent with the increase in measurement scale, and suggests that the difference among plant functional traits are a factor of plant size and hydraulic architecture rather than species *per se* (Meinzer, 2003; Wright et al., 2006).

In this chapter, I use the modified Jarvis-Stewart (MJS) model, conceptualised in Chapter 2 and tested against the PM equation and a statistical benchmark created using an artificial neural network (ANN), to explain hourly and day-to-day variation in stand transpiration across contrasting species and ecosystems. Five Australian sites have been chosen for this study, which differ in ambient environmental conditions, geographical location, species composition and soil type. Not only will this test the robustness of the model, but it will help determine if an average set of model parameters can be developed to operate across multiple ecosystems. The modelling work in this study will involve:

- Examining the variation and patterns of canopy water-use across multiple ecosystems
- Identifying the responses of water-use at the stand scale and how it varies across geographical location
- Identifying what the causes are (if any) that create variation in the response of canopy water-use across these multiple sites
- Investigating whether there is a functional converge of water-use amongst ecosystems

3.2 Methods

3.2.1 Site descriptions and data

It is acknowledged here that all measured data contained in this chapter were collected by a number of researches. Specifically Zeppel et al. (Paringa), Zeppel et al. (Castlereagh), O'Grady et al. (Pittwater), Yunusa et al. (Benalla) and Froend et al. (Gnangara). None of this data was collected by the author of this thesis.

This study incorporates the application of a simple empirical water-use model to data collected from five different sites around Australia. These sites are Paringa, located in the Liverpool Plains in north-western New South Wales (NSW); Castlereagh, located just west of Sydney in NSW; Benalla, located north-west of Melbourne in Victoria; Pittwater, located just east of Hobart in south-east Tasmania; and Gnangara just outside of Perth

in south-eastern Western Australia (WA). These sites have a diverse range of native Australian tree species, soil types and climate summarised in Table 3.1. All meteorological data were collected at half-hourly intervals throughout the respective sample periods at each site. Data for R_s (W m^{-2}), D_v (kPa), air temperature (T_a; °C) and rainfall (mm) were collected from nearby meteorological stations within close proximity of each site. Each of the five ecosystems used in this study are described below.

Paringa

The study site at Paringa is located approximately 70 km south of Tamworth in north-western NSW. The site is a remnant open woodland dominated by two native tree species, *E. crebra* and *Callitris glaucophylla*, with a canopy of approximately 15 m in height and these two species account for approximately 75% of the site's BA, while *Stipa* and *Aristada* grass species dominate the understorey. Woody characteristics for this site include a total basal area of 23.8 ± 3.4 m^2 ha^{-1} and a total of 212 stems ha^{-1} (Zeppel et al., 2004, 2008b). Canopy LAI varied only slightly during this study and was relatively constant, with a range of $0.9 - 1.1$ m^2 m^{-2}. The soil profile at this site was shallow and approximated to a sandy-loam, with some occasional exposed sandstone. The climate for the site is temperate, with a range in daily mean T_a of $20.0 - 34.2$ °C in summer and $3.4 - 16.8$ °C in winter, while mean daily maximum R_s and D_v range between $552.9 - 1040.6$ W m^{-2} and $0.85 - 3.68$ kPa respectively across the study period. Mean annual rainfall is 604 mm, and is summer dominant.

Castlereagh

This study site is located in a remnant woodland in the Cumberland Plain, approximately 47 km north-west of Sydney in NSW. This open woodland is dominated by two native tree species; *E. sclerophylla* and *Angophora bakeri*, standing at an average height of 14 m and accounting for 80% of the BA at the site. The canopy understorey is dominated by shrubs and grasses including *Pultenaea elliptica*, *Cryptandra amara* and *Melaleuca thymifolia*. Woody characteristics of the site include a total basal area of 12.2 ± 0.35 m^2 ha^{-1} and 85.5 ± 6.5 stems ha^{-1} (Zeppel et al., 2008a). Canopy LAI for this study period

TABLE 3.1: Site-specific information about the canopy, soil and climate for the Paringa, Castlereagh, Benalla, Pittwater and Gnangara sites used in this study; BA is basal area, LAI is leaf area index, $\overline{T_a}$ is the mean annual temperature and PPT is the annual precipitation. The initials for the species names are *Eucalyptus (E), Callitris (C) and Banksia (B).* The asterisk (*) denote the soil-types that are of a duplex nature.

SITE	**PARINGA**	**CASTLEREAGH**	**BENALLA**	**PITTWATER**	**GNANGARA**
Co-ordinates	31°30' S 150°42' E	33°39' S 150°46' E	36°36' S 145°56' E	42°94' S 147°30' E	31°60' S 115°50' E
Elevation (m)	390	40	190	51	19
Species Composition	*E. crebra* *C. glaucophylla*	*E. sclerophylla* *A. bakeri*	*E. camaldulensis* *E. microcarpa*	*E. globulus*	*B. attenuata* *B. ilicifolia*
BA (m^2 ha^{-1})	23.80	12.20	24.57	14.13	1.71
Height (m)	15.0	14.0	23.8	7.0	5.0
LAI (m^2 m^{-2})	0.9–1.1	1.3	1.0–1.2	3.0	0.57–0.61
Annual $\overline{T_a}$ (°C)	18.60	15.38	15.83	11.58	18.6
Annual PPT (mm)	604	729	670	500	868
Soil Type	Sandy Loam	Sandy-Loam/ Clay Loam*	Sandy-Clay/ Clay-Loam*	Loamy-Sand Clay-Loam*	Loamy Sand
Study Period	Jan–Feb (2004) Jul–Sep (2004)	Jan–Jul (2007)	Jan–Feb (2006) Jul–Aug (2006)	Jan–Dec (2007)	Oct–Nov (2008) Mar–Apr (2009)
Reference	Zeppel et al. (2008b)	Zeppel et al. (2008a)	Yunusa et al. *in review*	O'Grady et al. (2008)	Froend and Drake (2006)

was relatively constant at ≈ 1.3. The soil profile is duplex, consisting of a very sandy upper profile (≈ 0.8 m) overlying a deep clay profile (>10 m). This site experiences a temperate climate, with a mean summer T_a range of $18.7 - 29.3\,^{\circ}$C and a mean winter T_a range of $6.3 - 17.2\,^{\circ}$C. Mean daily maximum R_s and D_v range between $468.1 - 905.6$ W m^{-2} and $0.92 - 2.46$ kPa respectively across the study period. Mean annual rainfall is 729 mm and is seen to be slightly summer dominant.

Benalla

The Benalla study site is located in the Reef Hills State Park, in north-western Victoria. The site is as a heathy dry forest dominated by *E. camaldulensis* and *E. microcarpa*, standing at an average height of 25 m. The canopy understorey is dominated by wattles (*Acacia pynantha* and *Acacia meamsii*) and grasses (*Joycea pallida* and *Poa sieberiana*). Woody characteristics of the site include a mean basal area of 24.57 ± 2.13 m^2 ha^{-1} and LAI of a range between $1.0 - 1.2$ m^2 m^{-2} (Yunussa et al. *unpublished data*). The soil profile was duplex, and had contrasting soil textures in the upper profile (≈ 1.5 m), categorised by a depression and having a sandy-clay texture. *E. camaldulensis* was found to occupy 75% of the sandy-clay area. This site experiences a temperate climate, with a mean summer T_a range of $14.4 - 30.8\,^{\circ}$C and a mean winter T_a range of $3.9 - 14.2\,^{\circ}$C. Mean daily maximum R_s and D_v experienced large ranges of between $522.3 - 968.4$ W m^{-2} and $0.43 - 3.10$ kPa respectively across the study period. The mean annual rainfall is for this site is 670 mm and is slightly winter dominant, with a one third of this volume occurring during the months of June to August.

Pittwater

The Pittwater research plantation is located approximately 35 km east of Hobart, in south-eastern Tasmania. The site consists of 9 growth plots of 225 m^2, containing 25 trees of *E. globulus*. In each plot the trees are planted at a 3 x 3 m spacing, which approximates to 1111 stems ha^{-1} (O'Grady et al., 2008). The 9 plots are grouped into three treatments comprising of two irrigated and one rain-fed; for this study we have used data from the rain-fed plots only. The average height of the trees were approximately 7 m during the

study period and LAI remained constant at ≈ 3. The soil profile is duplex, with an upper profile ($1.5 - 2.0$ m) comprising a loamy-sand, overlying a deep sandy-clay to clay-loam profile. The regional climate is a cool temperate maritime, with a mean summer temperature range of $11.3 - 21.3\,^{\circ}$C and a mean winter temperature range of $2.2 - 11.5\,^{\circ}$C. Mean daily maximum R_s and D_v range between $436.8 - 866.1$ W m^{-2} and $0.58 - 1.48$ kPa respectively across the year of 2006. Mean annual rainfall is approximately 500 mm and is slightly summer dominant.

Gnangara

The Gnangara aquifer is located on the northern Swan Coastal Plain, approximately 35 km north of Perth, WA. The study site lies above this aquifer and is characterised by a Mediterranean-type climate with warm to hot, dry summers and mild, wet winters (Froend and Drake, 2006). During summer, the mean maximum T_a is approximately $30.1\,^{\circ}$C, while daily maximum R_s and D_v reach moderately high values of 1143 W m^{-2} and 6.63 kPa respectively. Mean annual rainfall is approximately 868 mm and is winter dominant, with $5 - 6$ month long dry season occurring between November and April. The site is typical of the Bassendean dune system, which is characterised by a deep sand profile that underlies an open woodland, dominated by a *Banksia* genus overstorey, with the predominant species being *B. attenuata*, *B. ilicifolia*, *B. menziesii* and *B. littoralis*.

Scaling tree water-use to the whole stand

The water-use of individual trees occupying the five stands used in this study were measured using sap flow techniques. Stand transpiration was scaled from the water-use of individuals trees up to the stand by multiplying the mean measured sap flow of the stand by the total sapwood area of the stand (Zeppel et al., 2004). This methodology is as follows: for each species, a number of trees were selected to cover the range in sizes observed at the stand. These trees were then instrumented with sap flow sensors and sap velocity derived using the heat-ratio (or heat-pulse) method. Sap flow was recorded at half-hourly intervals for the study period at each site (Table 3.1) and corrected for the effects of wounding, radial variability of flow, sapwood area and volumetric fractions of

wood and water (Burgess et al., 2001; Medhurst et al., 2002). The relationship between diameter at breast height (DBH) and sapwood area (SA) for the dominant species at the site was then used to determine the total sapwood area of each species at each site. Mean species sap flow was the multiplied by the total cross-sectional sapwood area of the stand, giving species water flux for the stand. The respective water fluxes of each species at each site were then added together to give the total water-use of the stand (Zeppel et al., 2004, 2008b).

3.2.2 The modified Jarvis-Stewart model

In Chapter 2 of this thesis, a simple empirical model was presented. This model estimated hourly rates of E_c by proportionally modifying a maximum potential transpiration rate via a set of reduction functions that described the variation in three major environmental variables known to drive transpiration. Thus E_c was determined by:

$$E_c = E_{cmax}\, f_1(R_s)\, f_2(D_v)\, f_3(\theta_s) \; + \; \varepsilon \tag{3.1}$$

where E_{cmax} represents the maximum potential transpiration rate (mm hr^{-1}), $f_{1...3}$ are the cost functions or the *limiting factors*, occupying values between 0 and 1, describing the percentage reduction in E_c with variations in the three driving variables. Additionally, ε represents the uncertainty in model predictions. However, not all ecosystems are affected by the soil water status for a number of reasons, including the trees in the stand having deep roots that are able to access ground water (GW) (Eamus et al., 2006b), the site being riparian (O'Grady, 2006), be both riparian and accessing GW (Boulten and Hancock, 2006), or have a soil profile with a high water retention due to its particle size distribution (Zeppel et al., 2008a). If such is the case, then E_c will no longer be affected by the soil water status, as $f_3(\theta_s) = 1$, ergo $f_3(\theta_s)$ in Equation 3.1 will disappear and E_c will then be determined by a much simpler equation defined as:

$$E_c = E_{cmax}\, f_1(R_s)\, f_2(D_v) \; + \; \varepsilon \tag{3.2}$$

To determine whether soil water status plays a major role in an ecosystem's water-use, analysis of the relationship between transpiration and θ_s is necessary; generally a slope in such a relationship will identify if any dependence exists. Additionally, Equations 3.1 and 3.2 can be statistically fitted to the data, and their relative performance will generally indicate whether θ_s is a factor in canopy water-use of an ecosystem.

The cost functions expressed in Chapter 2 for the functional response of E_c to variations in R_s and θ_s were found to be adequate descriptions of those relationships. The cost function for R_s is nonlinear and describes an asymptotic response defined as:

$$f_1(R_s) = \left(\frac{R_s}{1000}\right)\left(\frac{1000 + k_R}{R_s + k_R}\right) \tag{3.3}$$

where R_s is direct or global solar radiation (W m^{-2}), 1000 W m^{-2} is the typical value of R_s where saturation occurs (Jarvis, 1976; Stewart, 1988) and k_R is a fitted parameter. The cost function for θ_s is best described by the relative extractable water, given as a *broken stick* or piece-wise linear function defined as:

$$f_3(\theta_s) = \min\left\{1, \frac{\theta_s - \theta_w}{\theta_c - \theta_w}\right\} \tag{3.4}$$

where θ_s is the θ_s (m^3 m^{-3}), and θ_w and θ_c are the permanent wilting and critical points respectively and are also fitted parameters in this study[2].

The cost function that is used to describe the relationship between E_c and D_v, first proposed in Chapter 2, is now reviewed. Although this function was able to capture the three-phase response of leaf stomatal conductance (g_s) to increasing D_v as described by Monteith (1995) and shown by Thomas et al. (2000) and Eamus and Shanahan (2002), it was not normalised and therefore did not operate validly as a modifier. In order to bring the D_v function in line as a proper modifier such as those of Equations 3.3 and 3.4, a

[2]It is important to note that $\theta_c \neq \theta_f$, the field capacity of the soil. θ_c represents the level of saturated soil where transpiration is maximised and any further increases in θ_s will have no effect in increasing transpiration, as the rate of water loss is now being limited by the hydraulic architecture of the tree.

completely new function was developed for application in this chapter:

$$f_2(D_v) = \exp\left\{\frac{-k_{D1}(D_v - D_{peak})^2}{D_v + k_{D2}}\right\} \tag{3.5}$$

where D_v is the D_v (kPa), k_{D1}, k_{D2} and D_{peak} are fitted parameters found using nonlinear optimisation. The parameters k_{D1} and k_{D2} describe the shape of the D_v response curve. The parameter D_{peak}, describes the position of E_{cmax} at a specific value of D_v that is equivalent with the point of Regime B of the three-phase response. This is an important new addition to the model, as it allows the value of D_v at which E_{cmax} to shift along the x-axis, whereas before it was static.

3.2.3 Site-specific parameterisation

Equations 3.1, 3.2, 3.7 and 3.9 were optimised using the method of nonlinear least squares for each data-set to determine site-specific, species-specific, site-average and species-average model parameters. Due to the degree of nonlinearity in the model, a heuristic search algorithm was applied in order to properly cover the parameter space. In the past, genetic algorithms (GA) have been used to find the global minimum of highly complex parameter spaces, dictating the best fit parameters of the model based on the given data (Whitley et al., 2008, 2009). In the present application, a differential evolution (DE) optimisation GA was applied; a model that combines the evolutionary search routines of a GA, with a quasi-Newton gradient descent method that is capable of making better distinctions of the global minimum from local minima (Price et al., 2005). This optimisation was completed using the *GENetic Optimisation Using Derivatives* (GENOUD) function in *R Statistical Software*, an open source and freely available statistic package maintained by the *GNU* and *Comprehensive R Archive Networks* (http://www.r-project.org).

Optimisation was performed over an objective function defined as the sum of the square of error (SSE) between observed and modelled (Eqns 3.1 and 3.2) E_c expressed as:

$$\chi^2_{min} = \sum_{i=1}^{N}\left(\frac{Y_i - f(X_i, \beta)}{\sigma_i}\right)^2 \tag{3.6}$$

where χ^2_{min} is the SSE, Y_i is the data observed, $f(X_i, \beta)$ is the data modelled (X_i and β being the model variables and parameters respectively) and σ_i is the error in measurement. The combination of parameter values that reduces SSE to a minimum are deemed to be the *best fit* parameters for the data. Referring back to Chapter 2, a weighted fit is used to account for the heteroscedasity of the data, where $\sigma_i = b\,Y_i$, and b is a noise scale parameter describing the magnitude increase in error with the magnitude increase in measurement (Kirkup et al., 2004).

Using GENOUD, a large initial population of 10,000 samples was set to sufficiently cover the parameter space, and domains on the parameters were used to narrow the target area where the global minimum was believed to be. Parameter domains were created to constrain the optimisation and prevent problems of colinearity. These domains were set large enough so as not to dictate the optimisation towards a specific solution, but were also limited to within a physical range the parameters could only occupy. For example, values where $\theta_w > \theta_c$ or $E_{cmax} < 0.0$ occur would relate to impossible solutions as the θ_w must always be less than the θ_c, and E_{cmax} must always be larger than 0. Additionally, these constraints helped to reduce the colinearity between some of the parameter, such as E_{cmax} and θ_c, which are horribly correlated. The data were also scaled in order that all X variables were of the same or similar magnitude, in order to improve the topography of the parameter's space and hence make convergence easier for the algorithm. Parameter populations were run until a convergence to the global minimum was reached or the number of iterations had reached a maximum hard-limit.

3.2.4 Site-average parameterisation

The principle aim of this work was to determine a set of site-average parameters in order to see how sensitive the model is to the functional responses and to determine whether a set of average parameters can be applied to a number of disparate sites and still generate estimates of acceptable accuracy. In order to determine these average parameter values, all sites were concatenated into a large ensemble data-set. The MJS model was then fitted to the ensemble data-set using a mulitvariate-nonlinear-dummy regression (MNDR) procedure to determine a set of best-fit parameters that describe the average functional

responses across all sites (Kleinbaum et al., 1997). This optimisation incorporates the use of binary dummy variables that are assigned to each specific site. The use of dummy variables allows the turning *on* or *off* of the E_{cmax} at each site. With this in mind Equation 3.1 is therefore reformulated to include a set of dummy variables such that:

$$E_c = \{ k_{S0} + k_{S1}S_1 + k_{S2}S_2 + k_{S3}S_3 + k_{S4}S_4 \} f_1(R_s) f_2(D_v) f_S + \varepsilon \tag{3.7}$$

where $S_{1,2...4}$ are the dummy variables pertaining to each site and have values of either 0 or 1. The coefficients $k_{S\,1,2...4}$ represents the relative amount each site adds to k_{S0}; the result being the *actualised* E_{cmax} for each respective site. Equation 3.7 can be broken down into respective sites as:

$$\begin{aligned}
E_c^{Site1} &= k_{S0}\, f_1(R_s)\, f_2(D_v)\, f_S \\
E_c^{Site2} &= \{ k_{S0} + k_{S1}S_1 \} f_1(R_s)\, f_2(D_v)\, f_S \\
E_c^{Site3} &= \{ k_{S0} + k_{S2}S_2 \} f_1(R_s)\, f_2(D_v)\, f_S \\
E_c^{Site4} &= \{ k_{S0} + k_{S3}S_3 \} f_1(R_s)\, f_2(D_v)\, f_S \\
E_c^{Site5} &= \{ k_{S0} + k_{S4}S_4 \} f_1(R_s)\, f_2(D_v)\, f_S
\end{aligned} \tag{3.8}$$

Similarly, this was done for the species-specific data as well, where we define the multivariate model for the concatenated species data-set as:

$$E_c = \{ k_{T0} + k_{T1}T_1 + k_{T2}T_2 + k_{T3}T_3 \} f_1(R_s) f_2(D_v) f_S + \varepsilon \tag{3.9}$$

where $T_{1...3}$ represents the dummy variables for each site-dominant tree species and $k_{T1...3}$ are their respective coefficients. Therefore Equation 3.9 can also be broken down into the respective components for each tree species as:

$$\begin{aligned}
E_c^{Species1} &= k_{T0}\, f_1(R_s)\, f_2(D_v)\, f_S \\
E_c^{Species2} &= \{ k_{T0} + k_{T1}T_1 \} f_1(R_s)\, f_2(D_v)\, f_S \\
E_c^{Species3} &= \{ k_{T0} + k_{T2}T_2 \} f_1(R_s)\, f_2(D_v)\, f_S \\
E_c^{Species4} &= \{ k_{T0} + k_{T3}T_3 \} f_1(R_s)\, f_2(D_v)\, f_S
\end{aligned} \tag{3.10}$$

The component f_S represents the application of θ_s effects, that have already been optimised individually for each site, i.e. it is equal to Equation 3.4 but with known θ_w and θ_c inserted. This was done so as to reduce the complexity of Equations 3.7 and 3.9, and to more easily reach a convergence in the optimisation.

Site-average and species-average parameters were determined by optimising the objective function described by Equation 3.6 with GENOUD. Because the Castlereagh and Pittwater sites were significantly larger data-sets compared to the other sites (2 x and 4 x respectively), four months from both data-sets were selected to represent each site in the MNDR. The months that were selected for both sites were January, February, June and July and covered the summer and winter climatic forcing that is quantified by the other sites. GENOUD was then run until a convergence was reached, signifying the parameter values that give the best fit of the model to the ensemble data-set.

3.2.5 Model validation

In order to provide some evaluation of the site-specific, species-specific, site-average and species-average parameters, several statistical test were used. Individually, the explained variance (R^2) is not suitable as a measure of model performance, as it fails to account for model bias (see Mitchell, 1997). In order to provide a more robust statistical validation for the performance of models used in this study, the model efficiency (ME) and root mean square error (RMSE) were used to give additional measures of the variation in the error. The RMSE is an effective measure of the deviation of model predictions from the observed data, given as:

$$RMSE = \sqrt{\frac{\sum(\,Y_i - f(X_i, \beta)\,)^2}{N}} \tag{3.11}$$

and the ME estimates the proportion of variance of the data explained by the 1:1 line, and is given as:

$$ME = 1 - \frac{\sum(\,Y_i - f(X_i, \beta)\,)^2}{\sum(\,Y_i - \overline{Y}\,)^2} \tag{3.12}$$

Equation 3.12 provides information on what proportion of the modelled variance explains the measured variance. The ME can range from $-\infty$ to 1, where an efficiency of 1 (ME

= 1) corresponds to a perfect match between modelled and measured data, an efficiency of 0 (ME = 0) indicates that the model predictions are as accurate as the mean of the measured data, and an efficiency less than 0 (ME < 0) dictates that the measured mean is a better predictor than the model.

Artificial neural network

As well as the above measures of model performance, a self-organising linear output map (SOLO) ANN (Hsu et al., 2002) was also used in order create a statistical benchmark for *fitting*. This benchmark describes the best possible fit for the MJS model given the input data, and is used to compare both site-specific and site-summarised models (an explanation of SOLO was given in Chapter 2). SOLO uses a self-organising feature map (SOFM) (Kohonen, 1989) to create a set of weights, by grouping the three model input drivers (R_s, D_v and θ_s) into groups which are denoted as *nodes*; where the number of nodes used should be reflective of the size of the data-set for each site. A multiple linear regression is then performed across each of these nodes and the output variable of interest (E_c), producing a statistical reconstruction of the functional relationship between E_c and it's drivers (Abramowitz et al., 2009). Thus, this statistical reconstruction was used as the benchmark for *fitting* in this study and gives an idea on how well the models utilise the given meteorological data in predicting stand water fluxes. The settings for running SOLO and SOFM for each site are given in Table 3.2.

The SOFM for Paringa, Benalla and Gnangara sites was constructed using all three environmental drivers (R_s, D_v and θ_s) and described by a 5 x 5 matrix that resulted in 25 nodes. For the Castlereagh and Pittwater sites, only two drivers were used (R_s and D_v), as θ_s was seen to be non-limiting at these sites. Because these sites were larger data-sets, their respective SOFMs were described using a 10 x 10 matrix that resulted in 100 nodes.[3] All site SOFMs were constructed using 5000 iterations. Using the weights derived from the SOFM of each site and the above ranges given in Table 3.2, the data-set was trained and then simulated to produce the statistical benchmark.

[3]Although Pittwater had the largest data-set, increasing the node size beyond 10 did not result in an improved benchmark.

TABLE 3.2: The settings used to construct the statistical benchmark using the artificial neural network (ANN). Given are the number of variables considered to influence canopy transpiration (E_c) at each site (Vars), the number of nodes which the driver data are to be clustered into (Nodes) using the self-organising feature map (SOFM), the number of data available at each site (Data), the number of iterations used to create the SOFM, and finally the maximum (Max) and minimum (Min) values for solar radiation (R_s), vapour pressure deficit (D_v) and soil water content (θ_s) that are used to train the ANN in the self-organising linear optimisation (SOLO).

SITE	SOFM				SOLO							
	Vars	Nodes	Data	Iter	R_s (W m^{-2})		D_v (kPa)		θ_s (m^3 m^{-3})		E_c (mm hr^{-1})	
					Max	Min	Max	Min	Max	Min	Max	Min
PARINGA	3	5 x 5	2616	5000	1340.0	0.0	7.62	0.0	0.139	0.09	0.280	0.0
CASTLEREAGH	2	10 x 10	5088	5000	1153.3	0.0	5.50	0.0	-	-	0.196	0.0
BENALLA	3	5 x 5	2904	5000	1192.0	0.0	6.34	0.0	0.285	0.266	0.391	0.0
PITTWATER	2	10 x 10	8760	5000	1191.2	0.0	4.87	0.0	-	-	1.331	0.0
GNANGARA	3	5 x 5	2424	5000	1143.1	0.0	6.63	0.0	0.052	0.016	0.060	0.0

3.3 Results

3.3.1 Model fitting and convergence

The model was set up as follows for each site. Equation 3.1 was applied to the Paringa, Benalla and Gnangara data-sets, as they displayed a clear relationship between E_c and θ_s. Equation 3.2 was applied to the Castlereagh data-set, as these sites displayed no observable relationship between E_c and θ_s. In the case of Pittwater, it was unclear whether a relationship existed between E_c and θ_s due to the very sandy soil profile and the presence of shallow groundwater. However, initial testing of both Equations 3.1 and 3.1, showed that θ_s provided no improvement to the model estimates of E_c, and so Equation 3.2 was used for this site. The models were fitted successfully to the measured data at all sites by minimising the SSE using a GA, determining the best fit parameters for each site. However, due to the highly nonlinear structure of the model, some difficulties were encountered in acquiring statistically significant parameter estimates. This high nonlinearity is most prevalent in Equation 3.1 due to the inclusion of θ_s response function, causing a high collinearity to exist between the parameters E_{cmax} and θ_c, such that convergence towards the global solution becomes difficult to achieve. This was further supported by looking at

the eigenvalues Hessian matrix, which was determined from the best-fit parameters. The eigenvalues identified that the directions these parameters move in are dominated by many local minima (data not shown), so that despite sufficiently covering the parameter space with a large population of solutions using the GA, manual constraints were still necessary in order to reach the perceived global solution. Additionally, sites such as Pittwater and Castlereagh were halved in their resolution from half-hourly time-steps to hourly time-steps. Although this did not result in an improved fitting of the model to the Castlereagh data-set, it gave a significant improvement in fitting the model to the Pittwater data-set. The Pittwater data-set was characterised by some noise in the E_c data which was most likely due to equipment error, and a good portion of this noise was removed from halving the resolution of the data as described above. This improved fitting the model to the measured data, and allowed clear functional relationships to be observed between E_c and its environmental drivers.

3.3.2 Response of canopy transpiration to environmental drivers

Parameter estimates derived for all five sites gave well defined boundary curves to describe the non-limiting relationships between E_c and its environmental drivers. The optimised site- and species-specific parameter estimates are given in Table 3.3, while the site- and species-average parameter estimates are given in Table 3.4. The boundary curves that these parameters represent are graphically represented with the relationships between transpiration and its three primary environmental drivers in Figure 3.1. These results are explained below.

3.3.2.1 Response to solar radiation

The asymptotic response of E_c to increasing R_s was similar across all sites. However, the Castlereagh and Paringa sites showed R_s functional responses that tended to display weak and strong relationships respectively. For the Paringa site, a strong relationship between E_c and R_s was clearly observed, represented by a large k_R value. For the range of $0 < R_s < 1000$ W m^{-2} there is an almost direct relationship between these two quantities, and for $R_s > 1000$ W m^{-2} the response of E_c has still not saturated towards E_{cmax}

(Figure 3.1a). The Benalla, Pittwater and Gnangara sites displayed similar relationships between E_c and R_s, and therefore had similar k_R values, with E_{cmax} saturating at approximately $R_s = 1000$ W m^{-2} (Figure 3.1b,c,d). The R_s response for the Castlereagh site was the exact opposite of that observed for the Paringa site. The Castlereagh site displayed very little relationships to exist between E_c and R_s for $R_s > 200$ W m^{-2} and was represented by a very low k_R value (Figure 3.1e). This response suggests that $E_c \rightarrow E_{cmax}$ almost instantaneously over a low, small range of R_s. This is similarly conveyed in the model fits to the species-specific data , where the parameter estimate of k_R for *A.bakeri* is close to 0.0, which results in a large standard error (σ_{se}) and hence can be seen as statistically insignificant. However, the same estimates of k_R for the total stand and *E.sclerophylla* data, although very low as well, shows a convergence on values that are statistically significant and so the R_s response function was retained in the model for this site; testing the model without the R_s response function showed a failure of the parameter estimates to converge towards reasonable values and was therefore included. Comparing k_R among species at Castlereagh and Benalla, showed that the water-use of the stand favoured the response of one species over another to R_s. At Castlereagh, the species that displayed the stronger relationship between E_c and R_s was *E.sclerophylla*, while at Benalla this was *E.camaldulensis*. The site-average k_R value is comparable with the those of the Benalla, Pittwater and Gnangara sites, and shows the degree of deviation that the Paringa and Castlereagh sites take in respect to this. The disparity between the k_R values between Paringa and Castlereagh may suggest sites that are limited and not limited respectively by solar energy. Comparisons between k_R values among species at a site, showed a small variation around the total stand k_R, and suggests the stand value is an average between the two species responses. The σ_{se} for k_R values across all sites was variable, with Paringa and Benalla having the largest error; however the large σ_{se} at these sites may be a consequence of a more complicated parameter space due to the θ_s response function.

3.3.2.2 Response to vapour pressure deficit

A concave response of E_c to increasing D_v was observed to be generally similar across all sites. The sites at Paringa, Benalla and Gnangara displayed values of D_{peak} that were in the range of $2.3 - 2.5$ kPa, while those at Castlereagh and Pittwater had lower values

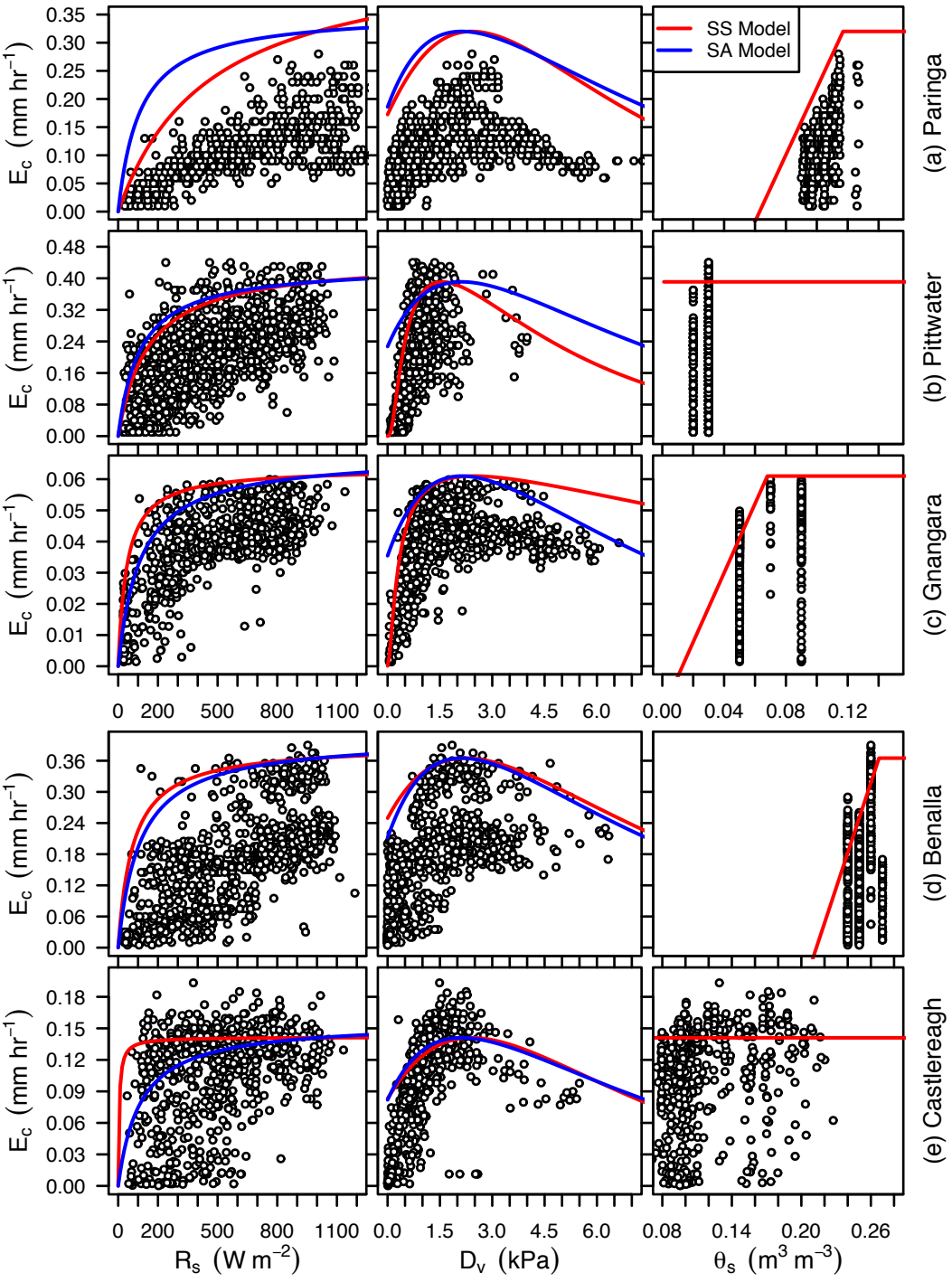

FIGURE 3.1: Functional response of canopy transpiration (E_c) to variations in solar radiation (R_s), vapour pressure deficit (D_v) and soil moisture content (θ_s) for the (a) Paringa, (b) Pittwater, (c) Gnangara, (d) Benalla and (e) Castlereagh sites. The red line represents the modelled non-limiting site-specific (SS) response, and the blue line represents the modelled non-limiting site-average (SA) response. The plots have been separated to distinguish between the sites that have sandy (a,b,c) and clay (d,e) soil profiles.

TABLE 3.3: Estimated parameter values that equate to the site-specific and species-specific functional responses of canopy transpiration (E_c) to solar radiation - $f_1(R_s|k_R)$, vapour pressure deficit - $f_2(D_v|k_{D1}, k_{D2}, D_{peak})$, and soil water content - $f_3(\theta_s|\theta_w, \theta_c)$. The functional responses that were used to parametrise the model for each site are listed. The values given here are those that were found to give the best fit of the model to the measured data, and were determined using the differential evolution genetic algorithm. Standard errors (σ) are given as a fraction of its respective parameter value .

Site	**Model**		E_{cmax} (mm hr^{-1})	k_R (kW m^{-2})	k_{D1} (kPa)	D_{peak} (kPa)	k_{D2} (kPa)	θ_w (m^3 m^{-3})	θ_c (m^3 m^{-3})
PARINGA	$E_{cmax}f_1(R_s)f_2(D_v)f_3(\theta_s)$	Value	0.320	0.260	0.270	2.408	0.523	0.063	0.117
		σ	(0.03)	(0.21)	(0.10)	(0.03)	(0.11)	(0.03)	(0.02)
CASTLEREAGH	$E_{cmax}f_1(R_s)f_2(D_v)$	Value	0.141	0.005	0.230	1.83	0.270	-	-
		σ	(0.01)	(0.001)	(0.11)	(0.02)	(0.16)	-	-
E.sclerophylla	$E_{cmax}f_1(R_s)f_2(D_v)$	Value	0.069	0.006	0.256	1.53	0.233	-	-
		σ	(0.01)	(0.01)	(0.11)	(0.03)	(0.23)	-	-
A.bakeri	$E_{cmax}f_1(R_s)f_2(D_v)$	Value	0.073	< 0.001	0.209	2.18	0.295		-
		σ	(0.01)	(1.00)	(0.13)	(0.03)	(0.21)	-	-
BENALLA	$E_{cmax}f_1(R_s)f_2(D_v)f_3(\theta_s)$	Value	0.365	0.061	0.153	2.289	0.279	0.213	0.267
		σ	(0.15)	(0.36)	(0.25)	(0.06)	(0.77)	(0.01)	(0.02)
E.camaldulensis	$E_{cmax}f_1(R_s)f_2(D_v)f_3(\theta_s)$	Value	0.171	0.077	0.182	1.738	0.118	0.205	0.263
		σ	(0.34)	(0.52)	(0.66)	(0.31)	(0.08)	(0.01)	(0.03)
E.microcarpa	$E_{cmax}f_1(R_s)f_2(D_v)f_3(\theta_s)$	Value	0.208	0.040	0.191	2.777	0.805	0.217	0.273
		σ	(0.19)	(0.32)	(0.43)	(0.05)	(0.49)	(0.01)	(0.03)
PITTWATER	$E_{cmax}f_1(R_s)f_2(D_v)$	Value	0.392	0.112	0.252	1.187	0.052	-	-
		σ	(0.02)	(0.10)	(0.17)	(0.04)	(0.85)	-	-
GNANGARA	$E_{cmax}f_1(R_s)f_2(D_v)f_3(\theta_s)$	Value	0.061	0.043	0.049	2.535	0.047	0.013	0.068
		σ	(0.01)	(0.10)	(0.14)	(0.04)	(0.51)	(0.01)	(0.02)

TABLE 3.4: Estimated model parameter values that have been derived by fitting the modified Jarvis-Stewart (MJS) model to all sites simultaneously at the stand scale (*site-average*) and to two sites (Castelreagh and Benalla only) simultaneously at the species scale *species-average*). Given below are the site-average parameter values that describe the functional responses of canopy transpiration ($k_{S,0...4}$) to solar radiation (k_R) and vapour pressure deficit (k_{D1}, k_{D2} and D_{peak}), as well as the species-average responses of canopy transpiration ($k_{T,0...3}$) to the same environmental drivers. Soil water content was incorporated into the optimisation as a known quantity and so $theta_w$ and $theta_c$ are not calibrated. The value listed here represent those that give the best fit of the MJS model to the measured E_c data determined from the nonlinear dummy regression. Standard errors (σ) are given as a fraction of the parameter values.

PARAMETER		Site-Average	Species -Average
k_{S0}/k_{T0}	Value	0.303	0.173
(mm hr^{-1})	σ	(0.03)	(0.02)
k_{S1}/k_{T1}	Value	-0.115	-0.102
(mm hr^{-1})	σ	(0.09)	(0.03)
k_{S2}/k_{T2}	Value	-0.184	-0.101
(mm hr^{-1})	σ	(0.04)	(0.04)
k_{S3}/k_{T3}	Value	0.043	0.000
(mm hr^{-1})	σ	(0.14)	(0.02)
k_{S4}	Value	-0.281	-
(mm hr^{-1})	σ	(0.04)	-
k_R	Value	0.110	0.030
(W m^{-2})	σ	(0.10)	(0.15)
k_{D1}	Value	0.172	0.202
(kPa)	σ	(0.25)	(0.24)
k_{D2}	Value	1.422	0.893
(kPa)	σ	(0.79)	(0.43)
D_{peak}	Value	2.123	2.171
(kPa)	σ	(0.06)	(0.05)

between 1.1−1.8 kPa. The parameter D_{peak} gave a representation of Regime B of the three-phase response, which dictates stomatal limitation to transpiration (Monteith, 1995). The Paringa, Benalla and Gnangara sites experienced a large range of D_v, with daily maximums reaching in the range of $6.3 - 7.6$ kPa during the study periods (Figure 3.1a,c,d), while the Castlereagh and Pittwater sites, also experiencing a moderate range of D_v, had slightly lower daily maximums in the range of $4.9 - 5.5$ kPa (Figure 3.1b,e). This lower range of D_v was the result of frequent rainfall in the case of Castlereagh, and low T_a at Pittwater during their respective study periods. Consequently, the D_{peak} values at these sites were

lower than the warmer or drier sites. A comparison of D_{peak} values among species at the Castlereagh and Benalla sites shows the stand values to be an approximate average of the species values. At Castlereagh, *A.bakeri* species displayed a much larger D_{peak} than the *E.sclerophylla* species; a difference of approximately 0.5 kPa despite having similar E_{cmax}. The same trend was seen for Benalla, where the D_{peak} for *E.microcarpa* was approximately 1.0 kPa larger than the *E.camaldulensis* species. This may suggest that some species are more sensitive to D_v than others. The parameters that describe the shape of the response curve were similar in value among the sites; of the ranges $0.04 < k_{D1} < 0.27$ kPa and $0.05 < k_{D2} < 0.50$ kPa. The site-average D_{peak} value gives a good approximation of the relationship between E_c and D_v across all five sites and species among sites, especially those of Paringa, Benalla and Castlereagh. However, a disparity is evident between the decline in E_c for $D_v > D_{peak}$ at the Pittwater and Gnangara sites. This appears to be due to the magnitude of the k_{D1} value, with a higher value (0.25 kPa) denoting a fast decline, while a low value (0.05 kPa) represents a slow decline. For Pittwater, the range in D_v is too low to properly display the decline in E_c that occurs at high D_v, while at Gnangara, although the range of D_v is sufficient, there may not be enough data to explain the same decline. The σ_{se} for D_{peak} and k_{D1} was consistently low for all sites, while the σ_{se} for the site-average k_{D1} value was moderately high, because of the different rates of decline in E_c at high D_v among the sites. The k_{D2} parameters displayed much a larger error, as a result of clumping of data around the Y-axis at $D_v < 0.5$ kPa and this was additionally seen for the site-average k_{D2} for the same reasons. Whether or not the model used the θ_s response function, seemed to have no effect on the σ_{se} of these parameters.

3.3.2.3 Response to soil water content

For sites that are limited by θ_s, the same *broken stick* response was observed. However, these relationships are not comparable due to the different magnitudes in θ_s as a result of disparate soil textures among sites. While sites such as Paringa, Benalla and Gnangara were able to show clear relationships, those sites that had access to deep water stores, such as ground water or highly saturated clay layers at Pittwater and Castlereagh respectively, displayed no such relationship. Paringa was characterised by a sandy-loam profile having a $\theta_w = 0.063$ and $\theta_c = 0.117$ m^3 m^{-3} (Figure 3.1a). Both the Pittwater and Gnangara sites

had much sandier profiles and hence, a lower soil-water retention. The Pittwater site was subject to a very low θ_s over the study period, in the range of $0.02-0.03$ m^3 m^{-3}. However, the site contained a shallow water table that was accessible to the tree roots, and provided an adequate water supply and removed any dependence between E_c and θ_s (Figure 3.1b). The Gnangara site, despite having a similar sandy soil profile, was able retain a larger volume of water and displayed a strong relationship between E_c and θ_s, with values of $\theta_w = 0.013$ and $\theta_c = 0.068$ m^3 m^{-3} (Figure 3.1c). The Benalla and Castlereagh sites were characterised by similar duplex profiles that consisted of a sandy-loam layer overlying a clay-loam layer. The Benalla site showed θ_s to vary little over the study period, having a range of $0.240 - 0.271$ m^3 m^{-3} (Figure 3.1d). Nevertheless, a relationship between E_c and θ_s could be determined, with $\theta_w = 0.213$ and $\theta_c = 0.267$ m^3 m^{-3}. For Castlereagh, θ_s covered a range of $0.071 - 0.468$ over the study period (Figure 3.1e). However, the underlying clay-loam layer provided a large water resource for the canopy, and so E_c was decoupled from θ_s and therefore no relationship was determined. Because the soil-profiles for each site were vastly different, no site-average response could be determined for θ_s. The site-specific parameters for θ_w and θ_c were still used as part of the site-average parameter set.

3.3.2.4 Relationship of model parameters with site characteristics

In order to investigate whether the model parameters vary across ecosystem as a function of site-defining characteristics, relationships were drawn for three of the MJS model's more critical parameters that are common across all sites (i.e. θ_s characteristics were not chosen). The site-specific model parameters of E_{cmax}, k_R, k_{D1}, k_{D2} and D_{peak} where therefore compared with BA, LAI and rainfall (Figure 3.2). In general, the site-specific parameters were found to have little or no linear relationship with BA, LAI or rainfall, with one exception. Site E_{cmax} and BA were highly correlated, but could not be described by a linear relationships unless the Pittwater site was removed from the regression ($P < 0.05$) (Figure 3.2a). This relationship was positive and E_{cmax} increased with increasing BA. Site E_{cmax} and LAI were positively correlated, but could not be described by a linear relationship even when removing the Pittwater site from the regression (Figure 3.2b). However, a trend of increasing E_{cmax} with increasing LAI is observable. Site E_{cmax} and

rainfall were negatively correlated, and could be described by negative linear relationship (Figure 3.2c). Removing the size factor (i.e. tree size) from the relationship between E_{cmax} and rainfall by dividing E_{cmax} by BA, did not improve the correlation. In the case of the site k_R parameter, no relationship was determined from BA, LAI or rainfall even when removing the Paringa site from the regression (Figure 3.2d-f). In the case of the k_{D1} shape parameter, no relationship was determined for BA or rainfall, but a direct positive relationship was found with LAI if the Pittwater site was removed from the regression ($P < 0.05$), such that k_{D1} increases with LAI (Figure 3.2g-i). No relationships were found between the k_{D2} shape parameter, BA, LAI and rainfall, even when removing the Pittwater site from the regression (Figure 3.2j-l); although this is not surprising as this parameter was subject to the largest σ_{se}. Similarly, no relationship between site D_{peak} and the site characteristics could be determined either (Figure 3.2m-o). On a final note, model parameters were plotted against site mean annual T_a, but no relationship was found in any case and so was omitted.

3.3.3 Model performance

The parameters in Tables 3.3 and 3.4, were used in the MJS model to determine site-specific model (SS) and site-average model (SA) estimates of E_c respectively. The SS and SA model estimates were compared with the measured data and a statistical benchmark constructed using the ANN at hourly and daily time scales. A comparison between modelled and measured estimates of E_c and the benchmark was done at the diurnal scale, by binning the data into monthly ensembles, that represents the mean diurnal course E_c for each month (Figure 3.3). Additionally, modelled and measured E_c and the benchmark was summed over the diurnal course to derive the daily course of E_c over the period (Figure 3.4), and for the entire time-series (Figure 3.6) to give a comparison of period total canopy water-use. Finally a regression analysis was performed for the SS and SA models and the benchmark (Figure 3.5), that statistics of which are given in Table 3.5..

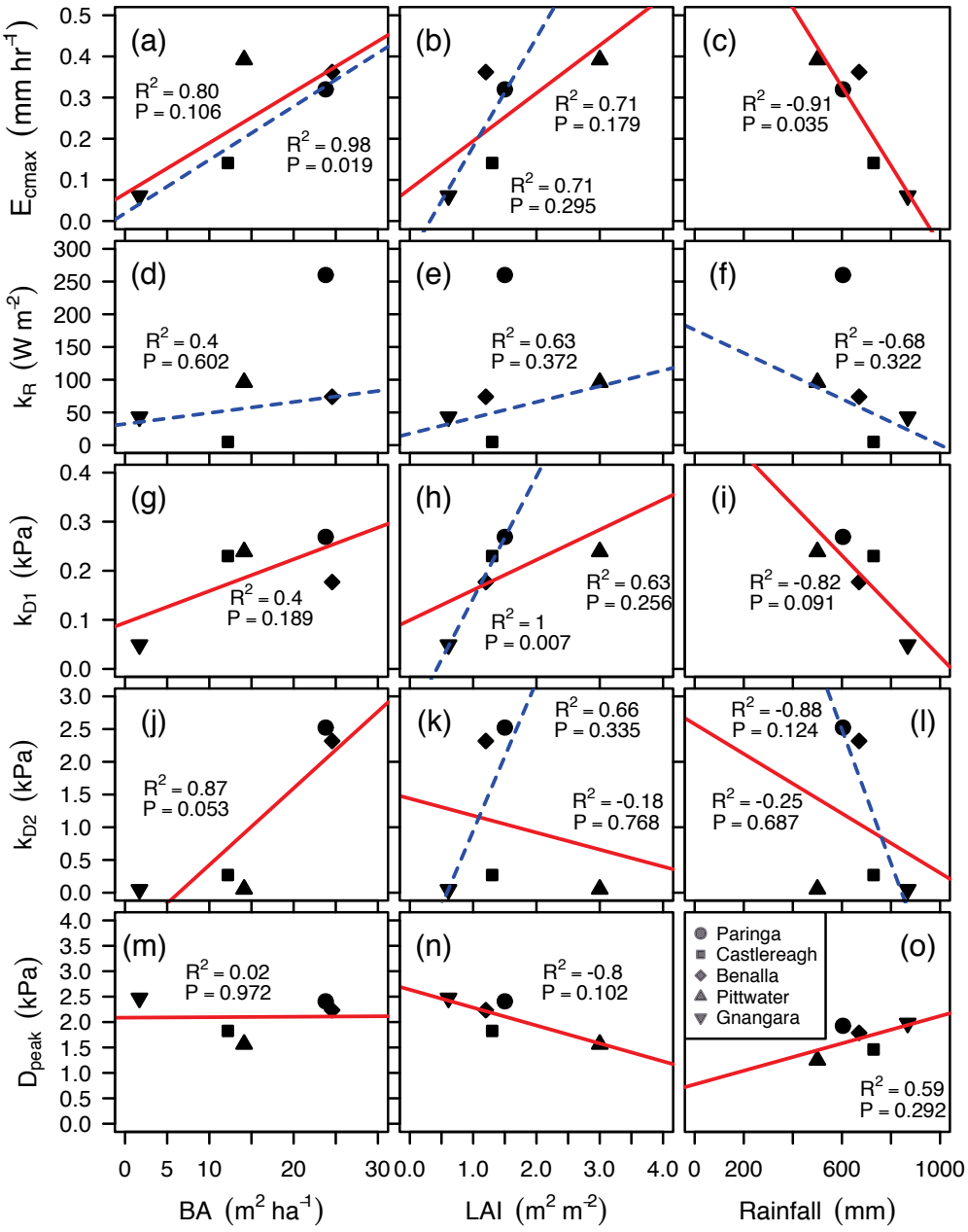

FIGURE 3.2: Relationships between the site potential-maximum transpiration rate (E_{cmax}) and (a) basal area (BA), (b) leaf area index (LAI), (c) rainfall; the site solar radiation response parameter (k_R) and (d) BA, (e) LAI, (f) rainfall; site vapour pressure deficit (VPD) shape parameter 1 (k_{D1}) and (g) BA, (h) LAI, (i) rainfall; site VPD shape parameter 2 (k_{D2}) and (j) BA, (k) LAI, (l) rainfall; site peak VPD (D_{peak}) and (m) BA, (n) LAI, and (o) rainfall. Symbols are represented for Paringa (●), Castlereagh (■), Benalla (♦), Pittwater (▲) and Gnangara (▼). Linear regressions were fitted with five (red line) and four (dashed blue line) sites, in order to determine relationships with the model parameters across site. The P values refer to the F tests of the null hypothesis that the regression coefficient is zero.

3.3.3.1 Paringa

For the Paringa site, both models gave a good approximation of the diurnal variation in measurement E_c within the regions of error (Figure 3.3a). Measured hourly E_c varied largely during the summer months (± 0.15 mm hr^{-1}), but less so in winter (± 0.08 mm hr^{-1}). Both models were able to capture this variation, with little difference in performance between models observed during the summer months; the exception being in Sep where the SA model fails to account for the afternoon decrease in E_c. Daily measured E_c varied largely over the study period between $0.8 - 2.7$ mm d^{-1} and both the SS and SA models were able to capture this variation (Figure 3.4a). The periods where the models failed to explained the measured data (14^{th} –22^{nd} Jan, 27^{th} –29^{th} Feb and 25^{th} –30^{th} Jul) could not be explained by the benchmark, and for these periods the models gave equivalent predictions to the benchmark. A regression analysis showed both models gave a comparable explanation of the measured data, producing regression lines close to the 1:1 line. The SS model performed only slightly better than the SA model, with the SA model subject to slight over- and under-estimation at high and low E_c respectively (Figure 3.5a). The SS model was able to explain 89% of the variance, with a high ME (0.79) and low RMSE (0.0015 mm hr^{-2}), while the SA model explained 87% of the variance, a high ME (0.72) and low RMSE (0.0060 mm hr^{-1}). Observed total period water-use was 111 mm and the benchmark predicted 112 mm. This SS model predicted a total of 91 mm, which under-estimated the observed total by 18%. The SA model gave a much closer prediction of 105 mm, under-estimating total water-use by only 5% (Figure 3.6a).

3.3.3.2 Castlereagh

For the Castlereagh site, both models were able to describe diurnal variation in measured E_c for the majority of the study period (Figure 3.3d). Over the course of the study period, measured hourly E_c was subject to both moderate (± 0.08 mm hr^{-1}) and large variations (± 0.12 mm hr^{-1}), the latter of which defined the May, Jun and Jul months. Both models and benchmark had difficulty capturing the mean diurnal response of measured E_c. Both models performed similarly, although the SA model tended to estimate the afternoon reduction in E_t to occur approximately 1 hr before the SS model; a result

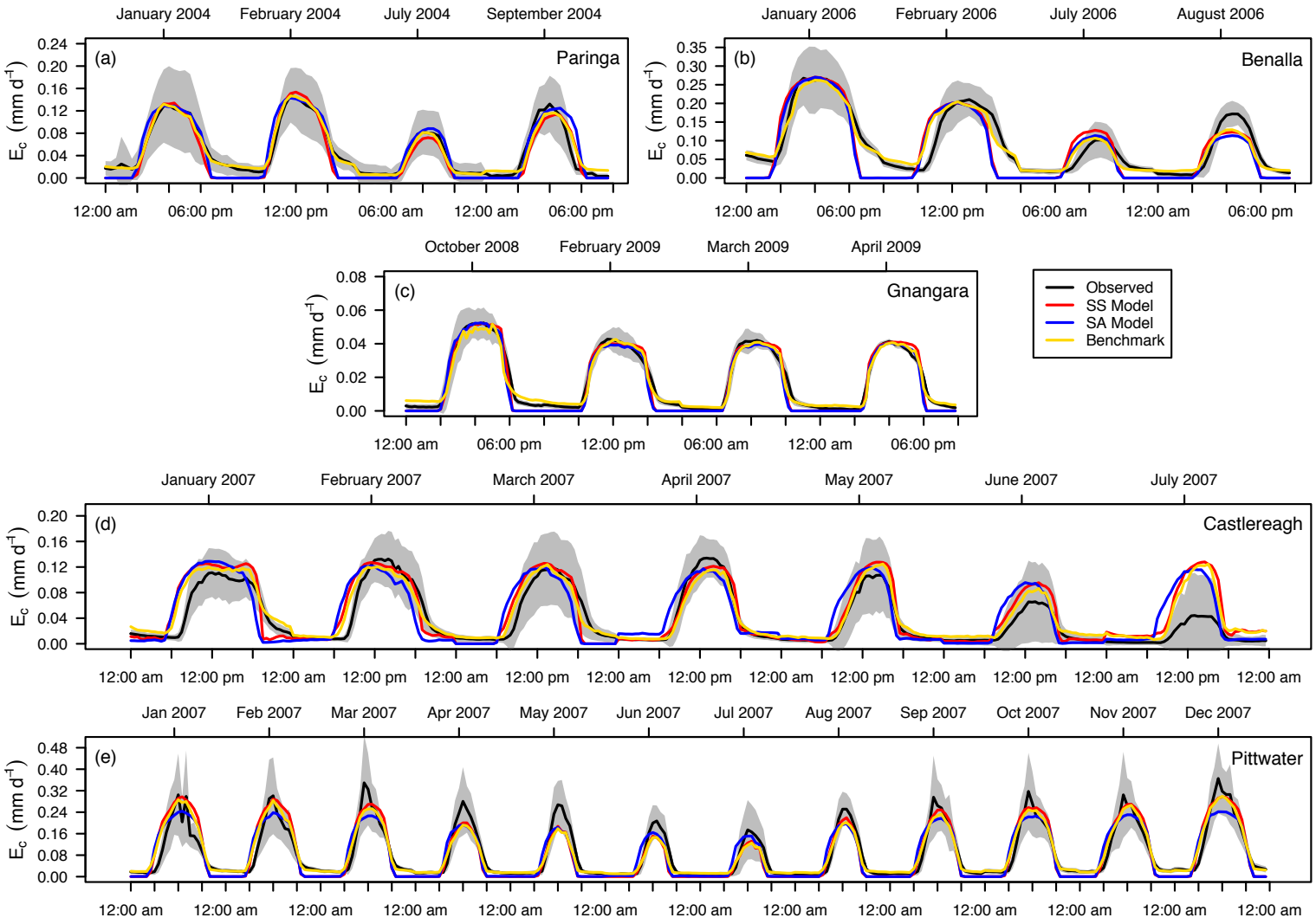

FIGURE 3.3: Monthly ensembles of mean measured canopy transpiration (E_c, black line) and the distribution of error around the mean (grey shaded region) for the (a) Paringa, (b) Benalla, (c) Gnangara, (d) Castlereagh, (e) Pittwater sites. The red and blue lines represent the modelled mean diurnal course of E_c using the site-specific (SS) and site-average (SA) model parameters respectively. The yellow line represents the best statistical fit that is possible by the MJS model using the meteorological data provided by each data-set; this statistical benchmark is constructed using the artificial neural network.

of small differences in the SS and SA response parameters. Additionally, the SS model was observed to follow the benchmark more closely. Periods of poor fitting are seen in Jan, Jun and Jul, where for the latter of these months, both models and the benchmark overestimated measured E_c significantly. Measured E_c tended to follow the diurnal trace of D_v, rather than R_s, which may explain the lack of synchronisation between modelled and measured. Measured daily E_c varied between $0.9-1.5$ mm d^{-1} over the study period, with large variations being due to cloud cover and rainfall events. The SS model overestimated measured E_c during the majority of Jan, early Feb, late April to early May and late June. In contrast to this, the SA model gave a slight, but consistent underestimation of measured E_c, with the exception of the mid-April to early May period were it was subject to overestimation (Figure 3.4b). The benchmark closely followed measured E_c, suggesting that variations in R_s and D_v are sufficient predictors. Despite the diurnal plots showing large overestimation in June and July for both models and benchmark, this was not translated when scaling up to the daily scale. A regression analysis show both models to give a reasonable explanation of the measured data, although they are subject to slight underestimation at low values of E_c (Figure 3.5b). The SS model was found to give the best fit to the data, explaining 83% of the variance, with a high ME (0.70) and low RMSE (0.0027 mm hr^{-1}), while the SA model did not perform as well explaining 68% of the variance, with a low ME (0.45), but retaining a low RMSE (0.0043 mm hr$_{-1}$). Observed period total water-use for this site was 198 mm, and the benchmark predicted total was 199 mm. The SS model was able to reach within 1% of the observed total by predicting total water-use to be 200 mm. The SA model did not perform as well, predicting a total water-use of 189 mm, 5% less than that observed total (Figure 3.6b).

3.3.3.3 Benalla

For the Benalla site, both the models and the benchmark were not able to provide a good description of measured E_c over the study period. The hourly variation in measured E_c was large in summer at the beginning of the study period ($\pm$0.08 mm hr^{-1}), but decreased moving into winter ($\pm$0.10 mm hr^{-1}) (Figure 3.3b). A good agreement between modelled and measured was observed for Jan. However, for the months following (Feb, Jul),

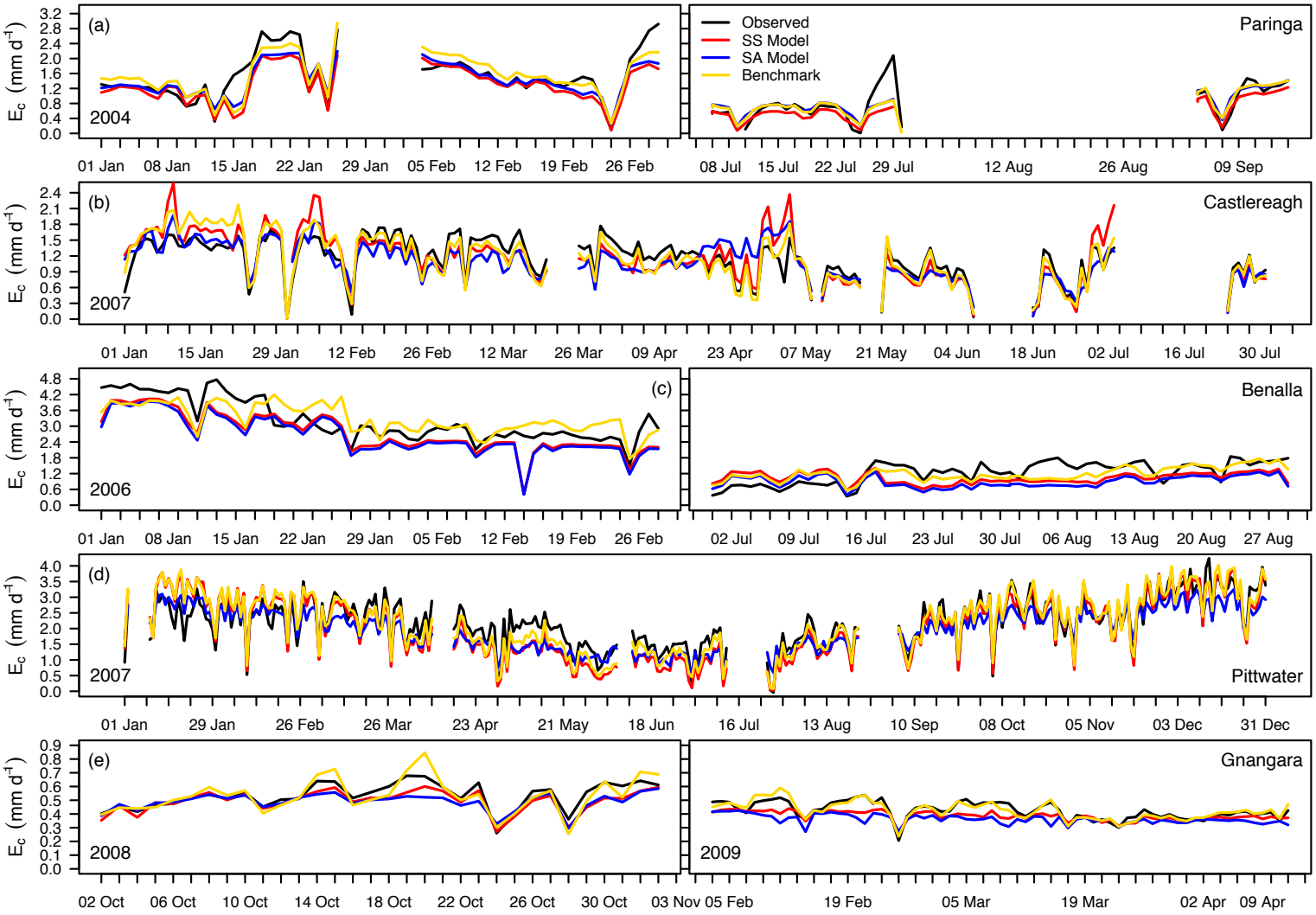

FIGURE 3.4: Time-series of the daily sum of measured and modelled canopy transpiration (E_c) for the (a) Paringa, (b) Castlereagh, (c) Benalla, (d) Pittwater and (e) Gangarra sites. The black line represents the daily time-course of measured E_c, while the red and blue lines represent the daily time-course of modelled E_c using the site-specific (SS) and site-average (SA) model parameters respectively. The yellow line represents the best statistical fit that is possible by the MJS model using the meteorological data provided by each data-set; this statistical benchmark is constructed using the artificial neural network.

modelled E_c was out of synchronisation with the measured data by approximately 1 hr, although by Aug this effect had disappeared. This is likely due to the k_R value being too low during these months. Both models were highly comparable in performance as a result of similar response parameters and followed the benchmark closely over the monthly diurnal courses. Modelled E_c traced R_s and therefore went to 0 during nocturnal hours, while the benchmark and measured values remained above 0 for a few hours after sunset, suggesting significant nocturnal transpiration at this site. The day-to-day variation of measured E_c was large, having a range of $0.6 - 4.6$ mm d^{-1} over the study period (Figure 3.4c). Both the models and benchmark failed to accurately capture this variation, with the models underestimating measured E_c for the majority of the study period and the benchmark predominantly overestimating E_c. The disparity between modelled and measured may be a factor of measurement error in the data-set, as the benchmark has difficulty producing the measured E_c signal from the given meteorological data. A regression analysis showed that the SA model provided a slightly better statistical fit to the data compared to the SS model, although both were subject to slight under-estimation at low values of E_c (Figure 3.5c). The statistical performance of the SA model matched closely with the benchmark. However, the benchmark did not give a reasonable explanation of the data, so this comparison is not very informative. The SS model was able to explain 77% of the variance, with a moderate ME (0.53) and moderate RMSE (0.0280 mm hr^{-1}). The SA model achieved slightly better statistics, explaining 81% of the variance, with a larger ME (0.61) and lower RMSE (0.0164 mm hr^{-1}). The observed total water-use for the period was 266 mm and was equally matched by the benchmark, which calculated the same total. However, a comparison of these totals is misleading as the benchmark could not accurately replicate the observed variations in measured E_c. Period total water-use predicted by the SS model was 241 mm, under-estimating the observed total by 9%, while the SA model predicted a total of 222 mm, under-estimating the total by 17% (Figure 3.6c). The lower predicted total by the SA model was a consequence of slightly lower estimates predicted during the Jul and Aug periods.

TABLE 3.5: Regression statistics for the site-specific, site-average models and the statistical benchmark that was determined using an artificial neural network (ANN) applied at each of the five sites. Listed are the R^2, the root mean-square error (RMSE; mm hr^{-1}), model efficiency (ME), and the number of data points (at the hourly time-step) that the data-sets consisted of (N).

	Site Specific			**Site Average**			**Benchmark**			
Site	R^2	RMSE	ME	R^2	RMSE	ME	R^2	RMSE	ME	N
PARINGA	0.89	0.0015	0.79	0.87	0.0060	0.72	0.90	0.0014	0.80	2616
CASTLEREAGH	0.83	0.0027	0.70	0.68	0.0043	0.45	0.85	0.0050	0.70	5088
BENALLA	0.78	0.0280	0.53	0.81	0.0164	0.62	0.81	0.0007	0.66	2904
PITTWATER	0.75	0.0067	0.55	0.70	0.0153	0.41	0.77	0.0122	0.58	8760
GNANGARA	0.91	0.0017	0.81	0.86	0.0023	0.68	0.87	0.0011	0.73	2424

3.3.3.4 Pittwater

At the Pittwater site, the SS and SA models performed reasonably well in estimating measured E_c. Diurnal variations in measured E_c were large over the study period (± 0.20 mm hr^{-1}). Additionally, the diurnal pattern in measured E_c was asymmetrical, displaying evident mid-morning peaks (Figure 3.3d). Both models were able to replicate the mean diurnal course of measured E_c for the majority of the study period, with the exception that it was not able to replicate the mid-morning peaks in E_c that were observed for the spring (Sep, Oct, Nov) and summer (Dec, Jan, Feb, Mar) months. These peaks reached between $0.40 - 0.48$ mm hr^{-2}, which was much higher than the determined value of E_{cmax} for this site (0.39 mm hr^{-1}). Additionally, the benchmark could not explain the cause of these peaks based on the intra-daily variations of R_s and D_v. Both models and benchmark under-estimated measured E_c from Mar to Jun, but gave a reasonable replication of mean E_c for all other months. The day-to-day variation in measured E_c was large, having a range of $1.0 - 3.5$ mm d^{-1}. Daily estimates of modelled and statistically determined E_c gave a close approximation to daily measured E_c (Figure 3.4d). However, the SA model slightly, but consistently, under-estimated measured E_c for much of the period. The Mar to Jun period was observed to have the largest degree of underestimation, which may be explained by high frequency of rainfall events during this period. A regression analysis showed both models were able to explain the measured data with little bias. However, the SA model is subject to an increasing underestimation as E_c increases, which is not evident

in the other models (Figure 3.5d). The SS model performed slightly better than the SA model, explaining 75% of the variance, having a moderate ME (0.55) and low RMSE (0.0067 mm hr^{-1}), while the SA model explained 70% of the variance, having a lower ME (0.41) and larger RMSE (0.0153 mm hr^{-1}). Observed total period water-use for this site was relatively high at 718 mm and this was closely matched by the benchmark at 713 mm. The SS model predicted a total period water-use of 667 mm, which under-estimated the observed total by 7%. while the SA model predicted a lower period total of 643 mm which, under-estimating the observed total by 10% (Figure 3.6d)

3.3.3.5 Gnangara

For the Gnangara site, both models performed well in explaining measured E_c. Measured E_c was observed to vary little over the study period ($\pm$0.02 mm hr^{-1}), and this variation decreased with time (Figure 3.3e). Both models were able to replicate diurnal variations in measured E_c, well within the small region of error. For this site, measured E_c was observed to be highly coupled with R_s, although some nocturnal transpiration was evident. Daily E_c was relatively constant over the study period, having a small range of $0.4 - 0.6$ mm d^{-1} (Figure 3.4e). At the daily scale, the SS model performed slightly better than the SA model in predicting measured E_c, although both models underestimated E_c over the Feb to mid-Mar period. Additionally, both models underestimated E_c over 4 days in the Oct period (16^{th} –20^{th}), the benchmark also failed to explain E_c. A regression analysis showed both models to display a high statistical performance, with regression lines showing both models and benchmark to be subject to some slight under-estimation at low values of E_c (Figure 3.5e). The SS model was able to explain 91% of the variance, with a high ME (0.81) and low RMSE of (0.0017 mm hr^{-1}), while the SA model performed equally well, explaining 86% of the variance, with a high ME (0.68) and low RMSE (0.0023 mm hr^{-1}). Observed total period water-use for this site was relatively low at 46 mm, which was matched by the benchmark. The SS model predicted a period total of 40 mm, under-estimating the observed total and benchmark by 13%, while the SA model predicted a near equal amount to the SS model at 39 mm, which under-estimated the observed total and benchmark by 15% (Figure 3.6).

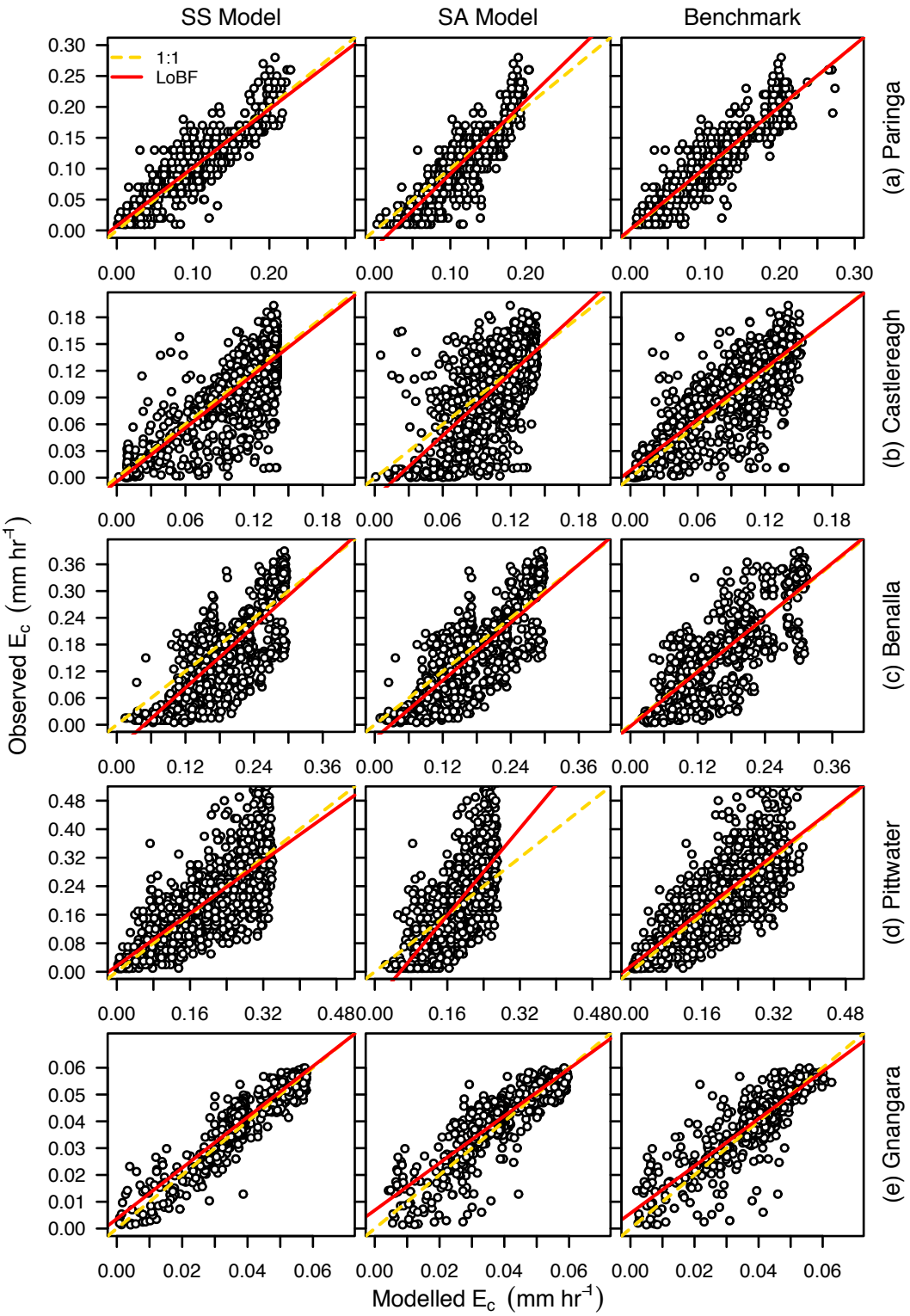

FIGURE 3.5: Regression plots showing the relationship between measured canopy transpiration (E_c) and modelled E_c for the (a) Paringa, (b) Castlereagh, (c) Benalla, (d) Pittwater and (e) Gnangara sites. Regression plots are shown for modelled E_c using site-specific and site-average model parameters. Additionally, regression plots for the statistical benchmark constructed using the artificial neural network are shown for each site. The red line indicates the line of best fit (LoBF) and the yellow line represents the one-to-one (1:1) line between the modelled and measured quantities.

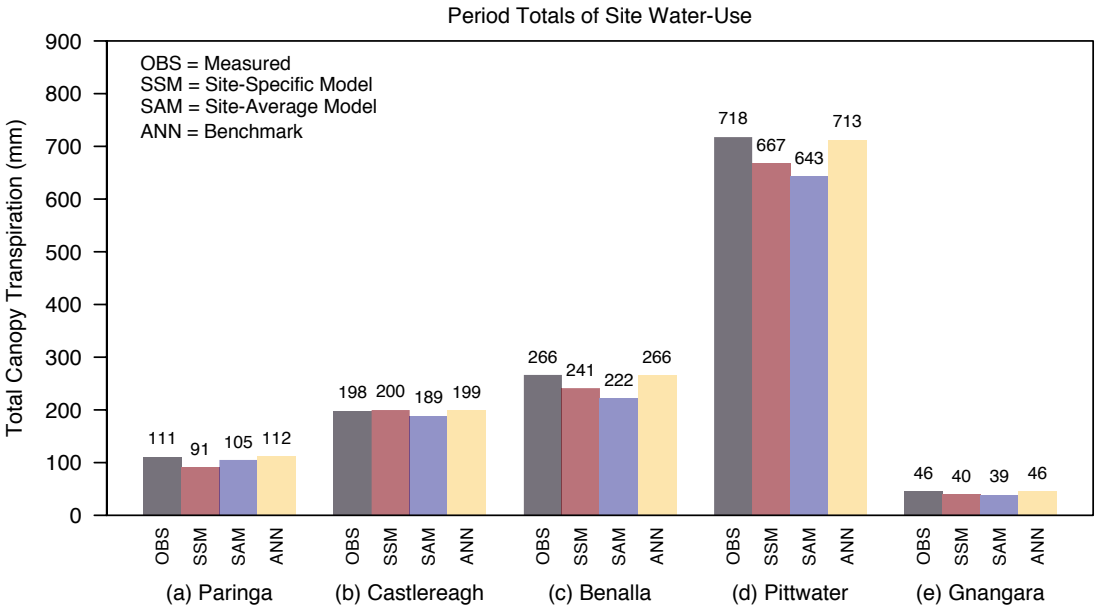

FIGURE 3.6: A comparison between the period totals of measured and modelled canopy transpiration (E_c) for the (a) Paringa (4 months), (b) Castlereagh (6 months), (c) Benalla (4 months), (d) Pittwater (1 year) and (e) Gnangara (2 months) sites. Total measured E_c (OBS) is shaded grey, while total modelled E_c using site-specific (SSM) and site-average (SAM) model parameters are shaded in red and blue respectively. The statistical total of estimated E_c derived from an artificial neural network (ANN) is shaded in yellow.

3.4 Discussion

The MJS model was parameterised individually for each data-set corresponding to one of five sites used in this study. This resulted in model parameters that described the responses of E_c to variation in R_s and D_v that were specific to each site. Using these *site-specific* model parameters, E_c was determined at the diurnal time-scales and was in high agreement with the measured data (SS model). The model was then parameterised across all five sites, to determine a set of model parameters that described the mean response of E_c to variations in R_s and D_v for all sites (SA model). Despite a disparity in value between the site-specific and site-average model parameters, a mean response was capable of determining a site's E_c with a reasonable degree of accuracy. Comparing the performance of the model using site-specific and site-average parameters at each site showed there was little observable difference in the modelled estimates of E_c; both sets of model parameters were sufficient to describe the diurnal (within day) and day-to-day

variations. This potentially reduces the number of model parameters that need to be identified in order for the model to applicable to a specific site, leaving only E_{cmax}, θ_w and θ_c to be determined by the user. Although there may be difficulty in assessing what E_{cmax} should be, θ_w and θ_c can be determined from field measurements of θ_s made over a reasonable period. Potential links between E_{cmax} and site variables, that offer a possible way for its determination are covered at the end of this section.

3.4.1 Model performance across the five sites

Application of the MJS model to the Paringa data-set resulted in few minor problems, and was predominantly similar to the results shown in Chapter 2 despite using a different D_v response function in the model. Using site-average parameters gave a much closer prediction of total water-use compared to using the site-specific parameters. However, this was due to slight but consistent over-estimation of daily E_c; using site-specific parameters also produced a better statistical fit to measured E_c. Model performance at the Castlereagh site, was generally high, although the site-specific parameters gave a better statistical fit to the measured data. The lower site-specific k_R value compared to the site-average one, allowed a stronger coupling between E_c and D_v, and may be why modelled E_c using site-average parameters resulted in a consistent underestimation. Although sufficient water could be accessed from the deeper clay layers, E_{cmax} was the lowest of all sites and this may be attributed to tighter stomatal regulation as a consequence of high D_v and infrequent rainfall, which have not been entirely captured in this study period (Zeppel et al., 2008a). This may also be a function of the low hydraulic conductance of clay, which could limit the rate of supply of water to the roots.

Evaluating model performance for the Benalla site was difficult, as the ANN, although capturing the mean diurnal response, could not capture the day-to-day variations of E_c. Modifying the size (or nodes) of the ANN SOFM and adding extra variables (such as T_a), did not improve the performance of the benchmark. The difficulty in producing a statistical benchmark that explains measured E_c may be a consequence of atypical circumstances that this site was subject to during the study period that could not be described by R_s, D_v and θ_s; for example, a reduction in leaf area through disease. The MJS model had to

describe a transition between a seasons of high and low θ_s that is not usually observed at this site (Yunusa et al., *unpublished data*). The year before the study was conducted, the site experienced higher than average rainfall that would have recharged the soil profile substantially. Consequently this allowed higher than average E_c to operate for a limited period, where part of this period has been captured in the Jan-Feb data. However, by the Jul-Aug period, E_c had declined to perceived normal rates (Yunusa et al., *unpublished data*), although θ_s had changed only marginally. Although both model and benchmark were able to capture this decline in E_c over the study period, both failed to account for the day-to-day variation.

The MJS model statistically performed the poorest at the Pittwater site and this was due to the large diurnal variations in measured E_c that was observed over the study period. Additionally, the Pittwater data-set was the largest and encompassed an entire year and was therefore subject to larger seasonal variations in E_c compared with the other sites. Seasonal variation in E_c followed R_s and T_a (and consequently D_v) rather than θ_s, which remained low ($\approx 0.02 - 0.03$ m^3 m^{-3}) over the study period. Sufficient water stores were therefore likely accessed from shallow ground water (O'Grady, *personal correspondence*). This influenced the high E_{cmax}, as well as the site having a high density of trees per ha, allowing the Pittwater site to maintain a high rate of canopy water-use over the study period. Additionally, the Pittwater site was also well fertilised in contrast to the other sites, and this allowed the maintenance of an extremely high LAI (O'Grady et al., 2008). The lower performance of the SA model was due to the D_v function, $f_2(D_v)$, being unable to correctly describe the response of E_c at low D_v, and resulted in an underestimation in the first half of the study period. The MJS model had the highest statistical performance at the Gnangara site, due to the relatively constant rate of canopy water-use over the study period. Compared with other sites, E_c was the lowest at this site, due to low LAI, a very sandy soil profile and little to no rainfall (that was recorded). As is seen at the Pittwater site, the lower performance of the SA model appears to be due to $f_2(D_v)$ incorrectly describing E_c at low D_v.

Comparing model performance across site, the drop in performance evident at Pittwater is due to a more variable climate that is a result of a longer study-period capturing more day-to-day and seasonal variability, which in contrast to Gnangara experiences a static climate

and covers a shorter time-series. Although the Paringa and Benalla data-sets are of a similar length, they encompass contrasting seasons, where R_s and D_v are very different, and so modelled E_c is subject to larger error. Also, for some of the sites, there was a clear lack of synchronicity between diurnal modelled and measured E_c, which approximated to a lag of 1 hr. This is likely due to the magnitude of the k_R parameter and for cases where the lag is present, the k_R value is too low. This lag may also represent a contribution of stored water in the stem entering the sap-flow, as been observed in other studies (Goldstein et al., 1998; Cermak et al., 2007). This is seen for sites at Benalla (Figure 3.3b; Feb, Jul), Castlereagh (Figure 3.3d; Jan-Apr) and Pittwater (Figure 3.3e; Jan-Feb), where the rate of increase in E_c towards saturation is too high. Despite some of the issues raised above, the MJS model displayed a high degree of statistical performance across all site using both site-specific ($R^2 = 0.75 - 0.91$; ME $= 0.53 - 0.81$; RMSE $= 0.0015 - 0.0280$ mm hr^{-1}) and site-average ($R^2 = 0.68 - 0.87$; ME $= 0.45 - 0.72$; RMSE $= 0.0023 - 0.0164$ mm hr^{-1}) model parameters. Additionally, both SS and SA models were capable of operating close to the statistical benchmark ($R^2 = 0.77 - 0.90$; ME $= 0.58 - 0.80$; RMSE $= 0.0007 - 0.0122$ mm hr^{-1}) and even matching it in some cases. This resulted in estimates of period total canopy water-use that was within a reasonable percentage ($\approx 10\%$) of the measured total.

3.4.2 The response of canopy water-use to solar radiation and vapour pressure deficit among species

Differences in sensitivity of E_c to variation in R_s and D_v among species were observable at the Castlereagh and Benalla sites. Species-specific model parameters varied between species, with the largest variation seen for the E_{cmax}, k_R and D_{peak} parameters. At the Castlereagh site, the *E.sclerophylla* trees had a lower D_{peak} value, but higher k_R value compared with the *A.bakeri* trees. At the Benalla site, the *E.camaldulensis* trees had a lower D_{peak} value, but higher k_R value compared with the *E.microcarpa* trees. This suggests that tree species with a low D_{peak} and high k_R tended to have a lower E_{cmax}, although not always significantly lower. These differences tend to suggest differing stomatal sensitivities to R_s and D_v among species that partially effect their E_{cmax}. A hypothesis can be proposed that a smaller E_{cmax} may be the result of a tighter stomatal regulation due to a higher sensitivity to D_v. This can be supported by leaf-scale measurements for

these species measured at this site by Zeppel et al. (2008a). The authors observed that the *A.bakeri* species has a higher pre-dawn leaf water potential ($\Psi_{pd} = -0.96$ MPa), a higher minimum leaf water potential ($\Psi_{lmin} = -1.88$ MPa) and larger whole plant conductance ($g_{plant} = 5.04$ mmol s^{-1} m^{-2} MPa^{-1}) when compared with the *E.camaldulensis* species ($\Psi_{pd} = -1.77$ MPa; $\Psi_{lmin} = -2.56$ MPa; $g_{plant} = 2.22$ mmol s^{-1} m^{-2} MPa^{-1}) for this site. This relationship is similarly seen at the Benalla site with *E.camaldulensis* maintaining a tighter stomatal control on E_c than *E.microcarpa*, such that a high D_{peak} and low k_R tends to suggest an ability to maintain a larger E_{cmax}. This is supported by *E.microcarpa* having a much higher observed canopy conductance ($g_c = 4.46$ mm s^{-1}) than *E.camaldulensis* ($g_c = 2.56$ mm s^{-1}) (Yunusa et al., *unpublished data*). These comparison also agree with Oren et al. (1999) in that different species have different the stomatal sensitivities. Although this may suggest a relationship between E_{cmax}, k_R and D_{peak}, no such relationship could be found in the present study as there were only 4 data points. Meinzer (2003) argues that all species converge towards the same physiological response curve at a site, and that different species may exert the same stomatal sensitivity to variation in D_v. However, such a conclusion could not be drawn here. The above comparisons of parameter values for the 2 species at the 2 sites, shows the possibility of one species to be more sensitive to either R_s or D_v. This suggests a convergence in behaviour through *different* mechanisms, rather than a convergence in sensitivity. It appears that the stand response of E_c to variations in R_s and D_v is an *average* of the response of the 2 species occupying the stand; although in the case of k_R parameter, it appears to be weighted towards the species with the lower D_{peak} value. However, there is not enough data to conclude that this averaging is indeed the convergence Meinzer describes. In order to test Meinzer's hypothesis, parameter values would have to be drawn for individual sites with a highly diverse range of species comprising the stand, as this would eliminate uncertainty due to variation among site-specific characteristics, such as LAI, BA and soil type.

3.4.3 The response of canopy water-use to solar radiation and vapour pressure deficit across sites

As well as varying among species at a site, the MJS model parameters were also shown to exhibit significant variance across ecosystems. Factors that may cause variation in these

parameters were tree size and density of the trees in the stand, vegetation cover, climate and soil particle size distribution (PSD). Although all model parameters (excluding θ_s ones) were compared across sites, relationships between the E_{cmax} parameter and site defining characteristics were deemed the most important, and while the same response of E_c to the environmental driving variables can be assumed across different sites and species, the magnitude of E_c is still site-specific.[4]

A relationship between E_{cmax} and BA was statistically significant across sites, and this agrees with the relationship between transpiration and tree size that has been observed in many other studies (i.e. Granier et al., 1996a, 2000; Whitehead, 1998; Goldstein et al., 1998; Ryan et al., 2000; Zeppel et al., 2008b). Additionally, a significant negative relationship was found between E_{cmax} and rainfall. However, it is debatable whether any true relationship between these quantities can be established, as a high E_{cmax} does not dictate a site that experiences high rainfall. Using the Gnangara site as an example, the site receives a large annual rainfall ($700 - 800$ mm annuallly), but is defined by a short and sparse vegetation cover (LAI $= 0.6$) sitting on a very sandy soil profile. Additionally, given the low LAI, the site is also likely to be limited by low nutrient availability. The site is characterised by distinct wet (winter) and dry (summer) seasons, where rainfall events are small and do not penetrate deeply into the soil profile. Additionally, sites such as Castlereagh and Pittwater have canopies that rely on access to abundant water resources through shallow aquifers or saturated clay layers, rather than soil water in the upper profile. It is therefore likely that E_{cmax} and rainfall are not coupled for all sites despite the high correlation observed here. Finally, a positive relationship between site E_{cmax} and LAI was evident, although not statistically significant. The relationship here is likely to be nonlinear rather than linear, where E_{cmax} saturates after a given LAI (≈ 1.5); a consequence of increased shading with the increase in LAI (Caldwell et al., 1986). Fitting an asymptote to the data points in Figure 3.2 did not improve the regression, a result likely due to a lack of data-points (or sites). However, the correlation observed, shows a relationship is likely to exist and this is supported by studies which have shown that LAI has a strong influence on E_c over the medium term when θ_s is high (Oren and Pataki, 2001; Wullschleger et al., 2001). The most likely reason for the problems in determining a relationship among E_{cmax}

[4] Although the same can be said for the θ_s and θ_c, these variable are subject to a much larger variation and are really only comparable for very similar sites.

and the site characteristics is due to a lack of data (or more precisely, a lack of sites). In order to better investigate why E_{cmax} may vary across ecosystems, a large number of sites (i.e. > 15) is ideally needed to better establish the variation in this parameter. The relationships between E_{cmax}, BA and LAI offer a way of explaining the variation in E_{cmax} across sites that is similar in structure to way the site-average parameters were derived. Such that a modification can be made to the MJS model so that the E_c across all sites may be explained as:

$$E_c = \{E_{cmin} + f(BA)\}\ f(R_s)f(D_v)f(\theta_s) + \varepsilon \tag{3.13}$$

or

$$E_c = \{E_{cmin} + f(LAI)\}\ f(R_s)f(D_v)f(\theta_s) + \varepsilon \tag{3.14}$$

where E_{cmin} is the residual amount of transpiration that occurs at each site. However, such an approach requires that sufficient information on the BA or LAI of a site be known, the measurements of which are not frequently collected.

No significant relationship was observable between the parameters k_R, k_{D1}, k_{D2} and D_{peak}, and the site characteristics of BA, LAI and rainfall, with the exception of k_{D1} and LAI. The k_R and k_{D2} parameters were subject to the largest σ_{se} and consequently made it difficult in identifying relationship with the site characteristics. Removing the Pittwater site in a few cases improved the correlation and regression line, although this did not translate in a statistically significant slope in all cases. Removing the Pittwater site from these regression can be justified, as it is a plantation rather than a native forest and is subject to a degree of control through the choice of species and tree density per hectare. It is likely that these model parameters are moderately insensitive to variation in value among sites, as a result of being drawn from wide distributions. Consequently the site-average parameter values are likely to be falling within 1–2 standard deviations of the site-specific parameter values and therefore sufficient to describe the site-specific response of E_c to R_s and D_v. Deviation in site-average parameter values outside the error of the site-specific values can be observed in the R_s function at the Castlereagh site. Here the site-average k_R falls outside the site-specific distribution of possible k_R values, and tries to fit a nonlinear response of E_c to light when there is close to no response at all. This is the likely reason

why the SA model performed the worst at this particular site, when compared with others. However, in contrast to this, the Paringa site displays a large difference between the site-specific and site-average k_R values. This difference is just over 100%, but did not greatly reduce model performance. However, the site-specific k_R is subject to a large degree of error ($\sigma_{se} = 36\%$) and so values much lower are likely to perform just as well. Despite a great degree of variation between site-specific and site-average parameter values being observed, using site-average parameters still gave a favourable outcome in estimating site E_c. Mäkelä et al. (2008) have used the same empirical approach in modelling gross primary productivity (GPP) across sites in Finland and attempted to determine the relationships between their model parameters and geographical location (latitude). Similar to the results of this study, Mäkelä et al. (2008) found that the response of GPP to variation in the environmental drivers could be describe by an average response. Additionally, the authors could not determine statistically significant relationships between model parameters and site-defining-characteristics, with the exception of their D_v parameter that varied with latitude. Their study, coupled with the one presented in this chapter shows the potential of using empirical Jarvis-type models for other gas-exchange fluxes.

On a final note, the success of the site-average parameters and the relative insensitivity of the model to variations in their values suggests that all sites may converge toward the same sensitivity of E_c to R_s and D_v. Considering that large variations in the magnitude of E_c across sites is related to site characteristics, a hypothetical response surface was constructed to describe the average functional response of canopy water-use to variation in light and evaporative demand (Figure 3.7). This response surface is created using Equations 3.3 and 3.5 and the site-average parameters derived from the pooled data-set of all five sites. The response of E_c to simultaneous variation in R_s and D_v may therefore characterise a response surface shared by multiple ecosystems. The topography of this response surface will shift due to site specific characteristics such as woody density, sapwood area and stem water storage capacity of the species constituting the stand (O'Grady et al., 2009). This topography suggests that on average, the ideal meteorological conditions that maximises E_c is in the mid-to-high range of R_s and low-to-mid D_v. This would represent the mid-morning to mid-day period which that can be generally identified in these data-sets to be the time when $E_c \rightarrow E_{cmax}$, after which E_c declines due to stomatal regulation

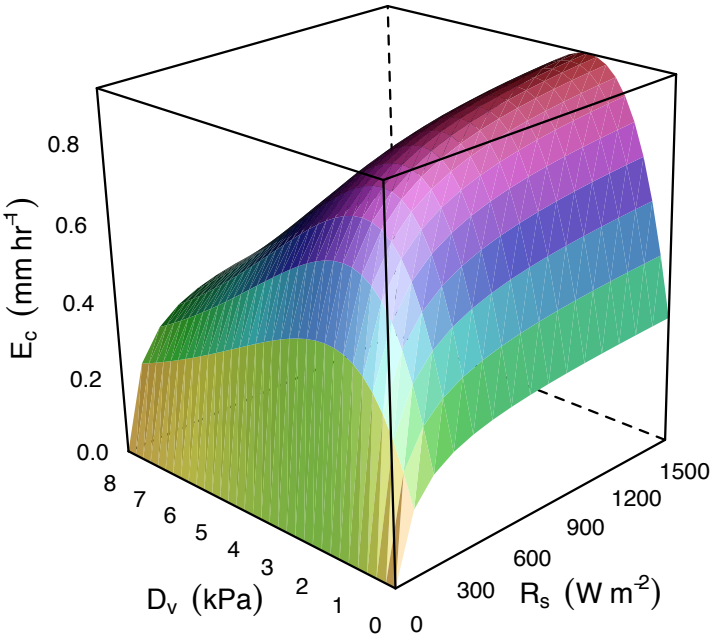

FIGURE 3.7: Representitive response surface of normalised canopy transpiration (E_c) to variation in solar radiation (R_s) and vapour pressure deficit (D_v), where the shape of the response curve is subject to change due to variations in site defining characteristics, such as leaf area index, basal area and soil type. The response surface was constructed using Equations 3.3 and 3.5.

to prevent xylem embolism (Tyree and Sperry, 1988).

3.5 Conclusion

This study has shown that a simple empirical model that is driven by solar radiation, vapour pressure deficit and soil water content, with a set of parameters that are not specific to an ecosystem, is able to explain hourly and day-to-day variation in stand transpiration for five Australian native forests to a reasonable degree of accuracy. The degree of performance was found to be consistent across the five sites used in this study, with only a slight drop in performance when using site-average parameters. Additionally, both site-specific and site-average parameterisations were comparable to a statistical benchmark that was created using an artificial neural network. Three of the five sites were limited

by soil moisture, while the other two sites had access to soil water stores through the presence of shallow aquifers or saturated clay layers. These results indicate that the responses of canopy water-use to available energy and evaporative demand are similar across sites indicating convergence in behaviour, with only the magnitude of water-use and soil water characteristics largely varying across ecosystems. Finally, period totals of modelled canopy water-use closely matched observed totals, showing the potential for the modified Jarvis-Stewart model to be used as a water management tool.

Chapter 4

Investigating C_3 and C_4 gas-exchange in a savanna ecosystem in northern Australia using a Soil-Plant-Atmosphere model

4.1 Introduction

Savannas are a significant component of the world's land surface, covering an area larger than that of wet tropical rainforests (15 x 10^{12} m^2; IPCC 2007). They are continentally and globally important to the carbon cycle, are major determinants of regional water budgets and have high conservation, social, cultural and economic value (Eamus and Prior, 2001). Savannas, also known as open woodlands, grassy woodlands, miombo, cerrado, chaco and caatinga (Eamus and Prior, 2001) consist of a discontinuous tree canopy above a continuous herbaceous layer, predominantly comprised of C_4 grasses. Within Australia, savannas cover approximately 25% of the land area (Hutley et al., 2000) and consequently make a significant contribution to the water and carbon cycle of Australia.

The savannas of northern Australia experience a monsoonal climate, with distinct wet (accounting for approximately 95% of the rainfall) and dry season. Seasonality is a significant factor influencing productivity and water-use of tropical ecosystems. For instance, seasonal reductions in water and carbon fluxes in a Brazillian rainforest have been observed as a result of increased the soil-root hydraulic resistance during the dry season (Williams et al., 1998). Similar reductions in water and carbon fluxes have been observed in west African Sahelian savannas (Verhoef et al., 1996; Hanan et al., 1998) and Brazillian cerrado (Miranda et al., 1997), following decreasing soil water availability and increasing evaporative demand between the wet to dry seasons. This seasonality can cause the savannas to cycle between being a carbon sink and carbon source over an annual period (Kanniah et al., 2010a). In northern Australia, savanna wet season productivity creates a carbon sink of between 0.1 and 0.2 mol C m^{-2} day^{-1}, but photosynthetic activity declines during the dry season and vegetation may become a source of carbon due to disturbance regimes such as fire (Chen et al., 2003; Beringer et al., 2007; Kanniah et al., 2010a,b).

The seasonality of savanna water-use varies along rainfall gradients, but generally declines between wet and dry seasons (Kelley et al., 2002). However, tree canopy water-use declines very little between wet and dry seasons, due to tree roots accessing ground water stores (Cook et al., 1998; O'Grady et al., 1999; Eamus et al., 1999, 2000; Hutley et al., 2000). Seasonality in productivity and water-use is often attributed to stomatal closure, increases in evaporative demand and leaf loss during the dry season (Eamus and Prior, 2001), but gas exchange is limited by a reduced stomatal conductance (g_s) in the afternoon in both seasons (Eamus et al., 1999; Chen et al., 2003). Furthermore, plant available water is determined by root access to soil moisture and influences annual carbon and water fluxes because soil water availability and atmospheric water content interacts with g_s (Thomas et al., 1999b, 2000; Ju et al., 2006). Coupling between seasonal rainfall patterns (and therefore soil water availability), savanna water-use and productivity has been observed at the leaf (Eamus et al., 1999), canopy (Eamus et al., 2001) and ecosystem scales (Chen et al., 2003). Additionally, while evidence suggests that plant available nutrients and fire are also key environmental factors that are responsible for savanna structure, function and dynamics (Beringer et al., 2007; Kanniah et al., 2010a), soil water availability has been

seen as the major determinant for savanna ecology in northern Australia, while fire and nutrients (although still significant) are seen as secondary (Hutley et al., 2000).

Approximately three quarters of the annual carbon flux of northern Australian savannas occurs during the wet season when the grasses often account for more than half of the total ecosystem leaf area index (LAI) (Williams et al., 1997; Eamus and Prior, 2001; Hutley et al., 2005). In contrast to this, the grasses may contribute a smaller percentage to total savanna water-use compared with the tree canopy, because C_4 vegetation is highly water-use efficient when compared to C_3 vegetation (Collatz et al., 1998). Stable isotope analysis of a Brazillian savanna suggests that approximately 40% of the annual net primary productivity (NPP) may have originated from C_4 grasses, even though the LAI of grasses was only 0.4 and 0.2 for the wet and dry seasons respectively and g_s of the C_4 grasses was equivalent to that of the C_3 trees (Miranda et al., 1997).

While C_4 grasses are a major carbon sink when they are active (the wet season), their contribution to whole ecosystem carbon uptake has been observed in only a few studies (Mordelet and Menaut, 1995; Miranda et al., 1997). There have been many studies to quantify savanna carbon and water fluxes in Australia at both leaf (Prior et al., 1997, 2004; Prior and Eamus, 1999; O'Grady et al., 1999, 2000; Eamus and Prior, 2001) and tree canopy scales (Eamus et al., 2000, 2001; Hutley et al., 2000, 2001, 2005; Kelley et al., 2002, 2007; Beringer et al., 2007). Additionally, these studies have been expanded upon by modelling carbon and water fluxes to investigate savanna structure and function (Schymanski et al., 2007, 2008b; Kanniah et al., 2009, 2010b). The work of Schymanski et al. (2007) in particular is of note, as they have used a multiple canopy layer approach to model the net carbon profit for a tropical savanna in northern Australia, with this work being further expanded into modelling canopy gas-exchange using an optimality approach (see Section **??**) in Schymanski et al. (2008b,b) and Schymanski et al. (2009). While the results presented in these bodies of work allow excellent insight into carbon and water fluxes of a whole ecosystem, they do not explore the dynamics of the two phenology types present in north Australian savannas. What is needed however is a way to fully explore the degree to which C_4 grasses contribute towards total savanna evapotranspiration (ET) and gross primary productivity (GPP).

Currently, there is no readily available model that can explore the diurnal, seasonal and annual variation in ET and GPP of ecosystems comprised of mixed C_3 (trees and shrubs) and C_4 (grasses) species. The Soil-Plant-Atmosphere (SPA) model of Williams et al. (1996a) is one of the most widely and successfully applied land surface exchange models and has been tested and validated across a range of diverse ecosystems, including Arctic tundra (Williams et al., 2000, 2001c, 2004), Brazilian tropical rainforests (Williams et al., 1996a; Fisher et al., 2006, 2007), temperate Ponderosa pine (Law et al., 2000; Williams et al., 2001a,b), boreal (Hill et al., 2008) and oak (Engel et al., 2002; Hernandez-Santana et al., 2009) forests, and temperate Australian woodlands (Zeppel et al., 2008a). The SPA model is a mechanistic model that predicts, amongst other parameters, carbon and water fluxes, leaf water relations and changes in soil moisture. However, it has not been applied to savannas because the productivity sub-model considers only the C_3 photosynthesis and therefore cannot account for the behaviour of the C_4 grass layer. Therefore, in this chapter, I describe the changes required to incorporate C_4 metabolism into the SPA model. This modified SPA model allows one to quantify ecosystem dynamics and to investigate the physiological mechanisms underlying the observed behaviour. The test of the modified SPA model, will therefore be its ability to reflect observed trends in gas flux across seasons. Both ET and GPP are chosen as the major determinants of model success, because seasonal changes in these fluxes in a savanna are strongly affected by seasonal changes in LAI arising from changes in the grass understorey.

The aims of this study were to first, modify the SPA model to incorporate both C_3 and C_4 photosynthesis, second, validate the modified model with five years of eddy covariance data for a savanna site, third investigate intra- and inter-annual variation in ET and GPP of a savanna and fourth, evaluate the sensitivity of ET and GPP to a number of abiotic and biotic factors. This exercise attempts to answer the the following questions:

- What photosynthesis model best simulates C_4 gas-exchange for savanna grasses?
- What are the relative contributions of C_3 and C_4 vegetation to total ecosystem ET and GPP?
- How water- and light-use efficient is C_4 vegetation for an Australian tropical savanna site?

- What environmental factors are dominant in driving savanna fluxes at this site, and do C_3 and C_4 vegetation respond similarly to these environmental drivers?

4.2 Methods

4.2.1 Study site

It is acknowledged here that all measured data contained in this chapter were collected by a number of researches. Eddy covariance data, as well as MODIS data for leaf area index, has been acquired with permission from Beringer et al. (2007). Additionally, leaf-scale measurements of stomatal conductance and photosynthesis for C_3 and C_4 species are taken from Eamus (2003) and Ghannoum et al. (2001b) and are used with their permission.

Eddy covariance (EC) data spanning five years (2001-2005) were collected near Howard Springs (131°09'09.00"E, 12°29'39.12"S), approximately 35 km southeast of Darwin, Northern Territory, Australia by Lindsay Hutley (Charles Darwin University) and Jason Beringer (Monash University). The site is an open forest savanna that is characterised by distinct dry (May-September inclusive) and wet (November-March inclusive) seasons. Approximately $90-95\%$ percent of the annual rainfall occurs between the start of November and the end of March and the long-term average annual rainfall is 1750 mm, however for this data-set, there are significant rainfall events in July 2001, May 2004 and October 2005, as is commonly observed in long-term records (Figure 4.1). Maximum solar radiation (R_s) levels vary a little between the wet season (typically $1000-1100$ W m^{-2}) and dry season (typically about 800 W m^{-2}), reflecting the high latitude of the site. In the dry season the absence of cloud results in relatively uniform radiation levels but in the wet season, highly extensive but variable cloud cover results in fluctuations in the daily variations of R_s (Figure 4.1a). Mean daily vapour pressure deficit (D_v) peaks in the dry season and is typically between 3.0 and 4.5 kPa (Figure 4.1b). In the wet season, D_v is generally low and is predominantly in the range $1.0-2.5$ kPa due to the high frequency of rainfall. Mean daily maximum temperatures (T_a) remain above 30°C throughout the year, irrespective of season. Fire events were also a frequent occurrence at this site during the dry season, and these ranged from low intensities in the early dry season (late April to June) to moderate

intensities at the end of the dry season (August to September) due to increased fuel loads and extreme weather conditions (see Beringer et al., 2007).

Vegetation at the site is representative of a mesic open forest savanna with an overstorey dominated by evergreens, *Eucalyptus tetrodonta* (F. Muell.) and *Eucalyptus miniata* (Cunn. ex Schauer), forming a discontinuous canopy of about 50% cover. These two species account for approximately 90% of the tree basal area of $8 - 10$ m^2 ha^{-1} (O'Grady et al., 2000). Overstorey LAI varies seasonally because of the presence of brevi- semi- and fully deciduous species, while the dominant evergreen species maintain canopy fullness throughout the dry season (Williams et al., 1997). The understorey includes semi-deciduous and deciduous small trees and shrubs but is dominated by C_4 grasses such as the annual species *Sarga spp.* and the perennial grass *Heteropogon triticeus*.

The soil profile for the site is a weathered lateritic red and yellow earth Kandosol (McKenzie et al., 2004), that is weakly acidic and low in nutrients (Russell-Smith et al., 1995). The soil surface is a well drained, sandy loam A-horizon, which transitions at approximately 1.5 m to a sandy clay loam B-horizon. Greater than these depths, ferricrete boulders occur in a matrix of mottled, heavy clays forming a duricrust of low permeability and variable depth. Additionally, ferricrete gravel is dispersed at the soil surface through to the entire profile, occupying between $20 - 50\%$ of soil volume (Hutley et al., 2000). Seasonal variation in volumetric soil water content in the upper profile is large, with high amplitudes between $0.20 - 0.30$ m^3 m^{-3} occurring during the peak wet season and dropping to lows of $0.03 - 0.04$ m^3 m^{-3} at end of the dry season (Figure 4.1c). For the deeper clay-loam subsoils, water contents can range from $0.26 - 0.40$ m^3 m^{-3} (Eamus et al., 2001). The storage capacity of soil water is poor with a volume release between field capacity and wilting point being 0.08 cm^3 cm^{-3} (Cook et al., 1998; Hutley et al., 2000). Additionally, the profile overlies a surface aquifer which can reach within 2 m of the soil surface during the wet season (Cook et al., 2002).

4.2.2 Eddy covariance data

The eddy covariance technique (Baldocchi et al., 1988) was used to calculate flux variables at 30 min time intervals. The instruments were mounted on a 23 m flux tower within a plot

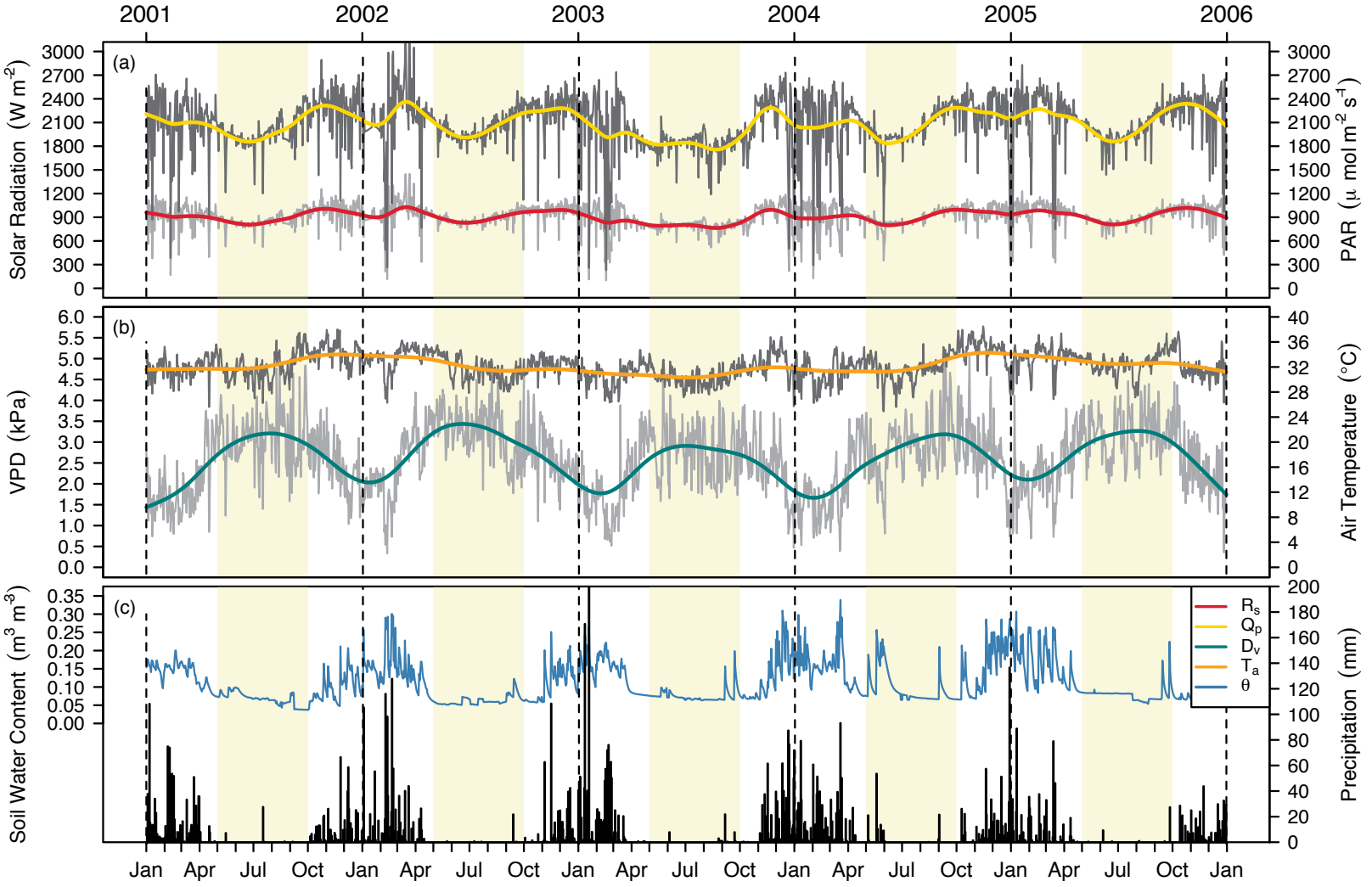

FIGURE 4.1: Five years of meteorological data that drive water and carbon flux cycles at Howard Springs taken from Beringer et al. (2007). These are (a) daily maximum solar radiation (R_s) and photosynthetically active radiation (PAR; Q_p), (b) daily maximum vapour pressure deficit (VPD; D_v) and ambient air temperature (T_a), and (c) soil water content at a depth of 10 cm (θ_s) and precipitation. In (a) and (b) the grey lines represent the EC data, while the coloured lines represent a spline fit that shows the underlying seasonal variation in these meteorological variables. The yellow shaded regions represent the annual dry season.

of open-forest savanna approximately 340 ha in size. The slope was less than 1° and the fetch was homogenous in all directions (> 1 km). Wind speed and direction was measured with a 3-D sonic anemometer (Campbell Scientific Inc. model CSAT3, Logan Utah, USA) and CO_2 and H_2O fluxes were measured at 10 Hz with an LI-7500 open-path CO_2/H_20 analyser (Licor Inc., Lincoln NE, USA). CO_2 fluxes were corrected for fluctuations in air density due to sensible and latent heat fluxes (Webb et al., 1980). Half-hourly values of rainfall, T_a, relative humidity, and net radiation were measured at the same height as the flux data. Soil moisture at 10 cm depth was measured on a daily time-step. Missing or invalid flux data were gap-filled using either linear interpolation (for gaps shorter than 3 hrs), or an artificial neural network (ANN) (for extended gaps). Details of gap-filling can be found in Beringer et al. (2007). GPP was a derived product, determined as the sum of net ecosystem exchange (NEE) and ecosystem respiration (R_e) and was assumed to be equivalent to night-time net CO_2 flux F_c under adequate wind speed conditions (where friction velocity values were larger than 0.15 m s^{-1}). Values of NEE collected under low wind speed conditions were excluded to avoid underestimation of R_e due to inadequate turbulent mixing (Baldocchi et al., 2000; Beringer et al., 2007). Using the ANN, daytime values of R_e were calculated from regression values of T_a and θ_s.

4.2.3 Photosynthesis models incorporated into the SPA model

An explanation of the SPA model has been covered in Chapter 1 and so will not be covered again here. However, parameterising of the model inputs and variables are covered below, as well as an extensive explanation of the photosynthesis models that are used in the half-hourly calculations of C_3 and C_4 canopy assimilation. Additionally, modifications that were made to the model have also been listed here such as how the seasonal patterns of leaf area and foliar nitrogen per canopy layer change throughout the year. Finally, a methodology for determining the efficiency parameter that describes stomatal sensitivity in the model is covered.

4.2.3.1 C_3 photosynthesis

C_3 photosynthesis operates by two distinct reactions; a light reaction, transforming light energy into a temporary form of stored chemical energy and a carbon-fixation reaction, which uses chemical energy from the light reaction to convert CO_2 into sugars (glucose) (Chapin III et al., 2002). In the light reaction, the chlorophyll captures energy from the visible spectrum and transforms this into chemical energy in the form of adenosine-5'-triphosphate (ATP) and nicotinamide adenine dinucleotide phosphate (NADPH). Carbon fixation occurs via the reaction between ribulose-bisphosphate (RuBP) and CO_2, and is catalysed by the enzyme ribulose-bisphosphate carboxylase-oxygenase (RuBisCO); the rate that is limited by light intensity and the intercellular CO_2 concentration (C_i). The products of this reaction are two sets of 3-carbon compound molecules 3-phosphoglycerate (hence the term C_3). This compound is then reduced via reactions with ATP and NADPH to form glucose (Nobel, 1999). Further photosynthesis is sustained by regenerating RuBP from ATP and NADPH, which is then used to react with more CO_2. The processes is cyclical and referred to as the photosynethetic carbon reduction cycle (PCR). There is however a side-effect of the enyzme RuBisCO to react with O_2 instead of CO_2 which is termed photorespiration, which inhibits photosynthesis due to high metabolic energy costs and is generally known as the photosynthetic carbon oxydation (PCO) cycle. To model these processes the intercellular transport (ICT) model developed by Farquhar et al. (1980) was used to calculate the amount of carbon fixation in C_3 vegetation.

Farquhar C_3 model

The net assimilation rate for C_3 photosynthesis describing the biochemical demand for CO_2 is calculated as:

$$A_n^{C_3} = A_g \left[1 - \frac{\Gamma^*}{C_i}\right] - R_d \tag{4.1}$$

where A_g (μmol m^{-2} s^{-1}) is the gross rate of photosynthesis limited by RuBisCO activity and RuP_2 regeneration through electron transport, Γ^* (μmol mol^{-1}) is the CO_2 compensation point in the absence of non-photorespiratory respiration, C_i (μmol mol^{-1}) is the intercellular CO_2 concentration and R_d (μmol m^{-2} s^{-1}) is the respiration rate . The gross

rate of carboxylation is limited by either RuBisCO activity or RuP_2 regeneration, and so the rate of carboxylation is determined by finding the minimum of the two:

$$A_g = \min\{A_c, A_j\} \tag{4.2}$$

The rate at which CO_2 is fixed by RuBisCO carboxylation (A_c), is given by:

$$A_c = \frac{V_{cmax} C_i}{C_i + K_c\left(1 + \frac{O_i}{K_o}\right)} \tag{4.3}$$

where O_i (μmol mol^{-1}) is the intercellular O_2 concentration, V_{cmax} (μmol m^{-2} s^{-1}) is the maximum carboxylation capacity, and K_c and K_o (μmol mol^{-1}) are Michaelis-Menton constants for enzyme catalytic activity for CO_2 and O_2 respectively.

The rate at which RuP_2 is regenerated (A_j), is given by:

$$A_j = \frac{J}{4}\frac{C_i - \Gamma^*}{C_i + 2\Gamma^*} \tag{4.4}$$

where J (μmol m^{-2} s^{-1}) is the electron transport rate, which is a function of J_{max} (μmol m^{-2} s^{-1}), the potential rate of whole chain electron transport, and Q_p (μmol m^{-2} s^{-1}) is the absorbed photosynthetic photon flux density and can be described by a non-rectangular hyperbolic function (Farquhar and Wong, 1984), given as:

$$\theta_j J^2 - (\alpha_j Q_p + J_{max})J + \alpha_j Q_p J_{max} = 0 \tag{4.5}$$

where θ_j is a parameter describing the shape of the non-rectangular hyperbola, α_j is the quantum efficiency, and J_{max} is the potential rate of whole-chain electron transport. The quadratic solution in terms of J is therefore described as:

$$J = \frac{-b + \sqrt{b^2 - 4ac}}{2a} \tag{4.6}$$

where

$$a = \theta_j$$
$$b = -\alpha_j Q_p + J_{max}$$
$$c = \alpha_j Q_p J_{max}$$

4.2.3.2 C_4 photosynthesis

The biochemical and physiological pathways of C_4 and C_3 photosynthesis are very different. The common factor is that both pathways use RuBisCO to fix CO_2 in the PCR cycle (Collatz et al., 1992). However, the difference occurs in the way the RuBisCO reaction is compartmented and how CO_2 is supplied to this site. The C_4 photosynthetic pathway works as follows. CO_2 diffuses from the intercellular air spaces to the mesophyll cell, where it is simultaneously fixed and converted into malate, a 4-carbon organic acid (hence the name C_4), by phosphoenolpyruvate (PEP) carboxylase (von Caemmerer, 2000). The acids then diffuse through to the bundle-sheath where they are decarboxylated back to CO_2, where the CO_2 either leaks back to the mesophyll cells or is fixed by RuBisCO in the PCR cycle. This mechanism can be thought of as a form of metabolic pump that supplies elevated CO_2 concentrations to the site of RuBisCO located in the bundle sheath cells. Because CO_2 must be fixed twice and PEP be regenerated as well as RuBP, the cycle requires more energy than is used in the C_3 pathway; generally at the cost of 30 mol ATP for 1 mol glucose compared to C_3 which requires only 18 mol ATP (von Caemmerer and Furbank, 1999). However the high CO_2 concentrations around the site of RuBisCO has the benefit of inhibiting photorespiration and reduces the need for a large g_s, making C_4 plants highly water- and nitrogen-use efficient (Sage et al., 1987; Ghannoum, 2009). Two models, both of which are based on the original work of Berry and Farquhar (1978) and Peisker (1979), have been used to describe the C_4 photosynthetic pathway in SPA. These are:

1. a mechanistic photosynthesis model developed by von Caemmerer and Furbank (1999) and

2. a simplified photosynthesis model developed by Collatz et al. (1992).

Both models have been tested to determine whether a highly detailed model describing the mechanisms of the C_4 pathway are necessary to correctly model C_4 photosynthesis, or if it can be determined from much simpler information.

The detailed von Caemmerer C_4 model

Given here are the equations of enzyme and light-limited assimilation rates that are approximations to the quadratic solutions given by von Caemmerer and Furbank (1999). Taking into account the mechanisms of the compartmentalised C_4 photosynthetic process, the net CO_2 assimilation rate is described by two equations. The first equation determines the rate at which CO_2 is supplied to the bundle-sheath and the second equation describes that rate at which CO_2 is assimilated in the bundle-sheath via the PCR cycle. The first equation describes the rate of CO_2 assimilation in terms of the reactions in the mesophyll cell:

$$A_e = V_p - L - R_m \tag{4.7}$$

where A_p is the rate of PEP carboxylation, R_m is mitochondrial respiration and L is the rate of CO_2 leakage from the bundle-sheath back to the mesophyll cell and is described as $L = g_{bs}(C_s - C_m)$, where g_{bs} is the conductance of CO_2 from the bundle-sheath to the mesophyll cell, and C_s and C_m are the bundle-sheath and mesophyll partial pressures respectively. When CO_2 is limiting the rate of PEP carboxylation is given as:

$$V_p = \min\left\{\frac{V_{pmax}C_i}{C_i + K_p}, V_{pr}\right\} \tag{4.8}$$

where V_{pmax} is the maximum PEP carboxylation rate, K_p is the catalytic constant for PEP and V_{pr} is V_p when rate of PEP regeneration is limiting. The rate of CO_2 assimilation given as the rate of decarboxylation of the C_4 acids is therefore be given as:

$$V_c = \frac{V_{pmax}C_i}{C_i + K_p} - g_{bs}(C_s - C_m) - R_m \tag{4.9}$$

The second equation describes the reaction in which CO_2 is decarboxylated from the C_4 acids and fixed by RuBisCO into sugars, and is given as:

$$A_e = V_c - 0.5V_o - R_d \tag{4.10}$$

where V_c and V_o are the rates of RuBisCO carboxylation and oxygenation respectively and R_d is the mitochondrial respiration such that $R_d = R_m + R_s$, where R_s is respiration in the bundle-sheath. The C_4 RuBisCO carboxylation rate is the same as Equation 4.3 (where C_i is replaced with C_s), and $V_o = 2V_c\gamma^* O_s/C_s$, such that Equation 4.10 becomes:

$$A_e = \frac{C_s V_{cmax}}{C_s + K_c(1 + O_s/K_o)} \left(1 - \frac{\gamma^* O_s}{C_s}\right) - R_d \tag{4.11}$$

where V_{cmax} is the maximum rate of RuBisCO activity, K_c and K_o are the Michaelson-Menton constants for CO_2 and O_2 respectively, γ^* is half the reciprocal of RuBisCO specificity and $O_s = \alpha A_e/(0.047 g_{bs}) + O_m$ and is the O_2 concentration in the bundle-sheath, where $(0 < \alpha < 1)$ describes the relative amount of O_2 evolution occurring.

The full enzyme limited CO_2 assimilation rate is calculated by solving for Equations 4.9 and 4.11 in terms of a quadratic expression of the form:

$$aA_c^2 + bA_c + c = 0 \tag{4.12}$$

where

$$A_e = \frac{-b + \sqrt{b^2 - 4ac}}{2a} \tag{4.13}$$

and

$$a = 1 - \frac{\alpha K_c}{0.047 K_o} \approx 1 \tag{4.14}$$

$$b = -\left(V_p - R_m + g_{bs} C_m\right) - \left(V_{cmax} - R_d\right) - g_{bs} K_c \left(1 + \frac{O_m}{K_o}\right) - \frac{\alpha \gamma^*}{0.047} \left(\gamma^* V_{cmax} + R_d \frac{K_c}{K_o}\right) \tag{4.15}$$

$$c = \left(V_{cmax} - R_d\right)\left(V_p - R_m + g_{bs} C_m\right) - \left(V_{cmax} g_{bs} O_m - R_d g_{bs} K_c \left(1 + \frac{O_m}{K_o}\right)\right) \tag{4.16}$$

The CO_2 assimilation rate limited by electron transport can be expressed by the shared energy requirement between the mesophyll and bundle-sheath cells, but is modelled as the whole electron transport chain by allocating fractions of energy to the C_3 and C_4 cycles for simplicity. Whole chain electron transport (J_t) is given as:

$$J_t = J_m + J_s \tag{4.17}$$

where the mesophyll electron transport is $J_m = J_t x$, the bundle-sheath electron transport is $J_s = J_t(1 - x)$, and $x \approx 0.4$ and is the partitioning factor between the bundle-sheath and mesophyll cells. J_t is derived from the same non-rectangular hyperbolic function that describes the relationship with absorbed irradiance that is used in the C_3 model (Eqn. 4.5). Based on the stochiometries given in von Caemmerer and Furbank (1999), the expression for whole chain electron transport required for C_4 acid regeneration is given as:

$$J_m = 2V_p \tag{4.18}$$

and whole chain electron transport required for the C_3 cycle is given as:

$$J_s = 4.5(1 + 7\gamma^* O_s / 3C_s) V_c \tag{4.19}$$

such that the two above equations can be incorporated into Equations 4.9 and 4.11 to

derive expressions for electron transport limited CO_2 assimilation rates in terms of the mesophyll cell:

$$A_j = \frac{xJ_t}{2} + g_{bs}(C_s - C_m) - R_m \tag{4.20}$$

and for the bundle-sheath cell:

$$A_j = \frac{(1 - \gamma^* O_s/C_s)(1-x)J_t}{3(1 + 7\gamma^* O_s/C_s)} - R_d \tag{4.21}$$

The full electron transport limited CO_2 assimilation rate is calculated from a quadratic expression derived by solving A_j simultaneously for Equations 4.20 and 4.21, resulting in the form of:

$$aA_j^2 + bA_j + c = 0 \tag{4.22}$$

where

$$A_j = \frac{-b + \sqrt{b^2 - 4ac}}{2a} \tag{4.23}$$

and

$$a = 1 - \frac{7\gamma^*\alpha}{3 \cdot 0.047} \tag{4.24}$$

$$\begin{aligned} b = &-(\frac{xJ_t}{2} - R_m + g_{bs}C_m) - \left(\frac{(1-x)J_t}{3} - R_d\right) - g_{bs}\left(\frac{7\gamma^* O_m}{3}\right) \\ &-\frac{\alpha\gamma^*}{0.047}\left(\frac{(1-x)J_t}{3} + R_d\right) \end{aligned} \tag{4.25}$$

$$\begin{aligned} c = &\left(\frac{xJ_t}{2} - R_m + g_{bs}C_m\right)\left(\frac{(1-x)J_t}{3} - R_d\right) \\ &-g_{bs}\gamma^* O_m\left(\frac{(1-x)J_t + 7R_d}{3}\right) \end{aligned} \tag{4.26}$$

Finally, the minimum between the Equations 4.13 and 4.23 describes the enzyme or light-limitied actual C4 CO_2 assimilation rate and is given by:

$$A_n^{C_4} = \min\{A_e, A_j\} \tag{4.27}$$

The simplified Collatz C_4 model

Alternatively the light and enzyme-limited C_4 assimilation rates can be determined from a more simplified model that is functionally equivalent to the above ICT model. Given here are the quadratic solutions from the coupled photosynthesis-stomatal conductance model as described by Collatz et al. (1992). The first quadratic expression is given as:

$$\theta_{tr} M_{cj}^2 - (V_{cmax} + \alpha_{rf} Q_p) M + V_{cmax} \alpha_{rf} Q_p = 0 \tag{4.28}$$

where, θ_{tr} is a parameter describing the transition between light-limited and RuBisCO limited CO_2 flux, α_{rf} is a combined constant describing the intrinsic quantum yield, and fraction of absorbed photons used by the reaction process, Q_p is the incident quantum flux density, V_{cmax} is the maximum C_4 RuBisCO carboxylation rate and M_{cj} is the CO_2 flux determined by both RuBisCO and light-limited photosynthetic capacities. Equation 4.28 is therefore solved for M_{cj} as follows:

$$M_{cj} = \frac{-b - \sqrt{b^2 - 4ac}}{2a} \tag{4.29}$$

where

$$a = \theta_{tr}$$
$$b = -\alpha_{rf} Q_p + V_{cmax}$$
$$c = \alpha_{rf} Q_p V_{cmax}$$

Overall net C_4 assimilation rate is similarly determined through a quadratic expression, which includes the RuBisCO and light-limited capacities described above as well as the CO_2 limited flux rate, and is expressed as:

$$\beta_{co} A_g^2 - (M + C_i k_T) A_g + M C_i k_T = 0 \tag{4.30}$$

where β_{co} is a parameter describing the co-limitation between light, RuBisCO and CO_2 limited flux, C_i is the intercellular CO_2 concentration of the mesophyll cells, $k_T = k_p - L/C_i$ and describes the interactions of k_p, a first-order rate constant for PEP carboxylase with

respect to the ratio between C_i and L; the amount of CO_2 leakage from the bundles sheath to the intercellular air spaces of the mesophyll. A_g is the gross C_4 photosynthetic rate, and is found by solving Equation 4.30 for A_g, given as:

$$A_g = \frac{-b - \sqrt{b^2 - 4ac}}{2a} \tag{4.31}$$

where

$$a = \beta_{co}$$
$$b = -M + C_i k_T$$
$$c = MC_i k_T$$

The net assimilation is then defined as:

$$A_n^{C_4} = A_g - R_d \tag{4.32}$$

The variables A_c, A_j and A_p for both C_3 and C_4 photosynthetic pathways are functions of C_i and temperature, with A_j having an additional dependence on Q_p. Consequently, the respective C_3 and C_4 parameters V_{cmax}, V_{pmax}, J_{max}, K_c, K_p, K_o, Γ^* and R_d are modified by temperature response functions from Chen et al. (1994) and Massad et al. (2007).

4.2.4 Model Parameterisation

4.2.4.1 Model canopy structure

The savanna canopy was constructed within the model to describe a savanna open woodland with five layers allocated to the overstorey (which included the mid-stratum) and understorey components respectively. The overstorey was comprised of the evergreen eucalypt trees as well as the deciduous and brevi-deciduous shrubs, which all operate along the C_3 photosynthetic pathway. The understorey was comprised of the grasses which operate along the C_4 photosynthetic pathway. The maximum height of the tree canopy was set to 14 m, and the height of the grasses was set to 1.5 m (Williams et al., 1997). Each understorey layer was 0.3 m deep (a total height of 1.5 m) and the overstorey layers were

each 2.5 m deep, taking the total canopy height to 14 m. Given the significant contribution of the grass to total LAI (up to 1.2 times the overstorey LAI during the wet season; Hutley et al. 2000), 50% of total LAI was allocated to the tree overstorey and grass understorey layers respectively.

Total LAI for Howard Springs was derived from Moderate-resolution Imaging Spectroradiometer (MODIS) 8-day 1 km Collection 5 (MOD15A2) composite LAI/FPAR[1] product for the 2001 to 2005 period from the National Aeronautics and Space Administration (NASA) Distributed Active Archive Centre (Figure 4.2a). Data were smoothed for obvious errors in the extracted LAI values by taking the mean between adjacent days (Palmer et al., 2008) and a spline function was fitted to the 5-year data-set to extract a smooth time-series response. The partitioning of the total savanna LAI into it's constituent C_3 and C_4 parts was done by following the records given in Williams et al. (1997) and Eamus (1999), which show the relative percentages that each vegetative component contributes to total savanna LAI. The understorey-dominant savanna grasses make up a significant portion of total LAI during the wet season, ranging from 0.05 m^2 m^{-2} with the onset of flushing of new leaves in early October, to a peak of 1.15 m^2 m^{-2} in February, during the peak of the wet season (Williams et al., 1997). In the dry season, grass LAI is 0.0, which is a result of their annual senescence. Canopy overstorey LAI reflects the seasonal patterns of the four phenological types described by Williams et al. (1997), and experiences a range of values between $0.6 - 1.10$ m^2 m^{-2} for dry and wet seasons respectively (Figure 4.2b).

The evergreen phenology was assigned to the top two canopy layers (9.0-11.5 m and 11.5-14.0 m canopy height) as the two dominant tree species are evergreen. Consequently the LAI of these layers remains reasonably constant throughout the year, while the bottom three canopy layers of the overstorey (1.5-4.0 m, 4.0-6.5 m and 6.5-9.0 m canopy height) incorporated components of the brevi-deciduous, semi-deciduous and fully deciduous species whose LAI values declined during the dry season. LAI for C_3 vegetation in the top five layers was assigned according to a normal distribution and was active all year round (Figure 4.2c). LAI in the five bottom canopy layers (0.0-0.3 m, 0.3-0.6 m, 0.6-0.9 m, 0.9-1.2 m, 1.2-1.5 m canopy height) layers, comprising of the C_4 grasses, was distributed uniformly (10% each) and went to 0% in the dry season. The senescent nature of the understorey

[1]FPAR is the Fraction of Photosynthetically Active Radiation

LAI was mapped into the LAI matrix, describing the seasonal increases and decreases in value.

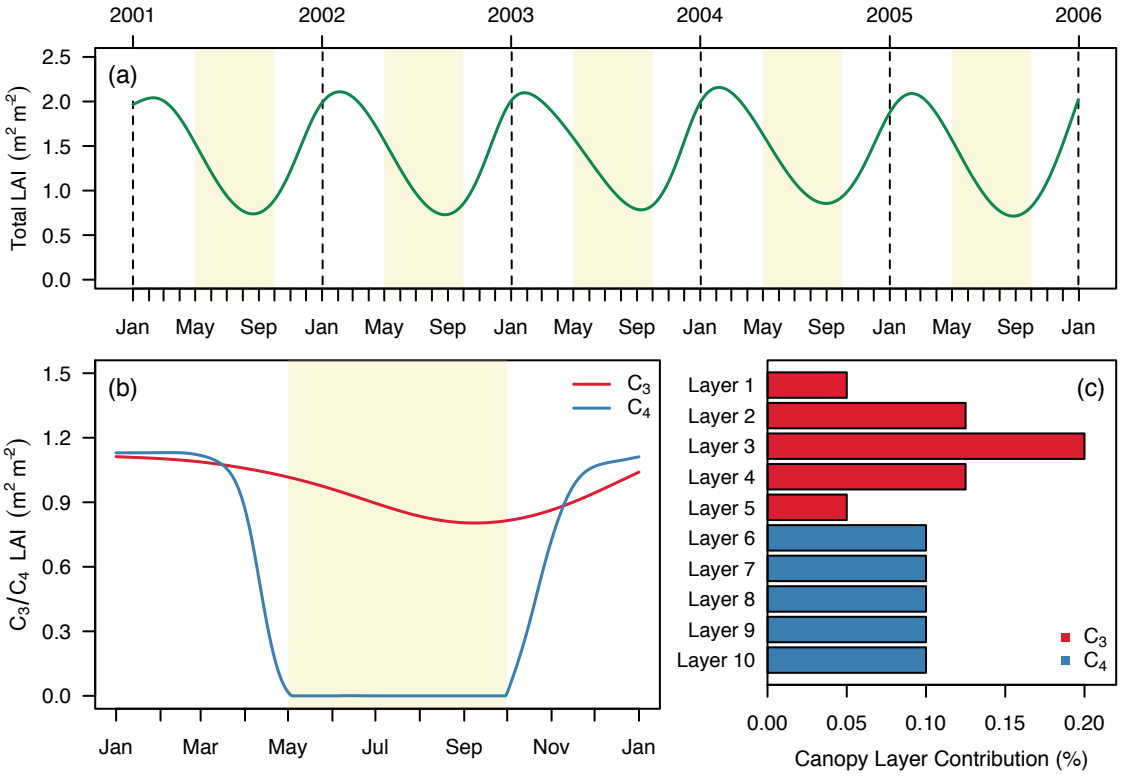

FIGURE 4.2: Representation of (a) savanna total leaf area index (LAI) at Howard Springs over the 5 year study period (2001–2005); (b) a one year example of the partitioning of total savanna LAI into the C_3 canopy overstorey and mid-term stratum and understorey C_4 grasses; (c) the percentage contribution of the 10 modelled canopy layers to total LAI during the wet season, where layers 1–10 represent the layers from the top of the tree canopy to the grasses on the surface. Yellow shaded regions represent the dry season period.

The model simulates leaf level productivity of the canopy by dividing it into 10 layers; this allows variations in absorbed Q_p through light interception, distribution of leaf area (L_A) and foliar nitrogen content (N_f) to be accounted for in each layer. The model requires that total canopy LAI and N_f be partitioned to each canopy layer so that each layer has a specific value of nitrogen per unit leaf area (N_{LA}). However, savanna ecosystems are comprised of different vegetation types (i.e. evergreen, deciduous and brevi-deciduous) that make up the the canopy and experience large and very different seasonal variations in L_A and N_f. In its original form, such seasonal changes are not accounted for by the SPA model. It was therefore important to incorporate the seasonality of savanna canopy

L_A and N_f in the model. This was achieved by defining L_A and N_f as dynamic rather than static variables, i.e. by supplying L_A and N_f matrices as model inputs, N_{LA} in each canopy layer was subject to change at the daily time-scale.

Concentrations of N_f were determined from the literature describing this site. *Myrtaceous* species typically have a leaf nitrogen concentration of 1.7 g m^{-2} leaf area (Prior et al., 2004) and the C_4 grass *Sorghum bicolor* typically may have a leaf nitrogen concentration of 1.6 g m^{-2} leaf area (Ghannoum et al., 2005). Based on maximum LAI of 2.25 and assuming the overstorey and understorey values were 1.10 and 1.15 m^2 m^{-2} respectively, the maximum N_f was 3.88 g m^{-2} ground area. The minimum N_f in the dry season was approximately 0.7 g m^{-2} ground area. Seasonal reductions were therefore incorporated in N_f on a leaf area basis consistent with Prior et al. (2004). The N_f matrix for the 10 canopy layers was based on a functional form of the LAI matrix described above.

4.2.4.2 Leaf biochemical parameters

Leaf level characteristics for the canopy were determined from the previous studies made for at this site (Prior and Eamus, 1999; Hutley et al., 2001; Prior et al., 2004) and the values of these parameters are given in Table 4.1. Maximum carboxylation capacity ($^{C_3}V_{cmax}$) and maximum electron transport rate ($^{C_3}J_{max}$) have not been determined, to my knowledge, for C_3 vegetation at this site. Similarly, C_4 photosynthetic parameters for maximum rates of carboxylation capacity ($^{C_4}V_{cmax}$), electron transport ($^{C_4}J_{max}$) and PEP carboxylase activity ($^{C_4}V_{pmax}$) have not been determined, to my knowledge, for this site either. Consequently, photosynthetic parameters for the C_3 and C_4 vegetation supplied to the model were determined from literature values. Values for $^{C_3}V_{cmax}$ and $^{C_3}J_{max}$ were taken from Zeppel et al. (2008a). Preliminary runs of the C_3 canopy with these parameters, were done to test how closely modelled A_n, g_s and leaf water potential (Ψ_l) matched with measurements from Prior and Eamus (1999). Measured and modelled results matched closely and so these parameter were deemed appropriate to describe the C_3 overstorey in the model. Photosynthetic parameters for the C_4 understorey were also taken from the literature. However, such information could only provide general values for $^{C_4}V_{cmax}$ based on a biochemical sub-type (i.e. NAD-ME and NADP-ME) or from crop families (i.e. *Zea*

mays and *sorghum*) (Massad et al., 2007; von Caemmerer and Furbank, 1999; Ghannoum et al., 2005). From comparing amongst studies, it was found that ${}^{C_4}V_{cmax}$ appears to be similar across most grass species, therefore an average value for *sorghum* was chosen from (Ghannoum et al., 2005). No measured values for ${}^{C_4}V_{pmax}$ could be found in the literature, and so a value was determined from a ratio of $V_{pmax}/V_{cmax} = 3$, based off the observations of von Caemmerer and Furbank (1999). The high value for ${}^{C_4}V_{pmax}$ is supported by Sage et al. (1987), who states that V_{pmax} is a highly regulated enzyme compared to V_{cmax} and should therefore be much higher. No measured values or adequate methods could be found to determine ${}^{C_4}J_{max}$ and so this was left at the value that is reported in von Caemmerer and Furbank (2003) and Massad et al. (2007). These values were tested using a sensitivity analysis (data not shown) and it was determined that modelled A_n was highly sensitive to variation in ${}^{C_4}V_{cmax}$, while changes in ${}^{C_4}V_{pmax}$ and ${}^{C_4}J_{max}$ had little effect on modelled A_n. A ${}^{C_4}V_{cmax} = 47$ μmol m^{-2} s^{-1} along with selected C_3 photosynthetic parameters (Table 4.1) was found to give the best fit to the data.

The value for whole plant hydraulic conductance (g_{plant}) was taken from Zeppel et al. (2008a) and tested in a sensitivity analysis, where changes in g_{plant} affected ET but not GPP. A comparison of modelled versus measured showed a value of 3.5 mmol m^{-2} MPa^{-1} to be adequate in describing savanna ET. Leaf capacitance (C_{leaf}) was left unchanged from the default value given in Williams et al. (1996a), as subsequent sensitivity test showed that it had very little effect on model outputs. Minimum leaf water potential, Ψ_{lmin} was determined from the measurements made at this site by Prior and Eamus (1999).

4.2.4.3 Stomatal efficiency parameters

At every 30 minute time-step, SPA uses a unique stomatal optimisation model to find the optimal g_s that maximises carbon gain per unit water loss and prevents xylem cavitation, based on the prevailing forces acting on the canopy at that time. The SPA model increases g_s to a point that maximises A_n under two constraints, i) the Ψ_l must remain above the minimum leaf water potential (Ψ_{lmin}) and ii) that any increase in g_s must give an appreciable increase in A_n. The latter of these constraints is termed as the threshold of

TABLE 4.1: This table lists the model variables and parameters that were used to describe and simulate the savanna ecosystem at the Howard Springs site. Descriptions of the model variables and parameters are given along with the symbols, SI units, values (if constant), as well as the reference source from which they have been taken.

Variable Description	Symbol	Units	Value	Reference
Solar radiation	R_s	W m^{-2}	*variable*	Beringer et al. (2007)
Photosynthetically active radiation	Q_p	μmol m^{-2} s^{-1}	*variable*	
Air temperature	T_a	°C	*variable*	
Vapour pressure deficit	D_v	kPa	*variable*	
Ambient atmospheric CO_2 concentration	C_a	μmol mol^{-1}	374	
Annual rainfall	P_{PT}	mm	$1219 - 2467$	
Leaf area index	L_{AI}	m^2 m^{-2}	$0.90 - 2.25$	MODIS Product
Foliar nitrogen	N_f	gN m^{-2}	$0.70 - 3.88$	Prior et al. (2004)
Minimum leaf water potential	Ψ_{lmin}	MPa	-2.5	Prior and Eamus (1999)
Whole leaf capacitance	C_{leaf}	mmol m^{-2} MPa^{-1}	5000	Williams et al. (1996a)
Whole plant conductance	g_{plant}	mmol m^{-2} MPa^{-1}	3.0	Zeppel et al. (2008a)
C_3 maximum RuBisCO carboxylation rate	${}^{C_3}V_{cmax}$	μmol m^{-2} s^{-1}	73.6	Zeppel et al. (2008a)
C_3 maximum electron transport rate	${}^{C_3}J_{cmax}$	μmol m^{-2} s^{-1}	129.8	
C_4 maximum RuBisCO carboxylation rate	${}^{C_4}V_{cmax}$	μmol m^{-2} s^{-1}	47.0	Ghannoum et al. (2005)
C_4 maximum PEP regeneration rate	${}^{C_4}V_{pmax}$	μmol m^{-2} s^{-1}	141.0	von Caemmerer and Furbank (1999)
C_4 maximum electron transport rate	${}^{C_4}J_{max}$	μmol m^{-2} s^{-1}	400.0	
C_3 stomatal efficiency	${}^{C_3}\iota_{op}$	%	0.07	Estimated this study
C_4 stomatal efficiency	${}^{C_4}\iota_{op}$	%	0.20	
Fine root radius	r_{root}	m	0.0001	Chen et al. (2003)
Root biomass	m_{root}	g biomass m^{-2}	1930	
Rooting depth	d_{root}	m	6.4	
Root resistivity	R_{root}	MPa s g $mmol^{-1}$	100	
Sand particle size distribution	$S_{\%}$	%	45.0	McKenzie et al. (2004)
Clay particle size distribution	$C_{\%}$	%	5.0	

stomatal efficiency, and is defined as:

$$\iota_{op} = \frac{\delta A_n}{\delta g_s} = \frac{A_{n,i}(g_{s,i})}{A_{n,i-1}(g_{s,i-1})} \tag{4.33}$$

where ι_{op} is a stomatal efficiency parameter and defines the point at which any further increase in g_s does not result in an appreciable increase in A_n. The ι_{op} parameter determines the maximum rate of assimilation (A_{max}) under well-watered conditions, and is therefore important that the value of this parameter be correctly defined. However, because C_3 and C_4 plants have very different water-use efficiencies (WUE), their respective responses of A_n to increasing g_s will be different and therefore result in different ι_{op} values. This being the case, separate stomatal efficiencies for the tree overstorey ($^{C_3}\iota_{op}$) and grass understorey ($^{C_4}\iota_{op}$) needed to be defined. The problem with this, is how to define what values these parameters assume at this site. Williams et al. (1996a) state that for their site (C_3 dominated), an $\iota_{op} = 0.07\%$ gave the best fit to their measured data. However this value may be too small for C_4 plants, which would saturate towards A_{max} at a much lower g_s compared to C_3 plants. I therefore theorise that C_4 species will have a larger ι_{op}, pertaining to a higher WUE. In order to test whether this theory and find a value for $^{C_4}\iota_{op}$, the following methodology was used.

A simple way of determining ι_{op} is to use the SPA model to estimate A_n and g_s over a range of Q_p, while keeping other driving variables (i.e. D_v) constant. A simplified version of SPA's stomatal optimisation model (StomOpt) was developed in *R Statistical Software* that could be used to accomplish this for C_3 and C_4 plants at this site.[2] This allows one to create a Ball-Berry-Leuning (BBL) -like relationship (Ball et al., 1987; Leuning, 1990) to be established, where the BBL relationship is given as:

$$g_s = g_{s0} + \frac{a_1 A_n}{(C_a - \Gamma^*)(1 + D_v/D_0)} \tag{4.34}$$

where g_s is the stomatal conductance (mmol m^{-2} s^{-1}) of the leaf, g_{s0} is the residual g_s in the absence of light, C_a is the ambient CO_2 concentration (μmol mol^{-1}), D_v (kPa) is the leaf to air vapour pressure deficit, and a_1 is the slope and D_0 is a coefficient (Lohammer et al., 1980), both of which are empirically determined.

[2] Although this could be done using the full version of SPA as well.

By using the SPA model to construct the relationship described by Equation 4.34, the a_1 parameter becomes equivalent to the ι_{op} parameter. The consequence of this is that changing the value of ι_{op} becomes equivalent to changing the slope of the BBL relationship. This allows SPA to be fit to leaf-scale measurements of g_s and A_n, where ι_{op} is adjusted so as to equal (or be as close as possible) to the slope (a_1) of the measured data. An $\iota_{op} \approx a_1$ would signify what stomatal efficiency is appropriate for the site and vegetation. Values of ι_{op} for the C_3 and C_4 vegetation were determined using this methodology (Table 4.1). The leaf-scale data used to calibrate ${}^{C_3}\iota_{op}$ in the model was taken from Eamus (2003) and consisted of measurements taken from a mix of native evergreen (*Eucalyptus*, *Alphitonia* and *Acacia*) and deciduous (*Planchonia*, *Terminalia* and *Cochlospermum*) tree species. Leaf-scale data used to calibrate ${}^{C_4}\iota_{op}$ was taken from Ghannoum et al. (2001a) and consisted of measurements from native *Dichanthium aristatum* and *D. sericeum* grass species.

4.2.4.4 Root and soil hydraulic parameters

The underlying soil profile at the site was defined as 20 soil layers over a depth of 6.5 m, with roots having access down to a depth of 6 m. The profile was structurally defined by sand and clay contents for each soil layer. The respective particle size distribution at each soil layer was a sandy-loam, clay-loam profile as defined by Hutley et al. (2001) and were given values derived from Kandosol information (for that region) provided by McKenzie et al. (2004). Values for root biomass, fine root radius, root resistivity and rooting depth were derived from Chen et al. (2002) and Eamus et al. (2002). The initial water content in each soil layer was set to be between 0.15 to 0.30, denoting high soil water stores that reflects the peak wet season period for which the model begins its simulation (Table 4.1).

4.2.5 Canopy simulations to compare photosynthesis models

Three photosynthesis models were simulated across the five year period in order to determine which model is the most effective in describing carbon uptake by the C_4 savanna grasses. The three models used to simulate the grass understory were,

- the C_3 photosynthesis model described Farquhar et al. (1980)
- the C_4 photosynthesis model described by von Caemmerer and Furbank (1999)
- the *simplified* C_4 photosynthesis model described by Collatz et al. (1992)

The C_4 models were tested over a five month period during the October 2002 to April 2003 wet season. The C_3 model was used for the tree canopy (top five layers) at all times, while the grass understorey (bottom five layers) were simulated separately with each of the three photosynthesis models mentioned above. This resulted in three different *canopies* being simulated, and modelled canopy performance was evaluated by comparing estimates of ET and GPP with total ecosystem measured derived from EC at hourly, daily and seasonal time-steps. The C_4 photosynthesis model that best described the grass understorey was then selected as the defining model for C_4 photosynthesis at this site and used to investigate the relative contribution that the C_4 grasses play in savanna gas-exchange.

4.3 Results

4.3.1 C_3 and C_4 thresholds for stomatal opening

Leaf-scale measurements of C_3 and C_4 g_s were plotted against a BBL relationship, established from measurements of assimilation A_n, C_a and D_v, with the parameter $D_0 = 3.0$ kPa. The Farquhar et al. (1980) model was used to predict $A_n^{C_3}$ and the Collatz et al. (1992) model was used to predict $A_n^{C_4}$. Both the Collatz et al. (1992) and von Caemmerer and Furbank (1999) C_4 models gave similar results, and so the Collatz model is used to represent the C_4 results in parameterising ${}^{C_4}\iota_{op}$. The slope derived from fitting the BBL model to these relationships was equivalent to the parameter g_1 in Equation 4.34. The slope (unitless) for the C_3 species was found to be 14.58, which was higher than the C_4 species at 4.22. A smaller slope for the C_4 species was to be expected as this indicated a more water-use efficient plant and describes higher rates of carbon being assimilated under a lower range of g_s.

The slope of the relationship, a_1 (which can be considered equivalent to the reciprocal of plant WUE), for C_3 and C_4 vegetation decreased exponentially with increasing stomatal

TABLE 4.2: The resulting slopes (a_1) and intercepts (g_0) from fitting the Soil-Plant-Atmosphere (SPA) model to a Ball-Berry-Leuning (BBL) relationship derived using leaf-scale measurements for C_3 and C_4 vegetation. The stomatal efficiency (ι_{op}) in SPA that determines an a_1 that matches a value determined by the BBL model is the ι_{op} for that species at that particular site.

	SPA C_3		SPA C_4	
ι_{op} (%)	g_0 (mol m^{-2} s^{-1})	a_1	g_0 (mol m^{-2} s^{-1})	a_1
0.01	0.0142	38.21	-0.0085	8.39
0.03	0.0090	22.43	-0.0080	6.34
0.07	0.0058	14.82	-0.0077	5.22
0.15	0.0041	10.62	-0.0074	4.48
0.20	0.0035	9.34	-0.0071	4.22
0.30	0.0029	7.82	-0.0070	3.95

efficiency (Table 4.2; Figure 4.3). For C_3 vegetation, a_1 ranged from 38.21 when $\iota_{op} = 0.01\%$ and 7.82 when $\iota_{op} = 0.30\%$. C_4 vegetation did not experience such a large range in g_1, but still dropped by half as ι_{op} increased from $0.01 - 0.15\%$; a_1 was 8.39 when $\iota_{op} = 0.01\%$ and 3.96 when $\iota_{op} = 0.30\%$. The lower range in a_1 experienced by the C_4 vegetation is directly related to the higher water-use efficiency of C_4 plants. The intercept g_0 (equivalent to the residual g_s as $A_n \to 0$ and $Q_p \to 0$) also decreased with increasing ι_{op} and moved close to 0 and this was more pronounced with the C_3 plants, than in the C_4 plants. The smaller drop in g_0 for the C_4 plants was most obviously due to fitting a linear relationship to a nonlinear one.

Figure 4.4 shows the simulated C_3 and C_4 assimilation rates plotted against simulated g_s from the 2001 wet season period. C_4 vegetation to reached a much higher A_{max} at a low g_s compared with the C_3 vegetation, which reached a lower A_{max} at a higher g_s. In the C_4 layers, A_n saturated at approximately $g_s = 0.2$ mol m^{-2} s^{-1}, while in the C_3 layers it saturated at approximately double this value ($g_s = 0.4$ mol m^{-2} s^{-1}). Even with stomata wide open ($\iota_{op} = 0.01\%$), g_s remained relatively low in the C_4 layers compared with the C_3 layers, which needed to increase g_s threefold in order to reach the same rates of A_n.

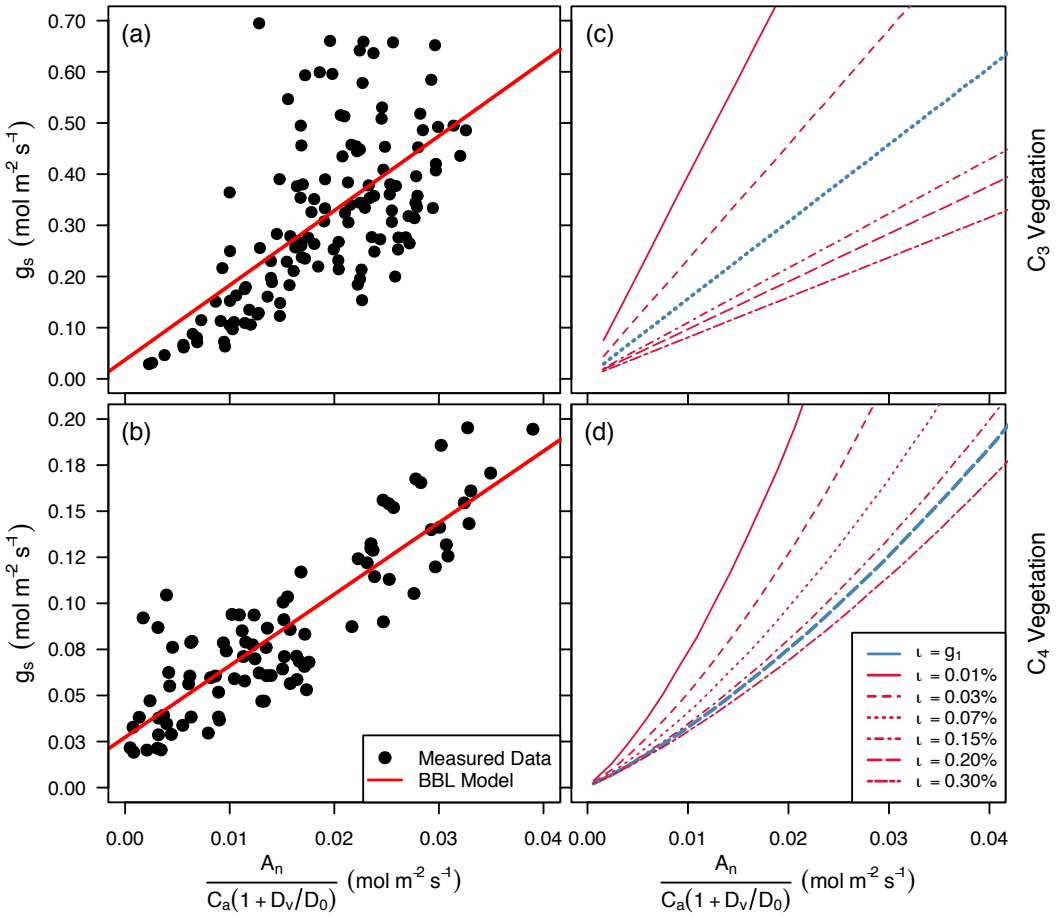

FIGURE 4.3: Measured stomatal conductance (g_s) for (a) C_3 and (b) C_4 species fitted with the Ball-Berry-Leuning (BBL) model to determine the parameter a_1 (the slope). Predicted g_s is plotted as a function of the BBL relationship at different stomatal efficiencies (ι_{op}) using (c) a C_3 photosynthesis model and (d) a C_4 photosynthesis model. The blue lines represent the ι_{op} that is equivalent to the a_1 derived from the measured data

4.3.2 Comparison between canopy simulations

Predictions from these simulated canopies were compared against EC derived measurements of ET and GPP at the daily, seasonal and annual scales. The canopy simulations to determine the most appropriate photosynthesis model were limited to the wet season period of October 2002 to April 2003. This was done as the period contained continuous measurements where prolonged gap-filling was minimal and contained no fire disturbances. Additionally, the C_4 models were only active during this period, as the dry season will contribute no information to the performance of the understorey photosynthesis models

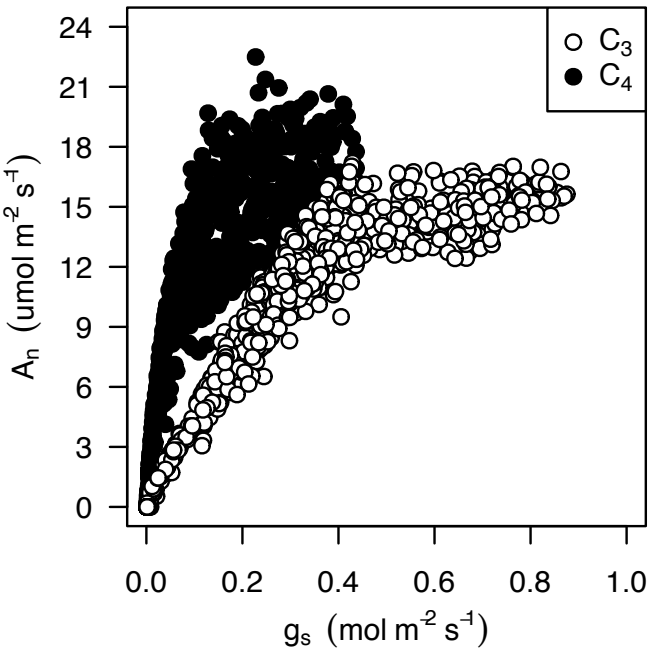

FIGURE 4.4: Simulated stomatal conductance (g_s) plotted against simulated net assimilation rate (A_n) for C_3 and C_4 model canopy layers for the 2001 year. The white circles denote the C_3 relationship using a stomatal efficiency (ι_{op} = 0.07%), while the black circles denote the C_4 relationship using an ι_{op} = 0.20%.

because the grasses are not active during the dry season. For the rest of this chapter the following definitions will be used:

- Total ecosystem = overstorey + understorey
- Overstorey = All C_3 trees, shrubs and mid-stratum vegetation
- Understorey = Only the C_4 grass

The word *'Canopy'* is used to describe the three different canopy simulations, where each simulation assumes a different photosynthesis model for the grass understorey; in Canopy 1 it is C_3 and in Canopy 2–3 it is C_4 (see Section 4.2.5). Additionally, when describing the daily results of savanna gas-exchange, ET is positive (flux moving from the canopy to the atmosphere) and GPP is negative (flux moving from the atmosphere to the canopy).

4.3.2.1 Hourly comparisons

Hourly predictions of ET and GPP derived from the three canopy simulations were compared against the respective EC derived measurements for the same period. Figure 4.5 was constructed by binning hourly measurements of ET and GPP by month, to show the average diurnal response of these quantities for each month over the test period. Measured peak ET values ranged between $0.15 - 0.36$ mm hr^{-1} and averaged at approximately 0.25 mm hr^{-1} over the test period; additionally there was some nocturnal water-use evident for most of this period. Measured peak ET increased over this period, but experienced a drop from December (0.28 ± 0.07 mm hr^{-1}) to January (0.21 ± 0.05 mm hr^{-1}) most likely as a result of increased cloud cover, frequent rain events and declining D_v (Figure 4.1b). All canopy simulations predicted very similar diurnal variations of ET across the wet season and were able to match the measured data well. There was hardly any discernible difference between the canopy simulations in predicting ET over this period. The simulations slightly underestimated average ET at the onset of the wet season by $\approx 10\%$, but then overestimated it for the rest of the season by $\approx 15\%$ with the exception of March which was able to match the measured average. The simulations did however stay within the range of error for the majority of the period.

Diurnal variations in measured peak values of GPP were large during the wet season test period, ranging from $11.0 - 26.0$ μmol m^{-2} s^{-1}, increasing from a low average peak in October (16.1 ± 5.5 μmol m^{-2} s^{-1}) to a high average peak in February (20.2 ± 4.9 μmol m^{-2} s^{-1}). A large difference in performance between the canopy simulations was clearly evident during this period. Canopy 1 consistently underestimated the average hourly rate of monthly GPP across this period by approximately $15 - 20\%$ (excluding Oct), with the highest average peak in February only reaching 14.9 μmol m^{-2} s^{-1}. For the majority of the period Canopy 1 remained within the range of measurement error, but was frequently tracing the lower limit, especially in October (9.3 μmol m^{-2} s^{-1}). Canopy 2 was able to match measured GPP to within the range of $2 - 8\%$ (excluding Oct); predicting similar monthly average peaks and remaining well within the monthly range of measurement error. Canopy 2 predicted close to the wet season maximum in February (15.8 μmol m^{-2} s^{-1}) but underestimated GPP in October (13.3 μmol m^{-2} s^{-1}) at the onset of the wet season.

Canopy 3 performed equally well, being able to match the measured GPP for most of the period to within the range of $2 - 10\%$ (excluding Oct). The wet season average peak in February was slightly underestimated at 19.8 μmol m^{-2} s^{-1}, but was still within the range of measurement error. Like Canopy 2, Canopy 3 underestimated peak GPP in October (12.4 μmol m^{-2} s^{-1}), but this traced the lower limit of the measurement error. Canopy 3 did not reach the peaks predicted by Canopy 2, and experienced slightly sharper drops from the mid-morning peaks. This is most likely due to the photosynthetic parameters in Canopy 3's C_4 model not being adequately set.

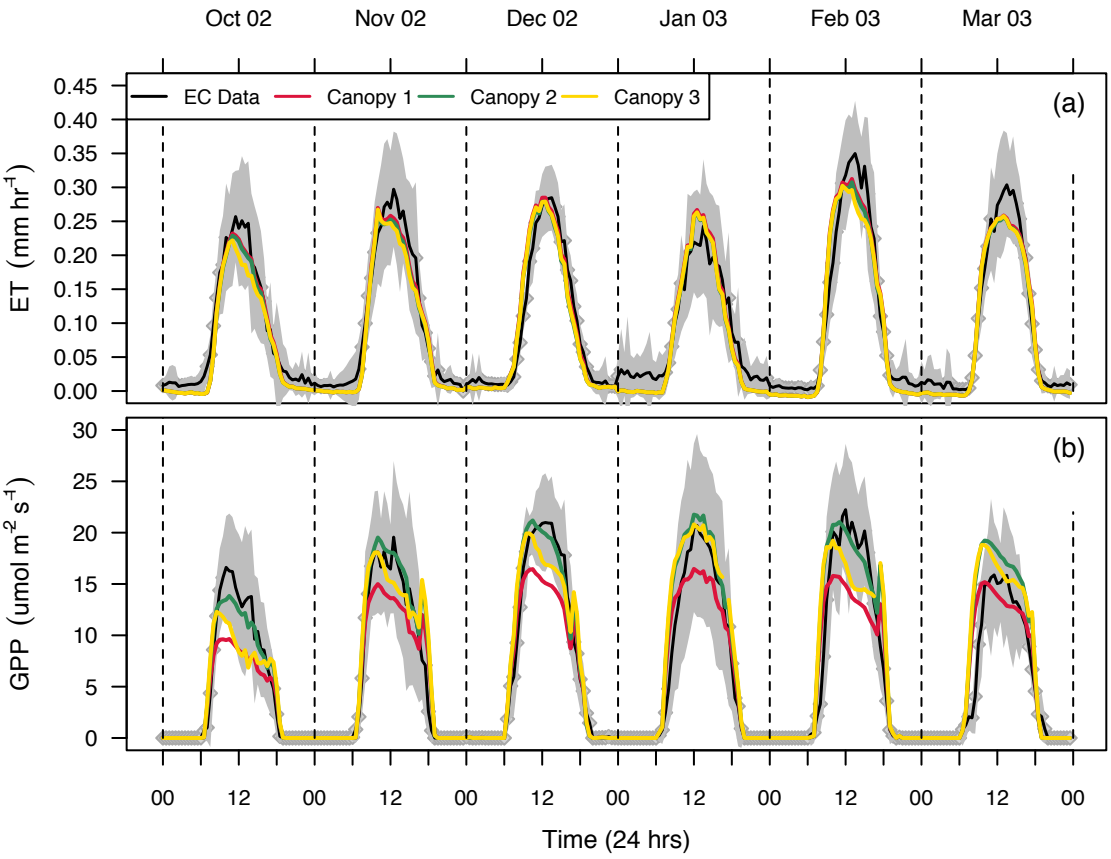

FIGURE 4.5: The three model canopies that have been used to simulate diurnal patterns of (a) evapotranspiration (ET) and (b) gross primary productivity (GPP) at the Howard Springs savanna site over the October 2002 to November 2003 wet season. The difference between the three different canopy simulations is the photosynthesis model assumed for the grass understorey: in Canopy 1 it is C_3 and in Canopies 2-3 it is C_4. Diurnal modelled and measured ET and GPP have been binned according to month, in order to show the mean diurnal responses over the test period. The mean modelled canopy outputs of ET and GPP (distinguish by colour) are compared against the mean measured diurnal responses (black line) derived from eddy-covariance (EC). The standard deviation of diurnal measured ET and GPP for each month is denoted by the gray shaded region.

4.3.2.2 Daily comparisons

Figure 4.6 shows modelled daily ET and GPP from each of the canopy simulations, plotted with daily EC measurements of ET and GPP for the October 2002 to April 2003 wet season. During this period, measured ET was typically within the range of $4.0 - 7.0$ mm d^{-1}, while GPP was within the range of $4.0 - 8.0$ gC m^{-2} d^{-1}. Measured ET and GPP fluctuated largely in February reflecting patterns in R_s and D_v. As was evident at the hourly scale, there was very little discernible difference in predictions of ET made among the canopy simulations. Modelled ET from the canopy simulations consistently overestimated measured ET by about 35% during October, but gave good agreement between modelled and measured values from the November to mid-January period. From mid-January onwards, there were frequent underestimations in daily values by approximately $10 - 20\%$. A regression analysis showed that canopy simulations were able to explain $63 - 64\%$ of the variance in measured ET, show a moderately low root mean square error (RMSE; $0.4395 - 0.5499$ mm d^{-1}) and a low model efficiency (ME; $0.17 - 0.24$). The regression lines did not match well with the 1:1 line, with all simulations having low, but similar slopes of $0.72 - 0.74$ and large intercepts of $1.43 - 1.45$ mm d^{-1} (Figure 4.7a-c). The large intercepts reflected overestimation at ET$>$ 5.5 mm hr^{-1} and underestimation at ET$<$ 5.0 mm hr^{-1}.

Daily predictions of GPP by the three canopy simulations displayed markedly different results, with the simulations that used a C_4 model performing better than one using only a C_3 model. On average, Canopy 1 underestimated measured GPP for the majority of the period. From January onwards, predicted GPP from Canopy 1 reached a daily average of about 5.0 gC m^{-2} d^{-1}, which was approximately 20% under the measured rate. The only exception was for mid-to-late February where measured GPP fluctuated largely around 4.0 gC m^{-2} d^{-1} and this gap was closed to about 9%. A regression analysis showed that Canopy 1 was able to explain 83% of the daily variation in GPP, however this is misleading as it performed poorly in predicting the correct level of daily GPP, which is shown by a low ME (0.29) and a high RMSE (1.1847 gC m^{-2} d^{-1}). The regression line poorly described the 1:1 line, having a small slope that showed increasing underestimation as the magnitude of measured GPP increased (Figure 4.7d). Canopy 2 performed well

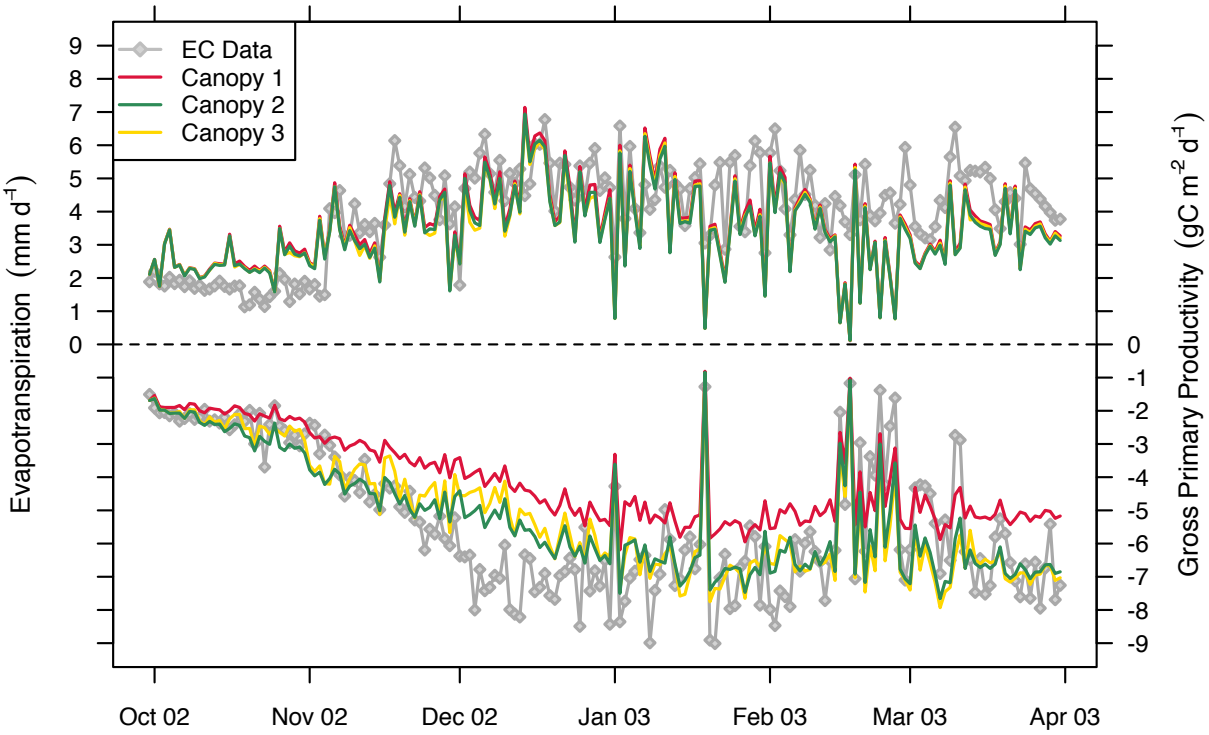

FIGURE 4.6: The three model canopies that have been used to simulate daily patterns of evapotranspiration (ET) and gross primary productivity (GPP) at the Howard Springs savanna site over the October 2002 to November 2003 wet season. The difference between the three different canopy simulations is the photosynthesis model assumed for the grass understorey: in Canopy 1 it is C_3 and in Canopies 2-3 it is C_4. The gray lines and points represent measured ET and GPP derived from eddy-covariance (EC), while the coloured lines represent the three different canopy simulations.

in predicting measured GPP, from October to November and January onwards predicting GPP to be in the range of $5.0 - 7.0$ gC m^{-2} d^{-1}, which was within 9% of the measured value. Between late November and most of December, the predictions were poor (5.5 gC m^{-2} d^{-1}) and underestimated measured GPP by about 15%. Canopy 3 gave almost equal predictions of GPP compared with Canopy 2; with predictions differing by less than 2% on average. The only divergence between these two simulations, occurred during the late November to late December period, where Canopy 3 gave slightly lower predictions at around 5.0 gC m^{-2} d^{-1}. A regression analysis showed Canopy 2 to be to explain 84% of the variation in daily GPP. A high ME (0.70) and low RMSE (0.0393 gC m^{-2} d^{-1}) gave a good indication that Canopy 2 performed well in it's predictions (Figure 4.7e). The regression was close to the 1:1 line, with a slope of 1.04 and an intercept close to zero.

Canopy 3 could only explain 69% of the variance which was lower than Canopy 1, but had a high ME (0.61) and low RMSE (0.0934 gC m^{-2} d^{-1}), indicating good model performance. The regression line for Canopy 3 was relatively close to the 1:1 line, with a slightly lower slope of 0.91 reflecting some slight underestimation of measured GPP (Figure 4.7f).

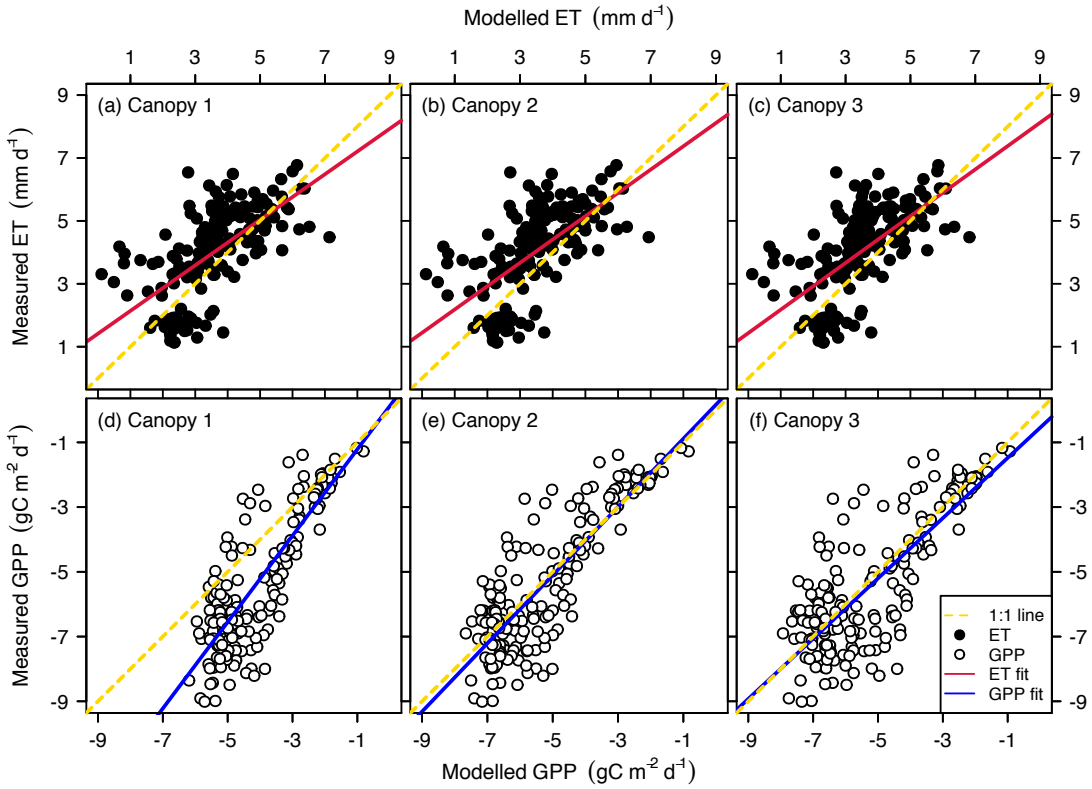

FIGURE 4.7: Regression plots that compare modelled and measured evapotranspiration (ET) for (a) Canopy 1, (b) Canopy 2 and (c) Canopy 3 simulations. Additionally, modelled and measured gross primary productivity (GPP) for (d) Canopy 1, (e) Canopy 2 and (c) Canopy 3 are compared. The yellow dotted line represents the 1:1 line, while the solid blue and red lines represent the fitted regression lines. The difference between the three different canopy simulations is the photosynthesis model assumed for the grass understorey: in Canopy 1 it is C_3 and in Canopies 2-3 it is C_4.

4.3.2.3 Residual analysis

A residual analysis was used to identify the causes of model failure in predicting daily measured ET and GPP. Plotting the ET residuals against time, showed that underestimation increased moving from the start to the middle of the wet season, before dropping back to the zero error point at the end of March. This showed the error to be the result

TABLE 4.3: Statistics of model performance for the three canopies that were used to simulate evapotranspiration (ET; *mm d^{-1}) and gross primary productivity (GPP; *gC m^{-2} d^{-1}) in the Soil-Plant-Atmosphere (SPA) model. The statistics listed here are the explained variance (R^2), model efficiency (ME) and root mean square error (RMSE), slope and intercept of the regression line.

	Model	R^2	ME	RMSE*	Slope*	Intercept*
ET	Canopy 1	0.64	0.24	0.4395	0.72	1.43
	Canopy 2	0.63	0.17	0.5549	0.73	1.45
	Canopy 3	0.63	0.18	0.5473	0.74	1.44
GPP	Canopy 1	0.83	0.29	1.1847	1.31	0.12
	Canopy 2	0.84	0.70	0.0393	1.04	0.18
	Canopy 3	0.69	0.61	0.0934	0.91	-0.54

of one of the environmental drivers during this period (Figure 4.8a). Residuals plotted against predictions of ET, showed that the error was stable when predictions of ET were high and underestimation was largely limited when predictions were low (< 3 mm d^{-1}) (Figure 4.8b). Plotting the ET residuals against the environmental drivers showed that most of the underestimation is also the result of a drop in total R_s and D_v (Figure 4.8c-d). The residuals plotted with D_v however, show that at $D_v > 3.0$ kPa, measured ET is most likely being reduced by a reduction in canopy g_s to prevent xylem cavitation, which is not being replicated in the model. Residuals plotted against θ_s and LAI however, show that increases in canopy L_A and soil water stores increased the understimation of ET by the model (Figure 4.8e-f). In the case of LAI, this could mean that too much L_A is being assigned to the overstorey which is reducing the amount of available energy reaching the understorey to evaporate water, regardless of θ_s.

A residual analysis was also used to identify the causes for failure of the photosynthesis models to adequately describe the measured GPP. Differences in intercepts between Canopy 1 and Canopies 2 and 3, are the result of Canopy 1 consistently underestimating daily GPP for the period. Plotting the residuals against time showed that underestimation increased from late November to late December period for all simulations (Figure 4.8 g). Plotting the residuals against predicted GPP, showed that the error was not a result of the magnitude of the predictions in all simulations (Figure 4.8h). Plotted against the

environmental drivers, the residuals showed a drop in daily total R_s (< 12 MJ m^{-2} d^{-1}) to cause an increase in model overestimation of measured GPP for all canopies (Figure 4.8i); no difference in the slope was seen between the slopes for Canopy 1, 2 and 3 ($P < 0.005$). Underestimation of measured GPP increased with increasing D_v (> 3.0 kPa). The underestimation is slightly more pronounced in Canopies 2 and 3, compared with Canopy 1, which has a slope that is almost zero (Figure 4.8j). Residuals plotted against θ_s showed no relationship for Canopies 2 and 3, but a slight relationship to exist for Canopy 1 (Figure 4.8k). Residuals plotted against LAI showed an irregular curve, where predictions of GPP decreased between a LAI of $1.4 - 1.8$ m^2 m^{-2} (Figure 4.8l). Outside this range, the residuals were well dispersed around the zero error mark, which suggests that the hump is a product of the other factors (i.e. D_v, R_s). This may therefore not be a problem in the model, but rather error in the EC measurements (Baldocchi et al., 1996).

4.3.2.4 Comparison of modelled and measured period totals

The cumulative sum of predicted ET and GPP from the three canopy simulations for the test period were compared against the cumulative sums of the measured period totals derived from EC (Fig. 4.9). Total measured ET and GPP for the period was 654 mm and 866 gC m^{-2} respectively. Canopy 1 overestimated measured total ET by 5.2% at 688 mm, but significantly underestimated total GPP by 19.1% at 701 gC m^{-2}. Canopy 2 gave the closet approximated totals of measured total ET and GPP. Measured total ET was overestimated, but only by 3.2% at 675 mm, while total measured GPP was underestimated by 5.8% at 816 gC m^{-2}. Canopy 3 gave the lowest prediction of total period ET at 591 mm, which was 9.6% under the measured total. However, despite the lower predicted total ET, Canopy 3 gave a very similar prediction of total GPP at 815 gC m^{-2}, which was 5.9% under the measured total. This suggests that those simulations which used a C_4 photosynthesis model were able to improve their prediction of the estimated total GPP by 13.3%. This did not have a great affect on estimated totals of ET, which at the worst was still within 10% of the measured total.

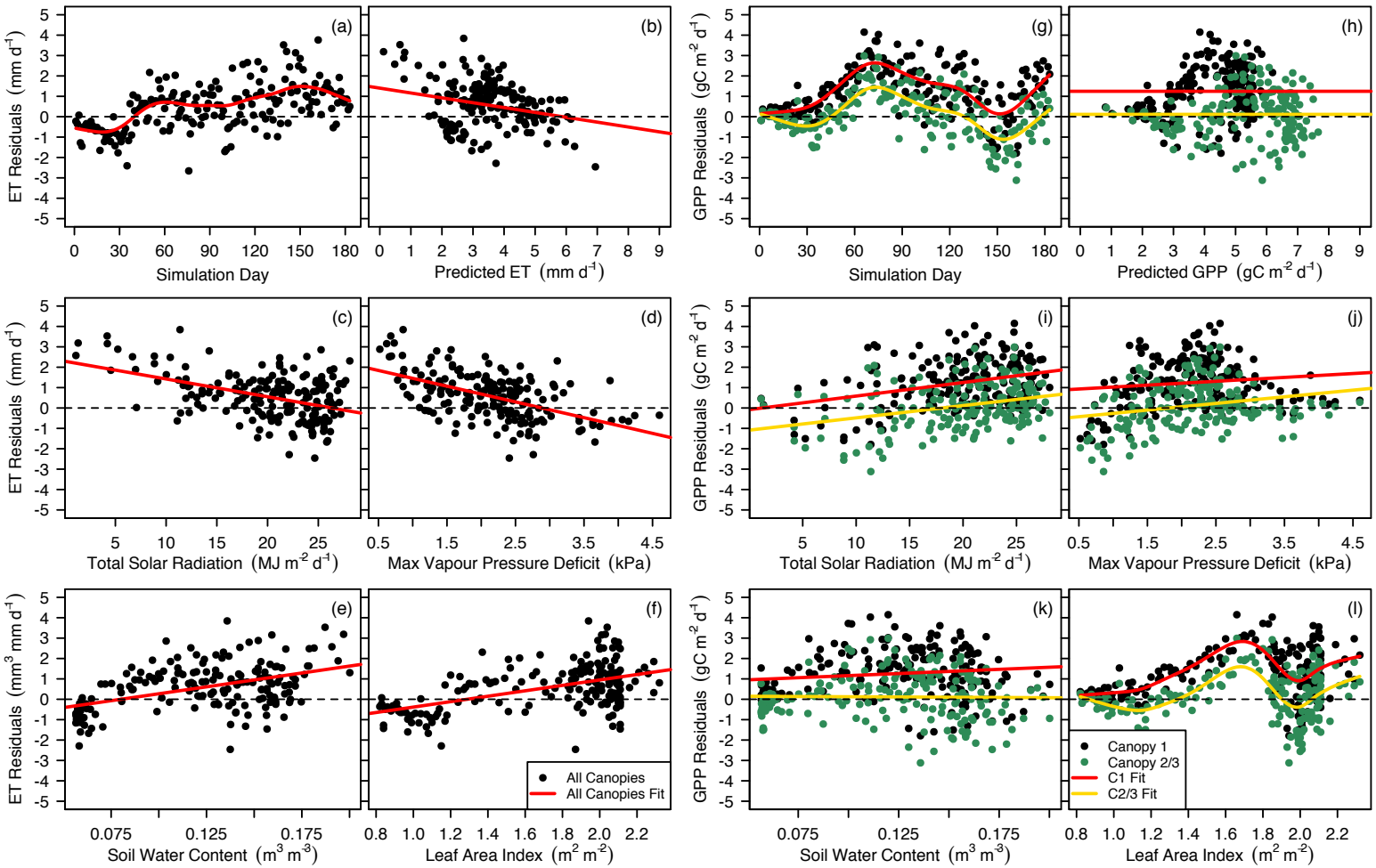

FIGURE 4.8: Residual analysis between modelled and measured evapotranspiration (ET) and gross primary productivity (GPP) for the three canopy simulations. The residuals for ET are plotted against (a) time, to determine periods of model failure, (b) model predictions, in order to determine model bias, (c) daily total solar radiation, (d) daily maximum vapour pressure deficit (VPD), (e) daily soil water content (SWC) and f) leaf area index (LAI) to determine the influence of the environmental drivers. For the same reasons, residuals of GPP are plotted against (g) time, (h) model predictions, (i) total solar radiation, (j) VPD, (k) SWC and (l) LAI. For the GPP model residuals, Canopy 1 is given by black circles and Canopies 2 and 3 are given by green circles. The red and yellow lines denote a regression fit to determine a pattern in the residuals.

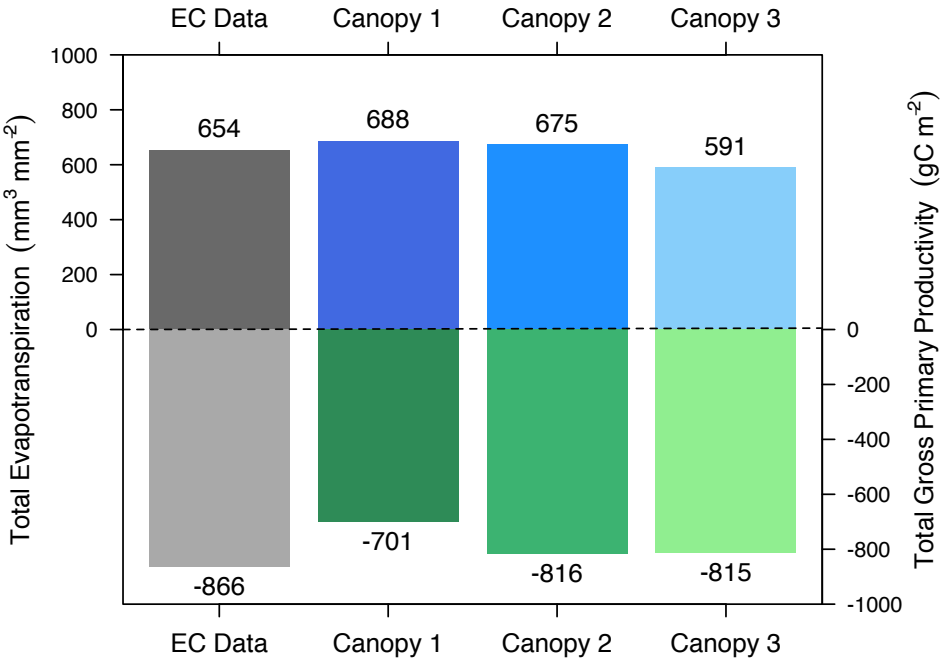

FIGURE 4.9: The cumulative sum of eddy-covariance (EC) measured evapotranspiration (ET) and gross primary productivity (GPP) compared with the cumulative sum of estimated ET and GPP derived from the three canopy simulations. These sums are taken over the October 2002 to April 2003 test period. The difference between the three different canopy simulations is the photosynthesis model assumed for the grass understorey: in Canopy 1 it is C_3 and in Canopies 2-3 it is C_4.

4.3.3 Modelled contributions to savanna fluxes of the C_3 overstorey and C_4

The incorporation of the C_4 photosynthesis model significantly improved the estimates of GPP over the simulation period. Canopy 2, using the Collatz et al. (1992) model for C_4 photosynthesis having performed the best of the three photosynthesis models in predicting ecosystem ET and GPP was then applied for the entire five year period (2001–2005) and compared against EC derived measurements. Additionally, overstorey and understorey components were examined to examine the relative contribution that the C_4 understorey plays in the savanna ecosystem.

4.3.3.1 Intra-daily patterns over a one year period

Modelled hourly rates of ET and GPP were compared against EC derived measurements on a monthly-average diurnal course over the 2001 year. Figure 4.11 was constructed by binning the hourly diurnal course of modelled and measured ET and GPP by month to show the average diurnal response for each month across the year. The diurnal course of measured ET from the wet season to the dry season showed a decrease in midday peak from 0.30 ± 0.07 mm hr^{-1} in April to 0.10 ± 0.02 mm hr^{-1} in September. Peak rates of ET increased with the arrival of monsoonal rains during late October, reaching a maximum in December. During the wet season nocturnal water-use was evident, fluctuating between $0.01 - 0.02$ mm hr^{-1}. Variations in ET were much larger during the wet season (0.20-0.37 mm hr^{-1}) than in the dry (0.11-0.13 mm hr^{-1}) because of frequent cloud cover and high intermittent rainfall. The diurnal course of measured GPP similarly followed the seasonal patterns seen in ET. With the onset of the dry season at the start of April, daily peak GPP fell from a high midday peak of 20.1 ± 4.9 μmol m^{-2} s^{-1} to a low midday peak of 5.2 ± 1.3 μmol m^{-2} s^{-1} in September, following the seasonal course of LAI (Fig. 4.2b). The midday peak of GPP increased in late October with the regeneration in canopy LAI and the onset of frequent rainfall events. By December, canopy vegetation had recovered from the aridity of the dry season and the GPP midday peak was close to the wet season average. The model was able to give a good approximation to the diurnal course of measured ET. During the wet season, ET tended to slightly over- or underestimate across the year, but generally gave predictions well within the bounds of measurement error. Predicted seasonal peaks were close to the measured ones, with a similar wet season high of 0.31 mm hr^{-1}, and dry season low of 0.14 mm hr^{-1}. The only exception occurred during September and October, where the model significantly overestimated ET above the upper boundary of error (Figure 4.10a). The model was also able to trace the diurnal course of measured GPP, matching the monthly-average midday peaks for the majority of the year. Overestimation tended to be limited to the end of the wet season, when LAI was high and θ_s non-limiting, while underestimation tended to occur during the mid-dry season (June–August), when LAI in the understorey had died off (Figure 4.10b). However, in most cases these variations were within the bounds of error. The model was able to predict similar

high midday peaks of GPP (22.5 μmol m^{-2} s^{-1}) during the wet season, and match the low midday-peak of 5.2 μmol m^{-2} s^{-1} well into the dry season.

In order to examine how canopy gas-exchange in the savanna differs between the C_3 and C_4 parts of the canopy, the canopy predictions in Figure 4.10 were partitioned into tree (C_3) and grass (C_4) transpiration (E_t) and A_n. Additionally the leaf-scale variables of g_s and Ψ_l were used to help explain the seasonal variations (Figure 4.11). Wet and dry season patterns of overstorey stomatal conductance ($^{C_3}g_s$) were asymmetrical over the diurnal course, with a much higher $^{C_3}g_s$ in the morning than in the afternoon (Figure 4.11a). Maximum wet season $^{C_3}g_s$ peaked at approximately 0.6 mol m^{-2} s^{-1} in the morning and decreased to around 0.4 mol m^{-2} s^{-1} in the afternoon, due to tight stomatal control in response to the drop in Ψ_l. Morning peak $^{C_3}g_s$ during the dry season did not reach the high levels achieved in the wet season and were limited to around 0.40 mol m^{-2} s^{-1}, being regulated by low overstorey Ψ_l. The distinct asymmetry in the diurnal course of $^{C_3}g_s$ observed in the wet season was not as severe in the dry season, and afternoon $^{C_3}g_s$ did not reduce by a significant amount falling to about 0.3 mol m^{-2} s^{-1}. Understorey stomatal conductance ($^{C_4}g_s$), maintained a relatively constant maximum at around 0.25 mol m^{-2} s^{-1}, with the exception of April which displayed a higher than average peak at about 0.4 mol m^{-2} s^{-1}. No asymmetry was observed in the diurnal courses of monthly $^{C_4}g_s$, due to high Ψ_l and low D_v. As the canopy moved into the dry season $^{C_4}g_s$ dropped from a high in April to a low in May following the severe drop in leaf area.

Patterns in the diurnal course of E_t in both the C_3 tree canopy and C_4 grasses reflected changes in g_s and Ψ_l (Figure 4.11b). The overstorey transpiration rate ($^{C_3}E_t$) remained fairly consistent over the course of the year at about 1.1 mmol m^{-2} s^{-1}, but increased during the wet-to-dry season transition period (April–June) to a high of 1.6 mmol m^{-2} s^{-1} as a result of high θ_s, large R_s and an increased D_v. However as Ψ_l dropped, so too did $^{C_3}E_t$ due to tighter stomatal control reaching a low of about 0.8 mmol m^{-2} s^{-1} in the dry season. The understorey transpiration rate ($^{C_4}E_t$) was relatively low and constant during the wet season, maintaining an hourly maximum $^{C_4}E_t$ of 0.4 mmol m^{-2} s^{-1}. There was an increase in $^{C_4}E_t$ to approximately 0.5 mmol m^{-2} s^{-1} moving out of the dry season (due to increasing LAI with θ_s), but this declined to a constant of 0.4 mmol m^{-2} s^{-1} with the seasonal drop in D_v.

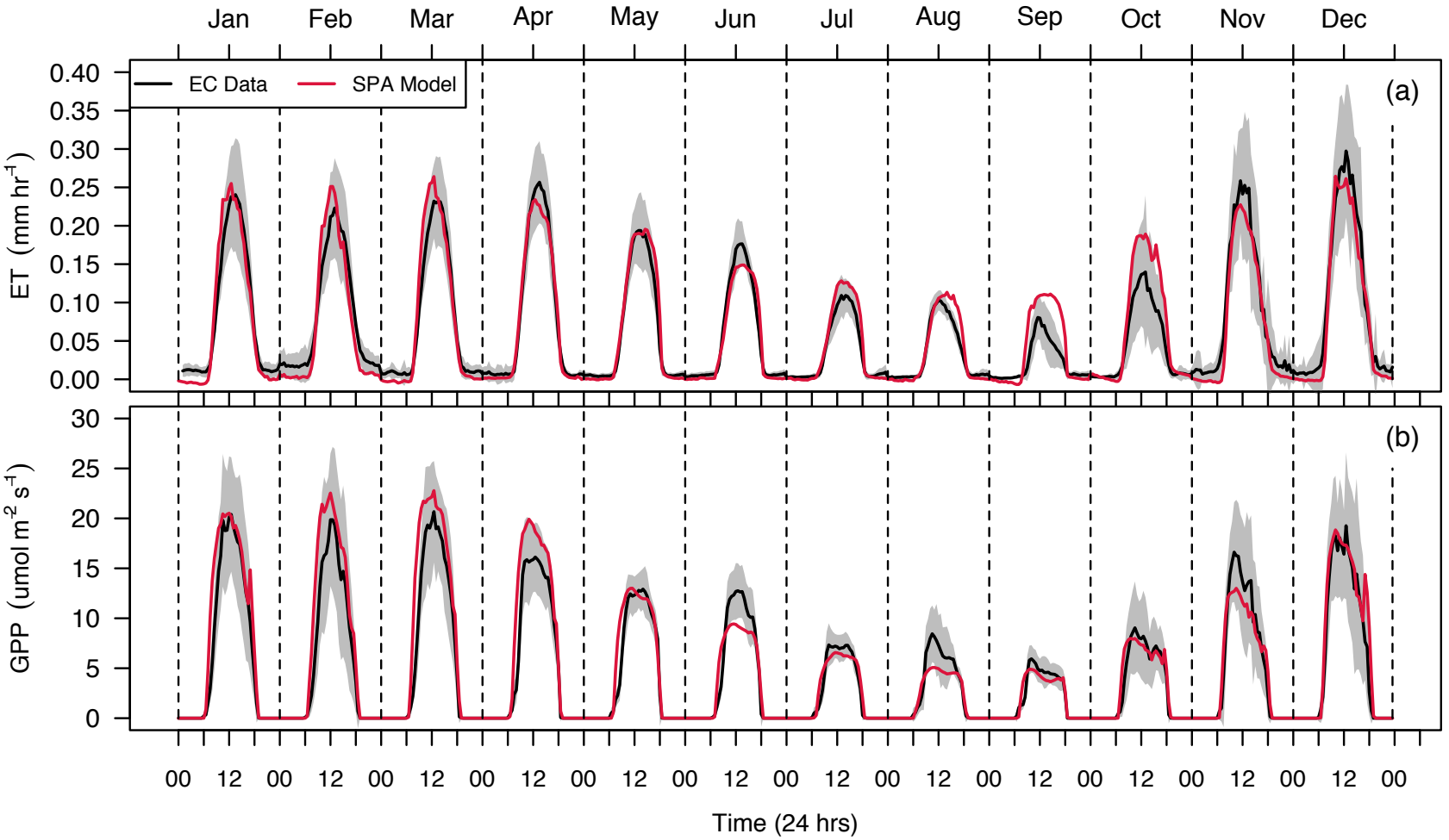

FIGURE 4.10: Binned monthly diurnal patterns of modelled (a) evapotranspiration (ET) and (b) gross primary productivity (GPP) compared with measurements derived from eddy-covariance (EC) for 2001. The mean measured responses of ET and GPP are given as black lines, while model predictions are given as red lines. The shaded gray regions denote the standard deviation of the measured mean ET and GPP.

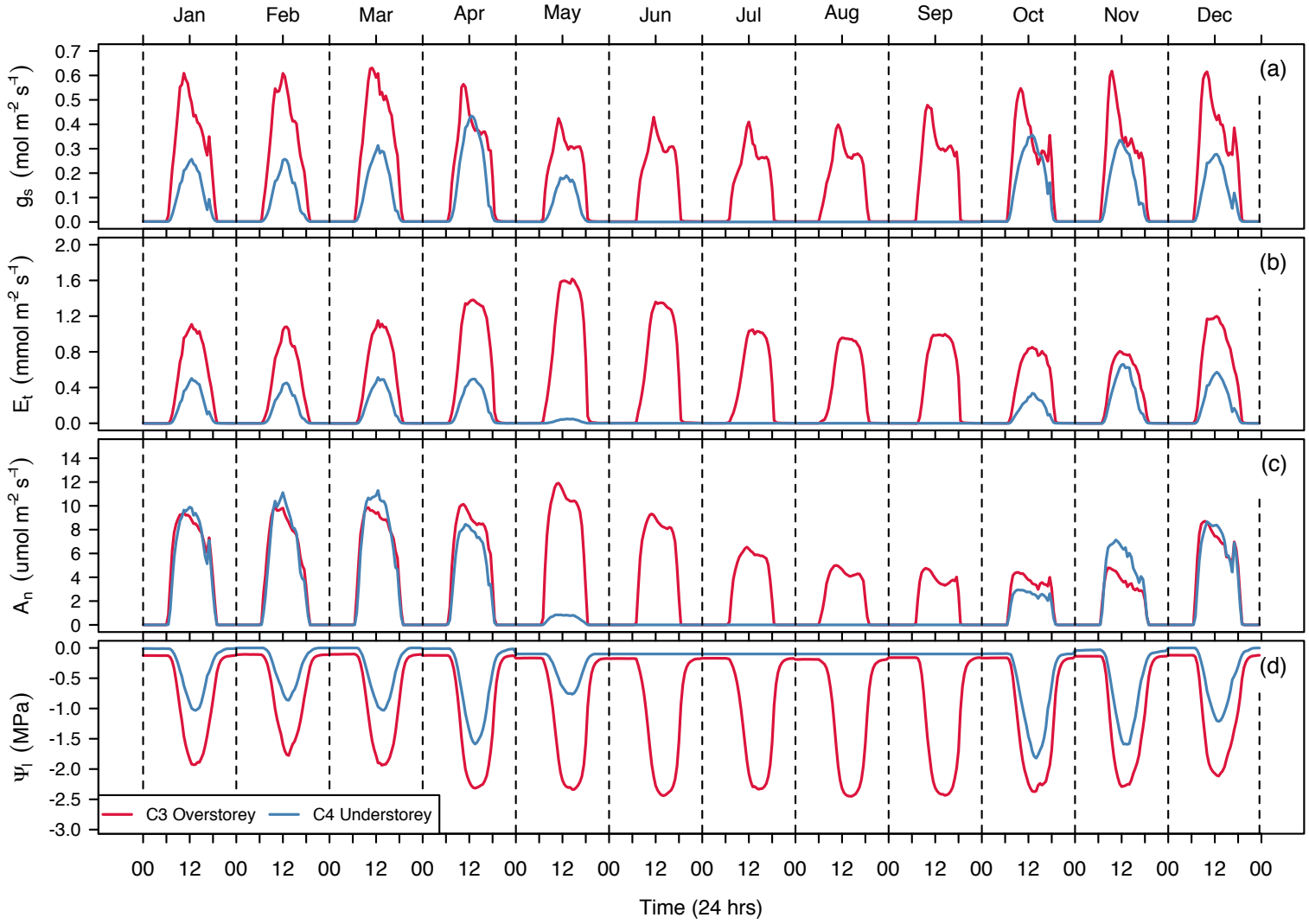

FIGURE 4.11: Binned monthly diurnal patterns of the simulated C_3 tree canopy and C_4 grass averaged leaf-scale gas-exchange quantities in 2001. These quantities include (a) the weighted stomatal conductance (g_s), (b) transpiration (E_t), (c) net assimilation (A_n) and (d) leaf water potential (Ψ_l). The red lines denote the C_3 tree canopy, while the blue lines represent the C_4 grasses.

Net CO_2 assimilation rates in the over- and understorey strongly reflected seasonal changes in over- and understorey LAI (Figure 4.2b). Overstorey net assimilation ($^{C_3}A_n$) remained consistent over the wet season period, with a midday peak of 10.1 μmol m^{-2} s^{-1}, with the exception of the dry-to-wet season transitional period (October–December) where $^{C_3}A_n$ was lower (Figure 4.11c). Dry season $^{C_3}A_n$ reached a reduced maximum of 4.0 μmol m^{-2} s^{-1} during September and is likely a result of a very low Ψ_l tracking close to the $\Psi_{l\,min}$ restricting stomatal opening. Understorey net assimilation ($^{C_4}A_n$) was high during the wet season, where peak rates were 10.3 μmol m^{-2} s^{-1}, equivalent with the overstorey. Following the seasonal course of LAI, $^{C_4}A_n$ dropped significantly in May to a peak rate < 1 μmol m^{-2} s^{-1}. Rates of $^{C_4}A_n$ increased gradually during the dry-to-wet transition period to reach large wet season rates in January.

Leaf water potentials between the canopy over- and understorey were significantly different over the course of the year (Figure 4.11d). Overstorey minimum leaf water potential ($^{C_3}\Psi_l$) was highest during the wet season with the highest $^{C_3}\Psi_l$ occuring in February at about -1.75 MPa. Moving into the dry season $^{C_3}\Psi_l$ decreased to an average low of -2.4 MPa tracking close to $\Psi_{l\,min}$ due to consistent water-use by the overstorey through the dry season at low soil moisture. In actuallity $^{C_3}\Psi_l$ would have fallen below $\Psi_{l\,min}$ frequently, causing a stronger stomatal regulation to water loss. Conversely, understorey leaf water potential ($^{C_4}\Psi_l$) remained relatively high during the wet season, staying above -1.0 MPa for most months, with the exception of the dry-to-wet transition period which reached an average minimum of -2.0 MP as a result of low soil moisture in the upper soil profile. $^{C_4}\Psi_l$ decreased with the increase in soil moisture of the upper soil profile, due the increased frequency of rainfall events. High $^{C_4}\Psi_l$ was maintained due to low $^{C_4}E_t$ as a result of the C_4 photosynthetic pathway being highly water-use efficient.

Abiotic factors controlling canopy gas-exchange

The tree overstorey (C_3) and grass understorey (C_4) outputs of E_t and A_n described above were plotted against four key abiotic variables known to regulate these fluxes, as a way of investigating how they responsed to changes in the environment. In the wet-dry tropics of Australia, variables known to drive water loss and carbon assimilation are R_s,

D_v and θ_s (Eamus et al., 2001). Figure 4.12 shows the response of tree over- and grass understorey rates of E_t and A_n to variation in these variables, as well as LAI. Quantile regression (Koenker and Bassett, 1978) was used to fit a set of nonlinear relationships for the responses of modelled over- and understorey A_n and E_t to variation in R_s and D_v, and linear relationships were used to explain the variation in θ_s and LAI. Fitting the 95% quantile of these relationships rather than the mean was done in order to capture the non-limiting responses of over and understorey gas-exchange to the driving abiotic variables (e.g. the response of A_n to R_s independent of D_v, θ and L_{AI}) (Jarvis, 1976; Stewart, 1988; Mäkelä et al., 2008).

Modelled C_3 over- and C_4 understorey A_n increased linearly with R_s until approximately 200 W m^{-2} where it tended towards an asymptote, saturating towards A_{max} at $R_s > 800$ W m^{-2} (Figure 4.12a). The understorey exhibited a slightly larger initial slope (proportional to ecosystem quantum yield) compared with the overstorey. Despite a drop in A_{max}, no discernible difference was observed in the slope between the wet and dry season responses (Figure 4.12b). In contrast, a significant difference was observed between the over- and understorey responses of E_t to variation in R_s. The response of overstorey E_t in the wet season showed an asymptotic response similar to that of A_n, but saturated towards E_{max} (1.6 mmol m^{-2} s^{-1}) at a much larger R_s ($\approx$ 900 W m^{-2}). The understorey response on the other hand was linear, with no observable asymptote observed (Figure 4.12c). The dry season response for the overstorey exhibited a linear increase at low R_s and E_{max} approached an asymptote much sooner than in the wet season ($\approx$ 300 W m^{-2}) (Figure 4.12d).

The modelled C_3 over- and C_4 understorey responses of A_n to D_v in the wet season showed rapid increases in A_n at low D_v, reaching A_{max} at approximately 1.0 kPa, after which a rapid decline was observed when $D_v > 1.5$ (Figure 4.12e). No difference in the slopes between the overstorey and understorey was observable, with both canopy components tending to exhibit the same rate of decay in A_n. There was a very weak overstorey response in the dry season, with no significant relationship being determined, except for a slight drop in A_n when $D_v > 2.5$ kPa (Figure 4.12f). The response of over- and understorey E_t to increasing D_v during the wet season was more pronounced than that of A_n. Overstorey E_t increased linearly at low values of D_v, reaching E_{max} at approximately 1.5 kPa, after

which it declined linearly (Figure 4.12g). However, understorey E_t reached E_{max} at a much higher D_v and did not decline with increasing D_v in contrast to the overstorey. Dry season overstorey E_t increased linearly to a much higher D_v than in the wet season at approximately 3.0 kPa, but experienced a sharp decline after this value (Figure 4.12h).

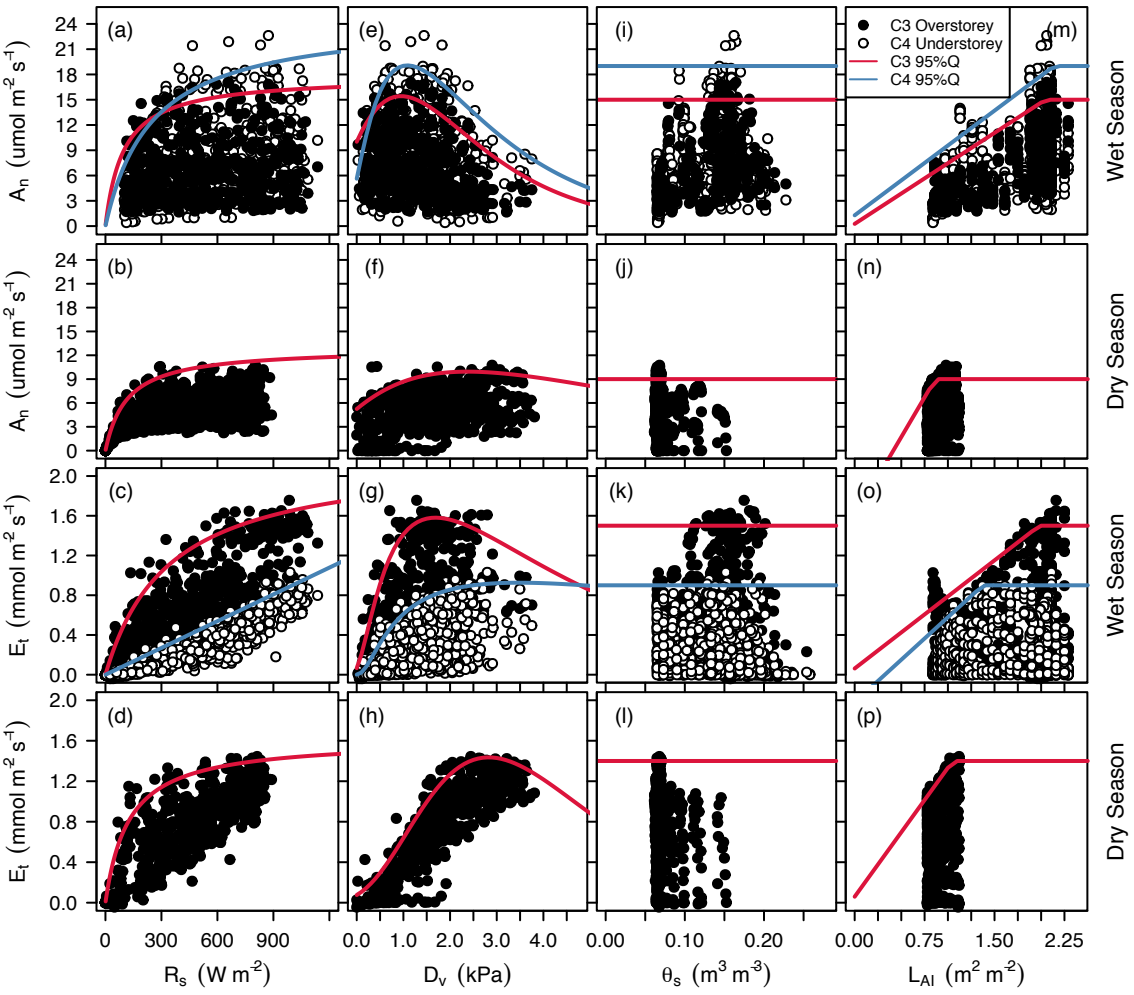

FIGURE 4.12: Relationships between modelled wet and dry season estimates of C_3 and C_4 net assimilation (A_n) and transpiration (E_t) and the primary environmental drivers of solar radiation (a-d) (R_s), (e-h) vapour pressure deficit (D_v), (i-l) soil water content (θ_s) and (m-p) leaf area index (L_{AI}). The black circles shows model estimates for the C_3 trees, and the white circles show the model estimates for the C_4 grasses. Quantile regression is used to fit the upper boundaries of the relationships in order to determine the underyling non-limiting responses, where the red and blue lines represent the quantile fits for C_3 and C_4 vegetation respectively.

The over- and understorey responses of A_n to increasing θ_s displayed piece-wise linear relationships, with the slope of the relationship being slightly larger in the understorey

than in the overstorey (Figure 4.12i). In contrast, the overstorey response in the dry season displayed no significant relationship, despite a much lower θ_s, likely due to the overstorey accessing deep water-stores (Figure 4.12j). The wet season response of overstorey E_t displayed a similar *broken stick* relationship and similar slope to that of A_n (Figure 4.12k). No significant relationship for understorey E_t was observed in the wet season, suggesting that the C_4 grasses are insensitive to soil water status. In the dry season no significant response was observed for the overstorey (Fig. 4.12l). It should be noted that the soil moisture measurements are only for the top 10 cm of the soil profile and no true response may be seen for both A_n and E_t in either season. It is therefore recommended that Figures 4.12i-l) be interpreted with caution.

Relationships between modelled over- and understorey A_n and LAI showed strong positive linear responses (Figure 4.12m). Both over- and understorey sections of the canopy displayed similar slopes in the relationship, with the understorey being slightly higher. The dry season response of the overstorey showed a strong relationship with LAI, producing a larger slope than in the wet season (Figure 4.12n). The wet season responses of over- and understorey E_t were markedly different, with the overstorey showing a strong significant relationship, and the canopy understorey showing no relationship (Figure 4.12o). For the dry season a significant response of the overstorey was observed (Figure 4.12p). Strong relationships for overstorey A_n and E_t in the dry season, is most likely due to adjustment of the canopy leaf-area in response to seasonal changes in D_v and θ. All modelled gas-exchange responses were found to have the same A_{max} and E_{max} across the 4 covariates.

4.3.3.2 Seasonal patterns over the 2001 to 2005 period

Total Canopy

Daily outputs of predicted ET and GPP from SPA were compared against EC derived measurements for the 2001 to 2005 study period (Figure 4.13). Ecosystem ET and GPP derived from EC measurements were largest in the wet season, typically within the ranges of 3.5-7.0 mm d^{-1} and 4.0-8.0 gC m^{-2} d^{-1} respectively; only rarely did GPP decline below 3.0 gC m^{-2} d^{-1} in the wet season. Day-to-day variations in ET and GPP in the wet season

closely reflected patterns in rainfall and R_s. From approximately mid-March through to September, both ET and GPP declined exponentially to an approximate minimum of 2.0 mm d^{-1} and 1.5 gC m^{-2} d^{-1} respectively. In the singular case of 2001, ET declined to an approximate low of 0.5 mm d^{-1}. Gradual increases in ET and GPP began following the dry season minima, generally between late September and mid-October, following the new growth of C_4 vegetation. The model predicted maximum ET in the wet season at values between 4.0 and 7.0 mm d^{-1}, while minimum values slightly overestimated dry season ET; predicting values within the range of 2.0-3.0 mm d^{-1}. It was only in 2003 that the model was able to clearly match measured dry season ET, with overestimation occurring for all other dry seasons. Model predictions of daily GPP match well with the EC derived measurements for the five year simulation period. The model predicted a maximum GPP of approximately 7.5 gC m^{-2} d^{-1} in the wet season agreeing well with the measurements. During the dry season predicted GPP fell to a minimum of 1.5 gC m^{-2} d^{-1} in September. The model was able to predict variations shown in the measurements especially in 2001 and 2003. The other years however had higher measured minimums of about 2.0-2.5 gC m^{-2} d^{-1}, which the model underestimated.

A regression analysis between modelled fluxes of ET and GPP and the EC derived measurements was done for each separate year and the entire simulation period (Figure 4.14). Plots of modelled *versus* measured are given for each year used in the simulation.[3] Figure 4.14 shows that across all five years of study, there was a significant positive relationship between modelled and measured for both GPP and ET; these statistics are given in Table 4.4. Modelled ET produced a moderate range of R^2 values, and was able to explain 68-81% of the variation in measured ET across the study period and explained 75% of the variance over the entire five years. The ME showed that out of these years, 2001 and 2002 gave close approximations to the 1:1 line with ME values in the range of 58 to 65. This was reflected in low values of RMSE in the range of $0.0656 - 0.1205$ mm d^{-1}, slopes closest to 1 and intercepts closest to 0. The years of 2003-2005 had much lower ME values in the range of 0.44 to 0.49. However, the RMSE was still low for these years, in the range of 0.0500-0.1929 mm d^{-1}, and the regression lines had reduced slopes and slightly larger intercepts. For the entire period, the model was able to explain 75% of the variance, but

[3]ET is plotted along a positive scale, while GPP is plotted against a negative scale

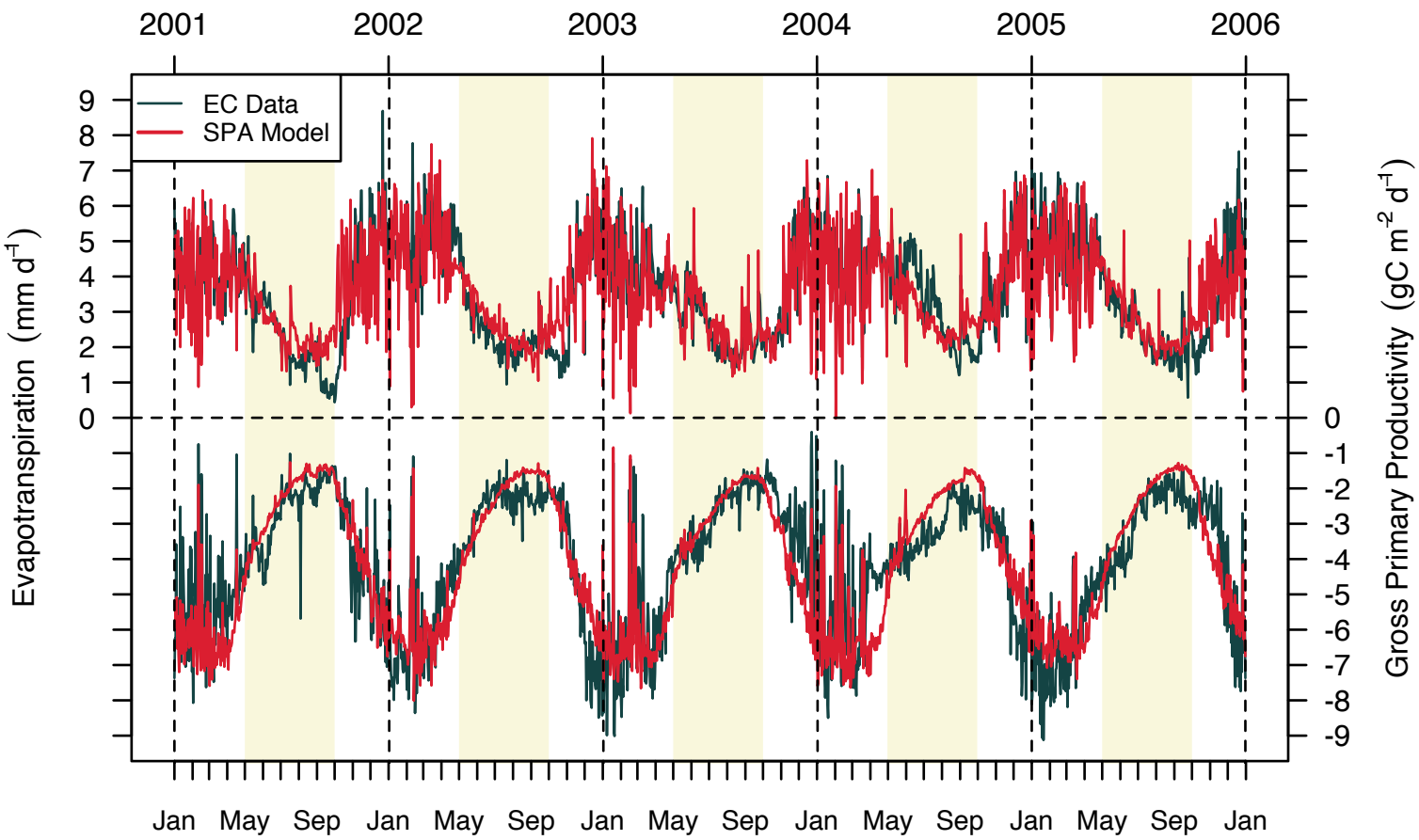

FIGURE 4.13: A comparison of estimated (red line) evapotranspiration (EC) and gross primary productivity (GPP) using the Soil-Plant-Atmosphere (SPA) model with the measured (black line) ET and GPP derived from eddy-covariance (EC) for the 2001 to 2005 study period. The yellow shaded regions denote the dry season period for each year.

a low ME due to overestimation for low measured ET (< 3 mm d^{-1}). The overall RMSE was low at 0.0376 mm d^{-1} and regression line gave a good approximation to the 1:1 line. Modelled GPP produced a high range of R^2 values across the simulation period, with the explained variance ranging from 80-90%. ME remained high in the range of 0.69 to 0.81, with the exception of 2004 where ME was lowest at 0.46. RMSE was relatively low across the five years, ranging from 0.0218 to 0.2517 gC m^{-2} d^{-1}; 2004 had the lowest RMSE, despite the model providing the least favourable fit to the data. The regression lines for 2002, 2003 and 2005 gave good approximations to the 1:1 line, with slopes close to 1 and intercepts close to 0. For 2001 and 2004 however, the regression lines had smaller slopes and larger intercepts reflecting periodic over- and underestimation and high and low GPP respectively. For the entire period, the model was able to account for 83% of the variation in measured GPP, had a large ME reflecting a good approximation of the 1:1 line, and a low RMSE of 0.0057 gC m^{-2} d^{-1}.

TABLE 4.4: Statistics of model performance in estimating evapotranspiration (ET; mm d^{-1}) and gross primary productivity (GPP; gC m^{-2} d^{-1}) for the 2001 to 2005 simulation period. Listed are the explained variance (R^2), model efficiency (ME) and root mean square error (RMSE), as well as the slope and intercept of the regression line.

		Model Results				
	Year	R^2	ME	RMSE	Slope	Intercept
ET	2001	0.77	0.58	0.1205	0.93	0.13
	2002	0.81	0.65	0.0656	0.89	0.32
	2003	0.73	0.46	0.1309	0.74	0.99
	2004	0.76	0.49	0.1929	0.76	1.07
	2005	0.68	0.44	0.0500	0.83	0.64
	All	0.75	0.54	0.0376	0.83	0.62
GPP	2001	0.87	0.69	0.0534	0.75	-0.90
	2002	0.90	0.81	0.1124	0.95	-0.31
	2003	0.88	0.75	0.2517	0.89	-0.16
	2004	0.80	0.46	0.0218	0.64	-1.47
	2005	0.87	0.74	0.2238	0.90	-0.60
	All	0.86	0.71	0.0057	0.83	-0.70

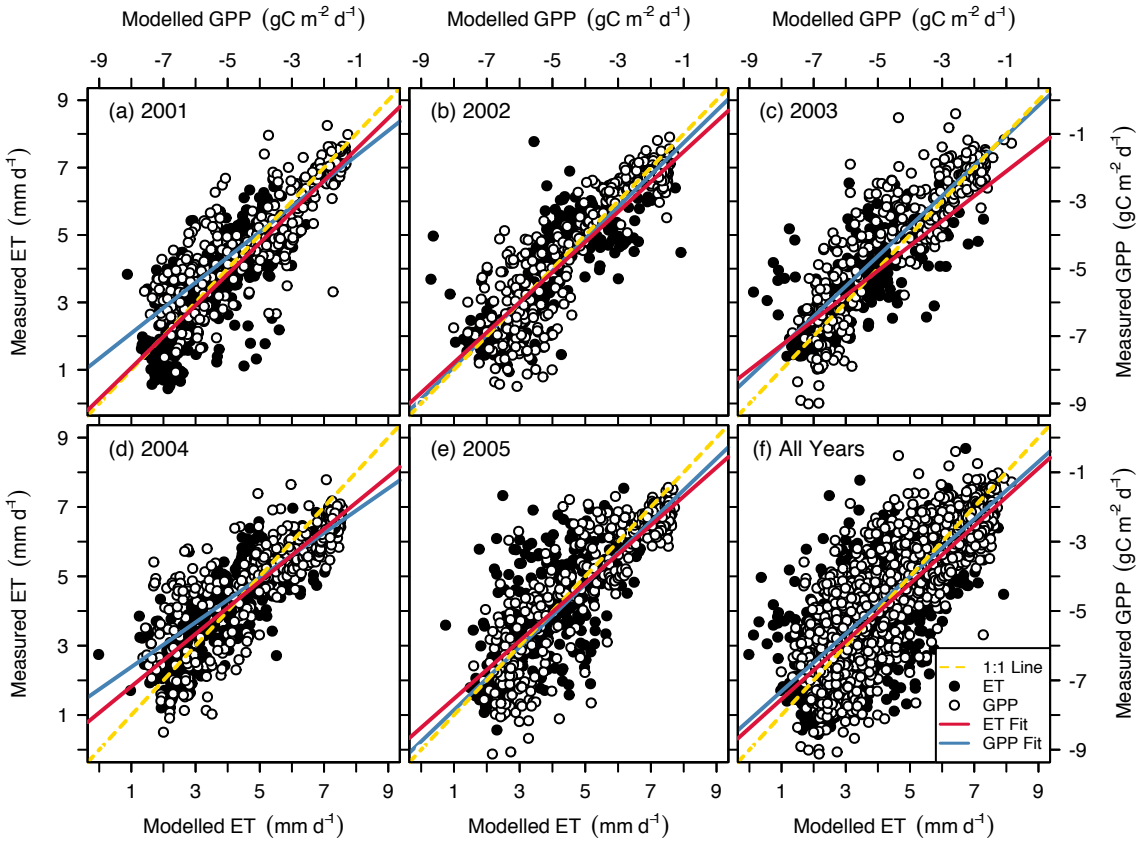

FIGURE 4.14: Correlation plots between modelled and measured evapotranspiration (ET; black circles), as well as modelled and measured gross primary productivity (GPP; white circles). Regressions are performed for (a) 2001, (b) 2002, (c) 2003, (d) 2004, (e) 2005 and (f) all years. The yellow line denotes the 1:1 line, while the red and blue lines represent the regressions lines for ET and GPP respectively. The relationship between modelled and measured GPP is plotted on a negative scale.

C_3 overstorey and C_4 understorey components

In order to see how the C_4 grasses contribute seasonally to the total savanna fluxes, modelled canopy E_t [4] and GPP was partitioned into the constituent C_3 over- and C_4 understorey components and examined over the same period (Figure 4.15). A spline function was applied to these results, and was used to distinguish the underlying seasonal patterns in these fluxes. Seasonal variations in total E_t over the study period traced variations in R_s, θ_s and LAI (Figures 4.1 & 4.2), while total A_n primarily traced the seasonal course of LAI. Modelled overstorey E_t displayed an average range of $1.8 - 4.2$

[4]Transpiration is used instead of evapotranspiration, as soil and wet canopy evaporation do not contribute to vegetation water use.

mm d^{-1}, and made up approximately 80% of the total savanna E_t during the wet season. The large variations in daily E_t were the result of frequent rainfall events, cloud cover and a seasonal decline in D_v which resulted in a significant drop in E_t around February. However, overstorey E_t increased towards the end of the wet season as rain events became less frequent and evaporative demand increased moving into the dry season. After this initial transition from the wet-to-dry period, overstorey E_t decreased progressively into the dry season due to increased regulation of g_s to minimise water-loss due in response to increasing D_v and decreasing θ_s in the upper profile. Understorey E_t contributed very little to total savanna E_t during the wet season ($\approx 20\%$), remaining roughly constant at about 1.0 mm d^{-1} following the wet season course of understorey LAI, with daily variations being due to cloud cover and the seasonal drop in mid February due to the low daily maximum VPD.

Seasonal variations in modelled over- and understorey GPP were highly correlated with the seasonal variation in LAI and gave almost equal contributions to total canopy GPP in the wet season. Overstorey GPP varied moderately in the wet season range from 1.5 gC m^2 d^{-1} at the start of the wet season and peaked to 4.0 gC m^2 d^{-1} at the end. A slight reduction in overstorey GPP occured during the February to March period as the result of the seasonal decline in D_v. After the wet-to-dry transitional period, understorey GPP decayed with LAI and to a lesser extent, reduced θ_s. Understorey GPP increased from 0.0 to 3.0 gC m^2 d^{-1} during October and increased slightly to 3.5 gC m^2 d^{-1} over the wet season. From April, understorey GPP declined to 0.0 due to a complete loss of understorey LAI as a result of the annual senescence of the savanna grasses.

4.3.3.3 Annual patterns over the 2001 to 2005 period

Modelled canopy over- and understorey water-use and GPP were totalled for wet and dry seasons in order to establish what seasonal and annual contributions they play as carbon sinks in the tropical savanna. Figure 4.16 shows annual and seasonal (wet and dry) water use and carbon gain for the savanna ecosystem partitioned into C_3 and C_4 vegetation. Annual and seasonal water-use efficiency (WUE), calculated as the ratio between moles of CO_2 assimilated to the moles of H_2O lost (A/E), was also determined for the five year

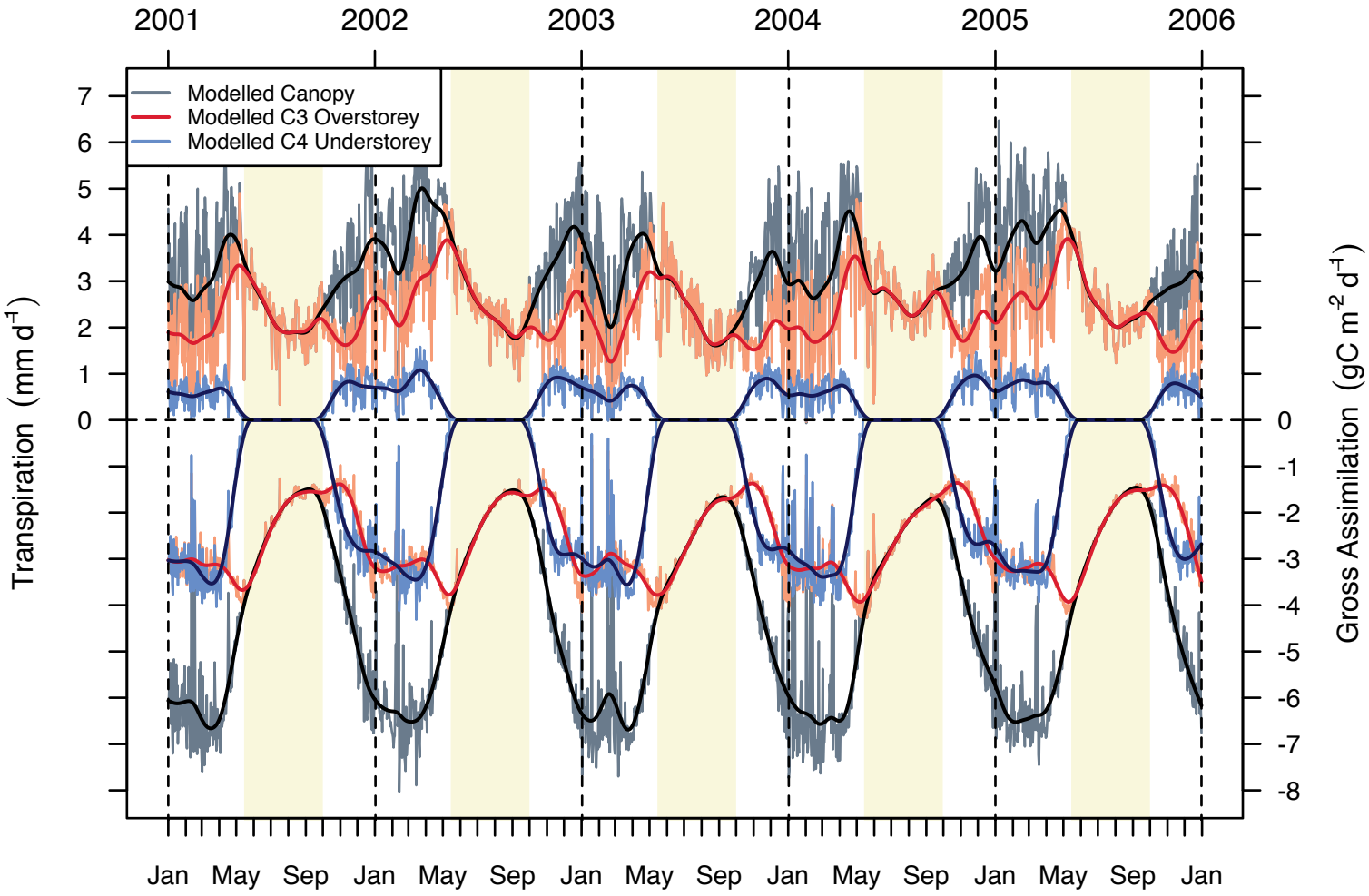

FIGURE 4.15: Modelled total canopy (grey lines) transpiration and gross primary productivity for the 2001 to 2005 period. Total canopy fluxes are partitioned into the C_3 tree overstorey (pink lines) and C_4 grass understorey (light-blue lines). Spline functions were applied to show the moving average for the total (black line), C_3 (red line) and C_4 (blue line) canopy fluxes. Yellow shaded regions represent the dry season.

period. Finally, annual and seasonal light-use efficiency (LUE), calculated as the ratio between moles of CO_2 assimilated to the moles of absorbed photons ($A/APAR$), was determined in order to determine the efficiency of the utilisation of light by the canopy and its over- and understorey components. Values for these measurements are given in Table 4.5.

Annual measured totals of ET were within a range of 1052-1213 mm (2001, 2004) over the five year period. This was made up of wet and dry season totals which were in the ranges of 826-901 mm (2003, 2002) and 207-324 mm (2001, 2004) respectively. Modelled totals of ET were overestimated across all years and seasons, with an annual range of 1181-1352 mm of water (2003, 2002) over the five year period. Modelled seasonal totals also overestimated measured totals, predicting a range of 850-1021 mm (2003, 2002) for the wet season and 331-378 mm (2002, 2004) for the dry season. Annual measured totals of total GPP were within a range of 1409-1560gC m^{-2} (2003, 2005), which was made up of wet and dry season totals in the range of 1082-1232 gC m^{-2} (03,05) and 289-385 gC m^{-2} (2002, 2004) respectively. Modelled totals of annual and seasonal GPP were within 10% of the measured totals over the five year period. Modelled carbon uptake by the ecosystem and canopy were deemed equivalent, as carbon uptake or release by the soil is not accounted for in the model. The model predicted the vegetation to sequester 1440-1501 gC m^{-2} (2001, 2003) annually, 1186-1214 gC m^{-2} (2001, 2005) during the wet season and 254-299 gC m^{-2} (2001, 2003) during the dry season. The canopy transpired 803-914 mm of water (2003, 2002) annually, 571-670 mm (2001, 2002) during the wet season, and 243-285 mm (2001, 2004) in the dry season in order to achieve these levels of carbon gain. The C_3 canopy overstorey sequestered 869-943 gC m^{-2} (2001, 2004) annually, 635-650 gC m^{-2} (2001, 2004) during the wet season, and 254-299 gC m^{-2} (2001, 2003) during the dry season. On average the overstorey canopy accounted for 53% of total wet season GPP and 62% of total annual GPP. The amount of water lost from the canopy overstorey to maintain this level of carbon uptake was in the range of 683-762 mm (2001, 2002) annually, 425-510 mm (2003, 2002) in the wet season, and 243-285 mm (2001, 2004) in the dry season. This averaged to the overstorey canopy accounting for 77% of the water lost during the wet season, and $35 - 38\%$ of the total water lost in evapotranspiration annually. Totals of GPP for the C_4 grass understorey were slightly less than the overstorey, sequestering

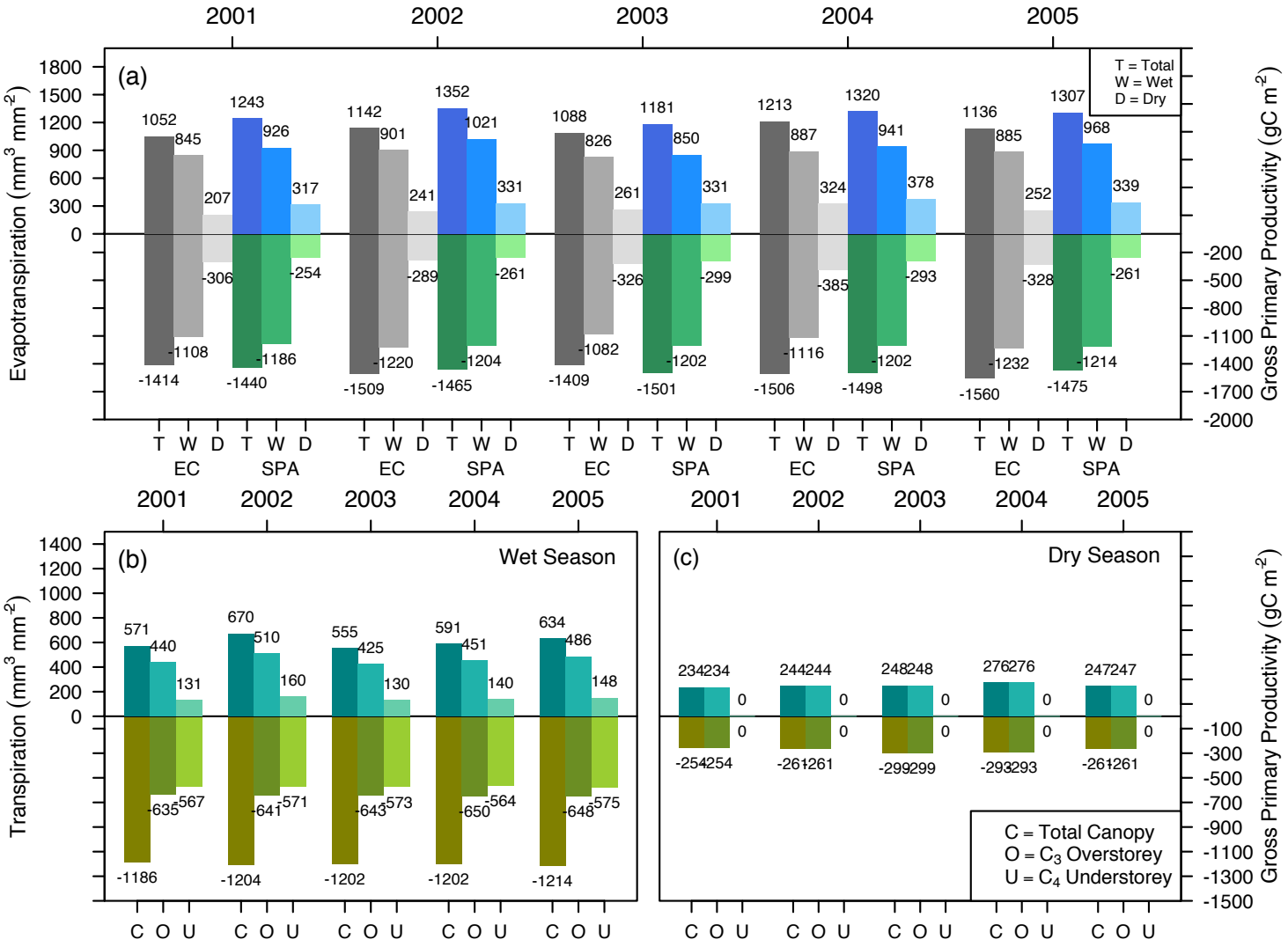

FIGURE 4.16: Modelled and measured period totals of savanna water-use (ET) and gross primary productivity (GPP) for the 2001 to 2005 study period. Modelled savanna fluxes are estimated from the Soil-Plant-Atmosphere (SPA) model, while measured fluxes are derived from eddy-covariance (EC). Totals derived from EC and SPA are given at the (a) annual (T), wet (W) and dry (D) season time-steps. Estimated (b) wet and (c) dry season totals of transpiration and GPP are partitioned from total canopy (C) into C_3 (O) and C_4 (U) components.

TABLE 4.5: Table of modelled annual, wet and dry season totals of water-use and carbon uptake for the 2001 to 2005 period. Additionally, canopy water-use (WUE) and light-use efficiency (LUE) are given. Totals are partitioned from the total ecosystem (Eco), to total vegetation (Can), and into C_3 overstorey (Ovr) and C_4 understorey (Und).

		Annual				**Wet Season**				**Dry Season**			
	Year	Eco	Can	Ovr	Und	Eco	Can	Ovr	Und	Eco	Can	Ovr	Und
Water Use (mm)	2001	1243	805	674	131	926	571	440	131	317	234	234	0
	2002	1352	914	754	160	1021	670	510	160	331	244	244	0
	2003	1181	803	673	130	850	555	425	130	331	248	248	0
	2004	1320	867	727	140	941	591	451	140	378	276	276	0
	2005	1307	881	733	148	968	634	486	148	339	247	247	0
Carbon Uptake (gC m^{-2})	2001	1440	1440	869	567	1186	1186	635	567	254	254	254	0
	2002	1465	1465	902	571	1204	1204	641	571	261	261	261	0
	2003	1501	1501	942	573	1202	1202	643	573	299	299	299	0
	2004	1498	1498	943	564	1202	1202	650	564	293	293	293	0
	2005	1475	1475	909	575	1214	1214	648	575	261	261	261	0
WUE (mmol CO_2 mol^{-1} H_2O)	2001		2.68	1.93	6.49		3.12	2.16	6.49		1.63	1.63	0
	2002		2.40	1.79	5.35		2.70	1.89	5.35		1.60	1.60	0
	2003		2.80	2.10	6.61		3.25	2.97	6.61		1.81	1.81	0
	2004		2.59	1.95	6.04		3.05	2.16	6.04		1.59	1.59	0
	2005		2.51	1.86	5.83		2.87	2.00	5.83		1.59	1.59	0
LUE (mol CO_2 mol^{-1} photon)	2001		0.0201	0.0164	0.0305		0.0221	0.0181	0.0305		0.0142	0.0142	0
	2002		0.0205	0.0170	0.0307		0.0224	0.0182	0.0307		0.0146	0.0146	0
	2003		0.0210	0.0178	0.0308		0.0224	0.0183	0.0308		0.0168	0.0168	0
	2004		0.0209	0.0178	0.0303		0.0224	0.0185	0.0303		0.0164	0.0164	0
	2005		0.0206	0.0172	0.0309		0.0226	0.0184	0.0309		0.0146	0.0146	0

from 564-573 gC m^{-2} (2004, 2003) in the wet season, which on average accounted for 47% of the total wet season GPP and 38% of the total annual GPP. The understorey was highly water-use efficient, transpiring only 130-160 mm of water (2003, 2002) during the wet season despite the large carbon gains, only accounting for 23% of the total water lost from the ecosystem and during the wet season and made up only $11-12\%$ of total annual evapotranspiration.

The annual WUE of the canopy varied only slightly within the range of 2.40-2.80 mmols CO_2 $mols^{-1}$ H_2O (2002, 2003). Removing the grass understorey component, leaving just the tree overstorey, reduced WUE to a much lower range of 1.51-1.82 mmols CO_2 $mols^{-1}$ H_2O (2002, 2003). Solely considering the wet season periods, the total canopy WUE increased to 2.70-3.25 mmols CO_2 $mols^{-1}$ H_2O (2002, 2003), while partitioning the canopy into over- and understorey parts shows the understorey to be highly efficient, having a WUE almost triple that of the overstorey, in the range of 5.35-6.61 mmols CO_2 $mols^{-1}$ H_2O (2002, 2003). During the dry season WUE droped by approximately half for the overstorey canopy, producing a range of 1.59-1.81 mmols CO_2 $mols^{-1}$ H_2O (2004, 2003), which was in response to an inactive understorey (grasses dead), reduced soil water supply and hence trees became more conservative in their water use.

Differences in canopy LUE were evident between wet and dry season period across all years, with a range of 0.2206-0.2258 mols CO_2 $mols^{-1}$ photon (2001, 2005) in the wet season, which was 50% larger than observed in the dry season at 0.1424-0.1676 mols CO_2 $mols^{-1}$ photon (2001, 2003). Comparing over- and understorey LUE in the wet season, shows the understorey to be more efficient in utilising available light; 0.3030-0.3078 mols CO_2 $mols^{-1}$ photon (Understorey; 2004, 2003) compared to 0.1824-0.1850 mols CO_2 $mols^{-1}$ photon (Overstorey; 2002, 2004). The higher LUE in the understorey is a product of the higher carbon yields and lower absorbed light by the grasses. Differences in LUE among years was statistically insignificant (ANOVA; $P > 0.05$) despite variability in wet and dry season lengths.

4.4 Discussion

The purpose of this study was to successfully incorporate a provision for C_4 vegetation within the SPA model, thereby allowing its application to savannas, as well as to provide a way of investigating the contribution of C_4 photosynthesis in the savanna ecosystem. Adding a C_4 photosynthetic sub-model gave a significant improvement in seasonal estimates of GPP via a larger A_n from the C_4 photosynthetic pathway. Additionally, this did not impact seasonal estimates of ET. The ability to describe variations in the seasonal distribution of LAI through an input matrix was also an important improvement, as the senescent nature of the C_4 grasses could be approximated for and handled by the model during the simulation period. Lastly, using SPA to fit a BBL-type relationship was an effective method in determining ${}^{C_3}\iota_{op}$ and ${}^{C_4}\iota_{op}$ at this site; a necessary parameterisation that constrained ${}^{C_4}g_s$ to values that are characteristic of plants using this photosynthetic pathway.

4.4.1 Modelled C_3 and C_4 stomatal efficiency

An important component of this study was in carefully and correctly parameterising the C_4 understorey that was present at this site. By simulating g_s and A_n over a range of Q_p at different levels of ι_{op}, outputs could be compared with leaf-scale measurements using a BBL relationship, where the correct level for ι_{op} matches a_1 slope parameter of the measured data. This allowed the determination of both ${}^{C_3}\iota_{op}$ and ${}^{C_4}\iota_{op}$ at this site. Although this value is a freely adjustable input in the model, the methodology given here does give a means of quantifying ι_{op} for particular vegetation types or the study site in particular. However, some unexpected inconsistencies did occur when applying the method to C_4 vegetation. The relationships were curved rather than linear (compared with the C_3 relationships) and this curvature increased with increasing ι_{op}. This may be related to the characteristic of C_4 photosynthesis to not saturate until high light levels (Collatz et al., 1992) or g_s being insensitive to D_v at low values (Leuning, 1995; Monteith, 1995). Either or both possible causes were not clearly apparent in the measured data, but when tested with the von Caemmerer and Furbank (1999) C_4 model as well, the same curvature was still present, so it is most likely due in part to a characteristic of the C_4 pathway.

The ι_{op} parameter has been parametrised in previous studies. Williams et al. (1996a) selected their ι_{op} in accordance with a desired maximum rate of g_s observed with measurements of northern red oak (*Quercus rubra*), which they believed to be 0.07%. Additionally, they used a sensitivity analysis in testing ι_{op} at relative levels from this value, with their value of 0.07% giving the best balance between water loss and carbon gain. They also found ι_{op} to be highly influential on the predictions of ET. However, in the present study this was not apparent. This may be in part due to this site having abundant soil water stores; in this study ι_{op} was parameterised for the wet season when the C_4 grasses were active. Similarly, Misson et al. (2004) parametrised ι_{op} for a very simplified version of the SPA stomatal model, by fitting it to measured g_s and found a slightly higher value of $\iota_{op} = 0.10\%$ to be most appropriate in matching measurements taken for ponderosa pine (*Pinus ponderosa* Dougl. ex Laws.). Although these methods of determining ι_{op} are feasible, the method described in this chapter is able to quantify the value of ι_{op} with the well established BBL relationship. It appears that for three very different tree species, ${}^{C_3}\iota_{op}$ had a range of $0.07 - 0.10\%$, and this may be reasonable range for most C_3 species in balancing water-loss and carbon gain without significant penalty.

This study is the first that attempts to parameterise ι_{op} for C_4 plants and the value derived here can not be compared with other studies. However, a comparison can be drawn with the C_3 ι_{op} values. The higher ι_{op} derived for C_4 plants is very likely, as they are by nature, very water conservative and a default $\iota_{op} = 0.07\%$ is most likely too high for this photosynthetic pathway. Based on the above comparison of the parametrised ι_{op} for different C_3 species being very similar, it is highly likely that this value will be very similar for other C_4 species. Even though a default value $\iota = 0.07\%$ is supplied, it is likely that this value increases stomatal aperture beyond the necessary limits for C_4 plants. C_4 plants are able to concentrate CO_2 at the site of RuBisCO and saturate A_n at low concentrations of CO_2 (unlike C_3), and so a large g_s is not needed (nor desirable). Additionally, maximising g_s beyond the general range of $0.2 - 0.4$ mol m^{-2} s^{-1} (Bunce, 1998; Ghannoum et al., 2001a) would not result in appreciable increases in A_n, as C_4 assimilation rates are generally saturated by this point (von Caemmerer and Furbank, 2003). Consequently, an increased ι_{op} reinforces the ability of C_4 species, simulated in the model, to be able to maximise their carbon gain within a low range of g_s that agrees with

the theory of C_4 photosynthesis (Pearcy and Ehleringer, 1984; Ghannoum et al., 2001b; Patrick et al., 2009).

The parametrised values for ι_{op} for C_3 and C_4 vegetation at this site, were able to constrain simulated g_s within a suitable range that is line with the literature for this site (Prior and Eamus, 1999; Eamus and Prior, 2001). The trace of simulated g_s from the wet season to the dry season, fell in the typical range for savannas (San José et al., 1998; Prior and Eamus, 1999; Prior et al., 2004). Additionally, modelled g_s over wet and dry season is within the range of what has been recorded in similar ecosystems, such as that observed by Myers et al. (1997) for *E. miniata* ($0.45-0.65$ in the wet season mol m^{-2} s^{-1} and $0.30-0.35$ mol m^{-2} s^{-1} in the dry season) and similarly by Prior et al. (1997) for *Terminalia ferdinandiana* ($0.69-0.78$ mol m^{-2} s^{-1} in the wet season and $0.31-0.37$ mol m^{-2} s^{-1} in the dry season). Unfortunately the g_s for the C_4 grass layers could not be directly compared to any previous studies made at this site, nor were there any measurements made for this particular grass contained in the literature. However, there is a good indication that estimates of C_4 g_s made by SPA are within a typical range for C_4 species. Bunce (1998) observed mid-range values of g_s to occur in Soybeans (*Glycine max*) of approximately $0.28 - 0.40$ mol m^{-2} s^{-1} and grain (*Amaranthus hypochondriacus*) of approximately $0.22 - 0.34$ mol m^{-2} s^{-1}, while Tezara et al. (1998) observes a similar range in weeds (*Alternanthera crucis*) of approximately $0.05 - 0.40$ mol m^{-2} s^{-1}. Although different species will have different strategies in water-use, simulated g_s agrees with the trend for C_4 species to operate at g_s within a low range of $0.2 - 0.4$ mol m^{-2} s^{-1} under well-watered conditions.

4.4.2 Comparison of C_4 photosynthesis models

The incorporation of a C_4 photosynthesis into the SPA model was important as it allowed improvements in predicting the correct levels of carbon uptake occurring in the savanna ecosystem, which were observed with measurements with EC. The savanna ecosystem that was modelled in this study is dominated by a layer of C_4 grasses in the wet season, which have an LAI of approximately 1.15 m^2 m^{-2} at full growth, while during the dry season the savanna is dominated by evergreen and semi-deciduous trees and shrubs (Williams et al., 1997). The understorey grasses are a significant contributor to total carbon uptake during

the periods for which they are active, but do not contribute in the dry season due to their annual senescence. Incorporating this dynamic into the model by daily adjustments to canopy layer leaf area allowed the model to replicate the life-span of the grasses over the simulation period. However, a more appropriate control might be to allocate the understorey layers a separate rooting distribution, thereby constraining productivity of the grasses during periods of low soil water availability. However, the approach used here was still valid as the grasses have been found to die off in the same time-frame annually, irrespective of soil water conditions (Beringer et al., 2007). For example, the 2003-2004 wet season period was longer than usual, having a length of 213 days which ended in mid June, which is usually well into the dry season. The EC measurements of GPP however do not seem to show a response to this extra water, remaining at levels comparable to other years. However, not all ecosystems match this dynamic and in order to broaden the applicability of this model to other sites, some quantification of the grass rooting distribution is still a much needed component.

Application of the C_4 photosynthesis models to the grass understorey layers significantly improved the estimates of GPP. Not accounting for the different photosynthetic pathways results in continuous predicted short-falls in estimated savanna productivity; this was observed when using a C_3 photosynthesis model to describe a C_4 grass understorey. The C_4 models did, however, fail to account for daily GPP during a certain periods (Figure 4.6; December 2002) in the course of model testing. This failure was difficult to identify within the model, as a residual analysis was not able to isolate what environmental forcing was causing the drop in performance. The only information procured was that it occurred for a mid range of LAI and that it was just after the onset of the wet season. This large discrepancy was thought to be in part due to the rapid flushing of the understorey grasses at the onset of the wet season, and the prescribed LAI being too low (Eamus et al., 2001). However, when looking at the measured data, it showed the diurnal course of GPP to contain large amounts of noise for a good proportion of this period. This was identified by looking at the modelled diurnal course of GPP, which on average, corresponded well with the measured diurnal course. The large noise in the data, when totalled over a day, created a large deviation from the expected measured daily total and this was the cause for the difference between measured and predicted in this period. Measurements

from EC are subject to their own errors, predominantly due uncertainty in nocturnal flux measurements, and the model cannot be expected to account for such errors (Baldocchi et al., 1996; Medlyn et al., 2005b; Beringer et al., 2007).

The simplified C_4 photosynthesis model developed by Collatz et al. (1992) gave a better correspondence with the EC measurements over the testing period, in part due to following a simpler calculation method of net CO_2 assimilation for the C_4 pathway. This is not to say the mechanistic model for C_4 photosynthesis by von Caemmerer and Furbank (1999) did poorly, as for a majority of the testing period it corresponded well with the measured data, and matched estimates made by the simpler C_4 model. However, there were some significant differences in the hourly values of GPP. This is most likely the result of the two models taking differing approaches in calculating C_4 photosynthesis. The mechanistic model requires more information on the stoichiometry of the C_4 vegetation being modelled; information which is not always available or easily obtained. The simplified C_4 model on the other hand circumvents the need for more detailed information by reducing the description of the C_4 pathway, which in general terms may be seen as removing the need to simulate the CO_2 concentrating mechanism, while still acknowledging it as a limiting factor in the pathway (Collatz et al., 1992). Rather than mathematically describing the complex path of CO_2 diffusion from the intercellular air spaces to the site of RuBisCO, the calculation of net assimilation is reduced to a set of quadratic expressions, which describes the transitions between the three limiting states of C_4 photosynthesis. This makes this type of C_4 model more broadly applicable, especially when coupling it with g_s models. This model has been broadly used across a number of dynamic global vegetation (DGVM) and land surface models (LSM) (Bonan, 1995; Sellers et al., 1996; Sitch, 2000), which have generally been used to investigate the impacts of variable climate forcing on global vegetation groups (i.e. Collatz et al., 1998; Collelo et al., 2003; Bondeau et al., 2007). Over a shorter study period, the mechanistic model may be a more desirable C_4 photosynthesis model, as it allows a quantification of important variables in the C_4 cycle, such as the CO_2 concentrations in the mesophyll and bundle-sheath cells, and a measure of the CO_2 concentrating mechanism. The ability to quantify the operation of the C_4 cycle to changes in the environment is important in developing robust climate change scenarios for savannas (Ghannoum, 2009) and it would be interesting to see how variable

forcing on the biochemical properties (i.e. CO_2 leakage, bundle-sheath cell conductance) of the C_4 pathway would translate up to the scale of a canopy. Other studies (Massad et al., 2007; Vico and Porporato, 2008; Carmo-Silva et al., 2008) have successfully applied the mechanistic model in investigating responses of C_4 assimilation to variations in meteorological and environmental forcing. However, no studies (that the author is aware of) have incorporated it into land-surface models which operate at the canopy and ecosystem scales, which was the intent of the present study. Despite being rather information heavy, the mechanistic model was still able to give very reasonable predictions based on a set of broad literature values of key parameters, owing to the robustness of the model itself.

4.4.3 The contribution of C_3 and C_4 vegetation to savanna productivity and water-use

The model performed well in explaining 80-90% of the measured savanna GPP, but was only able to explain 68-81% of savanna ET. There was a good correspondence between the productivity predicted by the model and that measured from EC for the majority of the five year period. Predictions of canopy productivity varied diurnally with incident R_s and D_v, and followed seasonal variation in LAI. Variations in measured wet season GPP were large, and generally matched by the model. The exception was in 2004, where the model corresponded poorly to a prolonged wet season. Measured GPP responded unusually for this period, as there was a decline in productivity before before reaching constant daily average value. This may be the result of some disturbance in measurements during this period, as the premature drop does not correspond with the environmental effects that are concurrently occurring. These results are comparable with MODIS derived estimates of GPP made by Kanniah et al. (2009), who have used an empirical model that rely on similar input information as the SPA model (i.e. R_s, D_v, LAI).

Partitioning savanna GPP into its constituent over- and understorey components, shows that the C_4 grasses constitute a very large part of total savanna productivity. The high LAI for the grasses at this site, coupled with the C_4 pathway and abundant soil water in the root zone of the grasses, allow the grasses to become a major carbon sink in the savanna during the wet season. Annual and seasonal totals of savanna GPP predicted in this study

compare well with those measured by Chen et al. (2003) at this site. Overstorey totals calculated in the present study also agree well with those found by Chen et al. (2003), and show the canopy overstorey to be a major carbon sink during the wet season, but only a minor one in the dry season. The understorey grasses are significant contributors to wet season productivity, contributing approximately 45% of the total, and therefore a major sink during this period. Similarly, Miranda et al. (1997) estimated C_4 grasses to contribute $30-35\%$ for a functionally similar cerrado savanna. However, despite this large contribution, the grasses become a large source of carbon during the dry season through decomposition and fire disturbances (Beringer et al., 2007; Kanniah et al., 2010b), and this according to Chen et al. (2003) results in $40-50\%$ loss in sequestered carbon, making the grass understorey carbon neutral (Chen et al., 2003). Annual totals of GPP modelled here tend to agree well with annual totals from other savanna sites that experience similar ranges in LAI and rainfall. Assuming that NPP is approximately half of GPP (Eamus et al., 2001), an average annual total of 1476 gC m^{-2} yr^{-1} estimated here, corresponds well with 1325 gC m^{-2} yr^{-1} for a Sahelian fallow savanna (Hanan et al., 1998), 1550 gC m^{-2} yr^{-1} and for a Brazilian cerrado savanna (Miranda et al., 1997). Additionally, the average total measured and modelled here is in contrast to 2360 gC m^{-2} yr^{-1} for Amazonian rainforests (Malhi et al., 1999) and 612 gC m^{-2} yr^{-1} for temperate European deciduous forests (Greco and Baldocchi, 1996).

Predictions of ET made by the model were hampered by large variations during the wet season, which was not seen in the EC measurements and resulted in a continuous over-estimation of total wet season water loss. The large error was the result of the model being highly sensitive to inter-daily variations in R_s and D_v that occurred during this period; this variability resulting from frequent, fluctuating cloud cover and rainfall events. Additionally, the inclusion of wet canopy evaporation may have caused additional error. Although this large variability was evident at higher spatial scales, it was averaged out in the monthly ensembles of ET, and gave a good match to monthly measured ET albeit frequent overestimation was still observable. Considering the E_t component of ET and partitioning it into it's constituent over- and understorey sub-components showed that a reduction in available energy and a low evaporative demand frequently constrained E_t in the overstorey. E_t in the understorey did not vary greatly during the same period, and

contributed 23-24% to the total water lost from the savanna. Although variability in ET is evident in the EC measurements, it is not to the degree which is predicted by the model. Regardless, estimates of savanna water-use correspond well with measurements made in the field by Hutley et al. (2000), who give a similar wet season total of 557 mm, but a much higher dry season total of 329 mm. However, where the understorey in this study has been solely defined as the C_4 grasses, and all C_3 vegetation relegated to the canopy overstorey. Hutley et al. included C_3 mid-term stratum of semi- and brevi-deciduous shrubs, as well as bare soil in their measurements of canopy understorey. Consequently, it is not possible to give a direct comparison of the water-use by the grasses to the data of these authors. However, one can still infer from corresponding canopy E_t totals that the grasses contribute less than C_3 vegetation in the overall water budget of savannas.

4.4.4 Environmental factors influencing savanna productivity and water-use

No relationship between annual and seasonal savanna ET and period total precipitation was found for any year ($P > 0.05$), similarly no relationship was found between annual and seasonal GPP and precipitation either ($P > 0.05$). Additionally, modelled and measured ET and GPP was not overly sensitive to variations in wet or dry season length. This is due to a lack of significant inter-annual variability in GPP, ET and rainfall (Eamus et al., 2001). However, spatial patterns in tree biomass have been observed across rainfall gradients in northern Australia, when moving inland there is a significant decrease in dry season length (110-221 days) and annual rainfall (300-1600 mm) (Williams et al., 1996b; Cook and Heerdegen, 2001; Cook et al., 2002; Kanniah et al., 2010a). Although rainfall and seasonal length provided no relationship with annual ET and GPP, partitioning modelled ET and GPP into its C_3 and C_4 components, showed A_n and E_t were highly sensitive to variation in their environmental drivers (R_s, D_v and LAI). However, no relationships were evident between A_n, E_t and θ_s for both C_3 and C_4 components of the savanna. This is in contrast to the results of Kanniah et al. (2009), who found that θ_s was a major determinant of the seasonal variation in GPP for this same site. Additionally, Kanniah et al. found that during the dry season, GPP was relatively insensitive to D_v and this

agree with the results found in this study (Figure 4.12f). However, the strong relationship between GPP and LAI in this study agrees with that found in Kanniah et al. (2009).

This leaves the question as to what accounts for the seasonal variability in ET and GPP at this site? A plot of savanna water-use and productivity through the wet and dry seasons over the five year period shows that θ_s and LAI are major determinants in the seasonality of over- and understorey gas-exchange. In order to test which of these environmental factors is governing (if at all) the seasonality of ET and GPP, one year from the study period was used to simulate two possible scenarios that may help to answer this question. Scenario 1 simulated the effects of the savanna that retains a full canopy through the dry season (constant LAI), but has the usual decline in θ_s, characteristic of the dry season. Scenario 2 simulated a canopy that undergoes normal leaf area adjustments but has access to permanent, abundant water supply. In order to keep the scenarios simple, only savanna E_t (instead of ET, to remove effects of soil and wet canopy evaporation) and GPP were considered. Results are given in Figure 4.17, where the black line represents a year under unchanged conditions and the coloured lines represent the two scenarios. Scenario 1 shows that the savanna site has an abundant water supply and is able to maintain high rates of E_t and GPP despite the drop in θ_s in the upper soil profile that characterises the dry season. The high rainfall in the wet season, which varied 1828-2467 mm over this five year period, recharged soil water stores to a point that the prevailing evergreen canopy wet season levels of E_t and GPP during the dry season. Tree rooting depth is sufficiently deep enough to access deep soil water stores in the lower profile (O'Grady et al., 1999; Eamus et al., 2001; Hutley et al., 2001; Kelley et al., 2002). Eamus et al. (2000) have shown that in ecosystems similar to this, evergreen trees across a rainfall gradient in northern Australia were able to maintain continuous rates of E_t despite the seasonality of rainfall. Scenario 2 shows that regardless of a modelled high soil water-status throughout the year, seasonal variation in LAI is constraining the level gas-exchange (E_t and GPP) occurring seasonally. There are some slight increases, but otherwise both E_t and GPP are operating equivalently in the dry season as if the conditions were arid. Williams et al. (1997) shows that for savannas in the dry tropics of northern Australia, adjust canopy fullness (LAI) to minimise water loss and maintain productivity during the dry season. This reduction in LAI is a biological response to low soil water availability and leaf to air D_v. In the case of

the C_4 grasses, their strategy is to die off completely and grow again when the monsoonal wet season returns, as their rooting depth is not sufficient to maintain water-use and productivity throughout the dry season. The drop in overstorey LAI, and consequently E_t and GPP, is a result of, principally but not exclusively, the deciduous and semi-deciduous vegetation components. This suggests that θ_s is not a limiting factor for vegetation at this site, provided that vegetation have deep enough roots in order to access soil water stores in the lower profile. Given the high annual rainfall and the above results on what drives E_t and GPP at this site, this savanna ecosystem can be thought of as an energy-limited rather than a water-limited (Budyko, 1974).

4.5 Conclusion

Modelling C_4 photosynthesis is an important requirement for correctly estimating savanna gas exchange. Furthermore, it is critical that the seasonal variation in understorey LAI of savanna grasses also be accounted for. A savanna ecosystem was simulated over a five year period, and model predictions were compared with EC derived measurements. A simplified C_4 photosynthesis model was found to be more appropriate lacking detailed information on the biochemistry of the understorey at this site, although the detailed C_4 photosynthesis model would be more appropriate in investigating climate change scenarios. The model was able to explain 80-90% of the variation in savanna GPP and 68-81% of the variation in savanna ET. Of these fluxes, the savanna understorey, dominated by C_4 grasses in the wet season, contributed almost half of total savanna GPP, while retaining a high WUE and contributing to only 20% of total water lost by vegetation during this period. Finally, by simulating two different scenarios of available soil water content and canopy LAI, it was found that the site is not water limited but rather energy limited. This conclusion was reached as seasonal variations in savanna gas-exchange were driven by changes in LAI, which in itself is limited by fire, and hence changes in energy absorption. In summary, with thew addition of a C_4 photosynthesis model and a seasonal description of LAI patterns, the SPA model was able to provide insight into the contribution that the C_4 grasses play in this savanna.

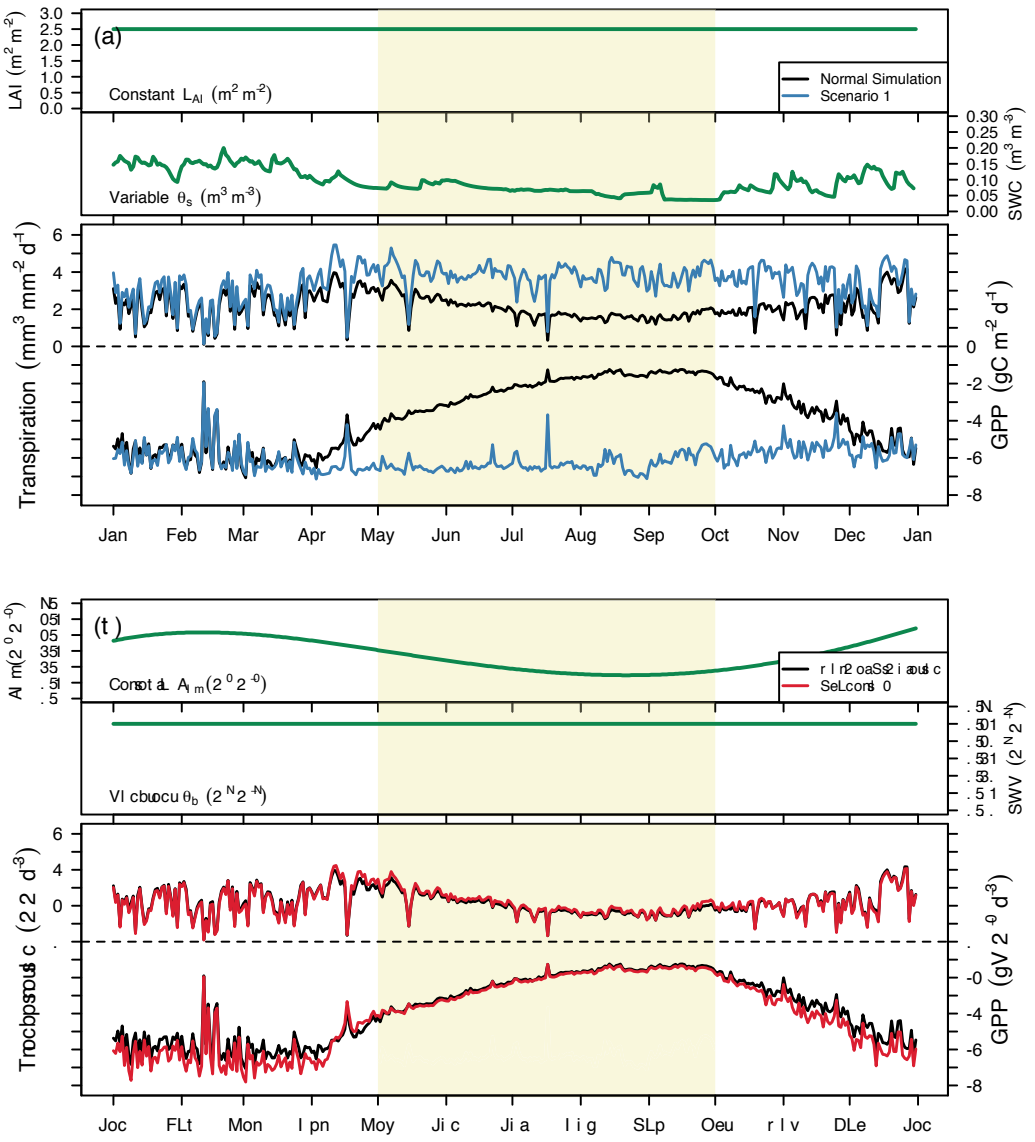

FIGURE 4.17: Two scenarios are simulated using the 2001 year to determine whether leaf area index (LAI) or soil water content (SWC) drives the seasonal variation in transpiration and gross primary productivity (GPP). These scenarios are (a) SWC is variable and LAI is held constant at 2.4 m^2 m^{-2} (blue line) and (b) LAI is variable, while SWC is held constant at approximately 0.30 m^3 m^{-3} (red line) over the entire year. The black line in both cases represents a normal simulated year where both LAI and SWC are variable. The yellow shaded region denotes the dry season.

Chapter 5

Stomatal regulation of photosynthesis and transpiration during drought

5.1 Introduction

Stomatal opening exerts the primary, short-term, biotic control on transpiration (E_t) from the leaf surface and the net assimilation (A_n) of atmospheric CO_2 (C_a). The function of this regulation is to restrict the loss of H_2O from the leaf cells, while permitting a constant diffusion of C_a into mesophyll cells for photosynthetic fixation (Farquhar and von Caemmerer, 1982). Stomatal aperture are widely influenced by environmental and physiological factors and are highly sensitive to changes in soil water availability (Leuning et al., 1998) and acts to prevent catastrophic failure of the hydraulic pathway (xylem; Tyree and Sperry, 1989). Uptake of C_a by the leaves for photosynthesis is a relatively well understood mechanism, with the seminal work by Farquhar et al. (1980) providing the widely accepted scheme of modelling leaf gas-exchange of C_a and water. The response of stomata to variations in environmental conditions and to physiological factors has been widely investigated (Jarvis and McNaughton, 1986; Tyree and Sperry, 1988; Mott and Parkhurst, 1991; Monteith, 1995; Whitehead, 1998; Eamus and Shanahan, 2002). However,

the underlying mechanisms of stomatal response to C_a and vapour pressure deficit (D_v) are not well understood (Buckley, 2005). Consequently, this has resulted in a number of models that attempt to explain the regulation of tree water-use via variations in stomatal conductance (g_s) using empirical, semi-empirical and optimality methods (Jarvis, 1976; Cowan, 1977; Ball et al., 1987).

The first approach to modelling g_s was through the purely empirical Jarvis-type models that proportionally modify g_s based on a set of response functions linked to critical abiotic drivers (Jarvis, 1976; Stewart, 1988, Chapters 2 and 3). These models require site-specific data and parameterisation in order to capture the dynamics of the system being modelled, but can be simplified to a model of only a few parameters without a sacrifice in performance (Chapter 3). The second method is semi-empirical and follows a more physiological approach, with g_s being directly linked to A_n and the environment (especially D_v). This correlation between g_s and A_n was first observed and modelled by Ball et al. (1987) and later modified by Leuning (1995); both of which are now termed as the Ball-Woodrow-Berry (BWB) and Ball-Berry-Leuning (BBL) models. Both of these models relate g_s to the ratio between A_n and the concentration of CO_2 in the atmosphere, boundary layer or intercellular air spaces depending on the study. The differences between these models is the use of relative humidity by the BWB model and the leaf-to-air vapour pressure deficit by the BBL model in describing atmospheric demand. Further modifications have been made to the BBW and BBL models in the past two decades, including the effects of plant water status on stomatal regulation, through i) declining soil water content (Leuning et al., 1998; Wang and Leuning, 1998), ii) leaf water potential (Williams et al., 1996a; Tuzet et al., 2003) and iii) root abscisic acid (ABA) (Tardieu and Davies, 1993; Tardieu and Simonneau, 1998; Dewar, 2002; Verbeeck et al., 2007). These models have been more widely used over their Jarvis-type variant, as there are fewer parameters required in linking g_s and A_n with leaf physiological characteristics, and additionally, can be readily applied to global change biology (GCB) models without the requirement of detailed parameterisation (Uddling et al., 2005; Medlyn et al., 2007). The final method of modelling g_s is through the optimisation of stomatal opening, so as to maximise the carbon gain per unit loss of water, proposed by Cowan (1977) and Cowan and Farquhar (1977). This type of model relates the intrinsic supply and demand for CO_2 and H_2O between the plant and

the atmosphere through A_n and E_t, the level of which is controlled via a *cost of water* parameter. Except for some notable studies of (Hari et al., 1986; Berninger and Hari, 1993; Mäkelä et al., 1996; Schymanski et al., 2008b), this type of model has not been as widely applied as the Jarvis- and BB-type models because of the difficulty in quantifying the *cost of water* parameter (Leuning, 1990; Katul et al., 2010). While there is no clear agreement on the choice of g_s model (van Wijk et al., 2000; Misson et al., 2004), all of the models described above give a viable means of replicating leaf-gas exchange.

In Chapter 1 the theory behind the operation of the hydraulic pathway of the soil-plant-atmosphere continuum (SPAC) was covered so as to explain the water balance of an ecosystem and the importance of modelling fluxes of water entering and leaving vegetation. In this chapter, the operation of stomata in regulating the flow of water along the SPAC and its consequences on photosynthesis is investigated using the soil-plant-atmosphere (SPA) model developed by Williams et al. (1996a) and expanded upon in Williams et al. (2001a), as was used to model a savanna ecosystem in Chapter 4. A more concise explanation of the SPAC theory is given here again but concentrates on the leaf gas-exchange component of the SPA model. The equations describing the supply of water by the roots, demand for water by the atmosphere, supply of CO_2 by the atmosphere and demand for CO_2 by the leaf are reviewed. An improvement of the representation of g_s in the SPA model is suggested, that includes a stronger coupling between E_t and D_v, such that there is a direct regulation in the model to balance the unit of carbon gained per unit of water lost. This improvement on the current gas-exchange model in SPA attempts to emulate the theory proposed by Cowan (1977), and which has also been successfully implemented by Hari et al. (1986), Berninger and Hari (1993), Mäkelä et al. (1996), Schymanski et al. (2008b) and Katul et al. (2010). Suggestions as to what value the arbitrary *cost of water* parameter should be is not investigated here, nor is its parametrisation discussed, as this is beyond the scope of this chapter. Rather, a sensitivity analysis is performed to test the relative effects of adjusting this parameter to see what impact this has on modelled leaf gas-exchange.

5.2 Methods

5.2.1 Model theory and structure

The rate of water and carbon exchange between a leaf and the atmosphere is directly controlled by several factors, including evaporative demand, stomatal opening, and the water available to the plant from the soil. The SPA model follows the theory that leaf stomata remain open as long as there is a sufficient water supply to meet atmospheric demand. When the atmospheric demand for water begins to exceed the supply of water to the canopy, stomata will begin to close to prevent embolism occurring in the xylem (Tyree and Sperry, 1989). Under conditions where the soil is sufficiently wet, stomata remain open so as to maintain a constant level of carbon gain (Cowan and Farquhar, 1977). This constant level can be technically defined by a point where further expenditure of water by the plant would not result in appreciable gains in carbon. This provides a framework to model leaf gas-exchange, which is limited by water availability and a measure of gas exchange optimality.

At a specific time-step, the respective level of A_n by a leaf and water lost from the leaf by E_t will be balanced at an *optimal* level of g_s. Additionally, the supply of CO_2 and atmospheric demand for H_2O must also be in equilibrium, which is also dependent on g_s. In the following section, an explanation of the structure and theory for leaf gas-exchange is given. Listed, are the general processes involved in the biochemical and hydrologic framework in the SPA model that describe the supply and demand for CO_2 and H_2O. In order to retain readability and to keep with the *circuit* analogue of the SPA pathway, both g_s and its inverse stomatal resistance (r_s), are used throughout the section.

5.2.1.1 Biochemistry framework

The model's leaf biochemistry calculates A_n through the supply and demand for CO_2. The rate of supply of CO_2 from the atmosphere to the intercellular air spaces of the stomata

(A_d) can be expressed by the diffusion equation as:

$$A_d = \frac{a_c M_w}{\mathcal{R} T_a} \frac{(C_a - C_i)}{(r_s + r_b)} \tag{5.1}$$

where r_s and r_b are the stomatal and boundary resistances to water loss (s m^{-1}), $a_c = 1/1.6$ and is a conversion factor between the relative diffusivities of H_2O and CO_2, C_a and C_i are the atmospheric and intercellular molar CO_2 concentrations respectively (μmol mol^{-1}), M_w is the molecular weight of water (18.02 g mol^{-1}), $\mathcal{R}$ is the universal gas constant and T_a is air temperature (°C).

The net biochemical demand for CO_2 is expressed as:

$$A_n = \min(V_c, V_j) - R_d \tag{5.2}$$

where V_c and V_j are the net assimilation rates limited by either RuBisCO activity or the RuBP regeneration rate, and R_d is dark respiration (μmol m^{-2} s^{-1}). Both V_c and V_j are functions of T_a and C_i, while V_j has the extra dependence of absorbed photosynthetically active radiation (Q_p). The equation described above is that which has been used in Section 4.2.3.1, Chapter 4.

In order to determine C_i, a solution between the supply and demand for CO_2 can be determined using one of the limiting factors of photosynthesis. At the top of the canopy the demand for CO_2 is co-limiting, meaning that A_n is limited equally by both V_c and V_j (Farquhar and von Caemmerer, 1982). Therefore, it can be expressed that $A_n = V_j$, so that:

$$A_n = \frac{J_e}{4} \frac{C_i - \Gamma^*}{C_i + 2\Gamma^*} - R_d \tag{5.3}$$

where J_e is the electron transport rate[1] (μmol m^{-2} s^{-1}) and Γ^* is the CO_2 compensation point (36.5 μmol m^{-2} s^{-1}).

By solving Equations 5.1 and 5.2 for $A_n = A_d$, and replacing the term $M_w P_a / [\mathcal{R} T_a (r_s + r_b)]$[2] with g_t, the total conductance of water through the stomata and boundary layer (mol

[1] see Section 4.2.3.1, Chapter 4 for the quadratic solution of the rectangular hyperbola that describes the relationship between electron transport and light.

[2] P_a is the atmospheric air pressure (101.3 kPa).

m^{-2} s^{-1}), the balanced equation can be written as:

$$\frac{J_e}{4}\frac{C_i - \Gamma^*}{C_i + 2\Gamma^*} - R_d - g_t(C_a - C_i) = 0 \tag{5.4}$$

and so a quadratic solution for C_i can be determined:

$$C_i = \frac{b - \sqrt{b^2 - 4ac}}{2a} \tag{5.5}$$

where $a = 4g_t$

$b = 4g_t(C_a - 2\Gamma^*) - a_c(J_e + 4R_d)$

$c = \Gamma^*(8a_cR_d - 8g_tC_a - a_cJ_e)$

5.2.1.2 Hydrologic framework

An Ohm's law analogue is used to describe the flow of water from the soil to the roots, to the leaf and to the atmosphere. The flow of water is controlled by a gradient of water potential (Ψ_w), which is defined by the difference in Ψ_w at the start (soil) and the end of the pathway (air). This gradient is equal to the rate of water flow and the hydraulic resistance along this pathway. Therefore, the flow of water over time along the SPA pathway can be described as:

$$\frac{dE}{dt} = \frac{1}{R}\frac{d\Psi}{dt} \tag{5.6}$$

where $d\Psi$ is the potential difference along the pathway (MPa), R is the total hydraulic resistance along the pathway (MPa m^2 s mol^{-1}) and E is the rate of water flowing along the pathway (mol m^{-2} s^{-1}). Equation 5.6 can be used to describe the flow of water from the soil to the leaf, and from the leaf to the atmosphere. The supply of H_2O from the soil to the leaves (J_w) is described by:

$$J_w = \frac{\Psi_s - \Psi_l - \rho_w g\, h}{R_{soil} + R_{root} + R_{plant}} \tag{5.7}$$

where Ψ_s and Ψ_l are the soil and leaf water potentials respectively (MPa), the term $\rho_w g\, h$ describes the gravitational pull on the transport of water up through the xylem, where ρ_w

is the density of water (0.001 MPa m^{-1}), g is the gravitational constant (9.807 m^2 s^{-1})and h is the height of the plant (m), R_{root} and R_{plant} are the hydraulic resistances from the soil to the roots, and the roots to the leaves respectively (MPa m^2 s mol^{-1}). Lastly, R_{soil} is the soil hydraulic resistance and is a function of the hydraulic conductivity of the soil and the root density (Tardieu and Simonneau, 1998), and can be described as:

$$R_{soil} = \frac{\ln(\bar{x}_{root}^2/r_{root}^2)}{4\pi K(\theta_s)} \tag{5.8}$$

where $\bar{x}_{root}$ is the mean distance between roots (m), r_{root} is the fine root radius (m) and $K(\theta_s)$ is the hydraulic conductivity dependent on the water content of the soil (m^2 MPa^{-1} s^{-1}).

The evaporative demand for H_2O from the leaf surface (E_t) is similarly described as:

$$E_t = \frac{M_w}{\mathcal{R}T_a}\frac{(e_s - e_a)}{(r_s + r_b)} \tag{5.9}$$

where e_s and e_a are the vapour pressures at saturation and in the air respectively (kPa) and r_s and r_b are the resistances[3] to water transport through the stomata and boundary layer respectively (s m^{-1}).[4]

The Ψ_l that equates to these levels for the supply and demand of water, can be calculated by combining Equations 5.7 and 5.9, assuming that $E_t = J_w$, such that:

$$E = \frac{\Psi_s - \Psi_l - \rho_w g\, h}{R_{soil} + R_{root} + R_{plant}} = \frac{M_w}{\mathcal{R}T_a}\frac{(e_s - e_a)}{(r_s + r_b)} \tag{5.11}$$

and can be simplified by again considering the term $M_w P_a/[\mathcal{R}T_a(r_s + r_b)]$ as the total conductance of water through the stomata and boundary layer (g_t, mol m^{-2} s^{-1}), $D_v =$

[3]Upper and lower case R has been used to distinguish between resistances along the soil-leaf pathway, and at the leaf.

[4]Though mentioned here for the sake of readability, the model uses the Penman-Monteith equation to calculate the evaporate demand for H_2O, so that the E_t is described as:

$$E_t = \frac{\Delta R_n + \rho_a c_p D_v/r_b}{\lambda[\Delta + \gamma(1 + r_s/r_b)]} \tag{5.10}$$

where R_n is the net radiation absorbed by the leaf (W m^{-2}), Δ is the slope of the relationship between the saturation vapour pressure and temperature (kPa $°C^{-1}$), ρ_a is the density or air (1.204 kg m^{-3} @ 20°C), c_p is the specific heat of air (1.013 MJ kg^{-1} $°C^{-1}$), γ is the psychometric constant (0.066 kPa $°C^{-1}$) and λ is the latent heat of vaporisation (2.39 MJ kg^{-1}).

$(e_s - e_a)$, and the sum of $R_{soil} + R_{root} + R_{plant}$, as the total above and below ground resistance ($R_{a,b}$). Equation 5.11 can then be rearranged in terms of Ψ_l as:

$$\Psi_l = \Psi_s - \rho_w g\, h - g_t D_v\, R_{a,b} \tag{5.12}$$

However, the above formulation is not exact, as there is some water stored within the plant tissue and this stored amount can be expended before the plant uses water located in the soil water stores. This creates a time-lag between evaporative demand for water and the flow of water through the plant (dE), such that for an instantaneous time-step $J_w \neq E_t$ and can be described as:

$$\begin{aligned} \frac{dE}{dt} &= J_w - E_t \\ &= \frac{\Psi_s - \Psi_l - \rho_w g\, h}{R_{a,b}} - g_t D_v \\ &= \frac{\Psi_s - \Psi_l - \rho_w g\, h - g_t D_v R_{a,b}}{R_{a,b}} \end{aligned} \tag{5.13}$$

This lag can however be incorporated into the above *circuit* analogue by considering the water stored in plant as a capacitor. Leaf capacitance (C_l) is described as:

$$C_l = \frac{dE}{d\Psi} \tag{5.14}$$

where C_l is the leaf capacitance (mol MPa^{-1} m^{-2}). Equations 5.13 and 5.14 are then combined such that:

$$C_l \frac{d\Psi}{dt} = \frac{\Psi_s - \Psi_l - \rho_w g\, h - g_t D_v R_{a,b}}{R_{a,b}} \tag{5.15}$$

and therefore the change in Ψ_l over time can be described as:

$$\frac{d\Psi}{dt} = \frac{\Psi_s - \Psi_l - \rho_w g\, h - g_t D_v R_{a,b}}{C_l R_{a,b}} \tag{5.16}$$

The above equation may be solved numerically, and allows a feedback between the soil water status and evaporative demand. Figure 5.1 shows a representation of the hydraulic framework, including resistance to water flow and capacitance for storage of water in the canopy, along the SPA pathway.

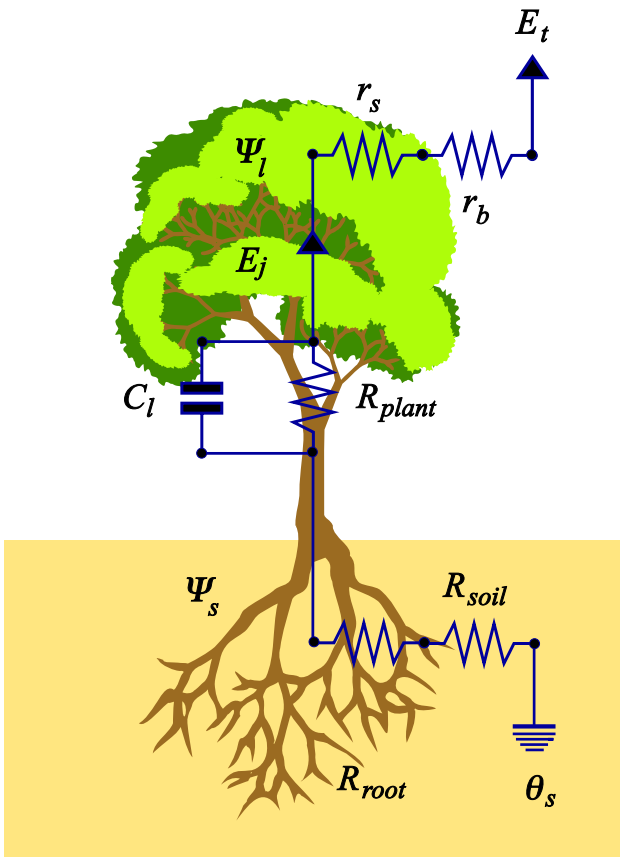

FIGURE 5.1: A circuit diagram of the soil-plant-atmosphere continuum (SPAC) showing the relative resistances to water flow along the pathway. Water is supplied from the soil (θ_s) and travels along the SPAC, where the flow of water (E_j), driven by a potential difference between the leaf (Ψ_l) and the soil (Ψ_s). This flow of water experiences resistance at the soil (R_{soil}), root (R_{root}) and plant (R_{plant}) interfaces. Once this water has reached the leaf, it moves to the atmosphere through transpiration (E_t), where E_t experiences resistance from the stomata (r_s) and from the boundary layer of air at the surface of the leaf (r_b). A portion of the water moving along the SPAC is stored within the plant tissue (C_l).

5.2.1.3 Control of stomatal opening

Two methods of describing the regulation of stomatal opening are described. First is the original hypothesis currently contained in the SPA model and described by Williams et al. (1996a) where g_s is solely regulated by gains in A_n. Second, a modification of this that includes the expenditure of water through E_t. Following the Williams formulation, g_s will increase incrementally to a point whereby A_n is maintained at a constant rate, the

operating point (ι_{op}) can be described as:

$$\iota_{op} = \frac{\delta A_n}{\delta g_s} = \frac{A_n(g_{s,i})}{A_n(g_{s,i-1})} \tag{5.17}$$

where δ describes an infinitesimal increase in g_s and A_n, which is equivalent to the ratio of A_n between increments, i, in g_s. Assuming adequate levels of irradiance and evaporative demand, both g_s and A_n will operate at a level around ι_{op}. However, there needs to be some feedback between the leaf and the demand for water by the atmosphere. Equation 5.17 describes a system where g_s is increased until such a point that no appreciable increases in A_n is gained. While this may be a reasonable approximation, any increases in g_s will result in appreciable increases in E_t, which at the level defined by ι_{op} may be excessive. Therefore, I propose that A_n must include a weighting term defined by E_t, such that increments in g_s is constrained not by an operating point, but by a *cost of water* parameter (λ_{cw}). This new constraint may be defined as:

$$\begin{aligned} \lambda_{cw} &= \frac{\delta A_n / \delta g_s}{\delta E_t / \delta g_s} \\ &= \frac{\delta A_n}{\delta E_t} \\ &= \frac{A_n(g_{s,i}) E_t(g_{s,i-1})}{E_t(g_{s,i}) A_n(g_{s,i-1})} \end{aligned} \tag{5.18}$$

which is functionally equivalent to the principle of optimality described by Cowan and Farquhar (1977). λ_{cw} can be seen as a cost parameter and allows A_n to be *maximised* while E_t is *minimised*, which results in a constant of carbon gained per water transpired.

The two schemes of stomatal optimisation however, are constrained by leaf water status or Ψ_l, such that A_n and E_t will remain constant while there is a sufficient supply water to maintain the levels demanded by the atmosphere, without inducing a Ψ_w that is too low and thereby inducing a reduction in g_s. Thus, in the absence of stomatal regulation, Ψ_l may drop to values that fall below a critical threshold, such that embolism will occur in the xylem preventing further water flow along the SPA pathway (Eamus et al., 2006b). Therefore, regulation of g_s needs to be quantified and this effect is incorporated into the model by the introduction of a critical threshold; the minimum leaf water potential

($\Psi_{l,min}$). The consequence of this is that g_s and A_n will be maximised and E_t minimised as long as $\Psi_l > \Psi_{l,min}$ holds. If Ψ_l is equal to, or less than Ψ_{lmin}, then no further increase in g_s will occur representing the prevention of xylem embolism.

The new model framework proposed in this study is therefore described by the following. Using Equations 5.1 and 5.2 to describe the supply and demand for CO_2, and Equations 5.7 and 5.9 to describe the respective supply and demand for H_2O, while the conditions hold that $\delta A_n/\delta g_s > \iota_{op}$ for g_s Model 1 or $\delta A_n/\delta g_s < \lambda_{cw}\delta E_t/\delta g_s$ for g_s Model 2 and $\Psi_l + d\Psi_l/dt > \Psi_{l\,min}$, determined from Equation 5.16, then the coupled leaf biochemical and hydrologic framework that operates on the above constraints can be represented as:

$$\begin{pmatrix} A_{n,1} & \cdots & A_{n,N} \\ E_{t,1} & \cdots & E_{t,N} \\ g_{s,1} & \cdots & g_{s,N} \\ \vdots & & \vdots \\ \Psi_{l,1} & \cdots & \Psi_{l,N} \end{pmatrix} = f_{SPA} \begin{pmatrix} Q_{p,1} & D_{v,1} & T_{a,1} \\ Q_{p,2} & D_{v,2} & T_{a,2} \\ Q_{p,3} & D_{v,3} & T_{a,3} \\ \vdots & \vdots & \vdots \\ Q_{p,N} & D_{v,N} & T_{a,N} \end{pmatrix} \text{ while } \begin{cases} \text{if } g_s \text{ Scheme 1} & \boxed{\begin{array}{l} \dfrac{\delta A_n}{\delta g_s} > \iota_{op} \\ \Psi_l > \Psi_{l\,min} \end{array}} \\ \text{if } g_s \text{ Scheme 2} & \boxed{\begin{array}{l} \dfrac{\delta A_n}{\delta g_s} < \lambda_{cw}\dfrac{\delta E_t}{\delta g_s} \\ \Psi_l > \Psi_{l\,min} \end{array}} \end{cases}$$

where meteorological inputs (i.e Q_p, D_v, T_a, etc) are passed to the SPA model, f_{SPA}, which uses either stomatal conductance model 1 or 2 to determine outputs of leaf gas-exchange (i.e. A_n, E_t, g_s, etc). While the respective conditions hold for the stomata to remain open, the leaf sub-models work iteratively in determining the gas-exchange variables and can be describe by the following procedure,

1. Increment g_s at a step size of ≈ 0.001 mol m^{-2} s^{-1}
2. Determine C_i from Equation 5.5
3. Determine A_n from Equation 5.2
4. Determine E_t from Equation 5.9
5. Determine $\dfrac{d\Psi_l}{dt}$ from Equation 5.16

6. Return to **1.**

A caveat of the model framework described here is that it will operate in an isohydric manner, so that g_s, A_n, E_t and C_i will operate at a constant rate irrespective of a decrease in Ψ_l *unless* it falls below $\Psi_{l,min}$, at which point limitations in g_s and hence A_n and E_t are seen.

5.2.2 Modelling approach

The two hypotheses on stomatal regulation described above in a leaf gas-exchange framework were tested for a hypothetical system that is subject to increasing water stress over a 30 day period. This methodology is similar to that which was undertaken by Tuzet et al. (2003). The system modelled was defined to represent a typical Australian native forest that is predominantly occupied by Eucalypt species.

Meteorological forcing on the system over the 30 day period was provided by a synthetic data-set constructed of 24 hr cycles of solar radiation (R_s), D_v and T_a (Figure 5.2). The diurnal course of these drivers is an idealised representation of the meteorological forcing exerted upon a forest canopy under conditions absent of rainfall and cloud cover for a temperate, Eucalypt woodland in eastern Australia during late September (Zeppel et al., 2008a). The diurnal course of R_s is symmetric around the midday peak, with a maximum value occurring at 900 W m^{-2}, with sunrise and sunset occurring at 5 am and 7 pm respectively. The diurnal course of T_a ranges between 12-24 °C over the day, and consequently D_v is peaks at 2.0 kPa at 2 pm. Both T_a and D_v track the course of daily irradiance but experience a lag of approximately 2 hours. Wind speed (U) was set to be constantly high at 8 m s^{-1} over the 30 day period, reducing the boundary layer resistance ($r_b \rightarrow 0$) and defining all water lost from the plant to be directly regulated by g_s, and therefore for all equations mentioned above, it holds that $g_t = g_s$ in this study. Although the meteorological conditions are low compared to peak summer values (Zeppel et al., 2008a), I wished to limit the effects of high D_v, so that the Ψ_l did not reach Ψ_{lmin} at the start of the 30 day simulation period. However, the effects of high D_v are explored in a sensitivity analysis.

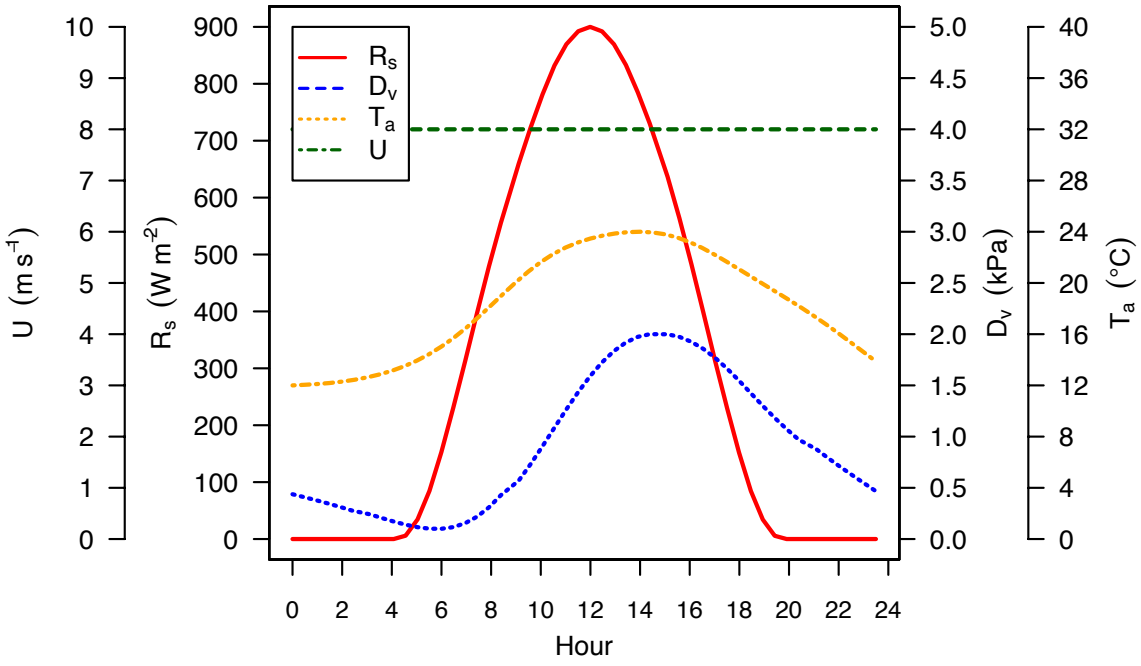

FIGURE 5.2: Diurnal course of solar radiation (R_s), vapour pressure deficit (D_v), air temperature (T_a) and wind speed (U) used in the simulation to test both leaf gas-exchange models. The diurnal course of these drivers are repeated over the 30 day simulation period.

Leaf biochemical parameters were chosen to reflect vegetation operating under the above idealised conditions, operating on a simple soil profile (Table 5.1). Simulations were performed for a 9 m tall tree with a LAI of 3 m^2 m^{-2} distributed evenly over 10 canopy layers. A low R_{plant} of 150 MPa m^2 $mmol^{-1}$ and low Ψ_{lmin} of -3.0 MPa was selected to allow a period where θ_s is non-limiting. The soil profile for this simulation was set to be 2 m deep, with roots having access down to a 1 m depth. The distribution of roots through the profile was exponential and fine root radius was selected to be 0.1 mm. Root biomass was set low at 3 kg m^3 in order to provide a reasonable feedback for below ground resistance in the system. The particle size distribution (PSD) of the profile was set as a sandy loam (65% Clay, 10% Sand), and the initial water content of the soil (θ_s) was set as saturated (0.18 m^3 m^{-3}). These values have not been selected to represent a specific site, but were selected to test the coupling of g_s with CO_2 exchange by the leaves and the flow of water through the SPAC within the SPA model.

Two representations of stomatal regulation were modelled for a 30 day drying-out period.

TABLE 5.1: Parameters used to describe the system's vegetation and soil profile. Parameter descriptions, symbols, units and values are given for the 30 day simulation period.

Description	Symbol	Units	Value
Canopy height	h	m	9.0
Leaf area index	L_{AI}	m^2 m^{-2}	2.0
Foliar nitrogen	N_f	gN m^{-2}	3.0
Whole leaf capacitance	C_l	mol m^{-2} MPa^{-1}	5.0
Whole plant resistance	R_{plant}	MPa m^2 $mmol^{-1}$	150
Maximum electron transport rate	J_{max}	μmol m^{-2} s^{-1}	160
Maximum RuBisCO activity	V_{cmax}	μmol m^{-2} s^{-1}	80
Minimum leaf water potential	Ψ_{lmin}	MPa	-3.0
Operating point for stomatal efficiency	ι_{op}	%	0.07
Carbon gained per unit water lost	λ_{cw}	μmol CO_2 mol^{-1} H_2O	75
Soil depth	d_{soil}	m	2.0
Rooting depth	d_{root}	m	1.0
Root biomass	m_{root}	kg biomass m^{-2}	3.0
Fine root radius	r_{root}	mm	0.1
Whole root resistance	R_{root}	MPa m^2 $mmol^{-1}$	400
Sand particle size distribution	$S_{\%}$	%	65.0
Clay particle size distribution	$C_{\%}$	%	10.0

The first representation (Scheme 1) is expressed by Equation 5.17, where g_s is maximised to maximise A_n (Williams et al., 1996a). The second representation (Scheme 2) is expressed by Equation 5.18, where g_s is maximised to maximise A_n while minimising E_t (Cowan, 1977). Both of these schemes contain the additional constraint that represents a fail-safe in the hydraulic system, such that g_s may only be maximised to a point where Ψ_l remains larger than Ψ_{lmin}. The point where g_s is said to maximise A_n (ι_{op} for Scheme 1 and λ_{cw} for Scheme 2) were chosen to emulate similar daily maximums of g_s on day 1. Because this study is purely theoretical and is not specified to a particular site, it was not possible to quantify the value of ι_{op} with λ_{cw}; although a method for site-specific parameterisation has been offered in Chapter 4. However, the relative effects of changing the magnitude of these parameters has been explored in a sensitivity analysis.

5.3 Results

5.3.1 Time-series of decreasing leaf and soil water potential and its impact on leaf gas-exchange

Schemes 1 and 2 were applied to an idealised site (Figure 5.2) for a 30 day period, where limiting soil water conditions were introduced. Figure 5.3 shows the effect of decreasing Ψ_s on modelled leaf gas-exchange produced by the respective schemes. Both schemes simulated similar below-ground water balances over the 30 day period, with soil water storage gradually declining from 360 to 264 mm (Figure 5.3a) in Scheme 1 and 360 to 262 mm (Figure 5.3b) in Scheme 2. Initial daily minimums of Ψ_l were slightly lower in Scheme 1 (-2.7 MPa; Figure 5.3c) than in Scheme 2 (-2.5 MPa; Figure 5.3d), which caused Scheme 1 to reach Ψ_{lmin} much sooner during the simulation period. However, this did not have a large impact on leaf gas-exchange over the simulation period.

Both schemes showed that while Ψ_s remained above -0.25 MPa, Ψ_l remained above Ψ_{lmin} and R_{soil} remained low and constant at 3.0 MPa m^2 s mmol^{-1}. Consequently, soil water was not limiting on gas-exchange under these conditions and g_s, A_n, E_t and C_i operated maximally and were symmetric around 12-noon peak (Figure 5.3e-l). However, while both schemes displayed similar daily maximums of g_s, A_n and C_i/C_a, the daily maximum E_t was larger in Scheme 1 (360 W m^{-2}) than in Scheme 2 (315 W m^{-2}). For Scheme 1, the period where θ_s was non-limiting lasted approximately 11 days, while for Scheme 2 it was longer, lasting 15 days. Once Ψ_s fell below -0.25 MPa, θ_s started to become limiting on the system; Ψ_l began to reach Ψ_{lmin} and R_{soil} increased slowly (3.0 $\rightarrow$ 4.0 MPa m^2 s mmol^{-1}). The decrease in Ψ_s over this period, which resulted in Ψ_l reaching Ψ_{lmin} caused an increasing asymmetry to occur in the diurnal courses of the leaf gas-exchange quantities. Diurnal g_s in both schemes displayed distinct mid-morning and afternoon peaks (Figure 5.3e,f), while A_n remain relatively unaffected (Figure 5.3g,h), E_t became asymmetric and dropped in its daily maximum values (Figure 5.3i,j) and C_i/C_a showed an increasing drop in the afternoon (Figure 5.3k,l). For Scheme 1, this period lasted 7 days, while in Scheme 2 this period was shorter, lasting 4 days. After Ψ_s fell below -0.8 MPa, θ_s began to reach critical levels (for this soil type; 0.08 m^3 m^{-3}) and water stress became

more evident and severe. As a result, Ψ_l reached Ψ_{lmin} for all daylight hours during this period and R_{soil} increased rapidly; in Scheme 1, this increase was from 4.0 to 29.0 MPa m^2 s $mmol^{-1}$, while in Scheme 2, the increase was smaller, moving from 4.0 to 20.0 MPa m^2 s $mmol^{-1}$. The decline in value of the gas-exchange quantities was similar for both schemes, however daily maximum g_s in Scheme 2 remained constant despite the significant drop in θ_s. For Scheme 1, the period of water stress lasted for 12 days, and for Scheme 2 the period lasted 11 days. By day 30, the rooting zone of the soil had dried out and gas-exchange had become severely limited.

5.3.2 Diurnal course of leaf gas-exchange in the two schemes

While gas-exchange showed a similar decline in both schemes over the 30 day period, there were differences in the shape and degree of asymmetry in the diurnal responses for some of the gas-exchange quantities. The most notable, was the difference in magnitude of daily maximum E_t that was observable between schemes at the start of the simulation period. Additionally Scheme 2 displayed an initial asymmetry in g_s that was independent of θ_s and was not seen in Scheme 1. Because these disparities observed among schemes relates to differences in stomatal regulation, a selection of days over the 30 day period were analysed in more detail.

Figure 5.4 shows the modelled diurnal course of g_s, A_n, E_t and C_i/C_a for days 1, 14, 18, 21, 26 and 30, demonstrating the effects of declining Ψ_s in Schemes 1 and 2. On day 1, under non-limiting soil water conditions, all variables in Scheme 1 were symmetrical around noon, tracing the diurnal course of R_s (Figure 5.4a-d). Scheme 2 showed similar symmetry for A_n and E_t (Figure 5.4f,g), but not for g_s and C_i/C_a, which were asymmetric even though θ_s was non-limiting (Figure 5.4e,h). This initial asymmetry in g_s was in response to increasing D_v and T_a in the afternoon and was independent of soil water status. The effect of high afternoon D_v and T_a was not observable in Scheme 1 as a result of poor coupling between g_s and D_v. The initial asymmetry seen in C_i/C_a is the result of the auto-correlation between g_s and C_i in Equation 5.1, such that $g_s \propto C_i$. From day 14 onwards, both schemes displayed an asymmetry in the diurnal patterns of the gas-exchange quantities as a result of $\Psi_l = \Psi_{lmin}$ and became more pronounced as Ψ_s decreased. This

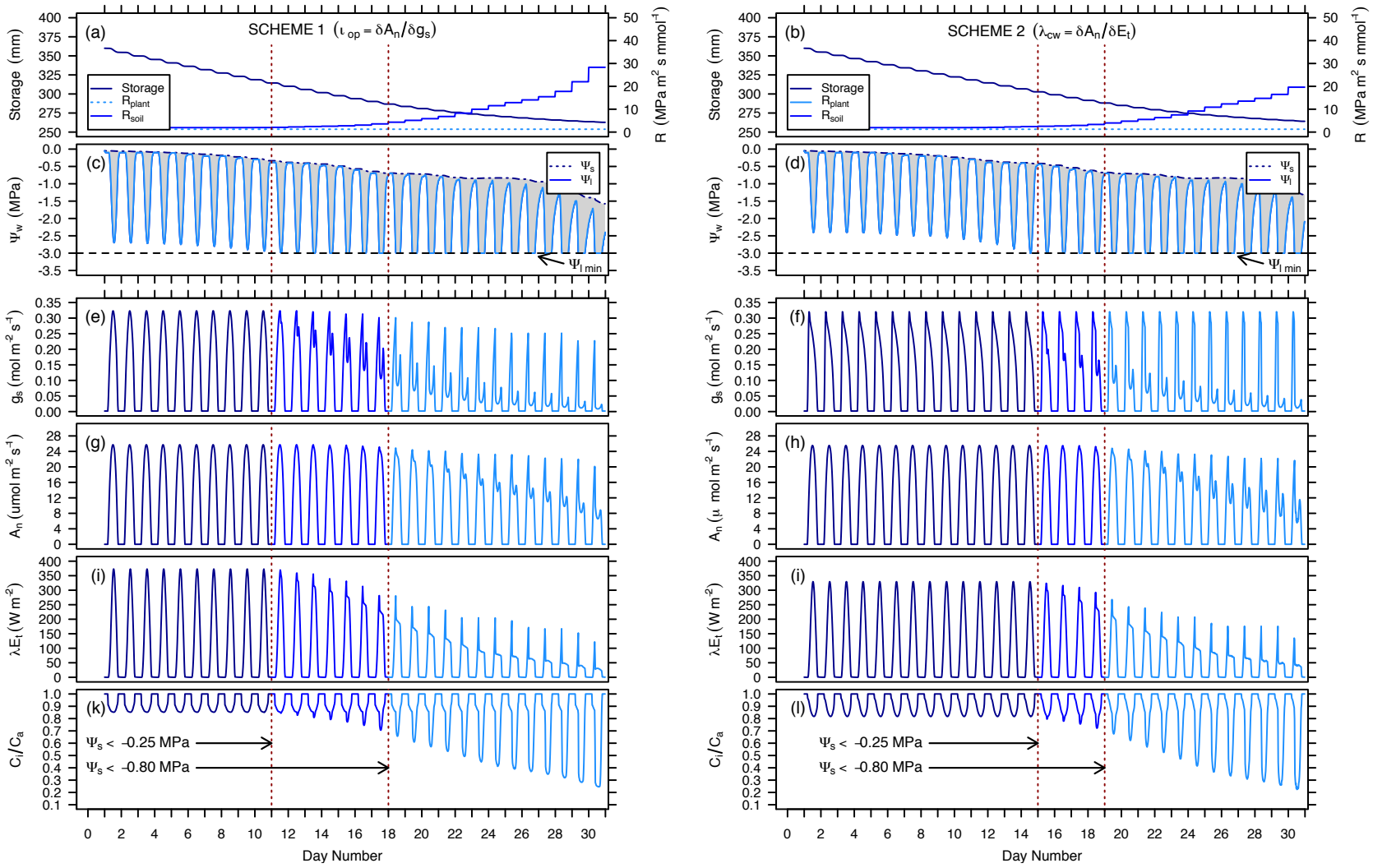

FIGURE 5.3: Simulated gas-exchange and soil water dynamics of Schemes 1 and 2 over the 30 day drying period. Shown above is the time course of (a-b) soil water storage, plant (R_{plant}) and soil (R_{soil}) resistance, as well as (c-d) the leaf (Ψ_l) and soil (Ψ_s) water potentials, and the minimum leaf water potential (Ψ_{lmin}). Estimates of leaf gas-exchange quantities are given along this trace for (e-f) stomatal conductance (g_s), (g-h) net assimilation rate (A_n), (i-j) latent energy (λE_t) and (k-l) the ratio of intercellular and atmospheric CO_2 (C_i/C_a). The dotted maroon lines and the change in colour (blue to light blue), denote the transition from well-watered to water-stressed conditions. Modelled A_n and E_t have been multiplied by L_{AI} to scale from leaf to canopy.

resulted in morning and afternoon peaks in the diurnal course of g_s and A_n, an initial morning peak and then decline in E_t, and an increasing draw-down of C_i in the afternoon as a consequence of the stomata beginning to regulate Ψ_l as water supply declined. The asymmetry in these quantities was the result of the reduced ability of soil to supply water to the canopy, due to a decrease in hydraulic conductivity and increase in R_{soil}.

In Scheme 1, the decrease in Ψ_l caused a decline in g_s after it had reached a midday peak at approximately 12-noon, falling to a minimum at 2 pm when $\Psi_l = \Psi_{lmin}$. As the soil dried out, the peak in g_s occurred earlier in the morning, and decreased from 0.32 to 0.22 mol m^{-1} s^{-1} (days 1 and 30 respectively) as a result of Ψ_l reaching Ψ_{lmin} sooner (Figure 5.4a). In contrast to this, A_n remained unresponsive to declining g_s until Ψ_s was less than -0.8 MPa (day 18 onwards), when the system became severely water stressed (Figure 5.4b). During this period A_n began to display increasing asymmetry that was coupled with the large draw-down in C_i/C_a and the increase in R_{soil} (Figure 5.3a). With the decline in Ψ_s, the diurnal course of E_t showed a distinct morning peak that then declined to a constant for the remaining daylight hours. Despite Ψ_l reaching Ψ_{lmin}, E_t did not experience a midday depression due to increasing D_v in the afternoon which counteracted the drop in g_s (Figure 5.3c). The draw-down of C_i/C_a increased with the progression of the drought and followed the increase in daily D_v and T_a and was limited by $\Psi_l = \Psi_{lmin}$ (Figure 5.3d). The increased draw-down was correlated with the midday depression in g_s.

Scheme 2 displayed an initial asymmetry in g_s under high Ψ_s, with a maximum g_s occurring at 8 am, which then decreased over the course of the day with increasing D_v and T_a and was limited by $\Psi_l = \Psi_{lmin}$ (Figure 5.3e). Morning peak g_s did not move in time, due to the effect of increasing D_v on g_s in the early morning, which was not yet limited by Ψ_l reaching $\Psi_{l,min}$. As a result, daily maximum g_s (0.32 mol m^{-1} s^{-1}) did not decrease over the 30 day period despite decreasing Ψ_s and did not display a midday depression until day 18. Compared to Scheme 1, the afternoon peaks of g_s in Scheme 2 were of a lower magnitude due to a stronger coupling between g_s and D_v. The response of A_n to decreasing Ψ_s was similar to Scheme 1, with the exception that Scheme 2 displayed deeper midday depressions in A_n and had slightly higher afternoon peaks (Figure 5.3f). Like Scheme 1, A_n was insensitive to g_s, but was sensitive to increasing R_{soil} and decreasing C_i/C_a. Scheme 2 E_t displayed a similar diurnal response to Scheme 1, although an asymmetry in the

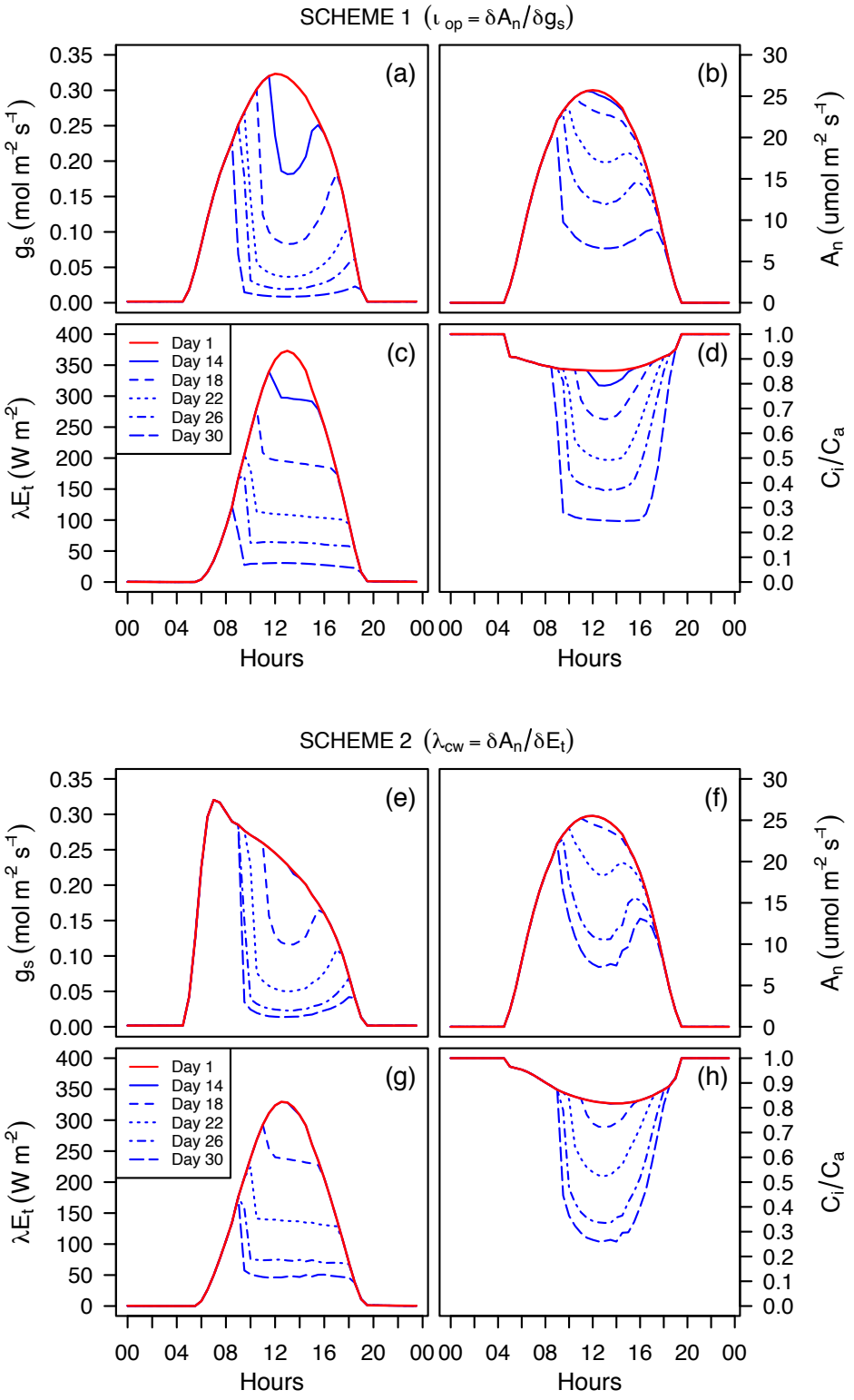

FIGURE 5.4: Diurnal course of leaf gas-exchange variables for days 1, 14, 18, 22, 26 and 30 during the 30 day drying period. Show above are (a) stomatal conductance (g_s), (b) net assimilation rate (A_n), (c) latent energy (λE_t) and (d) the ratio of intercellular and atmospheric CO_2 (C_i/C_a) in Scheme 1, and (e) g_s, (f) A_n, (g) λE_t and (h) C_i/C_a in Scheme 2. The red line denotes gas-exchange that is operating under non-limiting soil water conditions. Modelled A_n and E_t has been multiplied by L_{AI} to scale from leaf to canopy.

diurnal response was not observed until a later period (day 18 instead of 14). However, by day 30 the E_t of each scheme was at a very similar level (Figure 5.3g). There was a much smoother draw-down in C_i/C_a for Scheme 2 than Scheme 1, and the initial asymmetry of C_i/C_a was evident under non-limiting θ_s (Figure 5.3h). As was observed in Scheme 1, C_i/C_a was correlated with g_s in Scheme 2.

5.3.3 Relationships among leaf gas-exchange quantities

5.3.3.1 Between leaf gas-exchange quantities and environmental drivers

The relationships between leaf gas-exchange and the environmental drivers of R_s and D_v are shown in Figure 5.5 for Schemes 1 and 2, where days 1, 18, 22, 25 and 30 show the effects of progressive soil drying on these relationships. All quantities show a hysteresis loop in response to the diurnal changes in R_s and D_v, as well as the difference of pre-dawn leaf water potentials (Ψ_{lpd}) between days.

For Scheme 1, the relationship between g_s, D_v and R_s remains proportional under well-watered conditions. The response of g_s to R_s was positive, and highly correlated, displaying a tight hysteresis loop and showing that g_s retained a strong relationship with light throughout the day (Figure 5.5a). In contrast to this, the response to D_v showed a much weaker relationship and was less correlated, with the major effects of D_v on g_s limited to the afternoon (Figure 5.5b). In Scheme 2, the relationship between g_s and R_s was also positive, with the exception that towards midday a slight, negative relationship developed in response to increasing D_v (Figure 5.5c). This relationship was also less strongly correlated than in Scheme 1, displaying a larger degree of hysteresis. Scheme 2 exhibited a negative relationship of g_s with D_v during the morning compared with a positive one observed in Scheme 1 (Figure 5.5d). Thus g_s in Scheme 2 was more sensitive to D_v than in Scheme 1.

Little difference was observable between Schemes 1 and 2 for the responses of A_n, E_t and the C_i/C_a ratio to D_v and R_s. Any differences that arose were in part due to Scheme 2 regulating E_t and exhibiting a smaller decline in Ψ_s. A_n and E_t were highly correlated with R_s, with increasing hysteresis in the relationships occurring as the soil dried out.

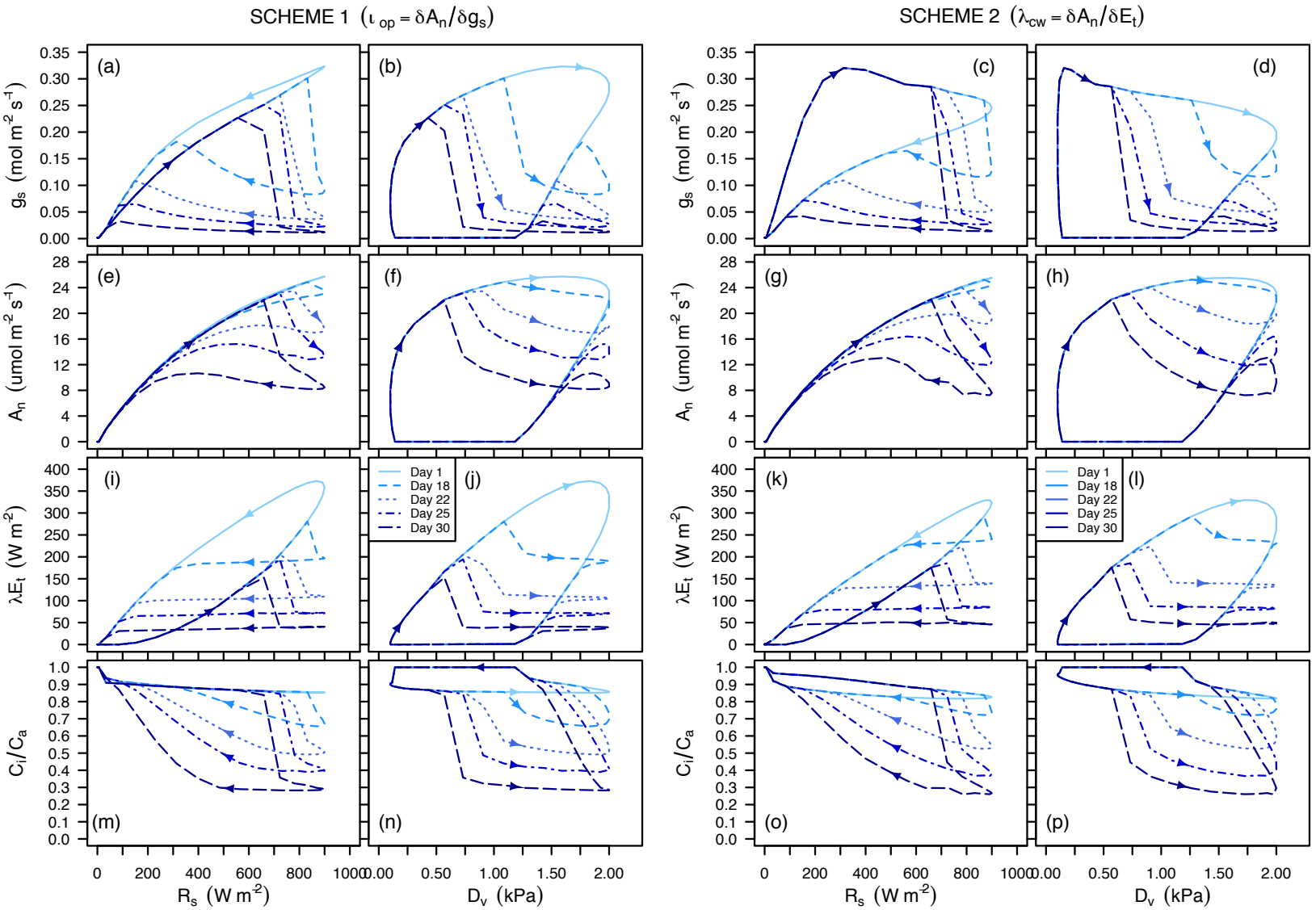

FIGURE 5.5: Shows the responses of Scheme 1 and 2 (a-d) stomatal conductance (g_s), (e-h) net assimilation rate (A_n), (i-l) latent energy (λE_t) and (m-p) the ratio of intercellular and atmospheric CO_2 (C_i/C_a), against solar radiation (R_s) and vapour pressure deficit (D_v) respectively. Relationships between these quantities are shown over the 30 day drying period for days 1, 18, 22, 25 and 30.

This caused A_n and E_t to become increasingly insensitive to R_s in the afternoon (Figure 5.5e,g,i,k). The relationships between A_n, E_t and D_v were positive under non-limiting soil water conditions, but displayed a large hysteresis. As the soil dried out, this hysteresis decreased, but the quantities A_n and E_t became increasingly insensitive to D_v for most of the day (Figure 5.5f,h,j,l). The opposite was seen for the C_i/C_a ratio, which was largely insensitive to R_s and D_v and displayed very little (for D_v) or no hysteresis (for R_s) under well watered conditions (Figure 5.5m-p). However, as soil water became limiting, hysteresis increased and the negative relationship became stronger.

For all quantities in both schemes, the effects of increasing soil water-stress caused g_s, A_n, E_t and the C_i/C_a ratio to become increasingly insensitive to R_s and D_v. In response to increasing D_v, the relationship with gas-exchange became increasingly, negatively correlated due to declining Ψ_s. The poor correlation and large hysteresis between gas-exchange and D_v under well-watered conditions is largely the result of a 2 hr time-lag that occurs between R_s and D_v, such that all quantities are initially out of synchronisation with D_v regardless of water status. For instance, g_s reaches a maximum at 12-noon while D_v reaches a maximum at 2 pm. The opposite effect was seen with R_s, with the relationship collapsing in response to the shift of daily maximum g_s from the midday mark (in synchronisation with daily maximum R_s) to earlier in the morning; creating an asymmetry in the diurnal course (Figure 5.4). This in turn was a consequence of tighter stomatal regulation as D_v increased under the conditions of decreasing Ψ_l.

5.3.3.2 Between stomatal conductance, assimilation and transpiration

Relationships between g_s, A_n and E_t are presented in Figure 5.6 for Schemes 1 and 2, using the same set of days representing the drying period mentioned in the last section. In Scheme 1, under non-limiting soil water conditions, the relationship between g_s and A_n was highly and positively correlated, such that $A_n \propto g_s$ (Figure 5.6a). As the soil dried out, there was an increasing draw-down in CO_2 during the afternoon, following an increase in D_v in the afternoon and Ψ_l reaching Ψ_{lmin}. This created a lag between A_n and g_s, which caused a disproportionality between these quantities and increased the degree of hysteresis as Ψ_s declined. This process similarly occurred in Scheme 2, with the exception

that the relationship was less correlated, due to a greater sensitivity of g_s to D_v and resulted in an initial hysteresis (Figure 5.6b). There was a positive and highly correlated relationship between g_s and E_t in Scheme 1 (Figure 5.6c). Declining Ψ_s resulted in a Ψ_l reaching Ψ_{lmin} and a decrease in the slope of the relationship between g_s and E_t. This caused E_t to become increasingly insensitive to g_s over the drying period. These patterns were similarly seen in Scheme 2, with the exception of an initial, large hysteresis that existed under well-watered conditions and was the results of a greater sensitivity to D_v (Figure 5.6d). This large hysteresis showed an insensitivity of E_t to increasing g_s during the early morning, which expanded to the rest of the day as the soil dried out.

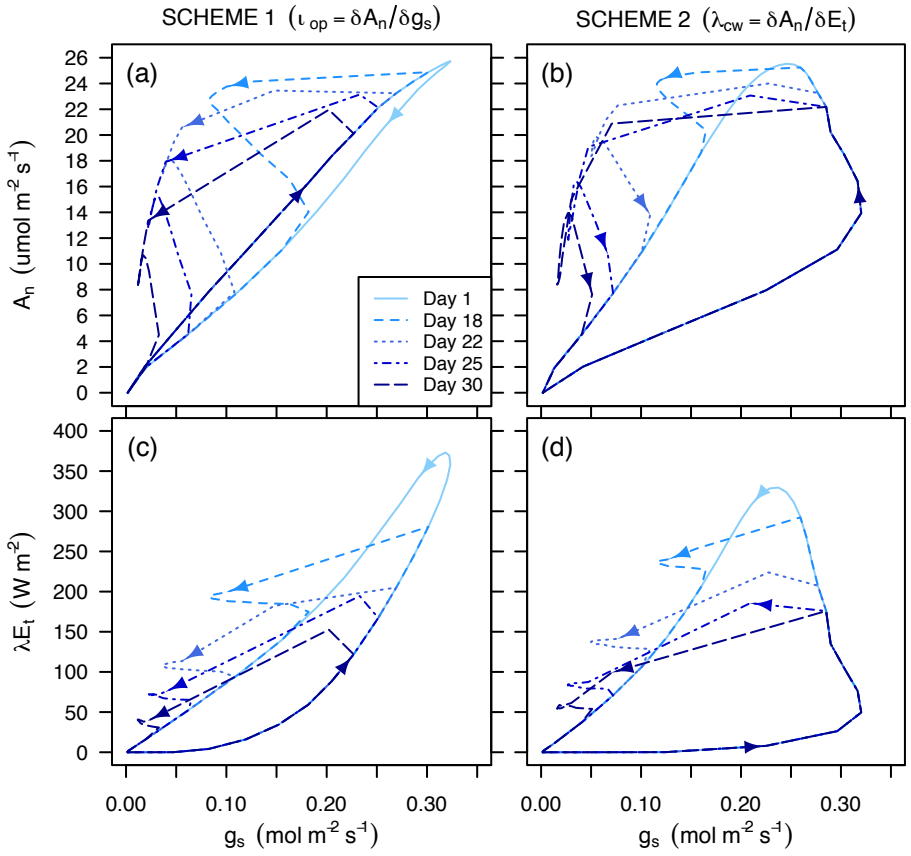

FIGURE 5.6: Plotted relationships between (a-b) stomatal conductance (g_s) and net assimilation rate (A_n), as well as (c-d) g_s and latent energy (λE_t) for Schemes 1 and 2 respectively. The effects of soil drying on these relationships is shown for a selection of days (1, 18, 22, 25 and 29) during the 30 day drying period.

5.3.3.3 Between leaf water potential, assimilation and transpiration

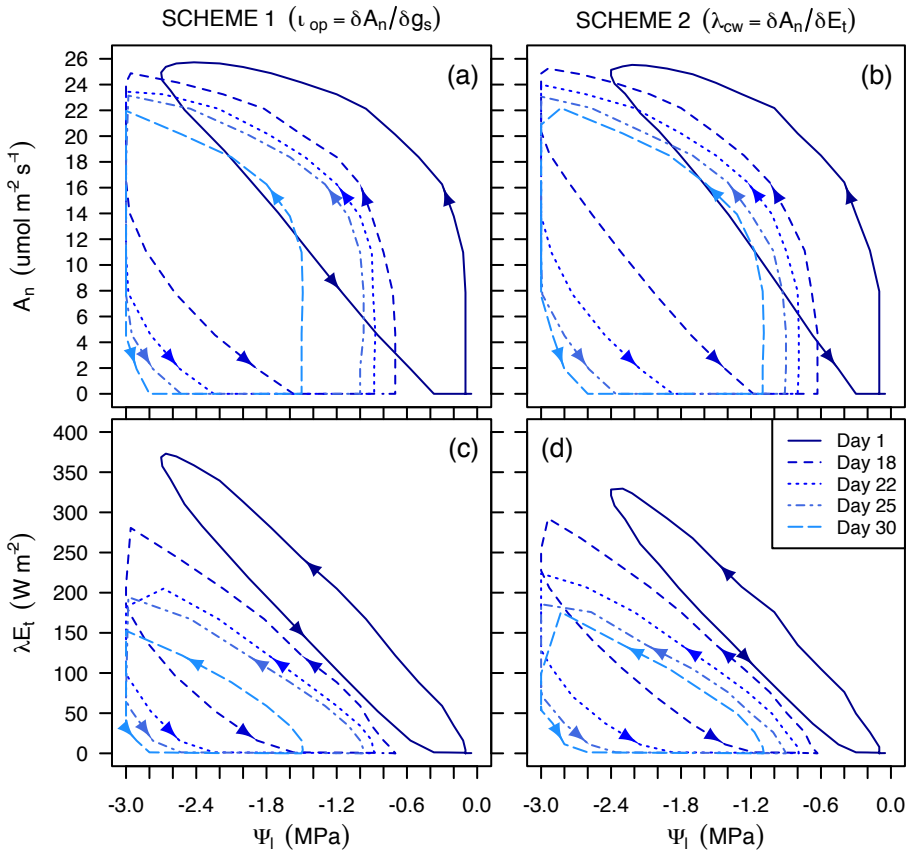

FIGURE 5.7: Plotted relationships between (a-b) leaf water potential (Ψ_l) and net assimilation rate (A_n), as well as (c-d) Ψ_l and latent energy (λE_t) for Schemes 1 and 2 respectively. The effects of soil drying on these relationships is shown for a selection of days (1, 18, 22, 25 and 29) during the 30 day drying period.

Figure 5.7 shows the sensitivity of A_n and E_t to decreasing Ψ_l for Schemes 1 and 2 over the 30 day drying period. Selected days showing these relationships are the same as those used in the last two sections. In Scheme 1, A_n was negatively correlated with Ψ_l and displayed initial hysteresis, where morning A_n was less sensitive to Ψ_l than in the afternoon (Figure 5.7a). With the decrease in Ψ_s, the relationship shifted towards Ψ_{lmin} as Ψ_{lpd} decreased. This caused an increase in hysteresis and the correlation between A_n and Ψ_l to decrease. Scheme 2 displayed a similar pattern to Scheme 1, however, there was a lesser degree of hysteresis and A_n was slightly more sensitive to Ψ_l in the morning (Figure 5.7b). A highly negative relationship existed between E_t and Ψ_l for Schemes 1

and 2 (Figure 5.7c,d), where E_t was highly sensitive to Ψ_l in both morning and afternoon. As the soil dried out and Ψ_l began to reach Ψ_{lmin}, E_t and Ψ_l became less correlated and the relationship slightly less negative. Scheme 1 had a higher maximum E_t and a Ψ_{lpd} that decreased much faster than in Scheme 2.

5.3.4 Sensitivity analysis

5.3.4.1 Sensitivity of gas-exchange to stomatal efficiency and the cost of water

Figure 5.8 shows the effect of changing the *stomatal efficiency* in Scheme 1, and *cost of water* in Scheme 2 on the daily mean values of modelled leaf gas-exchange. For convenience, both ι_{op} and λ_{cw} are denoted as the *operating points* (OP) for the respective schemes from this point on. The OPs were selected to cover the possible upper and lower limits; for Scheme 1 the range for ι_{op} was $0.3, 0.7, 0.2, 0.5$ and 1.0 %, and for Scheme 2 the range for λ_{cw} was $30, 75, 150, 300$ and 500 μmol mol^{-1}.

Variation in the value of OP in each scheme caused the initial values of the gas-exchange quantities to vary. In both schemes, increasing the OP increased the number of days for which the system was not limited by θ_s. The length of this period was the result of the initial values of mean diurnal stomatal conductance ($\overline{g}_s$), transpiration rate ($\overline{E}_t$) and the daily minimum of the ratio between intercellular and atmospheric CO_2 ($C_{i,min}/C_a$) having different magnitudes on day 1. However, increasing the OP showed very little effect on the initial values of mean diurnal net assimilation rate ($\overline{A}_n$). At the start of the 30 day drying period, $\overline{g}_s$ was found to be the most sensitive to variation in OP. In Scheme 1, increasing ι_{op} ($0.03 \rightarrow 1.00$ %) caused initial $\overline{g}_s$ to decrease from 0.35 to 0.07 mol m^{-2} s^{-1} (Figure 5.8a), while in Scheme 2, increasing λ_{cw} ($30 \rightarrow 500$ μmol mol^{-1}) caused initial $\overline{g}_s$ to decrease from 0.32 to 0.09 mol m^{-2} s^{-1} (Figure 5.8b). Initial $\overline{E}_t$ was also sensitive to variation in the OP. In Scheme 1, increasing ι_{op} resulted in a decrease in initial $\overline{E}_t$ from 253 to 119 W m^{-2} (Figure 5.8c), while in Scheme 2, increasing λ_{cw} resulted in a similar decrease in initial $\overline{E}_t$ from 236 to 126 W m^{-2} (Figure 5.8d). Increasing the OP had very little effect on the initial values of $\overline{A}_n$, with increases in ι_{op} and λ_{cw} resulting in very small decreases of 19.7 to 18.2 μmol m^{-2} s^{-1} in Scheme 1 (Figure 5.8e) and 19.7 to 18.5 μmol

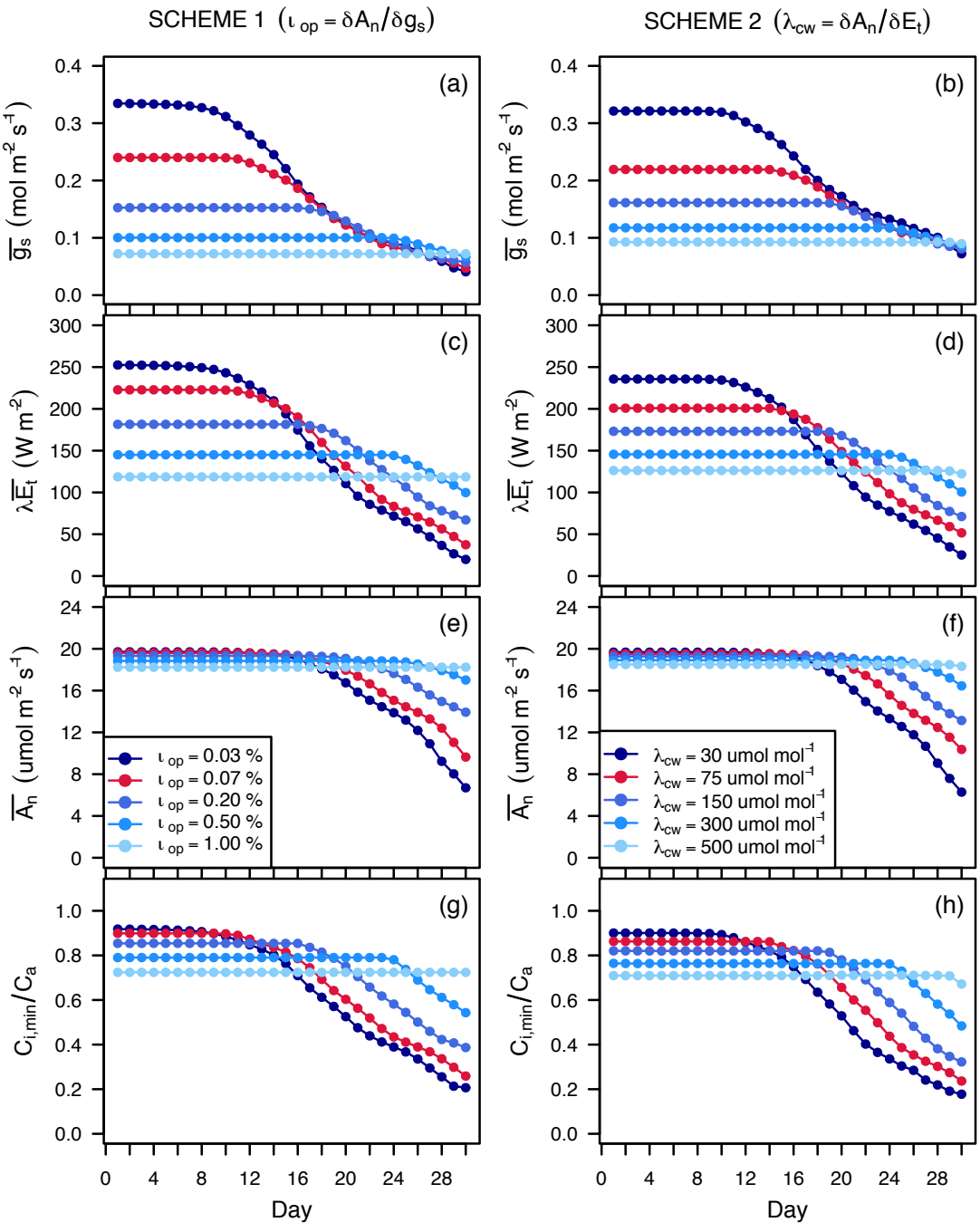

FIGURE 5.8: Sensitivity of daily mean (a) stomatal conductance ($\overline{g}_s$), (b) latent energy ($\lambda\overline{E}_t$), (c) net assimilation rate ($\overline{A}_n$) and (d) the daily minimum ratio between intercellular and atmospheric CO_2 ($C_{i,min}/C_a$) to *stomatal efficiency* ($\iota_{op} = 0.03, 0.07, 0.2, 0.5$ and 1.0 %) in Scheme 1, and (e) $\overline{g}_s$, (f) $\lambda\overline{E}_t$, (g) $\overline{A}_n$ and (h) $C_{i,min}/C_a$ to the *cost of water* ($\lambda_{cw} = 30, 75, 150, 300$ and 500 μmol m^{-2} s^{-1}) in Scheme 2. A run using the default operating points is given in red, while changes in ι_{op} and λ_{cw} are given in shades of blue.

m^{-2} s^{-1} in Scheme 2 (Figure 5.8f). Variation in OP had moderate effect on the starting values of $C_{i,min}/C_a$. In Scheme 1, the effect of increasing ι_{op} resulted in a decrease of initial $C_{i,min}/C_a$ from 0.91 to 0.72 (Figure 5.8g), while in Scheme 2, increasing λ_{cw} resulted in a decrease from 0.90 to 0.70 (Figure 5.8h).

High initial values of $\overline{g}_s$ and $\overline{E}_t$ resulted in a faster depletion of soil water over the 30 day period, and therefore, little to no gas-exchange by day 30. Values of $\overline{E}_t$, $\overline{A}_n$ and $C_{i,min}/C_a$ decreased substantially when θ_s became limiting and a low OP was selected. However, variation in the OP did not have a great effect on $\overline{g}_s$ for the same conditions, as it converged towards similar values at the end of the drying period (Figure 5.8a-b). This was observed in the small difference of OP derived values of $\overline{g}_s$ on day 30, where the difference in Schemes 1 and 2 were both 0.02 mol m^{-2} s^{-1}. For $\overline{E}_t$, a higher initial value dictated a larger decline in water-use over the drying period (Figure 5.8c-d). In Scheme 1, a low OP caused $\overline{E}_t$ to decrease from 253 to 20 W m^{-2} over the 30 day period, where θ_s became limiting on day 6. In Scheme 2 the decline in $\overline{E}_t$ over the same period was from 236 to 25 W m^{-2}, where θ_s became limiting on day 10. However, a high OP allowed both schemes to maintain a constant $\overline{E}_t$ (119 and 126 W m^{-2} for Schemes 1 and 2 respectively) over the drought, such that θ_s never became limiting on the system. Despite having little effect on $\overline{A}_n$ at the start of the drought, variation in the OP had a large impact on the final values of $\overline{A}_n$ (Figure 5.8e-f). In Scheme 1, a low OP caused a decline from 19.7 to 6.7 μmol m^{-2} s^{-1} over the 30 days, while in Scheme 2 this decline was from 19.7 to 6.3 μmol m^{-2} s^{-1}. However, a high OP allowed $\overline{A}_n$ to remain relatively unchanged over the drought in both schemes (19.7 μmol m^{-2} s^{-1} over 30 days). Similar to the effects seen on $\overline{E}_t$, a lower OP caused $C_{i,min}/C_a$ to decline at a faster rate (Figure 5.8g-h). In Scheme 1, this resulted in a decline from 0.91 to 0.20 over the 30 days, while in Scheme 2 the decline was from 0.90 to 0.18. As was observed with the other gas-exchange quantities, a high OP allowed $C_{i,min}/C_a$ to be maintained at a constant rate over the drought. Although this was predominantly true for both schemes, Scheme 2 experienced a minor drop in $C_{i,min}/C_a$ of 0.70 to 0.67 on the last day. Although this may be a numerical error in the model due to the extreme water-stressed conditions.

The effect on the total carbon gained and water lost over the period in both schemes is shown in Figure 5.9. The most significant result of varying the system OP was its impact

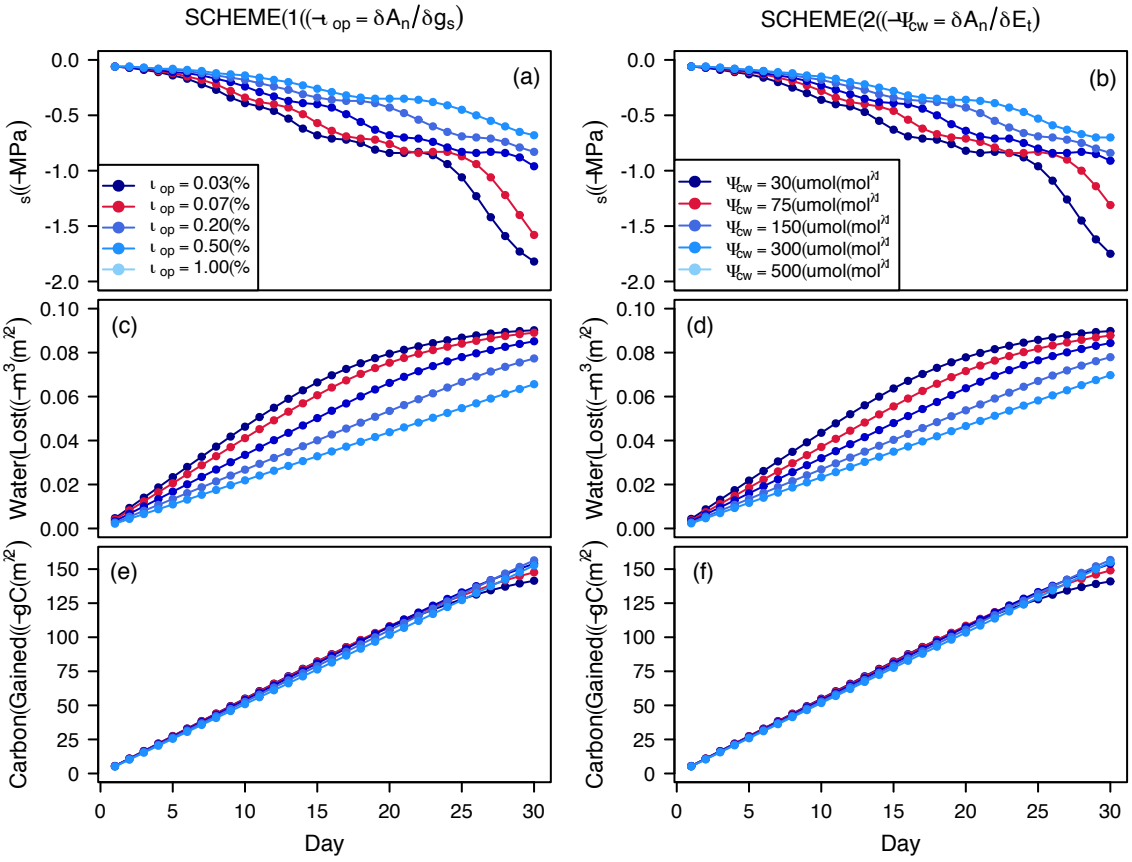

FIGURE 5.9: The sensitivity of (a-b) soil water potential (Ψ_s), (c-d) cumulative carbon gain and (e-f) cumulative water loss to variation in *stomatal efficiency* (ι_{op} = 0.3, 0.7, 0.2, 0.5 and 1.0 %) in Scheme 1 and the *cost of water* (λ_{cw} = 30, 75, 150, 300 and 500 μmol mol^{-1}) in Scheme 2. A run using default operating points is given in red, while changes in ι_{op} and λ_{cw} are given in shades of blue.

on the rate of soil water depletion during the simulation period (Figure 5.9a-b). A high OP resulted in smaller rate of decline in Ψ_s in Schemes 1 and 2 (-0.05 to -0.68 MPa), while a low OP resulted in a large decline in Ψ_s (-0.05 to -1.82 MPa). This resulted in large differences in the total amount of water lost by the end of the drying period (Figure 5.9c-d). In Scheme 1, a low ι_{op} (0.03%) resulted in a total water-use of 0.090 m^3 m^{-2}, while a high ι_{op} (1.00%) resulted in a total water-use of 0.066 m^3 m^{-2}. Similar totals were observed for Scheme 2, with low and high λ_{cw} values (30 and 500 μmol mol^{-1}) resulting in water-use totals of 0.089 and 0.70 m^3 m^{-2} respectively. However despite the large differences in total water-used, very little difference was observed between total carbon gained for different OP values (Figure 5.9e-f). In Scheme 1, the difference in total carbon gained for low and high ι_{op} was 142 and 153 gC m^{-2} respectively, while for Scheme 2 this

difference for low and high λ_{cw} was 141 and 155 gC m^{-2} respectively. These results show that there is no great benefit in maintaining a high g_s to marginally increase A_n, as this results in an excessive increase in E_t. This can be expressed by comparing the water-use efficiencies (WUE) for the low and high OPs, where the WUE is defined as total carbon gained divided by total water-use (A/E). In Scheme 1, a low ι_{op} has a WUE of 1.53 gC m^{-3} H_2O, while a high ι_{op} has a WUE of 2.33 gC m^{-3} H_2O. Similarly, in Scheme 2, a low λ_{cw} has a WUE of 1.57 gC m^{-3} H_2O and a high λ_{cw} has a WUE of 2.22 gC m^{-3} H_2O. Although a low OP may be reasonable during well-watered conditions, a high OP is more desirable in maintaining high levels of carbon gain while minimising water loss during a drought period.

5.3.4.2 Sensitivity of gas-exchange to vapour pressure deficit

Figure 5.10 shows the effect of increasing daily maximum vapour pressure deficit ($D_{v,max}$) on gas-exchange in each scheme. A range of $D_{v,max}$ (1.0, 2.0, 3.0, 4.0, 5.0 and 6.0 kPa) was selected to show the effects of a high and low evaporative demand that may be forced upon these systems. The most obvious result of changing $D_{v,max}$ was the change in the initial values of $\overline{g}_s$ and $\overline{E}_t$, and the length of time the system was not limited by θ_s. In Scheme 1, a high $D_{v,max}$ (6.0 kPa) caused the system to become water-limited immediately on day 1, while a low $D_{v,max}$ (1.0 kPa) prolonged the point of drying out until day 20. For Scheme 2 under a high $D_{v,max}$, soil water did not become a limiting factor until day 4, while a low $D_{v,max}$ similarly extended the non-limiting period to day 20. This showed that Scheme 2 was able to maintain a longer period where θ_s was not limiting to gas-exchange as $D_{v,max}$ increased and was the result of a greater coupling to D_v that allowed better regulation of E_t.

In Scheme 1, initial $\overline{g}_s$ under non-limiting θ_s, remained high and declined from 0.27 to 0.13 mol m^{-2} s^{-1} when $D_{v,max}$ increased from 1.0 to 6.0 kPa (Figure 5.10a). In Scheme 2, $\overline{g}_s$ was more sensitive to variation in $D_{v,max}$, with initial high values of 0.29 mol m^{-2} s^{-1} declining substantially to 0.10 mol m^{-2} s^{-1} as $D_{v,max}$ increased (Figure 5.10b). In both schemes, for $D_{v,max} \geq 2.0$ kPa, $\overline{g}_s \to 0$ as water-stress became more severe. Variation in $D_{v,max}$ produced the most significant change in initial $\overline{E}_t$ for Scheme 1, with a decline of

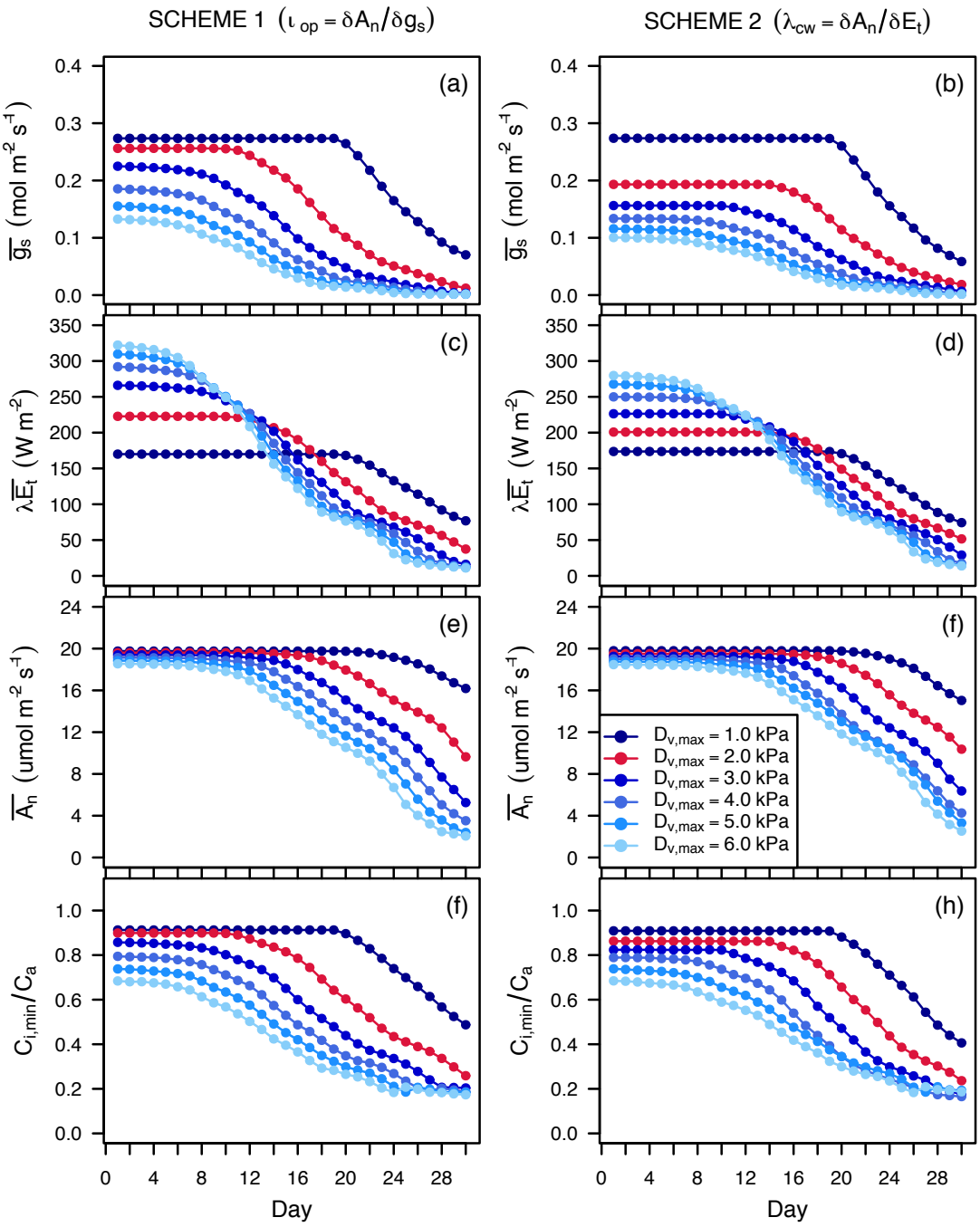

FIGURE 5.10: Sensitivity of daily mean (a-b) stomatal conductance ($\overline{g}_s$), (c-d) latent energy ($\lambda\overline{E}_t$), (e-f) net assimilation rate ($\overline{A}_n$) and (g-h) the daily minimum ratio between intercellular and atmospheric CO_2 ($C_{i,min}/C_a$) to variation in daily maximum vapour pressure deficit ($D_{v,max}$) for Schemes 1 and 2 respectively. The values of $D_{v,max}$ that were simulated are 1.0, 3.0, 4.0, 5.0 and 6.0 kPa, given in shades of blue, while the default $D_{v,max}$ of 2.0 kPa is given in red.

388 to 170 W m^{-2} with the increase in $D_{v,max}$ (Figure 5.10c). In Scheme 2, initial $\overline{E}_t$ was lower at 1.0 kPa and experienced a smaller decline from 285 to 174 W m^{-2} (Figure 5.10d). For $D_{v,max} > 2.0$ kPa, $\overline{E}_t \rightarrow 0$ as the drought progressed. Variation in $\overline{A}_n$ with increasing $D_{v,max}$ between schemes did not differ significantly, with initial range in $\overline{A}_n$ for low and high D_{vmax} decreasing from 19.76 to 18.54 μmol m^{-2} s^{-1} (Figure 5.10e-f). However, increasing evaporative demand largely affected $\overline{A}_n$ in the late drying period, with values declining to 2.53 to 2.06 μmol m^{-2} s^{-1} in Schemes 1 and 2 respectively under 6.0 kPa, while operating under a $D_{v,max} = 1.0kPa$, $\overline{A}_n$ decreased to only 14.36 to 15.90 μmol m^{-2} s^{-1}. Increasing $D_{v,max}$ had a moderate effect on $C_{i,min}/C_a$ and little difference in this response could be observed between schemes. An increase in $D_{v,max}$ from 1.0 to 6.0 kPa resulted in a moderate decline in initial $C_{i,min}/C_a$ from 0.91 to 0.68 (Figure 5.10g-h) and these values converged towards 0.19 by day 30. The more pronounced reduction in $\overline{g}_s$ that occurred in Scheme 2 was a result of a greater coupling with D_v. Scheme 1, although displaying some reduction in $\overline{g}_s$, contained no such feedback and changed little in its initial values despite a larger evaporative demand. For Scheme 1, an increase in $D_{v,max}$ did not impede g_s maximising towards ι_{op}, but rather increased the amount of water lost from the canopy and resulted in Ψ_l reaching Ψ_{lmin} much sooner. Scheme 2 showed a much higher sensitivity to D_v and therefore displayed a tighter regulation of E_t.

The effect of varying $D_{v,max}$ on total carbon gained and water lost over the period for both schemes is shown in Figure 5.11. A low $D_{v,max}$ resulted in Ψ_s declining at a much smaller rate due to a low $\overline{E}_t$, where it declined from -0.05 MPa on day 1 to -2.02 MPa in Scheme 1 (Figure 5.11a) and -1.94 MPa in Scheme 2 (Figure 5.11b) by day 30. Although this affected water-use during the middle of the drying period, this did not result in a large difference between period totals of water-use at high and low $D_{v,max}$. In Scheme 1, period total water use at a $D_{v,max}$ of 1.0 kPa was 0.084 m^3 m^{-2} and at a $D_{v,max}$ of 6.0 kPa was increased to 0.089 m^3 m^{-2} (Figure 5.11c). In Scheme 2, increasing $D_{v,max}$ from 1.0 to 6.0 kPa increased period total of water-use from 0.085 to 0.088 m^3 m^{-2} (Figure 5.11d). While different $D_{v,max}$ values produced similar water-use totals, there was a more noticeable difference in period totals of carbon gain. A large $D_{v,max}$ resulted in a lower carbon gained at the end of the 30 day drought, where Scheme 1 was showed a $D_{v,max}$ of 1.0 kPa resulted in a carbon gain of 161 gC m^{-2} and when increased to 6.0 kPa, this resulted in a

decrease in carbon gain at 107 gC m^{-2} (Figure 5.11e). This was similarly seen in Scheme 2, with increasing $D_{v,max}$ from 1.0 to 6.0 kPa resulting in total carbon gain declining from 162 gC m^{-2} to 115 gC m^{-2} (Figure 5.11f). These results were framed in terms of a scheme WUE at low and high $D_{v,max}$. For Scheme 1, a $D_{v,max}$ of 1.0 kPa produced a WUE of 1.92 gC m^{-3} H_2O and increasing $D_{v,max}$ to 6.0 KPa decreased WUE to 1.20 gC m^{-3} H_2O. Similarly, in Scheme 2, increasing $D_{v,max}$ from 1.0 to 6.0 kPa decreased WUE from 1.88 down to 1.31 gC m^3 H_2O. This showed that while Schemes 1 had a higher WUE under low D_v, when D_v was increased Scheme 2 retained a higher WUE.

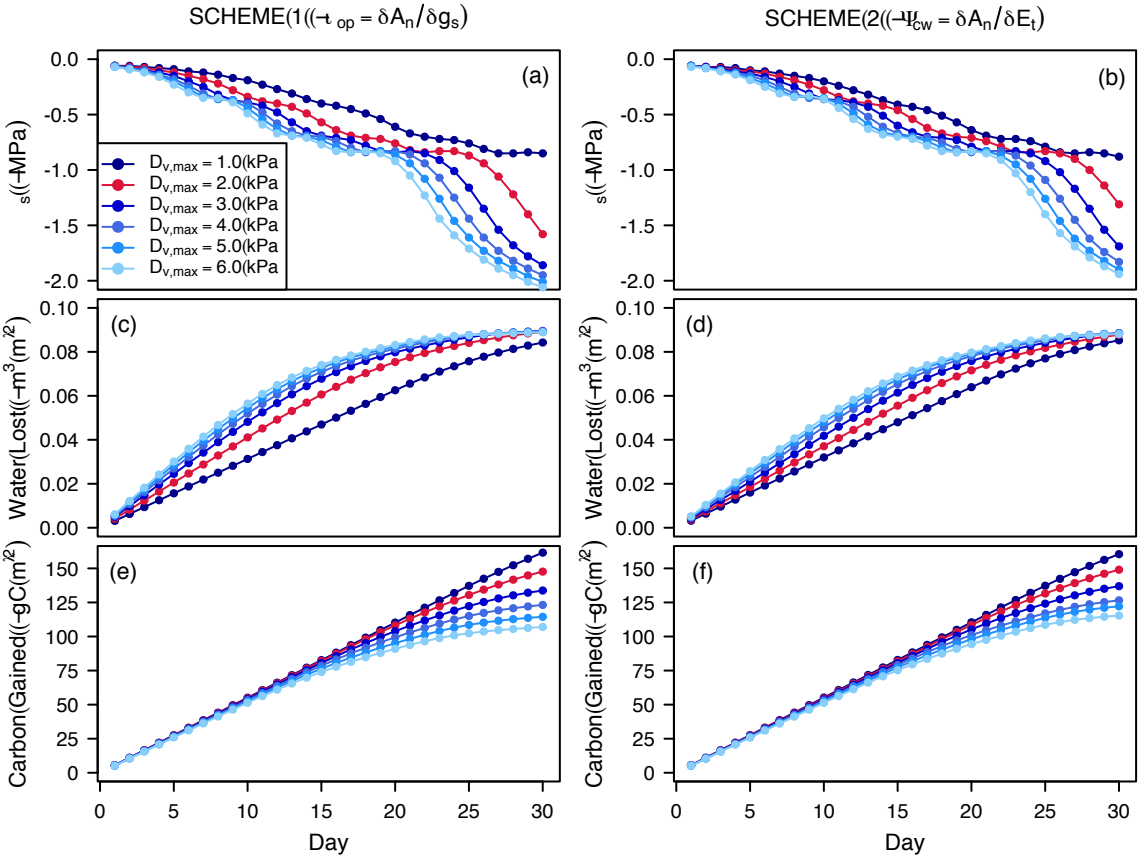

FIGURE 5.11: The sensitivity of (a-b) soil water potential (Ψ_s), (c-d) cumulative carbon gain and (e-f) cumulative water loss to variation in in daily maximum vapour pressure deficit ($D_{v,max}$) for Schemes 1 and 2 respectively. The values of $D_{v,max}$ that were simulated are 1.0, 3.0, 4.0, 5.0 and 6.0 kPa, given in shades of blue, while the default $D_{v,max}$ of 2.0 kPa is given in red.

5.4 Discussion

5.4.1 Performance of the SPA model using two descriptions of stomatal regulation

The aim of this study was to investigate the simulated process of leaf gas-exchange (particularly g_s) in the SPA model as it operates under drought. This involved simulating two schemes of leaf-gas exchange for a canopy operating under idealised environmental conditions and subjected to a 30 day drying period. The strategies of stomatal regulation tested in this work were defined by two schemes; (i) the maximisation of g_s to maximise A_n (Williams et al., 1996a) and (ii) the maximisation of A_n while E_t is minimised (Cowan and Farquhar, 1977). When soil water conditions were non-limiting, both schemes increased stomata aperture in order to increase carbon uptake. The point at which stomatal opening was maximised was defined by two respective operating points; ι_{op} for Scheme 1 and λ_{cw} for Scheme 2. The effect of water stress due to decreasing Ψ_s was reflected by the condition that g_s is limited (and therefore A_n and E_t) when $\Psi_l = \Psi_{lmin}$. Under non-limiting θ_s, Scheme 1 increased g_s until A_n was maximised, regardless of E_t. However, this process is not totally true as there must be some feedback between g_s and E_t which is sensitive to variations in D_v. The reasoning behind Scheme 2 was to include this feedback by necessitating that A_n be balanced with E_t. This increased the sensitivity of g_s and E_t to D_v and allowed g_s to be maximised so long as the canopy did not excessively transpire water in order to gain insignificant amounts of carbon. The consequences of this new strategy was a change in the diurnal response of g_s under well-watered conditions, which was defined by a reduction in daily maximum stomatal conductance (g_{smax}) and a distinct asymmetry (rather than symmetry) around noon in response to increasing evaporative demand as the day progressed. This resulted in a reduced E_t, which in turn resulted in a prolonged period where θ_s was not limiting to leaf gas-exchange. Additionally, Scheme 2 was more WUE than Scheme 1 under soil water-stress and when subjected to increases in daily evaporative demand.

The results of Scheme 1 and 2, compare well with the studies of Mäkelä et al. (1996) and Tuzet et al. (2003), which use similar modelling exercises to simulate leaf gas-exchange

over drought. The results given by Schemes 1 and 2 show similar reductions in A_n, E_t and C_i/C_a in response to decreasing soil water availability (Mäkelä et al., 1996; Tuzet et al., 2003). However, there are differences in the diurnal response of g_s between these studies. In Tuzet et al. (2003), the diurnal response of g_s is a symmetric pattern around noon, with a weak effect of increasing D_v and T_a, and this agrees with the daily response of g_s described by Scheme 1. In contrast, Mäkelä et al. (1996) shows the diurnal course of g_s to be similar to that produced by Scheme 2, which has a stronger coupling between g_s, D_v and E_t. These differences may be due to different modelling approaches in estimating leaf gas-exchange. Tuzet et al. use the semi-empirical BBL model to determine g_s, A_n and E_t, while Mäkelä et al. use the Cowan-Farquhar hypothesis to determine these same quantities. The BBL assumes an *a priori* functional response of g_s to D_v, whereas the Cowan-Farquhar hypothesis assumes that excessive E_t induces stomatal closure. This is why there is difference in the diurnal response of g_s between the studies mentioned above and between both schemes used in this study. The choice of which of these two diurnal stomata responses is true, constitutes to how stomata respond to soil water deficits and raises the question of *whether g_s is regulated by Ψ_l or by E_t at the evaporating sites of the stomata* (Tyree and Sperry, 1988; Monteith, 1995; Eamus and Shanahan, 2002; Leuning et al., 2003). Additionally, there is also the question of *what operating point should canopies function at, so as to benefit their productivity, while conserving water supplies* (Mäkelä et al., 1996; Thomas et al., 1999a,b; Schymanski et al., 2008b; Katul et al., 2010). These questions are now discussed below in the proceeding sections.

5.4.2 Response of stomata to transpiration and vapour pressure deficit

The diffusion of water vapour through the leaf stomata is described by $E_t = g_s D_v$, which shows a direct relationship between the quantities of E_t, g_s and D_v. For a low range of D_v ($0.0 - 2.0$ kPa), E_t increases asymptotically. However, as D_v increases further ($2.0 - 7.0$ kPa), E_t declines in response to decreasing Ψ_l (Prior and Eamus, 1999; Eamus and Shanahan, 2002; Zeppel et al., 2004). The response of g_s and E_t for a large range of D_v is characterised in the three-phase response as described by Monteith (1995), where g_s and E_t operate under three distinct regimes that describe the regulatory role of leaf stomata in preventing excessive water loss. While the three-phase response was observed

in Scheme 2, it was not in Scheme 1. The asymptotic increase in g_s with increasing D_v as displayed by Scheme 1 under non-limiting θ_s, did not follow the relationship that have been observed in other studies (Oren et al., 1999; Oren and Pataki, 2001; Pataki and Oren, 2003; Ewers et al., 2007). This relationship did not conform to the expected exponential decay of g_s to increasing D_v until θ_s became limiting and so any decline was likely the result of declining Ψ_l. In contrast to this, Scheme 2 displayed the expected exponential decline in g_s with increasing D_v under non-limiting θ_s. Additionally, Scheme 2 gave a clear representation of the three-phase response, showing the movement through regimes A, B and C as described by Monteith (1995), and observed by Thomas and Eamus (1999) and Eamus and Shanahan (2002). This is further supported by Oren et al. (1999), who have shown that all three regimes exist under well watered conditions, with a collapse of regime A (g_s decreases linearly with increasing E_t) as θ_s decreases. This response is also similar to the relationships shown by Oren and Pataki (2001); Misson et al. (2004); Uddling et al. (2005). While Scheme 1 shows some presence of regimes B and C, regime A appears to be only slightly present when the canopy was water-stressed. However, this response is similar to that found by Tuzet et al. (2003), whose model uses Ψ_l to regulate g_s under declining Ψ_s.

5.4.3 Response of assimilation to stomatal conductance and transpiration

There was an evident lag between g_s, E_t and A_n over the drought period, where modelled g_s had reached low values, yet still produced substantial values of A_n. This was the result of the increasing draw-down of C_i/C_a as the canopy became increasingly water-stressed, such that A_n became dampened by declining g_s in the late drying period. Although this effect is expected and has been observed in the field (Schulze, 1986; Sage, 1994; Prior et al., 1997; Lawlor and Cornic, 2002) and produced by other models (Mäkelä et al., 1996; Tuzet et al., 2003; Schymanski et al., 2007). This was also reflected in the sensitivity analysis, which showed that despite varying the OP or $D_{v,max}$ to create large differences in initial $\overline{g}_s$, $\overline{A}_n$ remained relatively unchanged. Again this is likely the result of declining C_i/C_a which dampens the proportionality between g_s and A_n. However, this explanation should be taken with caution, as initial C_i/C_a during the simulation of both schemes was higher

than observed in other studies (Fordyce et al., 1997; Prior et al., 1997; Eamus et al., 1999). Although the above argument offers a reasonable explanation for the lag and insensitivity between these quantities, there may still be a problem in the coupling between g_s and A_n in the SPA model, as some trial runs that were numerically unstable still produced reasonable values of A_n.

5.4.4 The level of stomatal efficiency and the cost of water

A large problem in this study was in defining the values of the OPs (ι_{op} and λ_{cw}). The problem with Equations 5.17 and 5.18 is that their respective OPs are abstract unless parameterised against field data (Hari et al., 1986; Mäkelä et al., 1996; Katul et al., 2010). If set incorrectly, this can result in the loss of copious amounts of water to gain only an infinitesimal amount of carbon, or conversely, results in very little water lost and so even less carbon gained (Williams et al., 1996a; Misson et al., 2004). In Chapter 4, a possible method in quantifying the level of ι_{op} was presented, and the same method should be equally applicable in quantifying λ_{cw}. However, the aim of this chapter was to explore two alternative schemes of declining g_s. Therefore, it was beyond the scope of this work to optimise these two OPs. If leaf-gas exchange is not limited by soil water availability, then the plant will maximise its productivity and so the OP can be relatively high. However the same OP under water-limited conditions would no longer be valid and should decrease with decreasing θ_s. The consequence of this feedback not being incorporated into SPA is that daily $g_{s,max}$ remains disproportionate to θ_s despite the forcing that should be applied by severe water stress; in Scheme 1, g_{smax} is seen to remain fairly high (Figure 5.4c), while in Scheme 2 it is constant (Figure 5.4c). Although it is not expected that g_{smax} would drop significantly with decreasing θ_s, there should be some decline nevertheless. The reasoning behind a constant g_{smax} occurring throughout the drought in Scheme 2, is because for this time of day R_s is high,and D_v low and $\Psi_l > \Psi_{l,min}$, such that g_s is able to increase to such a high value. Mäkelä et al. (1996) were able to solve this problem using the model of Hari et al. (1986), whereby their *cost of water* parameter (a function of the initial θ_s and probability of rainfall) changed under increased soil drying. A similar method linking the level of θ_s to the OP, possibly through some monotonic function, could be incorporated into SPA to solve this problem.

5.4.5 Effects of leaf water potential on gas-exchange

The stomatal control of leaf-gas exchange is a direct function of E_t, D_v and Ψ_l, all of which fluctuate over a daily time-course. In the absence of available energy (light) to evaporate water, leaf stomata remain shut and there is very little evaporative demand for water by the atmosphere. Before dawn, water is in equilibrium along the soil-root-leaf pathway (that is all plant cells are roughly saturated with water), so that $\Psi_{lpd} \approx \Psi_s$ (Eamus et al., 2006b). As the sun rises, light levels and temperature increase and stomata open so as to assimilate CO_2, and will continue to open their stomata to maximise A_n (Williams et al., 1996a). Consequently, E_t increases and so Ψ_l decreases. The level to which Ψ_l decreases, and its impact on leaf gas-exchange will differ depending on whether the plant is *ioshydric* or *anisohydric* in behaviour (Tardieu and Simonneau, 1998; Jarvis and Davies, 1998; Schultz, 2003). The SPA model contains the feedback of Ψ_l on gas-exchange described above, such that gas-exchange will remain unimpeded so long as conditions remain above that which causes xylem embolism to occur. This allows the model to keep g_s, E_t and A_n at maximised rates until further reductions in Ψ_s cause the condition $\Psi_l = \Psi_{lmin}$. The mechanism in both schemes can be related to isohydric behaviour, such that if water is available, then the plant will spend it regardless of depleting water availability so long as Ψ_l remains above Ψ_{lmin}. Modelled leaf gas-exchange in SPA is therefore operating on an *on* or *off* switch, with no long-term regulation by the available water supply unless it begins to lead to catastrophic failure of the plant's hydrology.

Despite the improvement offered by Scheme 2, the SPA model only considers leaves to operate in an isohydric manner, due to the constraint of Ψ_{lmin}. Such that modelled g_s does not decline with Ψ_l, but is only limited when $\Psi_l = \Psi_{lmin}$. There should therefore be some monotonic penalty function on g_s that is applied before the condition of $\Psi_l = \Psi_{lmin}$ is met. Tuzet et al. (2003) use a model that similarly incorporates a feedback between Ψ_l and Ψ_s to regulate stomata aperture. However, (ignoring structural differences of the model itself), Ψ_l tends to regulate gas-exchange through a monotonic cost function, where the decrease in Ψ_l, due to decreasing Ψ_s places a penalty on leaf gas-exchange. Additionally, their calculation of the water potentials along the SPA pathway is also more robust, as it incorporates the effects of root water potential (Ψ_r); an important factor in considering

the drying-out of the soil around the root-zone as the day progresses (and then to be re-saturated at night as stomata close and Ψ_l drops). Equation 5.12 and 5.16 relate directly to the Ψ_s itself, which is affected on a daily time-course not an hourly one, and so the effects of soil drying will be delayed by a day, before the effects of the regulation of g_s by Ψ_l will be seen. The problem with incorporating this dynamic is in establishing the flow of water from the soil to the roots, which can be done using the Richards' flow equation. However, this is not easily calculated, and requires a numerical solution in order to find it. It is something that should be considered in the future development of the SPA model, as this dynamic is important in establishing a truer measure of Ψ_l. Additionally, problems in defining the absolute value of the OP as discussed above, may result in higher than necessary g_s and so will needlessly reduce Ψ_l to operate close to Ψ_{lmin}. Work by Tardieu and Davies (1993) and expanded upon by Tardieu and Simonneau (1998), discusses using chemical signalling between the roots and the leaf (via concentrations in xylem [ABA]) to penalise leaf gas-exchange under increasing water stress. Results of these studies have shown that g_s responds to xylem [ABA] concentration and Ψ_r rather than Ψ_s, and this feedback could be incorporated into the SPA model in emulation of the work done by Dewar (2002).

5.5 Conclusion

The SPA model was tested over a 30 day drying cycle using two different schemes that were defined by their respective methods of regulating leaf gas-exchange. Scheme 1 was defined as a plant that increased its leaf stomatal aperture to maximise carbon uptake, so long as soil water was not limiting. Scheme 2 defined the increase in stomata aperture to maximise carbon uptake while minimising the water lost from the leaf. Meteorological and physiological conditions for the modelled canopy were idealised, to allow the effects of stomatal regulation to be a dominant factor in modelled gas-exchange. Under non-limiting soil water conditions, diurnal patterns in gas-exchange were symmetric and became asymmetric as the canopy became increasingly water stressed. Under these conditions, both schemes performed similarly, with the exception that Scheme 2 displayed a stronger response between stomatal conductance, transpiration and vapour pressure deficit. Stomatal

conductance displayed a continual diurnal asymmetry regardless of soil water status. The asymmetry of stomatal conductance in Scheme 2 resulted in a slower rate of depletion of soil water over the 30 day period, allowing assimilation rates to remain maximised for a longer period. A sensitivity analysis showed that the selection of OP is important in determining the rate of soil water-extraction and the impact this has on the rate of assimilation. Consequently a high OP in both schemes was found to be desirable in maintaining a maximised rate of assimilation and that the $\lambda_{cw} = \delta A_n/\delta E_t$ formulation is slightly more effective than $\iota_{op} = \delta A_n/\delta g_s$ at regulating leaf stomata under higher levels of vapour pressure deficit.

Chapter 6

Conclusions

This thesis aimed to answer four questions that are important in the process of modelling water and carbon fluxes from forest canopies in Australia. These questions are; (i) can water fluxes from a canopy be estimated using a simple empirical model without the need for canopy conductance? (ii) can a simple empirical model of canopy water-use be applied across multiple sites without the need for site-specific calibration? (iii) can a Soil-Plant-Atmosphere (SPA) model be used replicate canopy gas-exchange for a Australian tropical savanna? and (iv) can the leaf gas-exchange process in the SPA model be improved so as to maximise carbon gain while simultaneously minimising water loss from the leaf following the Cowan and Farquhar optimality hypothesis?

The result of the work described in this thesis is a body of work that (a) involved the development of a simple empirical model of canopy water-use; and (b) required the modification and improvement of a highly mechanistic and more complex soil-plant-atmosphere (SPA) continuum model (Williams et al., 1996a). The development of the simple canopy water-use model was in response to the problem of having to define surface conductance when using the Penman-Monteith equation (Monteith, 1965) to estimate transpiration. By removing surface conductance as a critical input, canopy water-use can be estimated from three readily available meteorological variables. The result is a model that is broadly applicable for many sites, and one that can be used as a tool in the management of water resources within industries such as forestry and mining. However, in order to investigate

the dynamics of water and carbon gas-exchange from forest canopies, and the mechanics underlying these dynamics, a more complex SPA model was used. While the SPA model has been successfully applied to various global ecosystems, the lack of an expression for C_4 photosynthesis in the model has limited its application to tropical savannas. Modification of the SPA model was therefore undertaken in order to improve its applicability to savannas through incorporation of C_4 photosynthesis. This was an important improvement to the SPA model, as savanna ecosystems contain C_4 vegetation, which contribute a large percentage of total ecosystem productivity. Additionally, this modification and subsequent application of the SPA model to a savanna site highlighted important issues in the leaf gas-exchange calculations when soil water became limiting. These problems were pursued by testing the SPA model for a simulated drought, where an improvement to modelled leaf gas-exchange was suggested and tested. In order to encapsulate the major findings of the work presented in this thesis, this chapter therefore provides a synthesis of the conclusions that have been drawn from each of the previous chapters. This is followed by a range of further questions that help to define the future direction of this research.

6.1 Modelling water fluxes from a forest canopy

Drawing from a general discussion on the important role of canopy water-use in an ecosystem's water balances (Chapter 1), models that are able to estimate water fluxes from the land surface, through evaporation and transpiration, have an important application as management tools in the areas of forestry, mining, and water and land resource management (Meyer, 1999; Raupach, 2001; Zhang et al., 2001). There is, therefore, a need for a simple canopy water-use model that is information-light (a small number of inputs that are readily available) and have a high applicability, which can be used to determine annual water budgets. The Penman-Monteith (PM) equation (Monteith, 1965) has been the most robust model for determining estimates of canopy water-use of a site via readily available inputs of meteorological data, such as solar energy, temperature, wind speed and humidity (Granier and Loustau, 1994; Zhang et al., 1997; Harris et al., 2004; Leuning et al., 2008). However, while the PM equation has experienced wide applicability and theoretical appeal, it is hindered by its requirement for estimates of canopy conductance (g_c) as a critical

input to run the model. Determining g_c for a site is a difficult process (Chapter 2), as measuring it requires extensive field campaigns where stomatal conductance (g_s) can be directly measured over short-term periods (days) using a porometer and then up-scaled to an estimate of g_c through the leaf area index (LAI) (Zeppel et al., 2008b). However, the application of the PM equation, and other canopy water-use models, are applied in the mid-term (annual) and so field measurements of g_c, although informative, are not entirely suitable for models that run for extensive periods. There are models available that can provide period estimates of maximum g_c (i.e. Kelliher et al., 1995), but such models still require the effects of soil water availability and a full coupling to the leaf physiology to be considered (Wang and Leuning, 1998; Tuzet et al., 2003). The other approach is through use of a Jarvis-Stewart (JS) model (Jarvis, 1976; Stewart, 1988) which incorporates a set of empirical cost functions which are calibrated according to the site. This approach has proved to be the most frequently used in the literature in overcoming the "g_c *problem*" and involves an inversion of the PM equation to properly calibrate the model. Although this methodology has been successful and offers an insight into seasonal trends of g_c (Granier et al., 1996b; Zhang et al., 1997; Harris et al., 2004), the process is still rather cumbersome and requires site-specific calibration of the model to work. Given the above difficulties in using the PM equation, one of the primary goals of this thesis was to develop a simple model that could be used to make short- to mid-term (annual) predictions of E_c without the need for g_c as an input.

6.1.1 Developing a simple model to estimate canopy water-use

Chapter 2 described the development and testing of a simple model of canopy water-use that is functionally equivalent to the PM equation and was based on the empirical framework of Jarvis (1976) and Stewart (1988). This empirical E_c model, called the modified Jarvis-Stewart (MJS) model, requires only three meteorological drivers as inputs, these being solar radiation (R_s), vapour pressure deficit (D_v), and soil water content (θ_s), as well as a set of empirically determined environmental response parameters that are calibrated for the model. This kept with the idea of limiting the number of required input parameters to those which are readily available and avoiding unnecessary model complexity. Initial testing showed a strong capability of the MJS model to estimate E_c for a

native Australian woodland, over a concatenated four month period, which encompassed contrasting seasons (two months of summer and two months of winter) and displayed variations in temperature, humidity and soil water availability. These results showed the MJS model to be perform equally well as (if not better than) the PM equation, giving a good explanation of the variation in the measured data (87%) and producing a low root mean square error (RMSE). Model performance and robustness was further supported through a strong comparison with a statistical benchmark, which was created using an ANN. The high correspondence between the MJS model and the statistical benchmark showed that R_s, D_v and θ_s provide adequate information to make reasonable predictions of E_c. Further information such as temperature or wind speed did not provide an increase in model performance. When applied to another four subsequent sites (Chapter 3), estimated E_c determined from the MJS model continued to correspond well with the measured data. Not all sites were water-limited and variation in R_s and D_v was adequate enough to explain the variation in E_c at these sites; this was further supported by the statistical benchmarks created for each site. Using only three readily available meteorological inputs to derive accurate predictions of E_c provides a favourable alternative to the PM equation, which requires g_c as an input and does not directly consider the effects of limiting θ_s. Furthermore, the MJS model is more accessible in contrast to typical land surface-exchange models (LSM) that need twenty to forty parameters of meteorology, soil hydraulics, leaf phenology and biochemistry information (which in itself requires extensive parameterisation) in order to run (Chapter 4).

6.1.2 Applicability of the modified Jarvis-Stewart model

It was shown in Chapter 3 that calibration of the MJS model across five disparate sites showed that the relationship between E_c, R_s and D_v was similar among sites. Consequently, the *site-specific* model parameters describing these relationships were similar in value despite differences in the species composition of the forest canopy and soil at each site. This led to the hypothesis that it may be possible to determine reasonable estimates of site E_c using an average set of model parameters. Calibrating the model for all five sites simultaneously produced a set of *site-average* model parameters, such that the model considers the response of E_c to variation in R_s and D_v to be the same across all sites. It

was established that differences in the parameter values between the sites was likely the result of these values varying around the site-average mean. From a numerical perspective, it was suggested that the parameter values are being drawn from very wide distributions (i.e. the variance of the parameter values is large), while from a biological perspective (assuming well-watered conditions) the response of E_c was strongly linked to D_v, and this response to D_v is similar among the five sites in study due to similar climatic conditions. However, not all model parameters could produce an average response across sites. The parameters describing the maximum canopy water-use (E_{cmax}) and soil hydraulic properties (wilting point, θ_w and critical point, θ_c) still need to be determined specifically for each site, as these directly relate to factors that will vary among ecosystems (LAI and soil type). Although these parameters could not be *averaged* across sites, their values can possibly be determined from other site-specific information. For example regressions of the model parameters against site characteristic information such as canopy basal area, LAI and annual rainfall were positive. However, only the relationship between E_{cmax} and basal area was statistically significant, LAI and rainfall were not. It must be noted, however, that there were only five data points from which to construct these relationships. Consequently, a statistically insignificant result was not surprising. If the model were applied to a further number of sites (say ten), thereby increasing the range of values, then a more confident conclusion could be drawn on linking site characteristics with E_{cmax}.

Application of the model with both site-specific and site-average parameter sets showed that despite some variation among parameter values, estimates of site E_c were highly comparable. Furthermore, applying the model to a site without initial calibration, will result in only a slight decrease in performance; at least for this set of sites (Chapter 3). Considering that the MJS model (using site-average parameters) was capable of producing reasonable estimates of site canopy water-use, this then reduces the required inputs to the model. In the case of sites that are limited by θ_s the number of model parameters reduces from seven to three , and for sites that are not limited by θ_s, the number of parameters reduces from five to one. The result is that the end user requires only the necessary meteorological inputs (R_s, D_v and θ_s), and information on the maximum rate of water-use for the site and soil water characteristics; information which can be proscribed from potential evaporation and the Saxton equations (Saxton and Rawls, 2006) respectively.

This offers a very useful management tool for water resource management in the industries of forestry, mining and land management, which are unlikely to undertake extensive field campaigns to determine information on leaf-level characteristics, root distributions and canopy phenology that is needed to run more complex LSMs.

6.2 Modelling canopy gas-exchange using a Soil-Plant-Atmosphere model

While the MJS model is a simple model able to provide estimates of canopy water-use, it has a greater applicability as a management tool than a research one, as it does not provide a detailed mechanistic understanding of forest canopy processes. Furthermore, it does not model carbon fluxes from forest canopies. The SPA model on the other hand, is able to provide reasonably accurate estimates of water and carbon fluxes from a canopy, as it is built upon a mechanistic understanding of canopy gas-exchange. The SPA model requires an extensively detailed parameterisation of a site in order to replicate the processes of gas-exchange, soil water balance and light interception correctly (Chapter 4). While models such as SPA have a large requirement of information, once the model is parameterised for a site, it can then be used to investigate processes that may not be possible in the field or ask detailed questions about the system. For example, "*What is the impact on the canopy if we increase the average daily maximum temperature?*" However, there are limits to the SPA model, and this thesis has attempted to overcome two of these limitations.

6.2.1 Investigating savanna canopy and water fluxes

The SPA model has been successfully applied over a number of disparate ecosystems. However, while successful, the application of this model has only considered ecosystems that are comprised entirely of C_3 vegetation. Because only C_3 photosynthesis is considered by the model, this prevents its application to tropical savannas, which contain a significant component of C_4 vegetation. Furthermore, this limits the SPA model as research tool, as tropical savannas are an important global biome that contributes approximately 26-30% of global gross primary productivity (GPP) (IPCC, 2007). Considering that C_4 vegetation

is a major component of global landscapes, the lack of a C_4 photosynthesis model severely limits the application of SPA in global climate models. There are a number of important characteristics of a savanna that distinguishes it from other ecosystems, (i) the canopy understorey is dominated by tall C_4 grasses which make an almost equal contribution to total ecosystem productivity, (ii) savannas exist in areas that experience highly seasonal rainfall (distinct wet and dry seasons) and so the C_4 grasses are only active during the wet season when there is a high water content in the upper soil profile. This seasonality in rainfall results in a seasonality in GPP and evapotranspiration (ET) The work outlined in Chapter 4 therefore described the modifications to the leaf-level processes of the SPA model that were needed to simulate the above characteristics, such that it could accurately replicate a tropical savanna located in northern Australia. In order to define the first (and major) characteristic of a savanna in the SPA model, two C_4 photosynthesis models were tested and incorporated. These were a simplified C_4 photosynthesis model (Collatz et al., 1992) and a more complex, mechanistic C_4 photosynthesis model (von Caemmerer and Furbank, 1999). Of these two models, the simple model was selected to describe C_4 vegetation in SPA, because it was less complex (requiring less leaf-scale information to work) and performed as well as the more detailed mechanistic model. To define the second savanna characteristic (the senescent nature of the savanna grasses), the model was further modified to incorporate a dynamic distribution of canopy leaf area. That is, the distribution of leaf area through the canopy was allowed to change on a daily basis rather than being constant throughout the year. The result was that the C_4 grass layers could be described as active during the wet season and inactive in the dry season, thereby capturing their senescent habit in the dry season.

Following a detailed parameterisation of the site, which included details of the leaf biochemistry of the C_3 canopy and C_4 grass and the underlying soil profile, the SPA model was run to replicate water and carbon flux measurements derived from eddy-covariance (EC) over five years for a tropical savanna in the northern Australia (Chapter 4). The use of a C_4 photosynthesis model to described the grass understorey improved wet season total estimates of GPP by 13 to 15% when compared with a simulation that considers only C_3 photosynthesis. However, the choice between C_3 and C_4 vegetation type did not result in any great difference in estimated ET. Consequently, having the SPA model correctly

parameterised to simulate a savanna ecosystem produced two important outcomes. The first outcome was that the C_4 grass understorey was shown to contribute largely (≈48%; $564 - 575$ gC m^{-2}) to total ecosystem GPP when it was active in the wet season. This level of contribution was almost equal to the level of productivity that was simulated for the C_3 canopy overstorey. Additionally, while the levels of productivity between the C_3 trees and C_4 grasses were almost equivalent, there was a great disparity in the levels of water-use. The C_4 grasses contributed much less to total savanna water-use ($\approx$ 23%; $130 - 160$ mm) than the overstorey, which highlighted the water-use efficient nature (the ratio of carbon gained to water lost) of C_4 vegetation. These values, as well as the overall simulated annual totals for the savanna compared well with totals measured with other savannas in the literature (Miranda et al., 1997; Hanan et al., 1998). The second insight arising from this research was that savanna ET and GPP were predominantly driven by the seasonal variation in LAI rather than changes in θ_s. Partitioning the canopy according to vegetation type showed the monthly diurnal variation in E_t for the C_3 trees remained constant and high throughout the year; that is, there was no seasonal decline in E_t during the dry season despite a decline in θ_s. This raised the question of what was driving the seasonality in canopy fluxes. This question was investigated by simulating two scenarios, i) a energy-limited scenario (limited by light-interception); where LAI was allowed to vary seasonally but θ_s remained constant and high, and ii) a water-limited scenario; where LAI was held constant, but θ_s was allowed to vary seasonally. The results from these scenarios showed that an abundant soil water supply in the upper soil profile did not allow ET and GPP to remain at wet season levels during the dry season, but a high and constant LAI throughout the year however, allowed ET and GPP to remain at wet season levels despite a large decline in θ_s. This shows that savanna ET and GPP are insensitive to variation of θ_s in the upper soil profile, due to the tree canopy having roots that are able to access deep soil water stores. Past studies conducted at this site indicated similar findings (O'Grady et al., 1999; Hutley et al., 2001; Eamus et al., 2001). Consequently, the modelled savanna was demonstrated to be limited by light interception, such that the decrease in GPP and ET during the dry season was driven by the seasonal decrease in total savanna LAI.

6.2.2 Parameterising the stomatal efficiency

Chapter 4 also looked at the impact on the leaf gas-exchange in the SPA model with the incorporation of the C_4 photosynthesis; that is the differences in modelled A_n, g_s and E_t between the two phenology types (C_3 and C_4 vegetation). The SPA model uses a unique coupled photosynthesis-stomatal conductance model, which operates to increase g_s until net CO_2 assimilation is maximised. The point at which modelled A_n is maximised (and therefore the upper limit of modelled g_s) is set by user-defined operating point (OP) (or *stomatal efficiency*; ι_{op}), which is representative of all vegetation modelled. This posed a problem, as C_4 vegetation (by nature) is able to maximise A_n at much lower levels of g_s than C_3 vegetation, due to its ability to inhibit photorespiration (von Caemmerer and Furbank, 1999). Consequently, the OPs between these two vegetation types will be different. It was therefore critically important that the C_4 species were assigned their own ι_{op}, as their A_n will be maximised at a much lower magnitude of g_s (and therefore have a lower E_t) compared with C_3 species. This problem was solved by incorporating a separate ι_{op} for C_3 and C_4 vegetation in the model. Additionally, a methodology was developed in order to parameterise ι_{op} (for both C_3 and C_4 species), by calibrating SPA with the slop of the Ball-Berry-Leuning (BBL) model (Chapter 4). This methodology required fitting the BBL relationship to C_3 and C_4 leaf-scale data that had been measured for the specific species types that were present at the site; the result being separate slopes for C_3 and C_3 species. The SPA model was then used to replicate the the BBL relationship, where the slope of this relationship is determined by the value of ι_{op}. An ι_{op} for both C_3 and C_4 species was then determined by adjusting its magnitude in order to match the slopes determined from the BBL model (Chapter 4). Although this methodology was quite involved, it allowed a way to quantify a critical parameter of the SPA model without having to calibrate the model to the data. Most importantly, however, it showed that the relationship between g_s and A_n for C_3 and C_4 species are very different. This difference being the result of C_4 vegetation being able to inhibit photorespiration and therefore be more water-use efficient than C_3 vegetation (Collatz et al., 1992; von Caemmerer and Furbank, 1999; Ghannoum et al., 2003).

6.2.3 Improving the leaf-level process in the Soil-Plant-Atmosphere model

Estimated period and annual totals of ET made by the SPA model in Chapter 4 were found to overestimate the measured totals of ET consistently over the five year study period. Although this was in part due to some error in the parameterisation of the model (i.e. whole plant conductance being higher than it should have been), it was also due to g_s, A_n and E_t not being well coupled in the model itself. Chapter 5 explored the sensitivity of the leaf gas-exchange sub-model in SPA to drought, with the purpose of investigating the covariance between g_s, E_t and A_n under a declining θ_s. The leaf gas-exchange scheme in the SPA model as described by Williams et al. (1996a) regulates g_s using two assumptions; (i) that the stomata regulate E_t through the leaf water potential (Ψ_l), and g_s will be limited when Ψ_l reaches a critical threshold value (Ψ_{lmin}) to prevent hydraulic failure in the xylem (Tyree and Sperry, 1988); (ii) while θ_s is not limiting, leaf stomata will remain open and transpire at a rate determined by D_v in order to maximise their carbon gain. The degree to which stomata may open is controlled by ι_{op}, defined as the point beyond which any increase in g_s will not result in a beneficial increase in A_n. While process (i) does occur in the field (e.g. Myers et al., 1997; Prior and Eamus, 1999), process (ii) fails to acknowledge that A_n is maximised while E_t is simultaneously minimised (Cowan, 1977). I therefore investigated a second scheme as a possible solution to this problem. This was achieved by replacing process (ii) with the theory of Cowan and Farquhar (1977), such that stomata aperture are regulated to maximise the balance between A_n and E_t; where this point is defined by a *cost of water* (λ_{cw}) parameter. The schemes of Williams et al. (1996a) and Cowan and Farquhar (1977) (labelled Schemes 1 and 2 respectively in Chapter 5), were tested in the SPA model, using an *idealised* site, constructed to simulate conditions of a temperate climate (indicative of a native Australian forest) over a 30 day drying period. Consequently, this study was purely theoretical, and provided a way of investigating improvements that could be made to the current leaf-gas exchange framework in SPA.

The sensitivities of the gas-exchange quantities g_s, E_t, A_n and the ratio between intercellular CO_2 concentration (C_i) and C_a, under both schemes were investigated under a drying

regime. The results showed that the framework of Scheme 1 caused the soil profile of the idealised site to decline in θ_s at a much faster rate than when using Scheme 2. Maximising g_s (and consequently increasing E_t) to gain a very small increase in A_n in Scheme 1, resulted in no net benefit to carbon uptake by the canopy. This was due to poor regulation in the amount of water transpired as a function of the cost/benefit ratio. In contrast to this, the framework of Scheme 2 displayed a tighter control on g_s, through a greater feedback with D_v (and therefore E_t) and consequently maintained a greater balance between A_n and E_t. This allowed A_n to operate at higher rates for a longer period during the drought. Scheme 2 was also found to be more water-use efficient (WUE) under increasing daily maximum D_v through a greater regulation of E_t compared to Scheme 1. The results of Scheme 1, may point to the overestimation of simulated ET observed in Chapter 4, as g_s was generally found to be too high. The magnitude of predicted g_s could be reduced through increasing the magnitude of the OP in both schemes (ι_{op} and λ_{cw} respectively). This also reduced the decline in θ_s and allowed more carbon to be gained in the long run. However, reasons for why a canopy will operate at different ι_{op} and λ_{cw} values were not investigated, as it was beyond the scope of this study. It is expected however, that a plant will assume an OP that results in the best balance between carbon gain and water loss; that is, the magnitude of the OP represents a measure of the regulation of E_t that is occurring. Developing upon the methodology of parameterising ι_{op}, mentioned in the last section may also offer the best possible way of parameterising λ_{cw}.

Although Scheme 2 displayed better regulation of g_s compared with Scheme 1, there were still evident problems that need to be investigated. Both schemes were poorly coupled with leaf water status during the drought, such that the gas-exchange quantities only became limiting when $\Psi_l = \Psi_{lmin}$. Additionally, modelled g_s was found to be poorly coupled with modelled A_n and this insensitivity may be the result of the structure of the leaf level process in SPA. Additionally, while both schemes operated in an isohydric manner, they do not display the necessary coordination between the liquid flow of water and g_s, such that Ψ_l is maintained within an acceptable range (Maseda and Fernandez, 2006). Although modifications to the current framework of SPA have provided a greater feedback between E_t, g_s and D_v, these quantities still need to have a greater coupling with Ψ_l to better simulate a plant under water-stress. This may be accomplished by linking changes in Ψ_l

to changes in root water potential (Ψ_r) rather than Ψ_s (discussed in the next section).This is critically important, as Australian forest canopies are subject to a high range of D_v and low θ_s compared with other forests globally (e.g. European boreal forests).

6.3 Empirical versus process-based modelling

This thesis has primarily dealt with the development, modification and use of two specific types of model. The empirical MJS model provided a relatively easy and successful way of estimating canopy water fluxes (with the potential application to carbon fluxes), while the process-based SPA model gave a more detailed estimation of both water and carbon fluxes, as well as information on the canopy and root-soil interface process that govern them. Generally speaking, the SPA model is the more advantageous model, as it allows us to ask insightful scientific questions about the effects of varying forces acting upon and within a system, as well as allowing us to simulate scenarios such as the impacts of climate change and land-use (Macinnis-Ng et al., 2010). However, while the SPA model has the advantage of giving a more detailed output of canopy processes, it still relies on empirical relationships to describe important responses, such as soil hydraulic characteristics (Saxton et al., 1986), temperature effects on the leaf (McMurtrie et al., 1992b; Massad et al., 2007) and leaf biochemistry (McMurtrie et al., 1992a) to name a few. Consequently, for the SPA model to work correctly, a detailed and accurate parameterisation of an ecosystem (or site) is required. However, even this does not guarantee a model's success, as any measurement of model performance is spatially and temporally specific (Abramowitz et al., 2009). In contrast, models based purely on empirical relationships, such as the MJS model, can be much easier to apply, as they are specifically calibrated to the conditions of an ecosystem and provide a high level of performance assuming that *such conditions* remain relatively constant (Medlyn et al., 2005b; Mäkelä et al., 2008). The disadvantage of using such a model though is obviously seen in the limitations of site specific calibration and a much reduced amount of output information when compared with process based models. There is therefore no easy answer to the question of which of the two model types is better, as both are more specific to certain purposes. Process-based models are effectively scientific tools that can be used to ask interesting and insightful questions, with specific

application to forecasting and experimental design, while conversely empirical models are more applicable in asking questions about the data itself, having application in gap-filling and benchmarking. It is therefore my hope that the work presented in this thesis has shown the merits of using both types of models, and will contribute to the larger body of work that is currently being accomplished by the international land-surface modelling community.

6.4 Further research

The MJS model provided a successful way of estimating canopy water fluxes. Additionally, modifications to the leaf gas-exchange framework of SPA, extended the applicability to estimating both water and carbon fluxes to environments where C_4 is a major component of the vegetation. Enumerated below are ideas for further research into modelling canopy water and carbon fluxes.

6.4.1 Future applications of the MJS model

1. To further the applicability of the MJS model, it would be ideal to test the model for ecosystems that experience a different climate to Australia. Additionally, it would also be valuable to see if the site-average parameter values are applicable for sites on other continents.

2. As well as further application of the model across other ecosystems, the MJS model should be tested with eddy-covariance and remote-sensing data. This would offer a simple model that could be readily applied to monitor ET from land surfaces without the need to quantify surface (stomatal) conductance.

3. Undertaking an analysis of greater depth into why average parameter values are as statistically significant as site-parameterised values. Using Bayesian analysis, one could investigate the distributions of each of the model parameters and compare whether they are being drawn from the same distribution. The benefit of this is that it would provide a robust quantification of the level of uncertainty in model predictions (predictions within a region of confidence).

4. The MJS framework could be applied to other canopy gas-exchange quantities such as GPP or respiration. Furthermore, this would raise the question "*Do these quantities display the same responses to R_s, D_v and θ_s that is observed for ET?*". If so, an average set of parameters (describing these similar responses) could be applied to various gas-exchange quantities and allow a simple means of estimating ecosystem gas-exchange (ET and GPP) without the need for highly complex LSMs.

6.4.2 Improvements and further testing of the SPA model

1. It would be ideal to test the robustness of SPA, with the added C_4 photosynthesis sub-model, to other savanna ecosystems, or ecosystems that have a large presence of C_4 vegetation. This would allow further assessment of the contributions of C_4 plants to carbon sequestration and provide a means of investigating the effects of climate change on tropical savannas.

2. Currently, SPA does not have a working carbon allocation or growth component model in its framework (that has been published). Incorporating a growth model into the SPA framework would not only further its applicability, but also provide a way of investigating carbon allocation that occurs in C_4 vegetation.

3. A critical addition that must be made in the future is a separate rooting distribution pattern for the understorey C_4 grass layers, or for any other dominant vegetation that is separate from the trees. Vegetation that has roots limited to the upper $1-2$ metres of the soil profile will be subject to greater effects of soil drying than vegetation which has deep reaching roots that are able to access deep stores of soil water. Considering that C_4 grasses play a dominant role in savanna landscapes, their below-ground access to water stores needs to be correctly represented.

4. Following on from the above suggestion, a better a description on the flow of water from the soil to the roots is needed in the SPA model. Because the saturated soil around the roots dries out over a diurnal time course, there needs to be some feedback between the water potentials of the root and the leaf, rather than just between the soil and the leaf. The work of Tuzet et al. (2003) offer a solution to simulating this process by use of the Richard's flow equation. I believe the same concept can be

applied to SPA quite easily. Whether or not this is numerically stable will need to be tested.

5. The leaf gas-exchange framework of SPA, needs the incorporation of some penalty to the *stomatal efficiency* and *cost of water* parameters when under conditions of drought. A solution to this may be to follow the idea of Mäkelä et al. (1996), who were able to associate their *cost of water* parameter using relationships between the probability of rainfall occurring for the current time-step and the level of the initial θ_s. SPA does not consider the probability of rainfall, but a relationship could still be drawn between the g_s operating point and the magnitude of θ_s.

Appendix A

Expressions for light- and enzyme-limited photosynthesis

Remembering that the diffusion rate of CO_2 from the air through to the stomata is expressed as:

$$A_d = g_s(C_i - C_a) \tag{A.1}$$

we re-express Equation A.1 in terms of C_i, such that:

$$C_i = \frac{A_d - g_s C_a}{g_s} \tag{A.2}$$

The net CO_2 assimilation rate limited by both RuBisCO activity and RuP_2 regeneration rate is expressed as:

$$A_n = \min\{A_c, A_j\} - R_d \tag{A.3}$$

such that there are two possible solutions that may be solved for A_n. Therefore, expressions of A_n for both light and enzyme limited capacities are determined. First, the net CO_2 assimilation limited by the rate of RuP_2 regeneration is determined by substituting Equation A.2 into:

$$A_j = \frac{J}{4}\frac{C_i - \Gamma^*}{C_i + 2\Gamma^*} \tag{A.4}$$

so that the above expression becomes:

$$A_j = \frac{J_e\left(\frac{A_d - g_s C_a}{g_s} - \Gamma^*\right)}{4\left(\frac{A_d - g_s C_a}{g_s} + 2\Gamma^*\right)} \tag{A.5}$$

eliminating C_i as an input, reducing the number of unknown parameters. Equation A.5 is rearranged as a quadratic expression using the assumption of that supply equals demand ($A_d = A_j$):

$$4A_j^2 - [4g_s(C_a - 2\Gamma^*) - J_e]A_j + g_s J_e(C_a + \Gamma^*) = 0 \tag{A.6}$$

and therefore A_j is determined from the quadratic solution:

$$A_j = \frac{-b - \sqrt{b^2 - 4ac}}{2a} \tag{A.7}$$

where $a = 4$

$b = -4g_s(C_a - 2\Gamma^*) - J_e$

$c = g_s J_e(C_a + \Gamma^*)$

Second, we now determine the net CO_2 assimilation limited by RuBisCO activity, by substituting Equation A.2 into:

$$A_c = V_{cmax}\frac{C_i - \Gamma^*}{C_i + K_m} \tag{A.8}$$

so that the above expression becomes:

$$A_c = V_{cmax}\frac{\left(\frac{A_d - g_s C_a}{g_s} - \Gamma^*\right)}{\left(\frac{A_d - g_s C_a}{g_s} + K_m\right)} \tag{A.9}$$

eliminating C_i as an input, reducing the number of unknown parameters. Equation A.9 is rearranged as a quadratic expression, and using the assumption of $A_d = A_c$:

$$A_c^2 - [g_s(K_m + C_a) + V_{cmax}]A_c + g_s(V_{cmax}\Gamma^* + g_s K_m C_a) = 0 \tag{A.10}$$

and therefore A_c is determined from the quadratic solution:

$$A_c = \frac{-b - \sqrt{b^2 - 4ac}}{2a} \tag{A.11}$$

where $a = 1$

$$b = -g_s(K_m + C_a) - V_{cmax}$$

$$c = g_s(V_{cmax}\Gamma^* + g_s K_m C_a)$$

The rate of electron transport (J) is given as non-rectangular hyperbola, which is a function of the incident photosynthetically active radiation (Q_p) (Farquhar and Wong, 1984). The quadratic equation for J is given as:

$$\theta_j J^2 - (\alpha_j Q_p - J_{max})J + \alpha_j Q_p J_{max} \tag{A.12}$$

where θ_j is a parameter describing the shape of the non-rectangular hyperbola, α_j is the quantum efficiency, and J_{max} is the potential rate of whole-chain electron transport. The quadratic solution in terms of J is therefore described as:

$$J = \frac{-b + \sqrt{b^2 - 4ac}}{2a} \tag{A.13}$$

where $a = \theta_j$

$$b = -\alpha_j Q_p + J_{max}$$

$$c = \alpha_j Q_p J_{max}$$

Appendix B

SPA stomatal model source code

B.1 Main file

Below is given the main file for running the stomatal model mentioned in Chapter 5.

```
PROGRAM TESTBED

! Declare the derived type to be used in this program
  USE STOMOPT

  IMPLICIT NONE

! <---- Start of variable declarations

  ! Number of simulation steps to be run
  INTEGER, PARAMETER :: N=(30*48)
  INTEGER :: i

  ! Create an array of the type LEAFDAT, with each index pertaining to a
    timestep
  ! with specific met values and photosynthetic paramters
  TYPE(LEAF_DATA_TYPE) :: leafC3(N)

  REAL :: CiCa, WSPD(N), Rain(N)
```

```
  CHARACTER(LEN=500) :: Directory, File_1, File_Headers, variable_names, &
                & variable_units, FMTS, FMTN

! Write the headings for the output variables and the corresponding units of
    measurement
  variable_names = "  Time, PAR, VPD, Ta, Ca, SWP, An, gs, Ci, Ci/Ca, Et, LWP
    , Rrs"
  variable_units = " ,umol m-2 s-1, kPa, oC, umol mol-1, MPa,          &
           & umol m-2 s-1, mol m-2 s-1, umol mol-1, , mmol m-2 s-1, MPa, MPa
    m2 s mmol"
! Format strings
  FMTS = '( A," ,A," ," ,A," ," ,A," ," ,A," ," ,A," ," ,A," ," ,A," ," ,A," ," ,A," ," ,A
    ," ," ,A," ," ,A )'
  FMTN = '( F10.4," ," ,F10.4," ," ,F10.4," ," ,F10.4," ," ,F10.4," ," ,F10.4," ," ,F10.4," ," ,    &
      & F10.4," ," ,F10.4," ," ,F10.4," ," ,F10.4," ," ,F10.4," ," ,F10.4," ," ,F10.4 )'

! <--- End of declarations


! Open the file that contains the data
  File_1 = "darwin met drivers.csv"

  OPEN( UNIT=101, FILE=File_1, STATUS='OLD')

! <---- Start reading in data
  READ(101,*) File_Headers
  DO i=1,N
    READ(101,*) leafC3(i)%Time, leafC3(i)%Ta, leafC3(i)%Ca, WSPD(i),    &
        & leafC3(i)%Rs, leafC3(i)%VPD,  leafC3(i)%PAR,  Rain(i), leafC3(i)%
    SWP
  ENDDO
! <---- End reading in data

  ! Boundary layer conductance (m s-1)
  DO i=1,N
    CALL BOUNDCOND( WSPD(i), leafC3(i)%Ta, leafC3(i)%gb )
  ENDDO

! leafC3%gb    = 10.0
```

```
  leafC3%LAI     = 2.0 ! Doesn't do anything yet
  leafC3%Nit     = 4.0 ! Doesn't do anything yet

! leafC3%SWP     = -0.05 ! Soil water potential (well watered)
  leafC3%MINLWP = -3.5  ! Minimum leaf water potential
  leafC3%Rp     = 0.1 ! Plant hyraulic resistance (constant)

  leafC3%PhoMod = 1    ! Photosynthesis model
  leafC3%Vcmax25  = 80.0
  leafC3%Jmax25 = 120.0
  leafC3%Vpmax25  = 0.0

  leafC3%OptMod = 1      ! Optimisation model
  leafC3%iota    = 1.0007   !150.0 <=== lambda   1.0007 <===== iota
  !leafC3%iota     = 250.0

! Open the output CSV files where the values will be stored
  OPEN(UNIT=102, FILE="Outputs_iota.csv", STATUS="UNKNOWN")

! .... and write the headers to go on these files
  WRITE(102,FMTS) variable_names
  WRITE(102,FMTS) variable_units


! <---- Run stomatal optimisation simulation model

  DO i=1,N

   ! Echo simulation step to the user
     WRITE(*,*) "Day ",leafC3(i)%Time

   ! Call the stomatal optimisation model
     CALL OPTIMISE_STOMATA( leafC3(i) )
     CiCa = leafC3(i)%Ci/leafC3(i)%Ca

   ! Write the result to an output file
     WRITE(102,FMTN) leafC3(i)%Time, leafC3(i)%PAR,  leafC3(i)%VPD,  leafC3(i)
    %Ta, leafC3(i)%Ca, leafC3(i)%SWP,  &
```

```
        & leafC3(i)%An, leafC3(i)%gs, leafC3(i)%Ci, CiCa,      leafC3(i)%Et,
    leafC3(i)%LWP, leafC3(i)%Rrs

  ENDDO ! End simulation

END PROGRAM TESTBED
```

stomoptim_main.f90

B.2 Leaf module

Below is the fortran code of the leaf gas-exchange module, for running the stomatal model mentioned in Chapter 5.

```
MODULE STOMOPT
! FILE:    stomoptim_module_leaf.f90
! AUTHOR: Rhys Whitley
! DATE:    August 2009
! EMAIL:   Rhys.J.Whitley@uts.edu.au
!
! This is a prototype of the stomatal conductance optimsation model using the
    pseudo object-oriented
! design.
!
! This sub-model of SPA is now stored inside the module STOMOPT and contains
    the operating paramters,
! functions and subroutines. Input information such as interactive met data
    and leaf scale photosynthetic
! data is now accessed via a locally declared derived type. The leaf scale
    subroutines and functions are
! now accessed to only operate on the leaf scale data and are contained
    within this module by point of the
! CONTAINS statement.
!
! Temperature functions still need to be added to the photosynthetic
    paramters AND the ODE derivation of
! LWP must also be included.
!
```

```
! ** This code may be added to any reformatted version of SPA in the future

  IMPLICIT NONE

  PRIVATE ! By default

  PUBLIC :: LEAF_DATA_TYPE, OPTIMISE_STOMATA, BOUNDCOND


! Create a derived type for holding data that is operated on by the leaf
    level
! subroutines and functions to find the optimum gs and A
  TYPE :: LEAF_DATA_TYPE

    INTEGER :: PhoMod, OptMod
    REAL    :: Time, PAR, APAR, Rs, VPD, Ta, Ca, gb, LAI, Nit
    REAL    :: MINLWP, OLDLWP, SWP, iota, Rp, Rrs
    REAL    :: Vcmax25, Vpmax25, Jmax25
    REAL    :: gs, An, Ad, Ci, Cm, Rd, Et, Tl, LWP

  END TYPE LEAF_DATA_TYPE

! Parameters used in this module
  REAL, PARAMETER :: C3Kc25 = 310.0    ! Catalytic constant for C4 CO2
    carboxylase @ 25C
  REAL, PARAMETER :: C3Ko25 = 155.0    ! Catalytic constant for C4 oxygenase @
     25C
  REAL, PARAMETER :: C4Kc25 = 650.0    ! Catalytic constant for C4 CO2
    carboxylase @ 25C
  REAL, PARAMETER :: C4Ko25 = 400.0    ! Catalytic constant for C4 oxygenase @
     25C
  REAL, PARAMETER :: C4Kp25 = 80.0     ! Catalytic constant for C4 PEP
    carboxylase @ 25C
  REAL, PARAMETER :: gammastar25  = 36.5  ! CO2 compensation point @ 25C

! Scientific constants used in this module
  REAL, PARAMETER :: Pi = 3.14159
  REAL, PARAMETER :: Ma = 29.0E-3      ! Molecular mass of air (kg mol-1)
  REAL, PARAMETER :: cp = 1010.0       ! Specific heat of air (J kg-1 K-1)
```

```
  REAL, PARAMETER :: Hd = 9.807E-3     ! Hydrualic head

  LOGICAL, PARAMETER :: TEMPON = .FALSE.   ! Turn on temperature functions

  INTEGER, PARAMETER :: SoilPSD = 1      ! Choose a soil type [ 1=Sandy Loam;
    2=Silt; 3=Loam ]

!
    ------------------------------------------------------------------------

  CONTAINS
!
    ------------------------------------------------------------------------


! Begin declaration of subroutines here


    SUBROUTINE OPTIMISE_STOMATA( leaf )
! Finds the optimal stomatal conductance (gs) based on the current weather
    conditions, sunlight and
! photosynthetic parameters. The optimal gs is then used by the subroutine
    STOMATA to find the desired
! leaf level outputs such as photosynthesis, internal CO2 concentration,
    respiration, leaf temperature
! and transpiration (water loss)

      IMPLICIT NONE

      TYPE(LEAF_DATA_TYPE), INTENT(INOUT) :: leaf

      REAL :: check1, check2, gs_low, gs_high, tol

      !EXTERNAL ZBRENT

      tol = 1.0E-5     ! Bisection tolerance
      gs_low = 1.0E-3    ! Lower gs limit
      gs_high = 2.0    ! Upper gs limit
```

```
    ! Check if conditions allow photosynthesis, also prevents night-time
    stomatal conductance
    ! being calculated
      check1 = STOMDIFF(gs_low, leaf)
      check2 = STOMDIFF(gs_high, leaf)

      IF( (leaf%PAR > 0.0) .AND. (check1*check2 < 0.0) ) THEN
    ! Brent's method to determine gs (mol m-2 s-1)
        leaf%gs = ZBRENT(STOMDIFF, leaf, gs_low, gs_high, tol)
        CALL STOMATA(leaf)
      ELSE
    ! Dark calculations - photosynthetic conditions poor
        leaf%gs = gs_low
        CALL STOMATA(leaf)
      ENDIF

    END SUBROUTINE OPTIMISE_STOMATA

  ! ------------------------------------------------------------------------------
  ! ------------------------------------------------------------------------------

    REAL FUNCTION STOMDIFF(opt_gs, leaf) RESULT(Gsmin)
! Efficiency check and caviation check to determine maximum gs - by testing
    whether an iota
! increase in stomatal conductance gives an efficient increase in
    assimilation. If FALSE,
! then gs is said to be at its MAX for that time-step. Additionally if gs can
     continue to be
! higher, the leaf water potential goes below it's MIN, then gs is said to
    have reached its MAX.

      IMPLICIT NONE

      TYPE(LEAF_DATA_TYPE),INTENT(IN) :: leaf
      TYPE(LEAF_DATA_TYPE) :: leaf1, leaf2

      REAL,INTENT(IN) :: opt_gs
      REAL :: delta, eff, cavchck
```

```
! Create copies of leaf
    leaf1 = leaf
    leaf2 = leaf

! Prescribed incremental change in stomatal conductance (mol m-2 s-1)
    delta = 7.0E-4

! Assign the gs values to the leaf copies to find the the resulting change
  in An and Et
    leaf1%gs = opt_gs
    leaf2%gs = opt_gs-delta

  ! Uptake at current gs
    CALL STOMATA(leaf1)
  ! Uptake at slightly lower gs
    CALL STOMATA(leaf2)

  ! Stomata efficiency check
    STOMOPT: IF( leaf1%OptMod == 1 ) THEN

    ! [ dA/dgs ] :: If either eff or minpsi are negative, then stomata is
  negative, stomata only open if
    !       both checks are positive

    ! Maximise stomatal conductance up to it's efficiency point
      eff    = (leaf1%An-leaf2%An) - (leaf1%iota-1.0)
    ! Perform xylem cavitation check
      cavchck = leaf1%LWP-leaf1%MINLWP
    ! Stop optimisation if caviation will occur
      Gsmin = MIN(eff,cavchck)

    ELSE

    ! [ dA/dE ] :: Stomata remain open until VPD becomes too high and must
  close to conserve water. Balance
    !       is reached between carbon-gain and water-loss
      eff = (leaf1%An-leaf2%An) - leaf1%iota*(leaf1%Et-leaf2%Et)
    ! Perform xylem cavitation check
      cavchck = leaf1%LWP-leaf1%MINLWP
```

```
      ! Stop optimisation if caviation will occur
        Gsmin = MIN(eff,cavchck)

      ENDIF STOMOPT

      RETURN

    END FUNCTION STOMDIFF

  ! ------------------------------------------------------------------------------
  ! ------------------------------------------------------------------------------

    SUBROUTINE STOMATA(leaf)
! Determines leaf level stable Ci, net assimilation rate, diffusion rate,
    mitochondrial respiration,
! leaf temperature and leaf evaporation for given gs.

      IMPLICIT NONE

      TYPE(LEAF_DATA_TYPE),INTENT(INOUT) :: leaf

      REAL,PARAMETER :: Pa=101.0, tol=1.0E-5

    ! Calculate leaf temperature based on this gs
      leaf%Tl = leaf%Ta
    ! Calculate APAR
      leaf%APAR = leaf%PAR*( 1-exp(-0.7*leaf%LAI) )
    ! Evaporation rate in mol m-2 s-1
      leaf%Et = MAX(0.0, PENMAN_MONTEITH(leaf%gs, leaf%Tl, leaf%APAR, leaf%
    VPD, leaf%gb))
    ! leaf%Et = leaf%gs*leaf%VPD !/Pa
    ! Calculate mitochondrial respiration
      leaf%Rd = 0.105*leaf%Nit*EXP(LOG(2.0)*(leaf%Tl-10.0)/10.0)
    ! Calculate total below and above ground resistance to water flow
      leaf%Rrs = HYDRORES(leaf%SWP) !/1000.0
    ! Calculate the leaf water potential (MPa)
      leaf%LWP = leaf%SWP-leaf%Et*1000.0*(leaf%Rp+leaf%Rrs)

    ! Calculate assimilation rate based on user declared photosynthesis model
```

```
      PATHWAY: SELECT CASE (leaf%PhoMod)
    ! Farqhuar C3 photosynthesis model (Farqhuar and Cowan, 1977)
      CASE(1)
         leaf%Ci = ZBRENT( CDIFF,leaf ,0.1 ,leaf%Ca,tol)
         leaf%An = FARQUHAR( leaf%Vcmax25, leaf%Jmax25, C3Kc25, C3Ko25, &
                   gammastar25, leaf%Rd, leaf%PAR, leaf%Tl, leaf%Ci )
    ! Collatz C4 photosynthesis model (Collatz et al. 1992)
      CASE(2)
         leaf%Ci = ZBRENT( CDIFF, leaf , 0.1, leaf%Ca, tol)
         leaf%An = COLLATZ( leaf%Vcmax25, leaf%Rd, leaf%PAR, leaf%Tl, leaf%Ci
    )
    ! von Caemmerer C4 photosynthesis model (von Caemmerer and Furbank, 1999)
      CASE(3)
         leaf%Ci = ZBRENT( CDIFF, leaf , 0.1, leaf%Ca, tol)
         leaf%An = VONCAEMMERER( leaf%Vcmax25, leaf%Vpmax25, leaf%Jmax25,
    C4Kc25, &
                   C4Ko25, C4Kp25, leaf%Rd, leaf%PAR, leaf%Tl, leaf%Cm )
      END SELECT PATHWAY

    ! Calculate demand for C
      leaf%Ad = leaf%gs*(leaf%Ca-leaf%Ci)

    END SUBROUTINE STOMATA

  !-------------------------------------------------------------------------
  !-------------------------------------------------------------------------

    REAL FUNCTION CDIFF( opt_Ci, leaf ) RESULT(Cimin)
! Difference between metabolic assimilation rate and diffusive assimilation
    rate

      IMPLICIT NONE

      TYPE(LEAF_DATA_TYPE),INTENT(IN) :: leaf

      REAL,INTENT(IN) :: opt_Ci
      REAL :: An, Ad, gt

      PATHWAY: SELECT CASE (leaf%PhoMod)
```

```
      ! Farqhuar C3 photosynthesis model (Farqhuar and Cowan, 1977)
        CASE(1)
          An = FARQUHAR(  leaf%Vcmax25, leaf%Jmax25, C3Kc25, C3Ko25,      &
                    gammastar25, leaf%Rd, leaf%PAR, leaf%Tl, opt_Ci )
      ! Collatz C4 photosynthesis model (Collatz et al. 1992)
        CASE(2)
          An = COLLATZ( leaf%Vcmax25, leaf%Rd, leaf%PAR, leaf%Tl, opt_Ci )
      ! von Caemmerer C4 photosynthesis model (von Caemmerer and Furbank,
    1999)
        CASE(3)
          An = VONCAEMMERER(  leaf%Vcmax25, leaf%Vpmax25, leaf%Jmax25, C4Kc25
    ,&
                      C4Ko25, C4Kp25, leaf%Rd, leaf%PAR, leaf%Tl, opt_Ci )
      END SELECT PATHWAY

    ! Catch negative values and set to 0.0
      IF( An<0.0 ) An = 0.0

    ! Demand for Carbon

      gt = 1/( 1/leaf%gs + 1/leaf%gb )

      !Ad = gt*(leaf%Ca-opt_Ci)
      !Ad = leaf%gs*(leaf%Ca-opt_Ci)
      Ad = ( gt-0.5*leaf%Et )*leaf%Ca - ( gt+0.5*leaf%Et )*opt_Ci

      Cimin = Ad - An

      RETURN

    END FUNCTION CDIFF

  ! ------------------------------------------------------------------
  ! ------------------------------------------------------------------

    REAL FUNCTION PENMAN_MONTEITH(gs, Ta, PAR, VPD, gb) RESULT(Et)
  !  Determine evapotranspiration rate (mol m-2 s-1) from PAR (W m-2), Ta (oC),
      D (Pa) and gb and gs (mol m-2 s-1)
```

```
    IMPLICIT NONE

      REAL,INTENT(IN) :: gs, Ta, PAR, VPD, gb

      REAL :: epsilon, lambda, s, slope, psych, Rn

    ! Convert PAR to Net Radiation (W m-2)
      Rn = (0.60*(PAR/2.3) - 50.0)

    ! Calculate the slope of saturation vapour pressure curve (Pa K-1)
      Slope = DSLOPEFUN(Ta)*1000.0
    ! Calculate psychometric constant (Pa K-1)
      Psych = PSYCHOFUN(Ta)*1000.0
    ! Calculate the latent heat of vaporisation (J mol-1)
      Lambda = LAMBDAFUN(Ta)*18.0

    ! Finally calculate the transpiration from the leaf (mol m-2 s-1)
      Et = (slope*Rn + Ma*cp*gb*VPD*1000.0)/( lambda*(slope+psych*(1.0+gb/gs)
    ) )

    ! Return result to user
      RETURN

    END FUNCTION PENMAN_MONTEITH



  !-----------------------------------------------------------------------
  !-----------------------------------------------------------------------

    SUBROUTINE BOUNDCOND(U, Ta, gb)
! A quick function for converting windspeed to boundary layer conductance (
    not sure if it's appropriate)
! given in mol m-2 s-1

      IMPLICIT NONE

      REAL,INTENT(IN) :: U, Ta
```

```
      REAL :: gb, Dw, delta, D0, T0, Tk

      Tk = Ta + 273.15  ! Ambient temperature (K)
      D0 = 1.025E-2   ! Reference diffusivity of water vapour @ Ta=20 (was
    1.025E-3 <- need to check)
      T0 = 293.15     ! Reference temperature (K) @ Ta=20

    ! Calculate the diffusivity of water at the ambient temperature
      Dw = D0*( Tk/T0 )**1.75
    ! Calculate the thickness of the boundary layer
      IF( U > 0.0 ) THEN
        delta = 0.004*(0.08/U)**0.5
      ELSE
        delta = 0.012
      ENDIF

    ! Calculate the boundary layer conductance to heat
      gb = Dw/delta

    END SUBROUTINE BOUNDCOND

  !-----------------------------------------------------------------------
  !-----------------------------------------------------------------------

    REAL FUNCTION FARQUHAR(Vcmax25,Jmax25,Kc25,Ko25,gammastar25,Rd,PAR,Tl,Ci)
     RESULT(An)
! Metabolic C3 assimilation rate according to Farquhar and von Caemmerer 1982

      IMPLICIT NONE

      REAL,INTENT(IN) :: Rd, PAR, Tl, Ci
      REAL,INTENT(IN) :: Vcmax25, Jmax25, Kc25, Ko25, gammastar25
      REAL :: Vcmax, Jmax, Kc, Ko, gammastar
      REAL :: Oi, alphaj, theta, J, Ac, Aj, Alim

      Oi = 210.0      ! Internal CO2 concentration
      alphaj = 0.385    ! Initial slope of quantum response curve
      theta = 0.7     ! Curvature of quantum response curve
```

```
    ! Apply appropriate temperature responses on the photosynthetic
    parameters
      TEFFECTS: IF( TEMPON ) THEN
        Vcmax = Vcmax25 * TEMP_POLYNOMIAL( 65.03, 30.0, 0.143, Tl )
        Jmax = Jmax25 * TEMP_POLYNOMIAL( 57.05, 30.0, 0.172, Tl )
        Kc = Kc25 * TEMP_ARRHENIUS_C3( 23.956, Tl )
        Ko = Ko25 * TEMP_ARRHENIUS_C3( 14.509, Tl )
        gammastar = gammastar25 * TEMP_ARRHENIUS_C3(9.46, Tl)
      ELSE
        Vcmax = Vcmax25
        Jmax = Jmax25
        Kc = Kc25
        Ko = Ko25
        gammastar = gammastar25
      ENDIF TEFFECTS

    ! Determine Rubisco limited carboxylation rate
      Ac = (Vcmax*Ci)/(Ci+Kc*(1.0+Oi/Ko))
    ! Determine potential rate of RuBP regeneration
      J = QUADRATIC(theta,-(alphaj*PAR+Jmax),alphaj*PAR*Jmax,-1.0)
    ! Determine RuBP regeneration limited carboxylation rate
      Aj = J*Ci/(4.5*Ci+10.5*gammastar)
    ! Determine limiting carboxylation rate
      Alim = MIN(Ac,Aj)
    ! Net photosynthetic rate
      An = Alim*(1.0-gammastar/Ci) - Rd
    ! Return answer to user
      RETURN

    END FUNCTION FARQUHAR

  !-----------------------------------------------------------------------
  !-----------------------------------------------------------------------

    REAL FUNCTION COLLATZ(Vcmax25,Rd,PAR,Tl,Ci) RESULT(An)
! Metabolic C4 assimilation rate from Collatz et al. 1992

      IMPLICIT NONE
```

```
      REAL,INTENT(IN) :: Rd, PAR, Tl, Ci, Vcmax25
      REAL :: Vcmax
      REAL :: alpharf, theta, beta, K, M, A

      alpharf = 0.067      ! mol/mol
      K = 0.7          ! mol/m2/s
      theta = 0.83       ! Curvature of quantum response curve, Collatz table2
      beta  = 0.93       ! Collatz table 2

    ! Apply appropriate temperature responses on the photosynthetic
    parameters (Massad et al. 2007)
      TEFFECTS: IF( TEMPON ) THEN
        Vcmax = Vcmax25 * TEMP_ARRHENIUS_C4( 67294.0, 144568.0, 472.0, Tl )
      ELSE
        Vcmax = Vcmax25
      ENDIF TEFFECTS

    ! Rubisco and light limited capacity
      M = QUADRATIC(theta,-(alpharf*PAR+Vcmax),alpharf*PAR*Vcmax,-1.0)
    ! M and CO2 limitation
      A = QUADRATIC(beta,-(M+K*Ci),M*K*Ci,-1.0)
    ! Net photosynthetic rate
      An = A-Rd
    ! Return answer to user
      RETURN

    END FUNCTION COLLATZ

  !-----------------------------------------------------------------------
  !-----------------------------------------------------------------------

    REAL FUNCTION VONCAEMMERER(Vcmax25,Vpmax25,Jmax25,Kc25,Ko25,Kp25,Rd,PAR,
    Tl,Ci) RESULT(A_actual)
! C4 assimilation rate is calucated using quadratic solutions for the enzyme
    and light
! limited rates of photosynthesis. All values and calculations are take from
    the
! von Caemmerer and Furbank (1999) paper.
! *Note: We express that Ci is equivalent to Cm
```

```
    IMPLICIT NONE

! Function inputs
    REAL, INTENT(IN) :: Rd, PAR, Tl, Ci
    REAL, INTENT(IN) :: Vcmax25, Vpmax25, Jmax25, Kc25, Ko25, Kp25
    REAL :: Vcmax, Vpmax, Jmax, Kc, Ko, Kp

! Function variables
    REAL :: a_c, b_c, c_c, a_j, b_j, c_j,    &
            gbs, low_gamstar, Oi, K, Rm, alpha, &
            Vp, Vpr, J, Q2, shape, x,        &
            A_enzyme, A_light

    alpha = 0.0         ! Degree of PSII activity occuring in the bundle
sheath cells (adjust between 0-1)
    Oi = 210.0          ! Intercellular O2 equivalent to Om
    gbs = 0.003         ! Bundle sheath conductance (mol m-2 s-1)
    low_gamstar = 1.93E-4 ! Half the reciprocal for Rubisco specificity (
NOT CO2 compensation point)
    x = 0.4           ! Partitioning of the electron transport between
mesophyll and bundle sheath cells
    shape = 0.7         ! Shape of the hyperbolic response curve (typical
value)
    Rm = 0.5*Rd         ! Mitchondrial respiration from the mesophyll cells
is half of Rd
    Vpr = 80.0          ! PEP limiting regeneration rate
    K = Kc*(1.0+Oi/Ko)      ! Combined Michelson-Menton constant for Ci and
Oi

! Apply appropriate temperature responses on the photosynthetic
parameters (Massad et al. 2007)
    TEFFECTS: IF( TEMPON ) THEN
      Vcmax = Vcmax25 * TEMP_ARRHENIUS_C4( 67294.0, 144568.0, 472.0, Tl )
      Vpmax = Vpmax25 * TEMP_ARRHENIUS_C4( 70373.0, 117910.0, 376.0, Tl )
      Jmax  = Jmax25  * TEMP_ARRHENIUS_C4( 77900.0, 191929.0, 627.0, Tl )
      Kc  = Kc25 * TEMP_Q10( 2.1, Tl )
      Kp  = Kp25 * TEMP_Q10( 2.1, Tl )
      Ko  = Ko25 * TEMP_Q10( 2.1, Tl )
```

```
    ELSE
      Vcmax = Vcmax25
      Vpmax = Vpmax25
      Jmax = Jmax25
      Kc = Kc25
      Kp = Kp25
      Ko = Ko25
    ENDIF TEFFECTS

  ! PEP carboxylation rate
    Vp = MIN(Ci*Vpmax/(Ci+Kp),Vpr)

  ! Quadratic solution for enzyme limited C4 assimilation
    a_c = 1.0 - (alpha/0.047)*(Kc/Ko)
    b_c = -( (Vp-Rm+gbs*Ci) + (Vcmax-Rd) + gbs*K + alpha*low_gamstar
/0.047*( low_gamstar*Vcmax+Rd*Kc/Ko ) )
    c_c = (Vcmax-Rd)*(Vp-Rm+gbs*Ci) - (Vcmax*gbs*low_gamstar*Oi + Rd*gbs*K)

    A_enzyme = QUADRATIC(a_c,b_c,c_c,-1.0)  ! Using negative quadratic
solution

  ! Non-rectangular hyperbola describing light effect on electron transport
   rate (J)
    Q2 = PAR*(1.0-0.15)/2.0
    J = QUADRATIC(shape,-(Q2+Jmax),(Q2*Jmax),-1.0)

  ! Quadratic solution for light-limited C4 assimilation
    a_j = 1.0 - 7.0*low_gamstar*alpha/(3.0*0.047)
    b_j = -( (x*J/2.0-Rm+gbs*Ci) + ((1.0-x)*J/3.0-Rd) + gbs*(7.0*
low_gamstar*Oi/3.0)  &
        + alpha*low_gamstar/0.047*((1.0-x)*J/3.0+Rd) )
    c_j = ( (x*J/2.0-Rm+gbs*Ci)*((1.0-x)*J/3.0-Rd) - gbs*low_gamstar*Oi
*((1.0-x)*J/3.0-7.0*Rd/3.0) )

    A_light = QUADRATIC(a_j,b_j,c_j,-1.0) ! Using negative quadratic
solution

  ! The minimum between enzyme and light limited respiration rates is the
  actual rate
```

```
      A_actual = MIN(A_enzyme, A_light)
    ! Return answer to user
      RETURN

    END FUNCTION VONCAEMMERER

  !-----------------------------------------------------------------------
  !-----------------------------------------------------------------------

    REAL FUNCTION HYDRORES(SWP) RESULT(Rrs)

! Calculates a rough idea of the soil-root resistance to water flow

      IMPLICIT NONE

      REAL, INTENT(IN) :: SWP

      REAL :: Rs1, Rs2, RSoil1, RSoil2, Rlen, Slen
      REAL :: Rrad, Rxar, Rmas, Rden, Ks, Lsoil

    ! Setup an adequate soil description
      Slen = 1.0
      Rrad = 0.0001
      Rxar = Pi*Rrad**2.0
      Rmas = 2000.0/Slen
      Rden = 5.0e5
      Rlen = Rmas/(Rden*Rxar)

    ! Get Hydraulic conductivity from Campbell equations (m2 s-1 MPa-1)
      Ks = CAMPBELL(SWP)
      Lsoil = Ks

    ! Exploited soil volume = 1.0 * soil depth; each canopy layer has lrv/
    numl root length and
    ! is soildp/numl deep - so the numl cancel
        Rs1 = SQRT(1.0/(Rlen*Pi))
    ! lrv = total length of roots, must be divided by number of layers in
    this case
        Rs2 = LOG(Rs1/Rrad)/(2.0*Pi*Rlen*Slen*Lsoil)
```

```
    ! Convert from MPa s m2 m-3 to MPa s m2 mmol-1
        RSoil1 = Rs2*1.0E-6*18.0*0.001
    ! Second component of below ground resistance related to root hydraulics
        RSoil2 = 400.0/( Rmas*Slen )
        Rrs = RSoil1 + RSoil2

      RETURN

    END FUNCTION HYDRORES

!-----------------------------------------------------------------------
!-----------------------------------------------------------------------

    REAL FUNCTION CAMPBELL(SWP) RESULT(Ks)

! Does a quick calculation of what the soil water content and hydraulic
    conductivity are
! at this SWP.

! Authors Note: This is only a quick fix solution for implementing a soil
    drying effect and
! is not meant to be an accurate respresentation of soil water dynamics

      IMPLICIT NONE

      REAL, INTENT(IN) :: SWP
      REAL :: SMC

      REAL, PARAMETER :: b1=3.31, We1=-0.91E-3, Ksat1=957.6E-6
      REAL, PARAMETER :: b2=4.38, We2=-1.58E-3, Ksat2=217.8E-6
      REAL, PARAMETER :: b3=6.58, We3=-1.88E-3, Ksat3=228.6E-6

    ! Need to choose a soil PSD
      SOILTYPE: SELECT CASE (SoilPSD)
    ! Sandy Loam
      CASE(1)
        SMC = 0.4/( (SWP/We1)**(1.0/b1) )
        Ks  = Ksat1*(SMC/0.4)**(2.0*b1+3.0)
    ! Silt
```

```
      CASE(2)
        SMC = 0.4/( (SWP/We2)**(1.0/b2) )
        Ks  = Ksat2*(SMC/0.4)**(2.0*b2+3.0)
    ! Loam
      CASE(3)
        SMC = 0.4/( (SWP/We3)**(1.0/b3) )
        Ks  = Ksat3*(SMC/0.4)**(2.0*b3+3.0)

      END SELECT SOILTYPE

      RETURN

    END FUNCTION CAMPBELL

  !-----------------------------------------------------------------------
  ! Temperature and generic module functions are listed below
  !-----------------------------------------------------------------------


    REAL FUNCTION QUADRATIC(a, b, c, sign) RESULT(x)
! Generic quadratic solution function

      IMPLICIT NONE

      REAL,INTENT(IN) :: a, b, c, sign

      IF(sign < 0.0) THEN
        x = (-b-SQRT(b**2.0-4.0*a*c))/(2.0*a) ! Negative quadratic equation
      ELSE
        x = (-b+SQRT(b**2.0-4.0*a*c))/(2.0*a) ! Positive quadratic equation
      END IF

    ! Return answer to user
      RETURN

    END FUNCTION QUADRATIC

  !-----------------------------------------------------------------------
  !-----------------------------------------------------------------------
```

```
  REAL FUNCTION PSYCHOFUN( Ta ) RESULT(Psych)
! This function calculates the psychometric constant based on the current
! ambient air temperature.

    IMPLICIT NONE

    REAL, INTENT(IN) :: Ta

  ! Psychometric constants (kPa K-1)
    Psych = 0.1*( 0.646*EXP(0.00097*Ta) )
  ! Return answer to user
    RETURN

  END FUNCTION PSYCHOFUN

!-----------------------------------------------------------------------
!-----------------------------------------------------------------------

  REAL FUNCTION LAMBDAFUN( Ta ) RESULT(Lambda)
! This function calculates the latent heat of vaporisation based on the
  current
! ambient air temperature.

    IMPLICIT NONE

    REAL, INTENT(IN) :: Ta

  ! Latent heat of vapourisation (J g-1)
    Lambda = ( 2501.0 - 2.364*Ta )
  ! Return answer to user
    RETURN

  END FUNCTION LAMBDAFUN

!-----------------------------------------------------------------------
!-----------------------------------------------------------------------

  REAL FUNCTION DSLOPEFUN( Ta ) RESULT( Dslope )
```

```
! This function calculates the slope of saturation of the vapour pressure
  deficit
! curve based on the current ambient air temperature

    IMPLICIT NONE

    REAL, INTENT(IN) :: Ta
    REAL :: Tk, s

    s = 6.1078*17.269*237.3*EXP( 17.269*Ta/(237.3+Ta) )
! Slope of saturation vapour pressure curve (kPa K-1)
    Dslope = 0.1*( s/(237.3+Ta)**2 )
! Return answer to user
    RETURN

  END FUNCTION DSLOPEFUN


!-------------------------------------------------------------------------------
!-------------------------------------------------------------------------------

  REAL FUNCTION TEMP_Q10( Q10, Tl) RESULT(fTk)
  ! Simple Q10 temperature response function

    IMPLICIT NONE

    REAL,INTENT(IN) :: Q10, Tl

    fTk = Q10**(Tl-25.0)/10.0

  ! Return result to user
    RETURN

  END FUNCTION TEMP_Q10

!-------------------------------------------------------------------------------
!-------------------------------------------------------------------------------

  REAL FUNCTION TEMP_ARRHENIUS_C3(b, Tl) RESULT(fTk)
```

```
    IMPLICIT NONE

    REAL,INTENT(IN) :: b, Tl

    fTk = EXP(b*(Tl-25.0)/(Tl+273.2))

    RETURN

  END FUNCTION TEMP_ARRHENIUS_C3

!-----------------------------------------------------------------------
!-----------------------------------------------------------------------

  REAL FUNCTION TEMP_ARRHENIUS_C4(Ea,Hd,DS,Tl) RESULT(fTk)
  ! Arrhenius function use with C4 metabolic parameters as described by
  ! Massad et al. 2007

    IMPLICIT NONE

    REAL,INTENT(IN) :: Tl, Ea, Hd, DS
    REAL :: R, Tk

    R = 8.3144       ! Universal gas constant
    Tk = Tl + 293.0   ! Convert leaf temperature from degrees to Kelvin

  ! Arrhenius expression as used by Massad et al. 2007
    fTk = EXP( Ea*(Tk-298.0)/(298.0*R*Tk) )        &
        * (1.0 + EXP( (298.0*DS-Hd)/(298.0*R) ))  &
        / (1.0 + EXP( (Tk*DS-Hd)/(Tk*R) ))

  ! Return answer to user
    RETURN

  END FUNCTION TEMP_ARRHENIUS_C4

!-----------------------------------------------------------------------
!-----------------------------------------------------------------------
```

```
    REAL FUNCTION TEMP_POLYNOMIAL(Tmax, Topt, Q, Tl) RESULT(fTk)

      IMPLICIT NONE

      REAL,INTENT(IN) :: Tmax, Topt, Tl, Q

      IF( Tl >= Tmax) THEN
            fTk = 0.0
      ELSE
            fTk = EXP( LOG((Tmax-Tl)/(Tmax-Topt)) &
                 *Q*(Tmax-Topt))*EXP(Q*(Tl-Topt))
      ENDIF

     ! Return answer to user
      RETURN

    END FUNCTION TEMP_POLYNOMIAL

  !-----------------------------------------------------------------------
  !-----------------------------------------------------------------------

    REAL FUNCTION ZBRENT(FUNC, PARPACK, X1, X2, TOL)
! Below is the simple bisection routine that finds the optimal gs and Ci
    values based on the current
! met data. Taken from Numerical Recipes in FORTRAN.

      IMPLICIT NONE

      TYPE(LEAF_DATA_TYPE),INTENT(IN) :: PARPACK

      REAL :: FUNC, X1, X2, TOL
      REAL :: EPS
      INTEGER :: i, IMAX

      PARAMETER ( IMAX=30, EPS=3.0E-8 )

      REAL :: A,B,C,D,E,FA,FB,FC,P,Q,R,S,TOL1,XM

      A = X1
```

```
      B = X2
      FA = FUNC(A,PARPACK)
      FB = FUNC(B,PARPACK)

      IF( (FA>0.0 .AND. FB>0.0) .OR. (FA<0.0 .AND. FB<0.0) ) THEN
        FA = FUNC(A,PARPACK)
        FB = FUNC(B,PARPACK)
        !WRITE(*,*)'       FA       FB       X1          X2'
        !WRITE(*,*) FA, FB, X1, X2
        !WRITE(*,*)'[== Root must be bracketed for ZBRENT ==]'
        ZBRENT = -9999.0
        RETURN
      ENDIF
      C = B
      FC = FB

      DO i=1,IMAX

        IF( (FB>0.0 .AND. FC>0.0) .OR. (FB<0.0 .AND. FC<0.0) ) THEN
          C = A
          FC = FA
          D = B-A
          E = D
        ENDIF

        IF( ABS(FC) < ABS(FB) ) THEN
          A = B
          B = C
          C = A
          FA = FB
          FB = FC
          FC = FA
        ENDIF

        TOL1 = 2.0*EPS*ABS(B) + 0.5*TOL
        XM = 0.5*(C-B)

        IF( ABS(XM)<=TOL1 .OR. FB==0.0 ) THEN
          ZBRENT = B
```

```
      RETURN
    ENDIF

    IF( ABS(E)>=TOL1 .AND. ABS(FA)>ABS(FB) ) THEN

      S = FB/FA
      IF(A==C) THEN
        P = 2.0*XM*S
        Q = 1.0 - S
      ELSE
        Q = FA/FC
        R = FB/FC
        P = S*( 2.0*XM*Q*(Q-R) - (B-A)*(R-1.0) )
        Q = (Q-1.0)*(R-1.0)*(S-1.0)
      ENDIF

      IF(P>0.0) Q = -Q
      P = ABS(P)
      IF( 2.0*P < MIN(3.0*XM*Q-ABS(TOL1*Q),ABS(E*Q)) ) THEN
        E = D
        D = P/Q
      ELSE
        D = XM
        E = E
      ENDIF
    ELSE
      D = XM
      E = D
    ENDIF
    A = B
    FA = FB
    IF( ABS(D)>TOL1) THEN
      B = B+D
    ELSE
      B = B+SIGN(TOL1,XM)
    ENDIF
    FB = FUNC(B,PARPACK)
  ENDDO
```

```
      WRITE(*,*) "ZBRENT exceeding maximum iterations"

      ZBRENT = B

      RETURN

    END FUNCTION ZBRENT ! End of function

  ! ------------------------------------------------------------------
  ! ------------------------------------------------------------------



END MODULE STOMOPT   ! End of module
```

stomoptim_module_leaf.f90

Bibliography

Abramowitz, G. (2005). Towards a benchmark for land surface models. *Geophysical Research Letters*, 32(L22702).

Abramowitz, G., Leuning, R., Clark, M., and Pitman, A. J. (2009). Evaluating the performance of land surface models. *Journal of Climate*, 21:5468–5481.

Alton, P., Fisher, R., Los, S., and Williams, M. (2009). Simulations of global evapotranspiration using semiempirical and mechanistic schemes of plant hydrology. *Global Biogeochemical Cycles*, 23:GB4023.

Anwar, M. R., O'Leary, G., McNeil, D., Hossian, H., and Nelson, R. (2007). Climate change impact on rainfed wheat in south-eastern Australia. *Field Crops Research*, 104(1-3):139–147.

Asseng, S., Jamieson, P. D., Kimball, B., Pinter, P., Sayre, K., Bowden, J. W., and Howden, S. M. (2004). Simulated wheat growth affected by rising temperature, increased water deficit and elevated atmospheric CO2. *Field Crops Research*, 85(2-3):85–102.

Baldocchi, D. D., Finnigan, J., Wilson, K., Paw, U. K. T., and Falge, E. (2000). On measuring net ecosystem carbon exchange over tall vegetation on complex terrain. *Boundary-Layer Meteorology*, 96:257–291.

Baldocchi, D. D., Hicks, B. B., and Meyers, T. P. (1988). Measuring biosphere-atmosphere exchanges of biologically related gases with micrometeorological methods. *Ecology*, 69:1331–1340.

Baldocchi, D. D., Liukang, X., and Kiang, N. (2004). How plant functional-type, weather, seasonal drought, and soil physical properties alter water and energy fluxes of an oak-grass savanna and an annual grassland. *Agricultural and Forest Meteorology*, 123:13–39.

Baldocchi, D. D., Valentini, R., Running, S., Oechel, W., and Dahlman, R. (1996). Strategies for measuring and modelling carbon dioxide and water vapour fluxes over terrestrial ecosystems. *Global Change Biology*, 2(3):159–168.

Ball, J. T., Woodrow, I. E., and Berry, J. A. (1987). A model predicting stomatal conductance and its contribution to the control of photosynthesis under different environmental conditions. In Biggins, J., editor, *Progress in Photosynthesis Research*, volume 4, pages 221–224. Martinus Nijhoff: Dordrecht.

Banks, R. (1998). Soil landscapes of the Blackville 1:1,000.000 sheet. Technical report, Department of Land and Water Conservation, Gunnedah.

Beringer, J., Hutley, L. B., Tapper, N. J., and Cernusak, L. A. (2007). Savanna fires and their impact on net ecosystem productivity in north Australia. *Global Change Biology*, 13:990–1004.

Berninger, F. and Hari, P. (1993). Optimal regulation of gas-exchange - evidence from field data. *Annals of Botany*, 71:135–140.

Berninger, F., Makela, A., and Hari, P. (1996). Optimal control of gas-exchange during drought: Empirical evidence. *Annals of Botany*, 77:469–476.

Berry, J. A. and Farquhar, G. D. (1978). The CO2 concentration function of C4 photosynthesis: a biochemical model. In Hall, D., Coombs, J., and Goodwin, T., editors, *Proceedings of the 4th International Congress of Photosynthesis*, pages 119–131, London, UK. Biochemical Society.

Bonan, G. B. (1995). Land-atmosphere CO2 exchange simulated by a land surface process model coupled to an atmospheric general circulation model. *Journal of Geophysical Research*, 100D:2817–2831.

Bondeau, A., Smith, P. C., Zaehle, S., Schaphoff, S., Lucht, W., Cramer, W., and Gerten, D. (2007). Modelling the role of agriculture for the 20th century global terrestrial carbon balance. *Global Change Biology*, 13(3):679–706.

Bosveld, F. and Bouten, W. (2001). Evaluation of transpiration models with observations over a Douglas-fir forest. *Agricultural and Forest Meteorology*, 108:247–264.

Boulten, A. J. and Hancock, P. J. (2006). Rivers as groundwater-dependent ecosystems: a review of degrees of dependency, riverine processes and management implications. *Australian Journal of Botany*, 54(2):133–144.

Buckley, T. N. (2005). The control of stomata by water balance. *New Phytologist*, 168:275–292.

Buckley, T. N., Mott, K. A., and Farquhar, G. D. (2003). A hydromechanical and biochemical model of stomatal conductance. *Plant Cell and Environment*, 26(10):1767–1785.

Budyko, M. I. (1974). *Climate and Life*, volume 18 of *International Geophysics Series*. Academic Press, New York.

Bunce, J. A. (1998). Effects of environment during growth on the sensitivity of leaf conductance to changes in humidity. *Global Change Biology*, 4:269–274.

Burgess, S. S. O., Adams, M. A., Turner, N. C., Beverly, C. R., Ong, C. K., Khan, A. A. H., and Bleby, T. M. (2001). An improved heat pulse method to measure low and reverse rates of sap flow in woody plants. *Tree Physiology*, 21:589–598.

Caldwell, M. M., Meister, H. P., Tenhunen, J. D., and Lange, O. L. (1986). Canopy structure, light microclimate and leaf gas exchange of *Quercus coccifera* l. in a portuguese *macchia*: measurements in different canopy layers and simulations with a canopy model. *Tree-Structures and Function*, 1(1):25–41.

Carmo-Silva, A. E., Powers, S. J., Keys, A. J., Arrabaca, M. C., and Parry, M. A. J. (2008). Photorespiration in C4 grasses remains slow under drought conditions. *Plant Cell and Environment*, 31:925–940.

Cermak, J., Kucera, J., Bauerle, W. L., Philips, N., and Hinckley, Thomas, M. (2007). Tree water storage and its diurnal dynamics related to sap flow and changes in stem volume in old-growth douglas-fir trees. *Tree Physiology*, 27:181–198.

Chapin III, F. S., Matson, P. A., and Mooney, H. A. (2002). *Principles of terrestrial ecosystem ecology*. Birkhauser, illustrated edition.

Chen, D.-X., Coughenour, M. B., Knapp, A. K., and Owensby, C. E. (1994). Mathematical simulation of C4 grass photosynthesis in ambient and elevated CO2. *Ecological Modelling*, 73:63–80.

Chen, X. Y., Eamus, D., and Hutley, L. B. (2002). Seasonal patterns of soil carbon dioxide efflux from a wet-dry tropical savanna of northern Australia. *Australian Journal of Botany*, 50(1):43–51.

Chen, X. Y., Hutley, L. B., and Eamus, D. (2003). Carbon balance of a tropical savanna of northern Australia. *Oecologia*, 137:405–416.

Choudhury, B. J. (1999). Evaluation of an empirical equation for annual evaporation using field observations and results from a biophysical model. *Journal of Hydrology*, 216:99–110.

Cleugh, H. A., Leuning, R., Mu, Q., and Running, S. W. (2007). Regional evaporation estimates from flux tower and MODIS satellite data. *Remote Sensing of Environment*, 106:285–304.

Collatz, J. G., Ball, T. J., Grivet, C., and Berry, J. A. (1991). Physiological and environmental regulation of stomatal conductance, photosynthesis and transpiration: a model that includes a laminar boundary layer. *Agricultural and Forest Meteorology*, 54:107–136.

Collatz, J. G., Berry, J. A., and Clark, J. S. (1998). Effects of climate and atmospheric CO2 partial pressure on the global distribution of C4 grasses: present, past, and future. *Oceologia*, 114(4):441–454.

Collatz, J. G., Ribas-Carbo, M., and Berry, J. A. (1992). Coupled photosynthesis-stomatal conductance model for leaves of C4 plants. *Australian Journal of Plant Physiology*, 19:519–538.

Collelo, G. D., Levis, S., Sitch, S., Vertenstein, M., and Oleson, K. W. (2003). A dynamic global vegetation model for use with climate models: concepts and description of simulated vegetation dynamics. *Global Change Biology*, 9:1543–1566.

Cook, G. D. and Heerdegen, R. G. (2001). Spatial variation in the duration of the rainy season in monsoonal Australia. *Journal of Climatology*, 21:1723–1732.

Cook, P. G., Hatton, T. J., Pidsley, D., Herczeg, A. L., Held, A., O'Grady, A. P., and Eamus, D. (1998). Water balance of a tropical woodland ecosystem, northern Australia: a combination of micro- meteorological, soil physical and groundwater chemical approaches. *Journal of Hydrology*, 210:61–177.

Cook, P. G., Williams, R. J., O'Grady, A. P., and Liedloff, A. C. (2002). Variation in vegetative water use in the savannas of the north Australian tropical transect. *Journal of Vegetation Science*, 13(3):413–418.

Cowan, I. R. (1977). Stomatal behaviour and the environment. *Advances in Botanical Research*, 4:117–227.

Cowan, I. R. and Farquhar, G. D. (1977). Integration of activity in the higher plant. In Jennings, D. H., editor, *Stomatal Function in Relation to Leaf Metabolism and Environment*, pages 471–505. Cambridge University Press, Cambridge.

Cramer, W., Bondeau, A., Woodward, F. I., Prentice, I. C., Betts, R. A., Brovkin, V., Cox, P. M., Fisher, V., Foley, J. A., Friend, A. D., Kucharik, C., Lomas, M. R., Ramankutty, N., Sich, S., Smith, B., White, A., and Young-Molling, C. (2001). Global response of terrestrial ecosystem structure and function to CO2 and climate change: results from six dynamic global vegetation models. *Global Change Biology*, 7(4):357–373.

David, T. S., Ferreira, M. I., David, J. S., and Pereira, J. S. (1997). Transpiration from a mature *Eucalyptus globulus* plantation in portugal during a spring-summer period of progressively higher water deficit. *Oecologia*, 110:153–159.

Dawson, T. E., Burgess, S. S. O., Tu, K. P., Oliveira, R. S., Santiago, L. S., Fisher, J. B., Simonin, K. A., and Ambrose, A. R. (2007). Nighttime transpiration in woody plants from contrasting ecosytems. *Tree Physiology*, 27:561–576.

Debruin, H. and Holtslag, A. (1982). A simple parameterization of the surface fluxes of sensible and latent-heat during daytime compared with the Penman-Monteith concept. *Journal of Applied Meteorology*, 21(1):1610–1621.

Dewar, R. C. (2002). The Ball-Berry-Leuning and Tardieu-Davies stomatal models: synthesis and extension within a spatially aggregated picture of guard cell function. *Plant, Cell and Environment*, 25:1383–1398.

Dolman, A. J., Gash, J. H. C., Roberts, J., and Shuttleworth, W. J. (1991). Stomatal and surface conductance of tropical rainforest. *Agricultural and Forest Meteorology*, 54:303–313.

Donohue, R. J., Roderick, M. L., and McVicar, T. R. (2007). On the importance of including vegetation dynamics in Budyko's hydrological model. *Hydrology and Earth System Sciences*, 11:983–995.

Eagleson, P. S. (2002). *Ecohydrology: Darwinian Expression of Vegetation Form and Function*. Cambridge University, Cambridge.

Eamus, D. (1999). Ecophysiological traits of deciduous and evergreen woody species in the seasonally dry tropics. *Trends in Plant Sciences*, 14(1):11–17.

Eamus, D. (2003). How does ecosystem water balance affect net primary productivity of woody ecosystems? *Functional Plant Biology*, 30(2):187–205.

Eamus, D., Chen, X. Y., Kelley, G., and Hutley, L. B. (2002). Root biomass and root fractal analyses of an open Eucalyptus forest in a savanna of north australia. *Australian Journal of Botany*, 50:31–41.

Eamus, D., Froend, R., Loomes, R., Hose, G., and Murray, B. R. (2006a). A functional methodology for determining the groundwater regime needed to maintain the health of groundwater-dependent vegetation. *Australian Journal of Botany*, 54:97–114.

Eamus, D., Hatton, T. J., Cook, P. G., and Colvin, C. (2006b). *Ecohydrology: Vegetation Function Water and Resource Management*. CSIRO Publishing, Melbourne.

Eamus, D., Hutley, L. B., and O'Grady, A. P. (2001). Daily and seasonal patterns of carbon and water fluxes above a north Australian savanna. *Tree Physiology*, 21:977–988.

Eamus, D., Myers, B., Duff, G., and Williams, D. (1999). Seasonal changes in photosynthesis of eight savanna tree species. *Tree Physiology*, 19(10):665–671.

Eamus, D., O'Grady, A. P., and Hutley, L. B. (2000). Dry season conditions determine wet season water use in the wet-dry tropical savannas of northern Australia. *Tree Physiology*, 20(18):1219–1226.

Eamus, D. and Prior, L. (2001). Ecophysiology of trees of seasonally dry tropics: Comparisons among phenologies. *Advances in Ecological Research*, 32:113–197.

Eamus, D. and Shanahan, S. (2002). A rate equation model of stomatal responses to vapour pressure deficit and drought. *BMC Ecology*, 2:1–14.

Eamus, D., Taylor, D. T., Macinnis-Ng, C. M. O., Shanahan, S., and de Silva, L. (2008). Comparing model predictions and experimental data for the response of stomatal conductance and guard cell turgor to manipulations of cuticular conductance, leaf-to-air vapour pressure difference and temperature: feedback mechanisms are able to account for all observations. *Plant, Cell and Environment*, 31:269–277.

Engel, V., Stieglitz, M., Williams, M., and Griffin, K. (2002). Forest canopy hydraulic properties and catchment water balance: observations and modeling. *Ecological Modelling*, 154:263–288.

Ewers, B. and Oren, R. (2000). Analyses of assumptions and errors in the calculation of stomatal conductance from sap flux measurements. *Tree Physiology*, 20:579–589.

Ewers, B. E., Mackay, D. S., and Samanta, S. (2007). Interannual consistency in canopy stomatal conductance control of leaf water potential across seven tree species. *Tree Physiology*, 27:11–24.

Farquhar, G. D. and von Caemmerer, S. (1982). Modelling of photosynthetic response to the environment. In Lange, O. L., Nobel, P. S., B, O. C., and H, Z., editors, *Physiological*

Plant Ecology II, volume 12B of *Encyclopedia of Plant Physiology, New Series*, pages 549–587. Springer-Verlag, Berlin.

Farquhar, G. D., von Caemmerer, S., and Berry, J. A. (1980). A biochemical model of photosynthetic CO2 assimilation in leaves of C3 species. *Planta*, 149:78–90.

Farquhar, G. D. and Wong, S. C. (1984). An empirical model of stomatal conductance. *Australian Journal of Plant Physiology*, 11:191–210.

Fisher, R. A., Williams, M., Da Costa, A. L., Malhi, Y., da Costa, R. F., Almeida, S., and Meir, P. (2007). The response of an eastern Amazonian rain forest to drought stress: results and modelling analyses from a throughfall exclusion experiment. *Global Change Biology*, 13(11):2361–2378.

Fisher, R. A., Williams, M., Do Vale, R. L., Da Costa, A. L., and Meir, P. (2006). Evidence from Amazonian forests is consistent with isohydric control of leaf water potential. *Plant Cell and Environment*, 29(2):151–165.

Fordyce, I. R., Duff, G. A., and Eamus, D. (1997). The water relations of *Allosyncarpia ternata* (*Myrtaceae*) at contrasting sites in the monsoonal tropics of northern Australia. *Australian Journal of Botany*, 45:259–274.

Froend, R. H. and Drake, P. L. (2006). Defining phreatophyte response to reduced water availability: preliminary investigations on the use of xylem cavitation vulnerability in Banksia woodland species. *Australian Journal of Botany*, 54:173–179.

Gash, J., Shuttleworth, W., Lloyd, C., Andre, J., Goutorbe, J., and Gelpe, J. (1989). Micrometeorological measurements in les landes forest during hapex-mobilhy. *Agricultural and Forest Meteorology*, 46:131–147.

Ghannoum, O. (2009). C4 photosynthesis and water stress. *Annals of Botany*, 103:635–644.

Ghannoum, O., Conroy, J. P., Driscoll, S. P., Paul, M. J., Foyer, C. H., and Lawlor, D. W. (2003). Nonstomatal limitations are responsible for drought-induced photosynthetic inhibition in for C4 grasses. *New Phytologist*, 159:599–608.

Ghannoum, O., Evans, J. R., Chow, W. S., Andrews, T. J., Conroy, J. P., and von Caemmerer, S. (2005). Faster RuBisCO is the key to superior nitrogen-use efficiency in NADP-malic enzyme relative to NAD-malic enzyme C4 grasses. *Plant Physiology*, 137(2):638–650.

Ghannoum, O., von Caemmerer, S., and Conroy, J. P. (2001a). Carbon and water economy of Australian NAD-ME and NADP-ME C4 grasses. *Australian Journal of Plant Physiology*, 28:213–223.

Ghannoum, O., von Caemmerer, S., and Conroy, J. P. (2001b). Plant water use efficiency of 17 Australian NAD-ME and NADP-ME C4 grasses at ambient and elevated CO2 partial pressure. *Australian Journal of Plant Physiology*, 28:1207–1217.

Goldberg, D. (1989). *Genetic Algorithms in Search, Optimization, and Machine Learning*. Addison-Wesley Professional, London.

Goldstein, G., Andrade, J., Meinzer, F., Holbrook, N., Cavelier, J., Jackson, P., and Celis, A. (1998). Stem water storage and diurnal patterns of water use in tropical forest canopy trees. *Plant, Cell and Environment*, 21:397–406.

Granier, A., Biron, P., Breda, N., Pontailler, J. Y., and Saugier, B. (1996a). Transpiration of trees and forest stands: Short and longterm monitoring using sapflow methods. *Global Change Biology*, 2(3):265–274.

Granier, A., Biron, P., and Leoine, D. (2000). Water balance, transpiration and canopy conductance in two beech stands. *Agricultural and Forest Meteorology*, 100:291–308.

Granier, A., Huc, R., and Barigah, S. (1996b). Transpiration of natural rain forest and its dependence on climatic factors. *Agricultural and Forest Meteorology*, 78:19–29.

Granier, A. and Loustau, D. (1994). Measuring and modelling the transpiration of a maritime pine canopy from sap-flow data. *Agricultural and Forest Meteorology*, 71:61–81.

Greco, S. and Baldocchi, D. D. (1996). Seasonal variations of CO2 and water vapor exchange rates over a temperate deciduous forest. *Global Change Biology*, 2:83–197.

Hanan, N. P., Kabat, P., Dolman, A. J., and Elbers, J. A. (1998). Photosynthesis and carbon balance of a Sahelian fallow savanna. *Global Change Biology*, 4(3):523–538.

Hari, P., Makela, A., Berninger, F., and Pohja, T. (1999). Field evidence for the optimality hypothesis of gas-exchange. *Australian Journal of Botany*, 26(3):239–244.

Hari, P., Makela, A., Korpilahti, E., and Holmberg, M. (1986). Optimal control of gas exchange. *Tree Physiology*, 2:169–175.

Harris, P. P., Huntingford, C., Coxb, P. M., Gash, J. H. C., and Malhi, Y. (2004). Effect of soil moisture on canopy conductance of Amazonian rainforest. *Agricultural and Forest Meteorology*, 122:215–227.

Hartung, W. (1983). The site of action of abscisic acid at the guard cell plasmalemma of *Valieranella locusta*. *Plant Cell and Environment*, 6:427–428.

Hernandez-Santana, V., Martinez-Vilalta, J., Martinez-Fernandez, J., and Williams, M. (2009). Evaluating the effect of drier and warmer conditions on water use by *Quercus pyrenaica*. *Forest Ecology and Management*, 258(7):1719–1730.

Hill, T. C., Williams, M., and Moncrieff, J. B. (2008). Modeling feedbacks between a boreal forest and the planetary boundary layer. *Journal of Geophysical Research-Atmospheres*, 113(D15):D15122.

Howe, P., Cook, P., O'Grady, A., and Hillier, J. (2005). Pioneer valley groundwater consultancy 3: Analysis of groundwater dependent ecosystem requirements. Technical report, Resource and Environmental Management Pty Ltd.

Hsu, K., Gupta, H., Gao, X., Sorooshian, S., and Imam, B. (2002). Self-organizing linear output map (SOLO): An artificial neural network suitable for hydrologic modeling and analysis. *Water Resources Research*, 38(12):1–17.

Hughes, L. (2003). Climate change and Australia: Trends, projections and impacts. *Austral Ecology*, 28(4):423–443.

Hutley, L. B., Leuning, R., Beringer, J., and Cleugh, H. A. (2005). The utility of the eddy covariance techniques as a tool in carbon accounting: tropical savanna as a case study. *Australian Journal of Botany*, 53(7):663–675.

Hutley, L. B., O'Grady, A. P., and Eamus, D. (2000). Evapotranspiration from eucalypt open-forest savanna of northern Australia. *Functional Biology*, 14(2):183–194.

Hutley, L. B., O'Grady, A. P., and Eamus, D. (2001). Monsoonal influences on evapotranspiration of savanna vegetation of northern Australia. *Oecologia*, 126:434–443.

Internantional Panel on Climate Change (IPCC) (2007). *Climate change 2007, The physical science basis. Contribution of Working Group I to the Fourth Assessment Report of the Intergovernmental Panel on Climate Change*. Cambridge University Press, Cambridge.

Jarvis, A. J. and Davies, W. J. (1998). The coupled response of stomatal conductance to photosynthesis and transpiration. *Journal of Experimental Botany*, 49:399–406.

Jarvis, P. G. (1976). The interpretation of the variations in leaf water potential and stomatal conductance found in canopies in the field. *Philosophical Transactions of the Royal Society London B*, 273:593–610.

Jarvis, P. G. and McNaughton, K. G. (1986). Stomatal control of transpiration: scaling up from leaf to region. *Advanced Ecology Research*, 15:1–49.

Jones, H. G. (1992). *Plants and Microclimate*. Cambridge University Press.

Jones, H. G. (1998). Stomatal control of photosynthesis and transpiration. *Journal of Experimental Botany*, 49:387–398.

Ju, W., Chen, J. M., Black, T. A., Barr, A. G., Liu, J., and Chen, B. (2006). Modelling multi-year coupled carbon and water fluxes in a boreal aspen forest. *Agricultural and Forest Meteorology*, 140:136–151.

Kanniah, K. D., Beringer, J., and Hutley, L. B. (2010a). The comparative role of key environmental factors in determining savanna productivity and carbon fluxes: A review, with special reference to northern Australia. *Progress in Physical Geography*, pages 1–32.

Kanniah, K. D., Beringer, J., Hutley, L. B., Tapper, N. J., and Zhu, X. (2009). Evaluation of collections 4 and 5 of the MODIS gross primary productivity product and algorithm improvement at a tropical savanna site in northern Australia. *Remote Sensing of Environment*, 113(9):1808–1822.

Kanniah, K. D., Beringer, J., Tapper, N. J., and Long, C. N. (2010b). Aerosols and their influence on radiation partitioning and savanna productivity in northern Australia. *Theoretical and Applied Climatology*, 100(3-4):423–438.

Katul, G. G., Leuning, R., and Oren, R. (2003). Relationship between plant hydraulic and biochemical properties derived from a steady-state coupled water and carbon transport model. *Plant Cell and Environment*, 26(3):339–350.

Katul, G. G., Manzoni, S., Palmroth, S., and Oren, R. (2010). A stomatal optimization theory to describe the effects of atmospheric CO2 on leaf photosynthesis and transpiration. *Annals of Botany*, 105:431–442.

Kelley, G., Hutley, L. B., and Eamus, D. (2002). Role of savanna vegetation in soil and groundwater dynamics in a wet-dry tropical climate. In *Proceedings of the International Association of Hydrogeologists, International Groundwater Conference, 'Balancing The Groundwater Budget'*, pages 12–17, Darwin, Northern Territory, Australia.

Kelley, G., O'Grady, A. P., Hutley, L. B., and Eamus, D. (2007). A comparison of tree water use in two contiguous vegetation communities of the seasonally dry tropics of northern Australia: the importance of site water budget to tree hydraulics. *Australian Journal of Botany*, 55(7):700–708.

Kelliher, F. M., Leuning, R., Raupach, M. R., and Schulze, E. D. (1995). Maximum conductances for evaporation from global vegetation types. *Agricultural and Forest Meteorology*, 73(1-2):1–16.

Kelliher, F. M., Leuning, R., and Schulze, E. D. (1993). Evaporation and canopy characteristics of coniferous forests and grasslands. *Oecologia*, 95:153–163.

Kirkup, L., Foot, M., and Mulholland, M. (2004). Comparison of equations describing band broadening in high-performance liquid chromatography. *Journal of Chromatography A*, 1030:25–31.

Kleinbaum, D. G., Kupper, L. L., Muller, K. E., and Nizam, A. (1997). *Applied regression analysis and other multivariable methods*. Duxbury Press, 3rd edition.

Koenker, R. and Bassett, G. (1978). Regression quantiles. *Econometrica*, 46(1):33–50.

Kohonen, T. (1989). *Self-Organising and Associative Memory*. Springer-Verlag, New York.

Komatsu, H., Kang, Y., Kume, T., Yoshifuji, N., and Hotta, N. (2006a). Transpiration from a *Cryptomeria japonica* plantation, part 1: aerodynamic control of transpiration. *Hydrological Processes*, 20:1309–1320.

Komatsu, H., Kang, Y., Kume, T., Yoshifuji, N., and Hotta, N. (2006b). Transpiration from a *Cryptomeria japonica* plantation, part 2: responses of canopy conductance to meteorological factors. *Hydrological Processes*, 20:1321–1334.

Kosugi, Y., Takanashi, S., Tanaka, H., Ohkubo, S., Tani, M., Yano, M., and Katayama, T. (2007). Evapotranspiration over a japanese cypress forest. I. Eddy covariance fluxes and surface conductance characteristics for 3 years. *Journal of Hydrology*, 337:269–283.

Lagergren, F. and Lindroth, A. (2002). Transpiration response to soil moisture in pine and spruce trees in sweden. *Agricultural and Forest Meteorology*, 112:67–85.

Law, B., Williams, M., Anthoni, P., Baldocchi, D., and Unsworth, M. (2000). Measurement and modelling seasonal variation of carbon dioxide and water vapour exchange of a *Pinus ponderosa* forest subject to soil water deficit. *Global Change Biology*, 6(6):613–630.

Lawlor, D. W. and Cornic, G. (2002). Photosynthetic carbon assimilation and associated metabolism in relation to water deficits in higher plants. *Plant Cell and Environment*, 25(2):275–294.

Leuning, R. (1990). Modelling stomatal behaviour and photosynthesis of *Eucalyptus grandis*. *Australian Journal of Plant Physiology*, 17:159–175.

Leuning, R. (1995). A critical appraisal of a combined stomatal-photosynthesis model for C3 plants. *Plant, Cell and Environment*, 18:339–355.

Leuning, R., Cleugh, H. A., Zegelin, S. J., and Hughes, D. (2005). Carbon and water fluxes over a temperate Eucalyptus forest and a tropical wet/dry savanna in Australia: measurements and comparison with MODIS remote sensing estimates. *Agricultural and Forest Meteorology*, 129:151–173.

Leuning, R., Dunin, F., and Wang, Y. P. (1998). A two-leaf model for canopy conductance, photosynthesis and partitioning of available energy. II. comparison with measurements. *Agricultural and Forest Meteorology*, 91:113–125.

Leuning, R., Tuzet, A., and Perrier, A. (2003). Stomata as part of the soil-plant-atmosphere continuum. In Mencuccini, M., Grace, J., Moncrieff, J., and McNaughton, K. G., editors, *Forests at the Land-Atmosphere Interface*. CAB International, Edinburgh, Scotland.

Leuning, R., Zhang, Q. Y., Rajaud, A., Cleugh, H. A., and Tu, K. (2008). A simple surface conductance model to estimate regional evaporation using MODIS leaf area index and the Penman-Monteith equation. *Water Resources Research*, 44(10).

Lohammer, T., Larsson, S., Linder, S., and Falk, S. O. (1980). FAST-simulation models of gaseous exchange in Scots pine. *Ecological Bulletin*, 32:505–523.

Lu, P., Yunusa, I. A., Walker, R., and Muller, W. (2003). Regulation of canopy conductance and transpiration and their modelling in irrigated grapevines. *Functional Plant Biology*, 30:689–698.

Lundbald, M. and Lindroth, A. (2002). Stand transpiration and sapflow density in relation to weather, soil moisture and stand characteristics. *Basic and Applied Ecology*, 3:229–243.

Macinnis-Ng, C. M. O., Zeppel, M. J. B., Williams, M., and Eamus, D. (2010). Applying a SPA model to examine the impact of climate change on GPP of open woodlands and the potential for woody thickening. *Ecohydrology*, DOI:10.1002/eco.138.

Mäkelä, A., Beringer, F., and Hari, P. (1996). Optimal control of gas exchange during drought: Theoretical analysis. *Annals of Botany*, 77:461–467.

Mäkelä, A., Pulkkinen, M., Kolari, P., Lagergren, F., Berbigier, P., Lindroth, A., Loustau, D., Nikinmaa, E., Vesala, T., and Hari, P. (2008). Developing an empirical model of stand GPP with the LUE approach: analysis of eddy covariance data at five constrasting conifer sites in Europe. *Global Change Biology*, 14:92–108.

Malhi, Y., Baldocchi, D. D., and Jarvis, P. G. (1999). The carbon balance of tropical, temperate and boreal forests. *Plant Cell and Environment*, 22(6):715–740.

Maseda, P. H. and Fernandez, R. J. (2006). Stay wet or else: three ways in which plants can adjust hydraulically to their environment. *Journal of Experimental Botany*, 57(15):3963–3977.

Massad, R.-S., Tuzet, A., and Bethenod, O. (2007). The effect of temperature on C4-type leaf photosynthesis parameters. *Plant Cell and Environment*, 30:1191–1204.

McKenzie, N., Jacquier, D., Isbell, R., and Brown, K. (2004). *Australian Soils and Landscapes: An Illustrated Compendium*. CSIRO Publishing, illustrated edition.

McMahon, T. A. and Finlayson, B. L. (2003). Droughts and anti-droughts: the low flow hydrology of Australian rivers. *Freshwater Biology*, 48(7):1147–1160.

McMurtrie, R. E., Comins, H. N., Kirschbaum, M. U. F., and Wang, Y. P. (1992a). Modifying existing forest growth models to take account of effects of elevated CO2. *Australian Journal of Botany*, 40:657–677.

McMurtrie, R. E., Leuning, R., Thompson, W. A., and Wheeler, A. M. (1992b). A model of canopy photosynthesis and water use incorporating a mechanistic formulation of leaf CO2 exchange. *Forest Ecology and Management*, 52:261–278.

Medhurst, J. L., Battaglia, M., and Beadle, C. L. (2002). Measured and predicted changes in tree and stand water use following high-intensity thinning of an 8-year old *Eucalyptus nitens* plantation. *Tree Physiology*, 22:775–784.

Medlyn, B. E., Berbigier, P., Robert, C., Grelle, A., Loustau, D., Linder, S., Wingate, L., Jarvis, P. G., Sigurdsson, B. D., and McMurtrie, R. E. (2005a). Carbon balance of coniferous forests growing in contrasting climates: Model-based analysis. *Agricultural and Forest Meteorology*, 131:97–124.

Medlyn, B. E., Pepper, D. A., O'Grady, A. P., and Keith, H. (2007). Linking leaf and tree water use with an individual-tree model. *Tree Physiology*, 27:1687–1699.

Medlyn, B. E., Robinson, A., Clement, R., and McMurtrie, R. E. (2005b). On the validation of models of forest CO2 exchange using eddy covariance data: some perils and pitfalls. *Tree Physiology*, 25:839–857.

Meinzer, F. C. (2003). Functional convergence in plant responses to the environment. *Oecologia*, 134:1–11.

Meyer, W. (1999). Standard reference evaporation calculation for inland, south standard reference evaporation calculation for inland, south eastern Australia. *Technical Report* 35/98, CSIRO Land and Water, Adelaide, South Australia.

Miranda, A. C., Miranda, H. S., Lloyd, J., Grace, J., Francey, R. J., Mcintyre, J. A., Meir, P., Riggan, P., R, L., and Brass, J. (1997). Fluxes of carbon, water and energy over Brazilian cerrado: An analysis using eddy covariance and stable isotopes. *Plant Cell and Environment*, 20(3):315–328.

Misson, L., Panek, J. A., and Goldstein, A. H. (2004). A comparison of three approaches to modeling leaf gas exchange in annually drought-stressed Ponderosa pine forests. *Tree Physiology*, 24:529–541.

Mitchell, P. L. (1997). Misuse of regression for empirical validation of models. *Agricultural Systems*, 54(3):313–326.

Monteith, J. L. (1965). Evaporation and environment. *Symposia of the Society of Experimental Biology*, 19:205–224.

Monteith, J. L. (1995). A reinterpretation of stomatal responses to humidity. *Plant, Cell and Environment*, 18:357–364.

Monteith, J. L. and Unsworth, M. H. (1990). *Principles of environmental physics*. Butterworth-Heinemann.

Mordelet, P. and Menaut, J. C. (1995). Influences of trees on aboveground production dynamics of grasses in a humid savanna. *Journal of Vegetation Science*, 6(2):223–228.

Moreno, F., Fernandez, J. E., Clothier, B. E., and Green, S. R. (1996). Transpiration and root water uptake by olive trees. *Plant and Soil*, 184(1):85–96.

Morton, F. I. (1983). Operational estimates of areal evapotranspiration and their significance to the science and practice of hydrology. *Journal of Hydrology*, 66(1-76).

Mott, K. A. (1988). Do stomata respond to CO2 concentrations other than intercellular. *Plant Physiology*, 86:200–203.

Mott, K. A. and Parkhurst, D. F. (1991). Stomatal responses to humidity in air and helox. *Plant Cell and Environment*, 14:509–515.

Mu, Q., Heinsch, F. A., Zhao, M., and Running, S. W. (2007). Development of a global evapotranspiration algorithm based on MODIS and global meteorology data. *Remote Sensing of Environment*, 111:519–536.

Myers, B. A., Duff, G. A., Eamus, D., Fordyce, I. R., O'Grady, A. P., and Williams, R. J. (1997). Seasonal variation in water relations of trees of differing leaf phenology in a wet-dry tropical savanna near Darwin, northern Australia. *Australian Journal of Botany*, 45:225–240.

Nobel, P. S. (1999). *Physicochemical and Environmental Plant Physiology.* Academic Press, 4, illustrated edition.

Novick, K. A., Stoy, P. C., Katul, G. G., Ellsworth, D. S., Siqueira, M. B. S., Juang, J., and Oren, R. (2004). Carbon dioxide and water vapor exchange in a warm temperate grassland. *Oecologia*, 138(2):259–274.

Ogink-Hendriks, M. (1995). Modelling surface conductance and transpiration of an oak forest in the Netherlands. *Agricultural and Forest Meteorology*, 74:99–118.

O'Grady, A. P. (2006). Comparative water use by the riparian trees *Melaleuca argentea* and *Corymbia bella* in the wet-dry tropics of northern Australia. *Tree Physiology*, 26:219–228.

O'Grady, A. P., Chen, X. Y., Eamus, D., and Hutley, L. B. (2000). Composition, leaf area index and standing biomass of Eucalypt open forests near Darwin in the Northern Territory, Australia. *Australian Journal of Botany*, 28:629–638.

O'Grady, A. P., Cook, P. G., Eamus, D., Dugoid, A., Wischusen, J. D. H., Fass, T., and Worldedge, D. (2009). Convergence of tree water use within an arid-zone woodland. *Oecologia*, 160:643–655.

O'Grady, A. P., Eamus, D., Cook, P. G., and Lamontagne, S. (2006). Groundwater use by riparian vegetation in the wet-dry tropics of northern Australia. *Australian Journal of Botany*, 54:145–154.

O'Grady, A. P., Eamus, D., and Hutley, L. B. (1999). Transpiration increases in the dry season: patterns of tree water use in the eucalypt open forests of northern Australia. *Tree Physiology*, 19:591–597.

O'Grady, A. P., Worldedge, D., and Battaglia, M. (2008). Constraints on transpiration of *Eucalyptus globulus* in southern Tasmania, australia. *Agricultural and Forest Meteorology*, 148:453–465.

Ol'dekop, E. M. (1911). On evaporation from the surface of river basins. *Transactions on meteorological observations*, 4.

Oren, R. and Pataki, D. E. (2001). Transpiration in response to variation in microclimate and soil moisture in southeastern deciduous forests. *Oceologia*, 127:549–559.

Oren, R., Sperry, J., Katul, G., Pataki, D., Ewers, B., Philips, N., and Schafer, K. (1999). Survey and synthesis of intra- and interspecific variation in stomatal sensitivity to vapour pressure deficit. *Plant, Cell and Environment*, 22:1515–1526.

Palmer, A., Fuentes, S., Taylor, D. T., Macinnis-Ng, C. M. O., Zeppel, M. J. B., Yunusa, I. A. M., February, E., and Eamus, D. (2008). The use of pre-dawn leaf water potential and MODIS LAI to explore seasonal trends in the phenology of Australian and southern African woodlands and savannas. *Australian Journal of Botany*, 56(7):557–563.

Pataki, D. and Oren, R. (2003). Species differences in stomatal control of water loss at the canopy scale in a mature bottomland deciduous forest. *Advances in water resources*, 26:1267–1278.

Patrick, L., Ogle, K., Bell, C. W., Zak, J., and Tissue, D. (2009). Physiological responses of two contrasting desert plant species to precipitation variability are differentially regulated by soil moisture and nitrogen dynamics. *Global Change Biology*, 15:1214–1229.

Pearcy, R. W. and Ehleringer, J. (1984). Comparitive ecophysiology of C3 and C4 plants. *Plant Cell and Environment*, 7:1–13.

Peisker, M. (1979). Conditions for low, and oxygen-independent, CO2 compensation concentrations in C4 plants as derived from a simple model. *Photosynthetica*, 13:198–207.

Penman, H. L. (1948). Natural evaporation from open water, bare soil and grass. *Proceedings of the Royal Society of London A*, 194(S):120–145.

Pike, J. G. (1964). The estimation of annual run-off from meteorological data in a tropical climate. *Journal of Hydrology*, 2:116–123.

Price, K. V., Storn, R. M., and Lampinen, J. A. (2005). *Differential Evolution: A Practical Approach to Global Optimization*. Natural computing series. Springer, illustrated edition.

Prior, L. D., Bowman, D. M. J. S., and Eamus, D. (2004). Seasonal differences in leaf attributes in Australian tropical tree species: family and habitat comparisons. *Functional Ecology*, 18(5):707–718.

Prior, L. D. and Eamus, D. (1999). Seasonal changes in leaf water characteristics of *Eucalyptus tetrodonta* and *Terminalia ferdinandiana* saplings in a northern Australian savanna. *Australian Journal of Botany*, 47:587–599.

Prior, L. D., Eamus, D., and Duff, G. A. (1997). Seasonal trends in carbon assimilation, stomatal conductance, pre-dawn leaf water potential and growth in *Terminalia ferdinandiana*, a deciduous tree of northern Australian savannas. *Australian Journal of Botany*, 45:53–69.

Rana, G., Katerji, N., and de Lorenzi, F. (2005). Measurement and modelling of evapotranspiration of irrigated citrus orcahrd under Mediterranean conditions. *Agricultural and Forest Meteorology*, 128:199–209.

Raupach, M. R. (2001). Combination theory and equilibrium evaporation. *Quarterly Journal of the Royal Meteorological Society*, 127:1149–1181.

Reich, P. B., Wright, I. J., Cavender-Bares, J., Craine, M., Oleksyn, J., Westoby, M., and Walters, M. B. (2003). The evolution of plant functional variation: Traits, spectra, and strategies. *International Journal of Plant Sciences*, 164:143–164.

Rollenbeck, R. and Dieter, A. (2007). Characteristics of the water and energy balance in an Amazonian lowland rainforest in Venezuela and the impact of the ENSO-cycle. *Journal of Hydrology*, 337:377–390.

Rouphael, Y. and Colla, G. (2004). Modelling the transpiration of a greenhouse zucchini crop grown under a Mediterranean climate using the Penman-Monteith equation and its simplified version. *Australian Journal of Agricultural Research*, 55:931–937.

Russell-Smith, J., Needham, S., and Brock, J. (1995). *Kakadu natural and Cultural Heritage and Management*, pages 94–126. Australian Nature and Conservation Agency and North Australia Research Unit.

Ryan, M. G., Bond, B. J., Law, B. E., Hubbard, R. M., Woodruff, D., Cienciala, E., and Kucera, J. (2000). Transpiration and whole-tree conductance in ponderosa pine trees of different heights. *Oecologia*, 124(4):553–560.

Sage, R. F. (1994). Acclimation of photosynthesis to increasing atmospheric CO2 - the gas exchange perspective. *Photosynthesis Research*, 39(3):351–368.

Sage, R. F., Pearcy, R. W., and Seemann, J. R. (1987). The nitrogen use efficiency of C3 and C4 plants. *Plant Physiology*, 85:355–359.

San José, J., Bracho, R., and Nikonova, N. (1998). Comparison of water transfer as a component of the energy balance in a cultivated grass (*Brachiaria decumbens* stapf.) field and a savanna during the wet season of the Orinoco Llanos. *Agricultural and Forest Meteorology*, 90:65–79.

Saxton, K. E. and Rawls, W. J. (2006). Soil water characteristic estimates by texture and organic matter for hydrologic solutions. *Soil Science Society of America*, 70:1569–1578.

Saxton, K. E., Rawls, W. J., Romberger, J. S., and Papendick, R. I. (1986). Estimating generalized soil-water characteristics from texture. *Soil Science Society of America*, 50(4):1031–1036.

Scanlon, B. R., Jolly, I., Sophocleous, M., and Zhang, L. (2007). Global impacts of conversions from natural to agricultural ecosystems on water resources: Quantity versus quality. *Water Resources Research*, 43(3):W03437.

Schreiber, P. (1904). Uber die beziehungen zwischen dem niederschlag und der wasserfuhrung der flusse in mitteleuropa. *Meteorology Z*, 21.

Schultz, H. R. (2003). Differences in hydraulic architecture account for near-isohydric and anisohydric behaviour of two field-grown *Vitis vinifera* l. cultivars during drought. *Plant Cell and Environment*, 26:1393–1405.

Schulze, E. D. (1986). Carbon dioxide and water vapour exchange in response to drought in the atmosphere and in the soil. *Annual Review of Plant Physiology*, 37:247–274.

Schymanski, S. J., Roderick, M. L., Sivapalan, M., Hutley, L. B., and Beringer, J. (2007). A test of the optimality approach to modelling canopy properties and CO2 uptake by natural vegetation. *Plant Cell and Environment*, 30(12):1586–1598.

Schymanski, S. J., Roderick, M. L., Sivapalan, M., Hutley, L. B., and Beringer, J. (2008a). A canopy scale test of the optimal water use hypothesis. *Plant Cell and Environment*, 31:97–111.

Schymanski, S. J., Sivapalan, M., Roderick, M. L., Beringer, J., and Hutley, L. B. (2008b). An optimality-based model of the coupled soil moisture and root dynamics. *Hydrology and Earth System Sciences*, 12:913–932.

Schymanski, S. J., Sivapalan, M., Roderick, M. L., Hutley, L. B., and Beringer, J. (2009). An optimality-based model of the dynamic feedbacks between natural vegetation and the water balance. *Water Resources Research*, 45(W01412).

Sellers, P. J., Berry, J. A., Collatz, J. G., Field, C. B., and Hall, F. G. (1992). Canopy reflectance, photosynthesis and transpiration. III. a reanalysis using improved leaf models and a new canopy intergration scheme. *Remote Sensing of Environment*, 42:187–216.

Sellers, P. J., Randall, D. A., Collatz, J. G., Berry, J. A., Field, C. B., Dazlich, D. A., Zhang, C., Collelo, G. D., and Bounoua, L. (1996). A revised land surface parameterization (SiB2) for atmospheric GCMs .1. Model formulation. *Journal of Climate*, 9(4):676–705.

Silberstein, R., Sivapalan, M., Viney, N., Held, A., and Hatton, T. (2003). Modelling the energy balance of a natural Jarrah (*Eucalyptus marginata*) forest. *Agricultural and Forest Meteorology*, 115:201–230.

Simonin, K., Kolb, T., Montes-Helu, M., and Koch, G. (2007). The influence of thinning on components of stand water balance in a ponderosa pine forest stand during and after extreme drought. *Agricultural and Forest Meteorology*, 143:266–276.

Sitch, S. (2000). *The Role of Vegetation Dynamics in the Control of Atmospheric CO2 Content*, chapter LPJ : a coupled model of vegetation dynamics and the terrestrial carbon cycle. Lund University.

Sommer, R., de Abreu Sa, T., Vielhauer, K., de Araujo, A., Folster, H., and Vlek, P. (2002). Transpiration and canopy conductance of secondary vegetation in the eastern Amazon. *Agricultural and Forest Meteorology*, 112:103–121.

Stewart, J. (1988). Modelling surface conductance of pine forest. *Agricultural and Forest Meteorology*, 43:19–35.

Tardieu, F. and Davies, W. J. (1992). Stomatal response to ABA is a function of current plant water status. *Plant Physiology*, 98:540–545.

Tardieu, F. and Davies, W. J. (1993). Integration of hydraulic and chemical signalling in the control of stomatal conductance and water status of droughted plants. *Plant, Cell and Environment*, 16:341–349.

Tardieu, F., Lafarge, T., and Simonneau, T. (1996). Stomatal control by fed or endogenous xylem ABA in sunflower: interpretation of correlations between leaf water potential and stomatal conductance in anisohydric species. *Plant Cell and Environment*, 19:75–84.

Tardieu, F. and Simonneau, T. (1998). Variability among species of stomatal control under fluctuating soil water status and evaporative demand: modelling isohydric and anisohydric behaviours. *Journal of Experimental Botany*, 49:419–432.

Tezara, W., Fernandes, M. D., Donoso, C., and Herrera, A. (1998). Seasonal changes in photosynthesis and stomatal conductance of five plant species from a semiarid ecosystem. *Photosynthetica*, 35(3):399–410.

Thomas, D. S. and Eamus, D. (1999). The influence of predawn leaf water potential on stomatal responses to atmospheric water content at constant Ci and on stem hydraulic conductance and foliar ABA concentrations. *Journal of Experimental Botany*, 50(331):243–251.

Thomas, D. S., Eamus, D., and Bell, D. (1999a). Optimization theory of stomatal behaviour I. A critical evaluation of fives methods of calculation. *Journal of Experimental Botany*, 50(332):385–392.

Thomas, D. S., Eamus, D., and Bell, D. (1999b). Optimization theory of stomatal behaviour II. Stomatal responses of several tree species of north Australia to changes in light, soil and atmospheric water content and temperature. *Journal of Experimental Botany*, 50(332):393–400.

Thomas, D. S., Eamus, D., and Shanahan, S. (2000). Influence of season, drought and xylem ABA on stomatal responses to leaf-to-air vapour pressure difference of trees of the Australian wet-dry tropics. *Australian Journal of Botany*, 48:143–151.

Thum, T., Aalto, T., Laurila, T., Aurela, M., Kolari, P., and Hari, P. (2007). Parameterization of two photosynthesis models at the canopy scale in a northern boreal Scots pine forest. *Tellus Series B - Chemical and Physical Meteorology*, 59:874–890.

Tuzet, A., Perrier, A., and Leuning, R. (2003). A coupled model of stomatal conductance, photosynthesis and transpiration. *Plant, Cell and Environment*, 26:1097–1116.

Tyree, M. T. and Sperry, J. S. (1988). Do woody plants operate near the point of catastrophic xylem dysfunction caused by dynamic water stress? *Plant Physiology*, 88:574–580.

Tyree, M. T. and Sperry, J. S. (1989). Vulnerability of xylem to cavitation and embolism. *Annual Reviews of Plant Physiology and Molecular Biology*, 40:19–38.

Uddling, J., Hall, M., Wallin, G., and Karlsson, P. E. (2005). Measuring and modelling stomatal conductance and photosynthesis in mature birch in Sweden. *Agricultural and Forest Meteorology*, 132:115–131.

van Wijk, M. T., Dekker, S. C., Bouten, W., Bosveld, F., Kohsiek, W., Kramer, K., and Mohren, G. (2000). Modeling daily gas exchange of a Douglas-fir forest: comparison of three stomatal conductance models with and without a soil water stress function. *Tree Physiology*, 20:115–122.

Verbeeck, H., Steppe, K., Nadezhdina, N., op de Beeck, M., Deckmyn, G., Meiresonne, L., Lemeur, R., Cermack, J., Ceulemans, R., and Janssens, I. A. (2007). Stored water used and transpiration in Scots pine: a modelling analysis with ANAFORE. *Tree Physiology*, 27:1671–1685.

Verhoef, A., Allen, S., De Bruin, H., Jacobs, C., and Heusinkveld, B. (1996). Fluxes of carbon dioxide and water vapour from a Sahelian savanna. *Agricultural and Forest Meteorology*, 80:231–248.

Vico, G. and Porporato, A. (2008). Modelling C3 and C4 photosynthesis under water-stressed conditions. *Plant and Soil*, 313:187–203.

von Caemmerer, S. (2000). *Biochemical models of leaf photosynthesis*. Techniques in plant sciences. CSIRO Publishing.

von Caemmerer, S. and Furbank, R. T. (1999). The modelling C4 photosynthesis. In Sage, R., editor, *The Biology of C4 Photosynthesis*, pages 169–207. Academic Press.

von Caemmerer, S. and Furbank, R. T. (2003). The C4 pathway: an efficient CO2 pump. *Photosynthesis Research*, 77:191–207.

Wang, Y. P. and Leuning, R. (1998). A two-leaf model for canopy conductance, photosynthesis and partitioning of available energy I: Model description and comparison with a multi-layered model. *Agricultural and Forest Meteorology*, 91:89–111.

Wartinger, A., Heilmeier, H., Hartung, W., and Schulze, E. D. (1990). Daily and seasonal courses of leaf conductance and abscisic acid in the xylem sap of almond trees (*Prunus dulcis* m.) under desert conditions. *New Phytologist*, 116:581–587.

Webb, E. K., Pearman, G. I., and Leuning, R. (1980). Correction of flux measurements for density effects due to heat and water vapour transfer. *Quarterly Journal of the Royal Meteorological Society*, 106:85–100.

Whetton, P. H., Fowler, A. M., Haylock, M. R., and Pittock, A. B. (1993). Implications of climate-change due to enhanced greenhouse-effect on floods and droughts in Australis. *Climate Change*, 25(3-4):289–317.

Whitehead, D. (1998). Regulation of stomatal conductance and transpiration in forest canopies. *Tree Physiology*, 18:633–644.

Whitley, R. J., Medlyn, B. E., Zeppel, M. J. B., Macinnis-Ng, C. M. O., and Eamus, D. (2009). Comparing the Penman-Monteith equation and a modified Jarvis-Stewart model with an artificial neural network to estimate stand-scale transpiration and canopy conductance. *Journal of Hydrology*, 373:256–266.

Whitley, R. J., Zeppel, M. J. B., Armstrong, N., Macinnis-Ng, C. M. O., Yunusa, I. A. M., and Eamus, D. (2008). A modified Jarvis-Stewart model for predicting stand-scale transpiration of an Australian native forest. *Plant and Soil*, 305(1-2):35–47.

Wilkinson, S. and Davies, W. J. (2002). ABA-based chemical signalling: the co-ordination of responses to stress in plants. *Plant Cell and Environment*, 25(2):195–210.

Williams, D. G., Cable, W., Hultine, K., Hoedjes, J. C. B., Yepez, E., Simonneaux, V., Er-Raki, S., Boulet, G., De Bruin, H. A. R., Chehbouni, A., Hartogensis, O. K., and Timouk, F. (2004). Evapotranspiration components determined by stable isotope, sap flow and eddy covariance techniques. *Agricultural and Forest Meteorology*, 125:241–258.

Williams, M., Bond, B., and Ryan, M. (2001a). Evaluating different soil and plant hydraulic constraints on tree function using a model and sap flow data from Ponderosa pine. *Plant, Cell and Environment*, 24:679–690.

Williams, M., Eugster, W., Rastetter, E. B., McFadden, J. P., and Chapin III, F. S. (2000). The controls on net ecosystem productivity along an Arctic transect: a model comparison with flux measurements. *Global Change Biology*, 6:116–126.

Williams, M., Law, B., Anthoni, P., and Unsworth, M. (2001b). Use of a simulation model and ecosystem flux data to examine carbon-water interactions in Ponderosa pine. *Tree Physiology*, 21:287–298.

Williams, M., Malhi, Y., Nobre, A., Rastetter, E., Grace, J., and Pereira, M. (1998). Seasonal variation in net carbon exchange and evapotranspiration in a Brazillian rain forest. *Plant Cell and Environmnet*, 21:953–968.

Williams, M., Rastetter, E., Fernandes, D., Goulden, M., Wofsy, S., Shaver, G., Melillo, J., Munger, J., Fan, S., and Nadelhoffer, K. (1996a). Modelling the soil-plant-atmosphere continuum in a *Quercus-Acer* stand at Harvard Forest: the regulation of stomata conductance by light, nitrogen and soil/plant hydraulic properties. *Plant, Cell and Environment*, 19:911–927.

Williams, M., Rastetter, E., Shaver, G., Hobbie, J., Carpino, E., and Kwiatkowski, B. (2001c). Primary production of an Arctic watershed: An uncertainty analsysis. *Ecological Applications*, 11(6):1800–1816.

Williams, R. J., Duff, G. A., Bowman, D. M. J. S., and Cook, G. D. (1996b). Variation in the composition and structure of tropical savannas as a function of rainfall and soil texture along a large scale climatic gradient in the Northern Territory, Australia. *Journal of Biogeography*, 24:747–756.

Williams, R. J., Myers, B. A., Muller, M. J., Duff, G. A., and Eamus, D. (1997). Leaf phenology of woody species in northern Australian tropical savanna. *Ecology*, 78:2542–2558.

Wong, S. C., Cowan, I. R., and Farquhar, G. D. (1978). Leaf conductance in relation to assimilation in *Eucalyptus pauciflora* sieb. ex spreng. Influence of irradience and partial pressure of carbon dioxide. *Plant Physiology*, 62:670–674.

Wong, S. C., Cowan, I. R., and Farquhar, G. D. (1985a). Leaf conductance in relation to rate of CO2 assimilation. I. Influence of nitrogen nutrition, phosphorous, nutrition, photon flux density, and ambient partial pressure of CO2 during ontogeny. *Plant Physiology*, 78:821–825.

Wong, S. C., Cowan, I. R., and Farquhar, G. D. (1985b). Leaf conductance in relation to rate of CO2 assimilation. II. Effects of short-term exposures to different photon flux densities. *Plant Physiology*, 78:826–829.

Wong, S. C., Cowan, I. R., and Farquhar, G. D. (1985c). Leaf conductance in relation to rate of CO2 assimilation. III. Influences of water stress and photoinhibition. *Plant Physiology*, 78:830–834.

Wright, I. J., Falster, D. S., Pickup, M., and Westoby, M. (2006). Cross-species patterns in the coordination between leaf and stem traits, and their implications for plant hydraulics. *Physiologia Plantarum*, 127:445–456.

Wright, I. R., Manzi, A. O., and da Rocha, H. R. (1995). Surface conductance of Amazonian pasture: model application and calibration for canopy climate. *Agricultural and Forest Meteorology*, 75:51–70.

Wullschleger, S. and Hanson, P. (2006). Sensitivity of canopy transpiration to altered precipitation in an upland oak forest: evidence from a long-term field manipulation study. *Global Change Biology*, 12:97–109.

Wullschleger, S., Hanson, P., and Todd, D. (2001). Transpiration from a multi-species deciduous forest as estimated by xylem sap flow techniques. *Forest Ecology and Management*, 143:205–213.

Wullschleger, S. D., Meinzer, F. C., and Vertessey, R. A. (1998). A review of whole-plant water use studies in trees. *Tree Physiology*, 18:499–512.

Wullschleger, S. D., Wilson, K. B., and Hanson, P. J. (2000). Environmental control of whole-plant transpiration, canopy conductance and estimates of the decoupling coefficient for large red maple trees. *Agricultural and Forest Meteorology*, 104:157–168.

Yunusa, I. A. M., Aumann, C., Rab, A., Merrick, N., Eberbach, P., and Eamus, D. (2010). Topographical and seasonal trends in transpiration by two co-occurring eucalypt species in a low rainfall environment. In review.

Yunusa, I. A. M., Walker, R. R., Loveys, B. R., and Blackmore, D. H. (2000). Determination of transpiration in irrigated grapevines: Comparison of the heat-pulse technique with gravimetric and micrometeorological methods. *Irrigation Science*, 20:1–8.

Zeppel, M. J. and Eamus, D. (2005). Tree water use under conditions of drought. *Agricultural Science*, 17:8–11.

Zeppel, M. J., Murray, B. R., Barton, C., and Eamus, D. (2004). Seasonal responses of xylem sap velocity to vpd and solar radiation during drought in a stand of native trees in temperate Australia. *Functional Plant Biology*, 31:461–470.

Zeppel, M. J. B. (2006). *The influence of drought and other abiotic factors on tree water use in a temperate remnant forest*. PhD thesis, University of Technology Sydney.

Zeppel, M. J. B. and Eamus, D. (2008). Coordination of leaf area, sapwood area and canopy conductance leads to species convergence of tree water use in a remnant evergreen woodland. *Australian Journal of Botany*, 56:97–108.

Zeppel, M. J. B., Macinnis-Ng, C. M. O., Palmer, A., Taylor, D. T., Whitley, R. J., Fuentes, S., Yunusa, I. A. M., Williams, M., and Eamus, D. (2008a). An analysis of the sensitivity of sap flux to soil and plant variables assessed for an Australian woodland using a soil-plant-atmosphere model. *Functional Plant Biology*, 35:509–520.

Zeppel, M. J. B., Macinnis-Ng, C. M. O., Yunusa, I. A. M., Whitley, R. J., and Eamus, D. (2008b). Long term trends of stand transpiration in a remnant forest during wet and dry years. *Journal of Hydrology*, 349:200–213.

Zhang, H., Simmonds, L., Morison, J., Payne, D., and Wullschleger, S. (1997). Estimation of transpiration by single trees: comparison of sap flow measurements with a combination equation. *Agricultural and Forest Meteorology*, 87:155–169.

Zhang, J. and Davies, W. J. (1990). Changes in the concentration of ABA in xylem sap as a function of changing soil water status can account for changes in leaf conductance and growth. *Plant Cell and Environment*, 13:277–285.

Zhang, J. and Davies, W. J. (1991). Changes in the concentration of ABA in xylem sap as a function of changing soil water status can account for changes in leaf conductance and growth. *Plant Cell and Environment*, 13:277–285.

Zhang, L., Dawes, W. R., and Walker, G. R. (1998). Prediciting the effect of vegetation changes on catchment average water balance. Technical report, CSIRO Land and Water.

Zhang, L., Dawes, W. R., and Walker, G. R. (2001). Response of mean annual evapotranspiration to vegetation changes at catchment scale. *Water Resources Research*, 37:701–708.